

AD-A252 656



DTIC
ELECTE
JUL 7 1992
S c D



WL-TR-91-2117
VOLUME II

ADVANCED THERMALLY STABLE JET FUEL DEVELOPMENT PROGRAM
ANNUAL REPORT
VOLUME II - COMPOSITIONAL FACTORS AFFECTING THERMAL
DEGRADATION OF JET FUELS

C. Song, S. Eser, H.H. Schobert, P.G. Hatcher, M.M. Coleman, Y. Peng, L. Selvaraj, M. Parzynski, J. Bortiatynski, Y. Liu, R.M. Copenhaver, R. Arumugam

The Pennsylvania State University
University Park, PA 16802

May 1992

Final Report for Period July 1990 - July 1991

Approved for public release; distribution is unlimited

92-17545



AERO PROPULSION AND POWER DIRECTORATE
WRIGHT LABORATORY
AIR FORCE SYSTEMS COMMAND
WRIGHT-PATTERSON AIR FORCE BASE, OHIO 45433-6563

92 17545 10

NOTICE

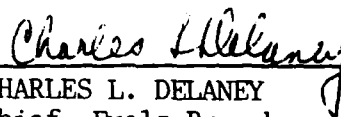
When Government drawings, specifications, or other data are used for any purpose other than in connection with a definitely Government-related procurement, the United States Government incurs no responsibility nor any obligation whatsoever. The fact that the government may have formulated, or in any way supplied the said drawings, specifications, or other data, is not to be regarded by implication or otherwise in any manner construed, as licensing the holder or any other person or corporation, or as conveying any rights or permission to manufacture, use, or sell any patented invention that may in any way be related thereto.

This report is releasable to the National Technical Information Service (NTIS). At NTIS, it will be available to the general public, including foreign nations.

This technical report has been reviewed and is approved for publication.

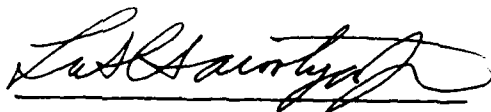


DONN M. STORCH, Major, USAF
Assistant Chief
Fuels & Lubrication Division
Aero Propulsion & Power Directorate



CHARLES L. DELANEY
Chief, Fuels Branch
Fuels & Lubrication Division
Aero Propulsion & Power Directorate

FOR THE COMMANDER



LEO S. HAROOTYAN, JR, Chief
Fuels & Lubrication Division
Aero Propulsion & Power Directorate

If your address has changed, if you wish to be removed from our mailing list, or if the addressee is no longer employed by your organization, please notify WL/POSF, Wright-Patterson AFB, OH 45433-6563 to help us maintain a current mailing list.

Copies of this report should not be returned unless return is required by security considerations, contractual obligations, or notice on a specific document.

REPORT DOCUMENTATION PAGE				Form Approved OMB No. 0704-0188	
1a. REPORT SECURITY CLASSIFICATION Unclassified			1b. RESTRICTIVE MARKINGS None		
2a. SECURITY CLASSIFICATION AUTHORITY N/A			3. DISTRIBUTION/AVAILABILITY OF REPORT Approved for public release; distribution is unlimited.		
2c. DECLASSIFICATION/DOWNGRADING SCHEDULE N/A					
4. PERFORMING ORGANIZATION REPORT NUMBER(S) N/A			5. MONITORING ORGANIZATION REPORT NUMBER(S) WL-TR-91-2117		
6a. NAME OF PERFORMING ORGANIZATION The Pennsylvania State University		6b. OFFICE SYMBOL (If applicable)	7a. NAME OF MONITORING ORGANIZATION Aero Propulsion and Power Directorate Wright Laboratory (WL/POSF)		
6c. ADDRESS (City, State, and ZIP Code) University Park, PA 16802			7b. ADDRESS (City, State, and ZIP Code) Wright-Patterson AFB, OH 45433-6563		
8a. NAME OF FUNDING / SPONSORING ORGANIZATION N/A		8b. OFFICE SYMBOL (If applicable) N/A	9. PROCUREMENT INSTRUMENT IDENTIFICATION NUMBER FY1455-89-N-0635		
8c. ADDRESS (City, State, and ZIP Code) N/A			10. SOURCE OF FUNDING NUMBERS		
			PROGRAM ELEMENT NO. 62203F	PROJECT NO. 3048	TASK NO. 05
11. TITLE (Include Security Classification) Advanced Thermally Stable Jet Fuels Development Program Annual Report: Volume 2 Compositional Factors Affecting Thermal Degradation of Jet Fuels					
12. PERSONAL AUTHOR(S) C. Song, S. Eser, H.H. Schobert, P.G. Hatcher, M.M. Coleman, Y. Peng, L. Selvaraj, M. Parzynski, J. Bortiatynski, Y. Liu, R.M. Copenhaver, R. Arumugam					
13a. TYPE OF REPORT Final		13b. TIME COVERED FROM 7/90 TO 7/91		14. DATE OF REPORT (Year, Month, Day) May 1, 1992	
15. PAGE COUNT 187					
16. SUPPLEMENTARY NOTATION None					
17. COSATI CODES			18. SUBJECT TERMS (Continue on reverse if necessary and identify by block number)		
FIELD	GROUP	SUB-GROUP			
19. ABSTRACT (Continue on reverse if necessary and identify by block number)					
<p>This project focuses on the compositional factors affecting jet fuel thermal stability at high temperatures. The chemical composition of the four jet fuel samples (JP-8C, JP-8P, JP-7P, Jet A-1) and Wilsonville middle distillates was characterized by using selective ion monitoring technique in GC-MS analysis. The thermal treatment tests have been performed on jet fuels and a series of model compounds including tetralin, decalin, ethylcyclohexane, butylcyclohexane, n-butylbenzene, t-butylbenzene, n-octane, n-decane, and n-tetradecane. Deposit samples from an actual aircraft fuel system as well as those produced from jet fuels and model compounds in microautoclaves were characterized by FTIR and polarized-light microscopy. Experiments were conducted to find the optimum amount of antioxidant 2,6-di-tert-butyl-4-methylphenol necessary to minimize the solid formation upon thermal stressing of JP8 neat and Jet A-1 fuel samples. The chemistry of thermal degradation of the fuel and antioxidant mixtures was studied by using FTIR to characterize the liquid products from thermal stressing.</p>					
20. DISTRIBUTION/AVAILABILITY OF ABSTRACT <input checked="" type="checkbox"/> UNCLASSIFIED/UNLIMITED <input type="checkbox"/> SAME AS RPT. <input type="checkbox"/> DTIC USERS			21. ABSTRACT SECURITY CLASSIFICATION Unclassified		
22a. NAME OF RESPONSIBLE INDIVIDUAL WILLIAM HARRISON			22b. TELEPHONE (Include Area Code) 513-255-6601		22c. OFFICE SYMBOL WL/POSF)

SUMMARY	1
TECHNICAL PROGRESS	4
TASK 1. Identification and Characterization of Stable Hydrocarbon Species	
Present in Coal-Derived Fuels.....	4
Activity 1. Identification of Hydrocarbon Species.....	4
Activity 2. Stressing of Model Compounds.....	8
TASK 2. Identification and Characterization of Mixtures of Stable Hydrocarbon	
Species Present in Coal-Derived Fuels.....	42
Activity 1. Fractionation of Jet Fuels.....	42
Activity 2. Thermal Stressing of JP-8C.....	43
TASK 3. Identification and Characterization of Stable Hydrocarbon Species Present in	
Petroleum-Derived Fuels.....	72
Activity 1. Identification of Hydrocarbon Species.....	72
Activity 2. Stressing of Model Compounds.....	79
TASK 4. Identification and Characterization of Mixtures of Stable Hydrocarbon	
Species Present in Petroleum-Derived Fuels	94
Activity 1. Fractionation of Jet Fuels.....	94
Activity 2. Thermal Stressing of JP-8P and Its Saturate Fraction.....	94
Mechanistic Considerations.....	127
TASK 5. Characterization of Solid Deposits.....	126
Aircraft System Deposits.....	126
Solids Produced in Laboratory Microautoclaves.....	137
TASK 6. Exploratory Studies for Fuel Thermal Stability Enhancement	147
Addition of 2,6-di-tert-butyl-4-methylphenol to JP8 Neat Fuel	148
Addition of 2,6-di-tert-butyl-4-methylphenol to Jet A-1 Fuel.....	148
Addition of 2,4,6-tri-tert-butylphenol and 2,4,6-trimethylphenol to JP8 Neat.....	161
REFERENCES	174

Table 1.	Gas products from thermal stressing of model compounds at 450°C for 4 h in N ₂	14
Table 2.	Gas products from thermal stressing of t-butylbenzene at 450°C with and without quartz	18
Table 3.	Identified compounds for peaks designated in Figures 12-15.....	27
Table 4.	Fractional composition of liquid products from n- and t-butylbenzene	29
Table 5.	Identified compounds in fraction 2 of 450°C-1 h liquid product of t-butylbenzene.....	36
Table 6.	Identified compounds in fraction 2 of 450°C-4 h liquid product of t-butylbenzene.....	37
Table 7.	Identified compounds in fraction 2 of 450°C-8 h liquid product of t-butylbenzene.....	38
Table 8.	Identified compounds in fraction 2 of 400°C-1 h liquid product of n-butylbenzene.....	39
Table 9.	Identified compounds in fraction 2 of 450°C-1 h liquid product of n-butylbenzene.....	40
Table 10.	Identified compounds in fraction 2 of 450°C-8 h liquid product of n-butylbenzene.....	41
Table 11.	Chromatographic separation of JP-8C and JP-8P fuels on neutral alumina gel	43
Table 12.	Identified compounds in saturate fraction of JP-8C jet fuel	45
Table 13.	Identified compounds in monoaromatic fraction of JP-8C jet fuel	49
Table 14.	Identified compounds in aromatic fraction of JP-8C jet fuel.....	53
Table 15.	Tentative assignments of ¹ H NMR spectra of jet fuels	64
Table 16.	Identified compounds in thermally treated JP-8C at 450°C for 16 h in N ₂ by GC-MS using modified procedure	70
Table 17.	Identified compounds in thermally stressed tetradecane at 475 °C for 6 h in N ₂	93
Table 18.	Identified compounds in saturate fraction of JP-8P jet fuel	96
Table 19.	Identified compounds in monoaromatic fraction (fraction 2) of JP-8P jet fuel	99
Table 20.	Identified compounds in aromatic fraction of JP-8C jet fuel.....	102

Table 21.	Gas products from thermal stressing of JP-8P at 450°C for 0.5-16 h in N₂...	107
Table 22.	Identified compounds in thermally treated JP-8P at 450°C for 16 h in N₂ by GC-MS using modified procedure	118
Table 23.	Aromaticity of the solids from the reactions of t-butylbenzene as a function of reaction time at 450°C.....	142



Accession For	
DTIC	<input checked="" type="checkbox"/>
DTIC TAB	<input type="checkbox"/>
Unannounced	<input type="checkbox"/>
Justification	
By	
Distribution/	
Availability Codes	
Dist	Avail and/or Special
A-1	

Figure 1.	Total and specific ion chromatograms of coal-derived jet fuel JP8-C from GC-MS using split injection of undiluted sample.....	5
Figure 2.	Total and specific ion chromatograms of Wilsonville middle distillate derived from two-stage coal liquefaction	7
Figure 3a.	Retention time window I (1-16:53 minutes) of GC-MS profile for JP-8C using split injection of undiluted sample.....	9
Figure 3b.	Retention time window II (16:54-33:43 minutes) of GC-MS profile for JP-8C.....	10
Figure 4.	Retention time window III (24-45 minutes) of GC-MS profile for JP-8C.....	11
Figure 5.	Time-pressure profile for thermal stressing of model fuel components for coal-derived jet fuels.....	12
Figure 6.	Formation of solids from t-butylbenzene as a function of time at 450, 475, and 500°C.....	16
Figure 7.	Apparent first-order plots for the formation of solids from t-butylbenzene..	16
Figure 8.	Apparent Arrhenius plot for the formation of solids from t-butylbenzene...	17
Figure 9.	Capillary gas chromatograms of liquids from t-butylbenzene stressed at 450°C for 15 min with (top) and without quartz insert (bottom)	19
Figure 10.	Capillary gas chromatograms of liquids from t-butylbenzene stressed at 450°C for 30 min with (top) and without quartz insert (bottom).....	20
Figure 11.	Capillary gas chromatograms of liquids from t-butylbenzene stressed at 450°C for 1 h min with (top) and without quartz insert (bottom).....	21
Figure 12.	Capillary gas chromatograms of liquids from t-butylbenzene stressed at 450°C for 15 (A), 30 (B) and 60 minutes (C).....	22
Figure 13.	Capillary gas chromatograms of liquids from t-butylbenzene stressed at 450°C for 4 (A), 8 (B) and 72 h (C)	23
Figure 14.	Capillary gas chromatograms of liquids from n-butylbenzene stressed at 450°C for 15 (A), 30 (B) and 60 minutes (C).....	24
Figure 15.	Capillary gas chromatograms of liquids from n-butylbenzene stressed at 450°C for 4 (A), 8 (B) and 72 h (C).....	25
Figure 16.	A separation scheme for concentrating minor components of liquid products.....	28
Figure 17.	GC/MS total ion chromatogram of fraction 2 of the 450°C-1 h liquid product from t-butylbenzene.....	30
Figure 18.	GC/MS total ion chromatogram of fraction 2 of the 450°C-4 h liquid product from t-butylbenzene.....	31

Figure 19.	GC/MS total ion chromatogram of fraction 2 of the 450°C-8 h liquid product from t-butylbenzene.....	32
Figure 20.	GC/MS total ion chromatogram of fraction 2 of the 400°C-1 h liquid product from n-butylbenzene.....	33
Figure 21.	GC/MS total ion chromatogram of fraction 2 of the 450°C-1 h liquid product from n-butylbenzene.....	34
Figure 22.	GC/MS total ion chromatogram of fraction 2 of the 450°C-8 h liquid product from n-butylbenzene	35
Figure 23.	GC-MS TIC of saturate fraction (n-pentane elute) of JP-8C jet fuel (split injection of undiluted sample without delay to ionization).....	44
Figure 24.	GC-MS TIC of monoaromatic fraction (5% benzene-pentane elute) of JP-8C jet fuel (splitless injection of diluted sample with 4 min delay to ionization)	48
Figure 25.	GC-MS TIC of aromatic fraction (benzene elute) of JP-8C jet fuel (splitless injection of diluted sample with 4 min delay to ionization)	52
Figure 26.	Liquid depletion and gas formation from JP-8C and its saturate fraction at 450°C.....	56
Figure 27.	Liquid depletion and gas formation from coal-derived JP-8C versus the residence time at 450°C in a N ₂ atmosphere	57
Figure 28.	Thermal decomposition of coal-derived jet fuel JP-8C at 450°C to form gas and solid deposits.....	58
Figure 29.	Thermal stability comparison between petroleum- and coal-derived JP-8 fuels	59
Figure 30.	¹ H NMR spectrum of the original, coal-derived JP-8C fuel	60
Figure 31.	¹ H NMR spectrum of the thermally stressed JP-8C at 450°C for 0.5 h.....	61
Figure 32.	¹ H NMR spectrum of the thermally stressed JP-8C at 450°C for 4 h	62
Figure 33.	¹ H NMR spectrum of the thermally stressed JP-8C at 450°C for 8 h	63
Figure 34.	Retention time window I (1-16:53 min) of GC-MS profiles for thermally stressed coal-derived JP-8C fuel for 0.5, 1 and 4 h	65
Figure 35.	Retention time window II (16:54-33:43 min) of GC-MS profiles for thermally stressed, coal-derived JP-8C fuel for 0.5, 1 and 4 h.....	66
Figure 36.	Retention time window III (24-45 min) of GC-MS profiles for thermally stressed, coal-derived JP-8C fuel for 0.5, 1 and 4 h	67
Figure 37.	Total ion chromatogram of liquids from thermally treated whole JP-8C at 450°C for 16 h in N ₂	69

Figure 38.	Specific ion chromatograms of petroleum-derived JP-8P from GC-MS using split injection of undiluted sample.....	73
Figure 39.	Specific ion chromatograms of petroleum-derived JP-7P from GC-MS using split injection of undiluted sample	74
Figure 40.	Specific ion chromatograms of petroleum-derived Jet A-1 from GC-MS using split injection of undiluted sample	75
Figure 41.	Total ion chromatogram of petroleum-derived JP-8P from GC-MS using split injection of undiluted sample.....	76
Figure 42.	Total ion chromatogram of petroleum-derived JP-7P from GC-MS using split injection of undiluted sample.....	77
Figure 43.	Total ion chromatogram of petroleum-derived Jet A-1 from GC-MS using split injection of undiluted sample.....	78
Figure 44.	Retention time window I (1-16:53 minutes) of GC-MS profile for JP-8P using split injection of undiluted sample.....	80
Figure 45.	Retention time window II (16:54-33:43 minutes) of GC-MS profile for JP-8P.....	81
Figure 46.	Retention time window III (24-45 minutes) of GC-MS profile for JP-8P...	82
Figure 47.	Time-pressure profiles for thermal stressing of model compounds at 450°C in N ₂	83
Figure 48.	Time-pressure profiles for thermal stressing of JP-8P and JP-8C at 450°C.....	84
Figure 49.	Maximum amount of solids produced by decane, dodecane, and tetradecane as a function of temperature.....	86
Figure 50.	A comparison of the rate constants calculated for solid formation from decane, dodecane and tetradecane using a variable maximum conversion as a function of temperature (k for decane at 475°C by extrapolation)	86
Figure 51.	Formation of solids from straight-chain octane, dodecane, and tetradecane at 400, 425, 450 and 475 °C as a function of stressing time.....	87
Figure 52.	Chromatograms of thermally stressed n-tetradecane at 400 °C for 4.5 (top) and 48 (bottom) h in N ₂	88
Figure 53.	Chromatograms of thermally stressed n-tetradecane at 425 °C for 6 (top) and 24 (bottom) h in N ₂	89
Figure 54.	Chromatograms of thermally stressed n-tetradecane at 450 °C for 3 (top) and 24 (bottom) h in N ₂	0
Figure 55.	Chromatograms of thermally stressed n-tetradecane at 475 °C for 1 (top) and 6 (bottom) h in N ₂	91
Figure 56.	GC-MS TIC of thermally stressed n-tetradecane at 475 °C for 6 h in N ₂	92

Figure 57.	GC-MS TIC of saturate fraction (n-pentane elute) of JP-8P jet fuel (split injection of undiluted sample without delay to ionization)	95
Figure 58.	GC-MS TIC of monoaromatic fraction (5% benzene-pentane elute) of JP-8P jet fuel (splitless injection of diluted sample with 4 min delay to ionization)	98
Figure 59.	GC-MS TIC of aromatic fraction (benzene elute) of JP-8P jet fuel (splitless injection of diluted sample with 4 min delay to ionization)	101
Figure 60.	Liquid depletion and gas formation in the thermal stressing of the saturate fraction Fr.1) as well as the whole fuel of JP8-P at 450°C for 4 h in N ₂ ...	103
Figure 61.	Liquid depletion and gas formation from petroleum-derived JP-8P versus residence time at 450°C under 100 psi N ₂	104
Figure 62.	Thermal decomposition of petroleum-derived jet fuel JP-8P at 450°C to form gas and solid deposits.....	105
Figure 63.	¹ H NMR spectrum of original JP-8P fuel	108
Figure 64.	¹ H NMR spectrum of thermally stressed JP-8P at 450°C for 1 h.....	109
Figure 65.	¹ H NMR spectrum of thermally stressed JP-8P at 450°C for 2.5 h	110
Figure 66.	¹ H NMR spectrum of thermally stressed JP-8P at 450°C for 4 h.....	111
Figure 67.	¹ H NMR spectrum of thermally stressed JP-8P at 450°C for 8 h	112
Figure 68.	Retention time window I (1-16:53 min) of GC-MS profiles for thermally stressed, petroleum-derived JP-8C fuel for 0.5, 1 and 4 h. The peak with scan number of 97 in the top TIC is due to solvent contamination	113
Figure 69.	Retention time window II (16:54-33:43 min) of GC-MS profiles for thermally stressed, petroleum-derived JP-8C fuel for 0.5, 1 and 4 h.....	114
Figure 70.	Retention time window III (24-45 min) of GC-MS profiles for thermally stressed, petroleum-derived JP-8C fuel for 0.5, 1 and 4 h	115
Figure 71.	Total ion chromatogram of thermally treated whole JP-8P at 450°C for 16 h in N ₂	117
Figure 72.	FTIR absorbance spectrum of globular particles from actual fuel system deposits	128
Figure 73.	Polarized-light micrographs of the actual engine deposits in the form of flakes.....	130
Figure 74.	Polarized-light micrographs of the actual engine deposits in the form of flakes.....	131
Figure 75.	Polarized-light micrographs of the actual engine deposits in the form of globules.....	133

Figure 76.	Polarized-light micrographs of the actual engine deposits in the form of globules.....	135
Figure 77.	X-Ray Diffraction profiles of flakes found in actual fuel system deposits and those of Si and SP-1 single crystal graphite.....	136
Figure 78.	Scanning electron micrographs of the flakes and the globules found in actual engine deposits	138
Figure 79.	CPMAS ^{13}C NMR spectrum of the solids produced from t-butylbenzene in 8 h at 450°C	139
Figure 80.	CPMAS ^{13}C NMR spectrum of the solids produced from t-butylbenzene in 20 h at 450°C	140
Figure 81.	FTIR absorbance spectrum of solids produced from Jet A-1 at 425°C for 18 h under 100 psi air pressure.....	141
Figure 82.	FTIR absorbance spectrum of solids produced from Jet A-1 at 425°C for 18 h under 100 psi air (a) and nitrogen (b) pressure.....	143
Figure 83.	Polarized-light micrographs of solids from triple stressing of tetradecane at 450°C for 8 h in nitrogen	146
Figure 84.	Effects of adding 2,4-di-tert-butyl-4-methylphenol on solid formation from JP8 Neat at 425°C in 100 psi N_2 (cold)	149
Figure 85.	Effects of adding 2,4-di-tert-butyl-4-methylphenol on solid formation from JP8 Neat at 425°C in 100 psi air (cold)	149
Figure 86.	Solid formation at 425°C under 100 psi nitrogen pressure from JP8 neat mixed with 2,6-di-tert-butyl-4-methylphenol	150
Figure 87.	Solid formation at 425°C under 100 psi air pressure from JP8 neat mixed with 2,6-di-tert-butyl-4-methylphenol	150
Figure 88.	Effect of A.O. concentration on formation of solids from Jet A-1 at 425°C for 24 h	151
Figure 89.	FTIR absorbance spectra of the liquid products obtained from reactions of Jet A-1 + 0.3% A. O. at temperatures 190°C - 310°C for 4 h in nitrogen	152
Figure 90.	FTIR absorbance spectra of the liquid products obtained from reactions of Jet A-1 + 0.3% A. O. at temperatures 190°C - 310°C for 4 h in air	154
Figure 91.	FTIR absorbance spectra of the liquid products obtained from reactions of Jet A-1 + 0.3% A. O. at 425°C for 0-24 h in nitrogen	155
Figure 92.	FTIR absorbance spectra of the liquid products obtained from reactions of Jet A-1 + 0.3% A. O. at 425°C for 0-24 h in air.....	156
Figure 93.	FTIR absorbance spectra of the liquid products obtained from reactions of Jet A-1 + 0.3% A. O. at temperatures 190°C - 310°C for 4 h in nitrogen	157

Figure 94.	FTIR absorbance spectra of the liquid products obtained from reactions of Jet A-1 + 0.3% A. O. at temperatures 190°C-310°C for 4 h in air	158
Figure 95.	FTIR absorbance spectra of the liquid products obtained from reactions of Jet A-1 + 0.3% A. O. at 425°C for 0-24 h in nitrogen	159
Figure 96.	FTIR absorbance spectra of the liquid products obtained from reactions of Jet A-1 + 0.3% A. O. at 425°C for 0-24 h in air	160
Figure 97.	FTIR absorbance spectra of the liquid products obtained from reactions of Jet A-1 + 0.3% A. O. at temperatures 190°C-310°C for 4 h in nitrogen	162
Figure 98.	FTIR absorbance spectra of the liquid products obtained from reactions of Jet A-1 + 0.3% A. O. at temperatures 190°C-310°C for 4 h in air.....	163
Figure 99.	FTIR absorbance spectra of the liquid products obtained from reactions of Jet A-1 + 0.3% A. O. at 425°C for 0-24 h in nitrogen	164
Figure 100.	FTIR absorbance spectra of the liquid products obtained from reactions of Jet A-1 + 0.3% A. O. at 425°C for 0-24 h in air.....	165
Figure 101.	FTIR absorbance spectra of the liquid products obtained from reactions of Jet A-1 + 0.3% A. O. at temperatures 190°C-310°C for 4 h in nitrogen	166
Figure 102.	FTIR absorbance spectra of the liquid products obtained from reactions of Jet A-1 + 0.3% A. O. at temperatures 190°C-310°C for 4 h in air	167
Figure 103.	FTIR absorbance spectra of the liquid products obtained from reactions of Jet A-1 + 0.3% A. O. at 425°C for 0-24 h in nitrogen.....	168
Figure 104.	FTIR absorbance spectra of the liquid products obtained from reactions of Jet A-1 + 0.3% A. O. at 425°C for 0-24 h in air.....	169
Figure 105.	Percent transmittance of the products obtained from thermal treatment of 10 ml JP 8 Neat alone and in the presence of 2,4,6-tri-t-butylphenol (TTBP) and 2,4,6-trimethylphenol (TMP)	171
Figure 106.	GC trace of JP-8 neat and mixtures of JP-8 neat with 2,4,6-trimethylphenol treated at 400°C for 2 h in 100 psi N ₂	172
Figure 107.	GC trace of JP-8 neat and mixtures of JP-8 neat with 2,4,6-tri-t-butylphenol treated at 400°C for 2 h in 100 psi N ₂	173

SUMMARY

The chemical composition of the four jet fuel samples (JP-8C, JP-8P, JP-7P, Jet A-1) and Wilsonville middle distillates was characterized by using selective ion monitoring technique in GC-MS analysis. The components in the liquid chromatographic fractions of JP-8C and JP-8P were identified by using GC-MS. The thermal treatment tests have been performed on the jet fuels derived from coal (JP-8C) and petroleum (JP-8P), and a series of model compounds including tetralin, decalin, ethylcyclohexane, butylcyclohexane, n-butylbenzene, t-butylbenzene, n-octane, n-decane, and n-tetradecane. The thermal decomposition behavior of the hydrocarbon components in coal-derived JP-8C and petroleum-derived JP-8P jet fuels was studied by ^1H NMR and GC-MS analyses of thermally stressed JP-8C and JP-8P samples at 450°C for 0.5-8 h. Short-time stressing of model compounds including n- and t-butylbenzene and n-tetradecane were conducted to examine the initial degradation products. A sample of actual aircraft fuel system deposits was characterized by solid-state ^{13}C NMR and FTIR, SEM, XRD, and optical microscopy using plane-polarized light. Selected solids produced from samples of Jet A-1 under nitrogen and air overpressures in microautoclaves were also characterized by FTIR; whereas solids obtained from JP8-P and JP8-C, n- and t-butylbenzene, decane, dodecane, and tetradecane were analyzed by optical microscopy. The solids produced from t-butylbenzene were also analyzed by ^{13}C NMR spectroscopy. Experiments were conducted to find the optimum amount of antioxidant 2,6-di-tert-butyl-4-methylphenol necessary to minimize the solid formation upon thermal stressing of JP8 neat and Jet A-1 fuel samples. The chemistry of thermal degradation of the fuel and antioxidant mixtures was studied by using FTIR to characterize the liquid products from thermal stressing.

Thermal stressing of petroleum-derived (JP-8P) and coal-derived (JP-8C) fuels at 450°C for periods ranging from short time (0.5 h) to long time (16 h) showed that there is an induction period for solid formation, which appeared to be longer for JP-8C than for JP-8P at 450°C . The extents of liquid depletion, gas formation and solid deposition were always higher with JP8-P than with JP-8C, indicating that JP-8C is more stable than JP-8P at 450°C both in short and long time stressing at 450°C in N_2 . There are also differences between JP-8C and JP-8P in the mechanisms of thermal degradation, in view of the time-dependences of liquid depletion and the formation of gaseous products and solid deposits. The higher thermal stability of the coal-derived JP-8C fuel can be attributed mainly to its higher contents of cycloalkanes and hydroaromatics.

The ^1H NMR spectra of thermally stressed JP-8C show some progressive change in hydrogen distribution as a function of stressing time at 450°C in N_2 . The original JP-8C has a spectrum with several major peaks in the chemical shift region of 0.5-1.05, 1.05-1.60, 1.60-2.00 ppm, respectively. The peak within 1.05-1.60 ppm diminishes in intensity, while that within 0.5-

1.05 ppm increased with increasing time at 450°C up to 4 h. These changes are accompanied by progressive increase in the contents of aromatics (6.0-9.0 ppm) and methyl hydrogens alpha to an aromatic ring (2.0-2.6 ppm). Extending the stressing time at 450°C from 4 to 8 h further decreased the intensity of peaks within 0.5-1.60 ppm, and increased that of aromatic (6.0-9.0 ppm) and alpha-methyl hydrogens (2.0-2.6 ppm). The increase in alpha-methylene hydrogens (2.6-3.4 ppm) was also observed after 4 to 8 h stressing. The NMR spectrum of petroleum-derived JP-8P is different from that of JP-8C. The former has two main peaks, a most predominant peak in the chemical shift range of 1.05-1.60 ppm and a relatively smaller peak within 0.5-1.05 ppm. These two peaks represent paraffinic methylene and methyl hydrogens, respectively. The intensity of methylene hydrogens (1.05-1.6 ppm) progressively decreased, while that of methyl hydrogens (0.5-1.0 ppm) gradually increased with the increase in stressing time at 450°C up to 4 h. As also observed in the case of JP-8C, there appears a monotonic increase in the contents of aromatic hydrogens and alpha-methyl hydrogens with increasing stressing time. These NMR results revealed some general features of the chemical decomposition processes of jet fuels.

The comparative GC-MS analysis of stressed JP-8C using expanded retention time windows provided valuable information on the thermal stability ranking of hydrocarbon components in JP-8C. In general, the stability of the cycloalkanes is higher than long-chain paraffins present in JP-8C. At 450°C, the stability of alkylcyclohexanes decrease with increase in chain length. Multi-substituted cyclohexanes are more stable than the n-alkyl substituted cyclohexanes with the same or larger carbon number. Among the cycloalkanes, the most stable components are methylcyclohexane, dimethylcyclohexane, and trans-decalin (major components in JP-8C) as well as cyclohexane (present in JP-8C in much lower concentration relative to the above components). It also appears that the stability of cycloalkanes decreases with increase in ring-size, namely cyclohexane > decalin > octahydrophenanthrene or octahydroanthracene. Among the two-ring cycloalkanes, trans-decalin is much more stable than cis-decalin. The intensity of n-C₁₂ through n-C₁₇, cis-decalin, C₁ - to C₂-decalins, C₀ - to C₂-tetralins decreased with increasing residence time at 450°C up to 4 h. Almost all the long-chain paraffins, n-C₁₂ through n-C₁₇ that are also present in the original JP-8C, disappear after 4 h. Tetralin and methyltetralins are the major hydroaromatic components in original and in stressed JP-8C at 450°C for 1 h, but they almost disappear after 4 h. This seems to be a result of their H-donation to some reactive radicals, which may have contributed to suppressing the undesirable reactions. As we have reported previously, JP-8C is much more stable than JP-8P at 450°C in nitrogen, both for short and long stressing time. GC-MS analysis of thermally stressed JP-8P at 450°C for 0.5-4 h revealed that the long-chain paraffinic components undergo significant decomposition reactions at high temperatures. While long-chain paraffins are still the major components of JP-8P after 1 h at 450°C, all the C₁₁ to C₁₇ components almost disappear after 4 h. This is accompanied by the progressive increase in the contents of lower alkanes and olefins (C₅-

C8) and those of alkylbenzenes, methylnaphthalenes and dimethylnaphthalenes as well as other polyaromatic compounds. The mechanistic considerations involving the initial fuel degradation and solid formation are also discussed in this report. .

FTIR and microscopic analyses of the actual fuel system deposits have shown that the constituent particles with two different morphologies, thin flakes and porous globules, have different chemical composition and different microstructures. Thin flakes appeared to have formed via gas phase reactions under stringent thermal stress, whereas the globules were formed in the liquid phase. In contrast to the thin flakes, the globular solids exhibited the formation of an isotropic pitch containing pools of carbonaceous mesophase. The differences in the microstructures and chemical constitutions of the liquid-phase and gas-phase solids suggest that the both gas phase and liquid phase reactions are important in studying the solid formation from jet fuels. The solids produced in microautoclave reactors from jet fuel samples and model compounds showed similarities in microstructure and chemical constitution to those of actual aircraft fuels system deposits. Solids produced from JP8-P appeared to have different microstructures than those obtained from JP8-C.

As part of the exploratory studies to enhance the thermal stability of fuels, experiments were conducted on mixtures of fuel samples (JP8 neat and Jet A-1) and 2,6-di-tert-butyl-4-methylphenol at 425°C in nitrogen and air. It was found that 0.005 g is the optimum amount of antioxidant required for 10.0 ml of JP8 neat fuel in an overpressure of nitrogen as well as air. The optimum concentration of antioxidant for Jet A-1 is in the range of 0.02 -0.03 g / 10.0 ml of fuel. FTIR analysis of the reaction products from Jet A-1 in the presence of the antioxidant showed degradation of the antioxidant as well as formation of CH₂ functionalities which are converted to aromatic compounds during stressing. This process appears to be closely related to solid formation.

The stressing of JP8 neat mixed with 2,4,6-trimethylphenol (TMP) and 2,4,6-tri-t-butylphenol (TTBP) showed that the mixtures of the fuel and TTBP were substantially less stable due to higher thermal reactivity of TTBP.

TECHNICAL PROGRESS

Task 1. Identification and Characterization of Stable Hydrocarbon Species Present in Coal-Derived Fuels.

The objective of Task 1 is to identify hydrocarbon species present in coal-derived jet fuels that are different from species in petroleum-derived jet fuels, and to examine the thermal stability of these species by thermal stressing of model compounds in microautoclaves.

Activity 1. Identification of Hydrocarbon Species

The coal-derived fuel samples examined are JP-8C from hydrotreating of liquids produced from the Great Plains Gasification plant, and middle distillate (MD) produced from Wilsonville two-stage coal liquefaction plant. In the previous report [1], JP-8C was analyzed by GC-MS using splitless injection of diluted sample (1/500 volume concentration in pentane), where 4 min delay to ionization was applied to cut off the solvent. In this way, the compounds whose retention time in GC at 40°C is shorter than 4 min could not be analyzed. In order to detect the lighter molecules that might be present in the fuels, a modified GC-MS method was used in the work reported here, which is characterized by the split injection of undiluted sample without delay to ionization. The Hewlett-Packard HP-17 column previously used in the Kratos MS80 GC-MS system was replaced with a new fused silica capillary column DB-17 purchased from J&W Scientific Co. (Coating phase: 50% phenyl-50% methyl polysiloxane; coating film thickness: 0.25 μm ; column dimension: 30 m x 0.258 mm i.d.).

Figure 1 shows the total ion chromatograms (TIC) and specific ion chromatograms (SIC) obtained from GC-MS analysis of JP8-C. The GC-MS using the modified method revealed that there are considerable amounts of low molecular weight components (retention time: < 4 min) in JP-8C which were not detected by previous GC-MS method [1]. The most predominant peak (retention time: 2.91 min; scan No.: 174) in the TIC of JP-8C was found to be methylcyclohexane (molecular ion mass: 98, base peak: 83). In the GC-MS spectra, the fragment ion of m/z 71 is characteristic of long chain paraffins, ions of m/z 81-83 are indicative of cycloalkanes, the ion of m/z 91 is a well-known troplium ion indicating the presence of *n*-alkylbenzenes, and ions of m/z 141-142 are characteristic of alkynaphthalenes. The main peaks in SIC at m/z 81-83 correspond to the major peaks in TIC of JP8-C, indicating that JP8-C is rich in cycloalkanes. The other peaks in TIC of JP-8C correspond to those in the SIC of m/z 71, 91-92 and 141-142. JP8-C consists

DS90 Chromatogram report Run: SONG660001, 17-Dec-90 20:15
SONG JP-8C SPLIT 0.1 UL DB-17 40-5 TO 280-10 AT 4 KRA MS80

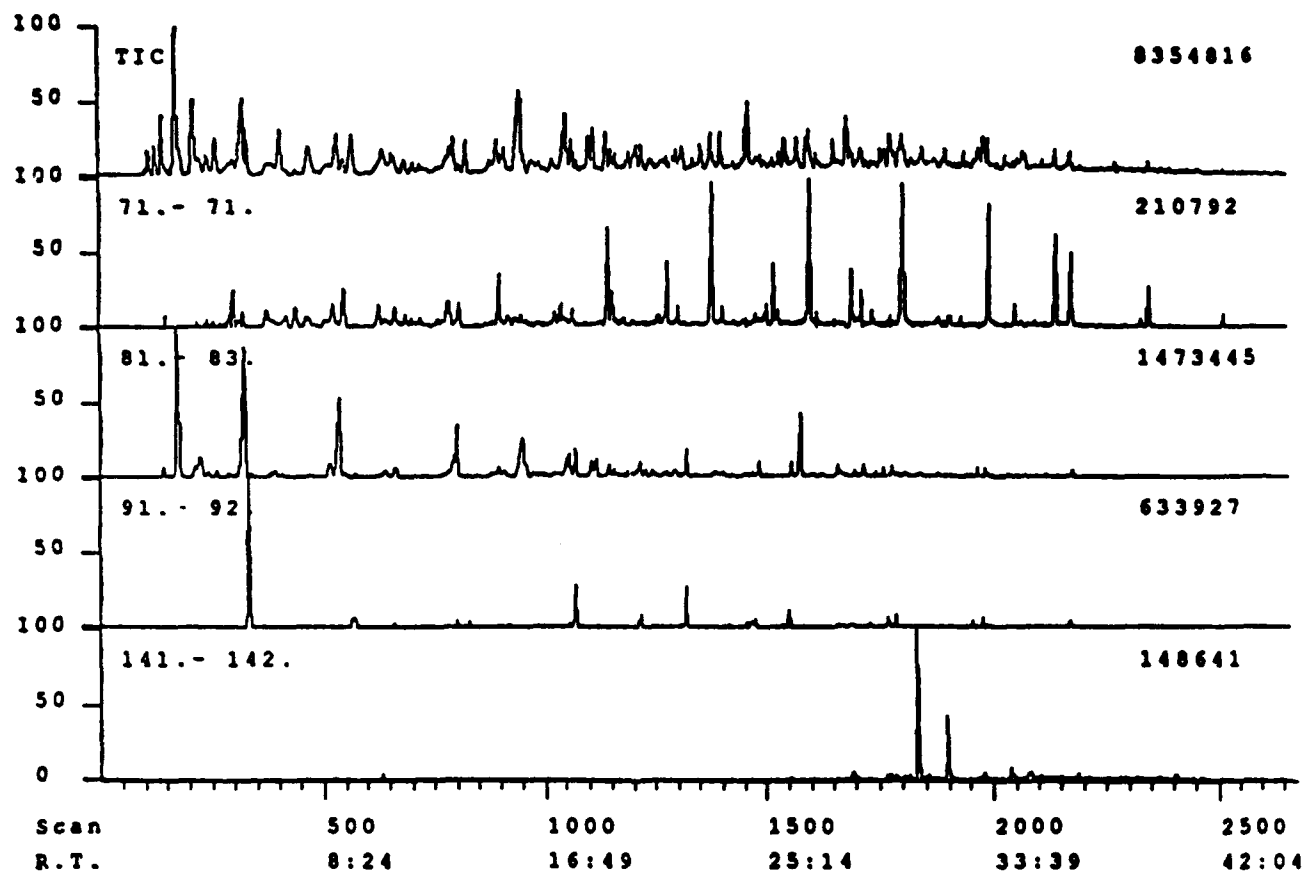


Figure 1. Total and specific ion chromatograms of coal-derived jet fuel JP8-C from GC-MS using split injection of undiluted sample.

mainly of monocyclic, bicyclic and tricyclic alkanes and two-ring hydroaromatic compounds as well as some alkylbenzenes. Alkyl-substituted cyclohexanes, decalins, and tetralins are the major components [1-2]. In contrast, petroleum-derived jet fuels are mainly composed of long-chain paraffins together with low concentrations of alkylbenzenes and alkylnaphthalenes (see Task 3).

Figure 2 shows the total ion chromatograms (TIC) and specific ion chromatograms (SIC) obtained from GC-MS analysis of Wilsonville middle distillate. Several features are apparent by comparing Figure 2 with Figure 1. First, Wilsonville MD appeared to be heavier than JP-8C, and there are few lighter molecules whose retention time in GC is shorter than 20 min. Second, there are only three peaks in the SIC at m/z 71 corresponding to three small peaks in the TIC, indicating that Wilsonville MD contains very limited amounts of the long-chain paraffins. Third, Wilsonville MD contains more aromatic compounds whose ring sizes are equal to or larger than two-ring. This is reflected by the fact that many peaks in the TIC correspond to those in the SIC at m/z 153-154 (acenaphthenes and biphenyls), m/z 165-166 (fluorenes) and m/z 177-178 (phenanthrenes or anthracenes). The most predominant peak at retention time of 59.45 min (scan: 3533, Figure 2) was identified as pyrene (molecular ion: 202). The above analytical results seem to suggest that Wilsonville MD has too high an aromatic content to become jet fuel. According to the data received from Wilsonville Advanced Coal Liquefaction Facility operated by South Clean Fuels (a Division of Southern Electric International), this sample was derived from two-stage liquefaction of the Pittsburgh N.8 seam bituminous coal from Ireland Mine coal in Run 259E (during April 16-20 in 1990) using Shell 324 Ni-Mo/ Al_2O_3 catalyst both in the first stage (reaction temperature, 825°F or 441°C; inlet H_2 partial pressure, 2650 psi H_2) and second stage (790°F or 421°C, 2490 psi H_2). Detailed data for Run 259 can be found elsewhere [2]. The coal conversion in the Run 259E was 95.7wt%, the total yield of C_4^+ distillates was 73.9 wt%, and the yield of middle distillate (b.p. 204-343°C) was 12.9 wt% (maf coal basis). Based on these data, it is clear that the Wilsonville MD was directly produced from coal, which has not been further refined to meet with the requirement of aviation jet fuel. On the other hand, the JP-8C sample is a clean distillate fraction which was derived from extensive hydrotreating of liquid by-product streams (tars) produced by the gasification of low-rank coal (lignite) at the Great Plains Gasification plant located in Beulah, North Dakota. Details of the hydrotreating are not available for the JP-8C sample received from WPAFB (dated 5-30-89). It is likely that the JP-8C was produced by two stage hydrotreating of the gasification tars from lignite [3]. As described later, the JP-8C exhibited higher thermal stability than the petroleum-derived JP-8P. One anticipates that further refining of Wilsonville MD could also produce high quality jet fuel.

DS90 Chromatogram report Run: SONG660007, 19-Dec-90 15:53
 WILSONVILLE 204-343oC MD 40-5 to 280-10 at 4 SPLIT 0.04 UL

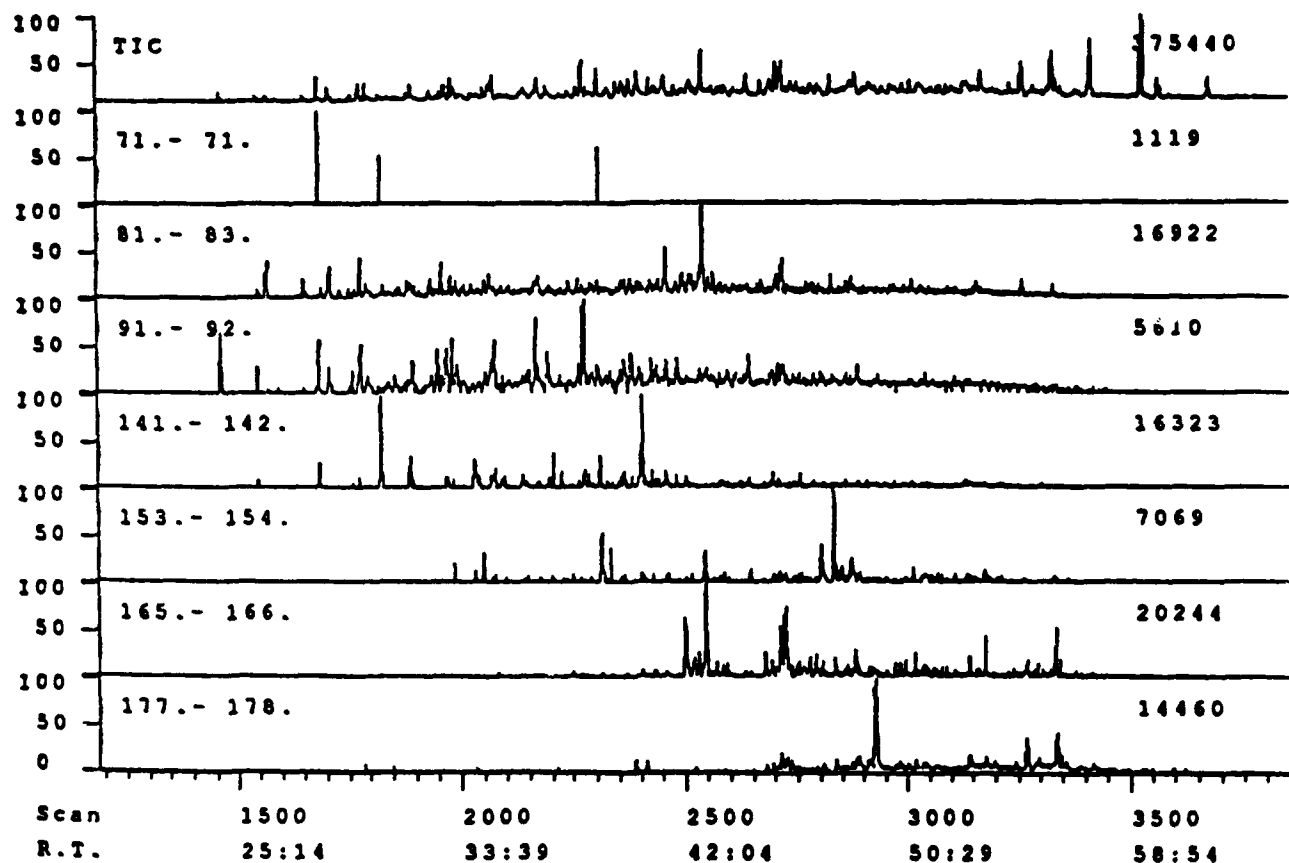


Figure 2. Total and specific ion chromatograms of Wilsonville middle distillate derived from two-stage coal liquefaction.

The major hydrocarbon species in JP-8C were identified by analyzing the mass spectra from GC-MS. The column used in GC-MS was a new fused silica capillary column DB-17 (Coating phase: 50% phenyl-50% methyl polysiloxane; coating film thickness: 0.25 μm ; column dimension: 30 m x 0.258 mm i.d.). Figure 1 shows the expanded retention time windows of GC-MS profile for GC-MS of JP-8C using split injection of undiluted sample, together with the structures of the compounds identified. These results serve as baseline for the comparative examination of the thermal stability of various hydrocarbon components in JP-8C, as described in Task 2.

Note that many peaks in TIC of JP-8C shown in Figures 3a and 3b are mixtures of two or more compounds due to co-elution. In terms of number of components and complexity of their mass spectra, the identification of JP-8C components is much more difficult than that of JP-8P. This is also because JP-8C is rich in cycloalkanes. Although the molecular ions of cycloalkanes are more abundant than those of their acyclic counterparts, their spectra are often more difficult to interpret [4]. The structures shown in Figures 3 and 4 only represent the tentative identification of major components. Detailed hydrocarbon distribution of JP-8C is characterized by GC-MS analysis of its chromatographic fractions, as described in Task 2.

Activity 2. Stressing of Model Compounds

Cycloalkanes and Tetralin

We have conducted the thermal stressing of a suite of model compounds including cycloalkanes, normal alkanes, alkylbenzenes and tetralin. From the compositional differences between different fuels described in Task 1 and Task 3, it is apparent that testing of alkylcyclohexanes, decalin and tetralin is more pertinent to coal-derived jet fuel, while the testing of alkylbenzenes is relevant to both coal- and petroleum-derived fuels.

The comparative examination of thermal stability of several model compounds was conducted under the same conditions (20 ml microreactor; 5 ml sample; 450°C; 4 h; 100 psi UHP grade N₂). The experimental details have been described previously [1]. Decalin (consisting of trans- and cis-decalin), ethylcyclohexane, n-butylcyclohexane, and tetralin were selected as the model fuel components for coal-derived jet fuels. Figure 5 shows the time-pressure profile for the thermal stressing of these compounds. Since the static reactor was used, the sample is always confined with the reactor. Therefore, the pressure increase after equilibrium boiling is indicative of the thermal decomposition of the compounds tested. As shown in Figure 5, when the reactor was

DS90 Chromatogram report Run: SONG660001, 17-Dec-90 20:15
 SONG JP-8C SPLIT 0.1 UL DB-17 40-5 TO 280-10 AT 4 KRA MS80

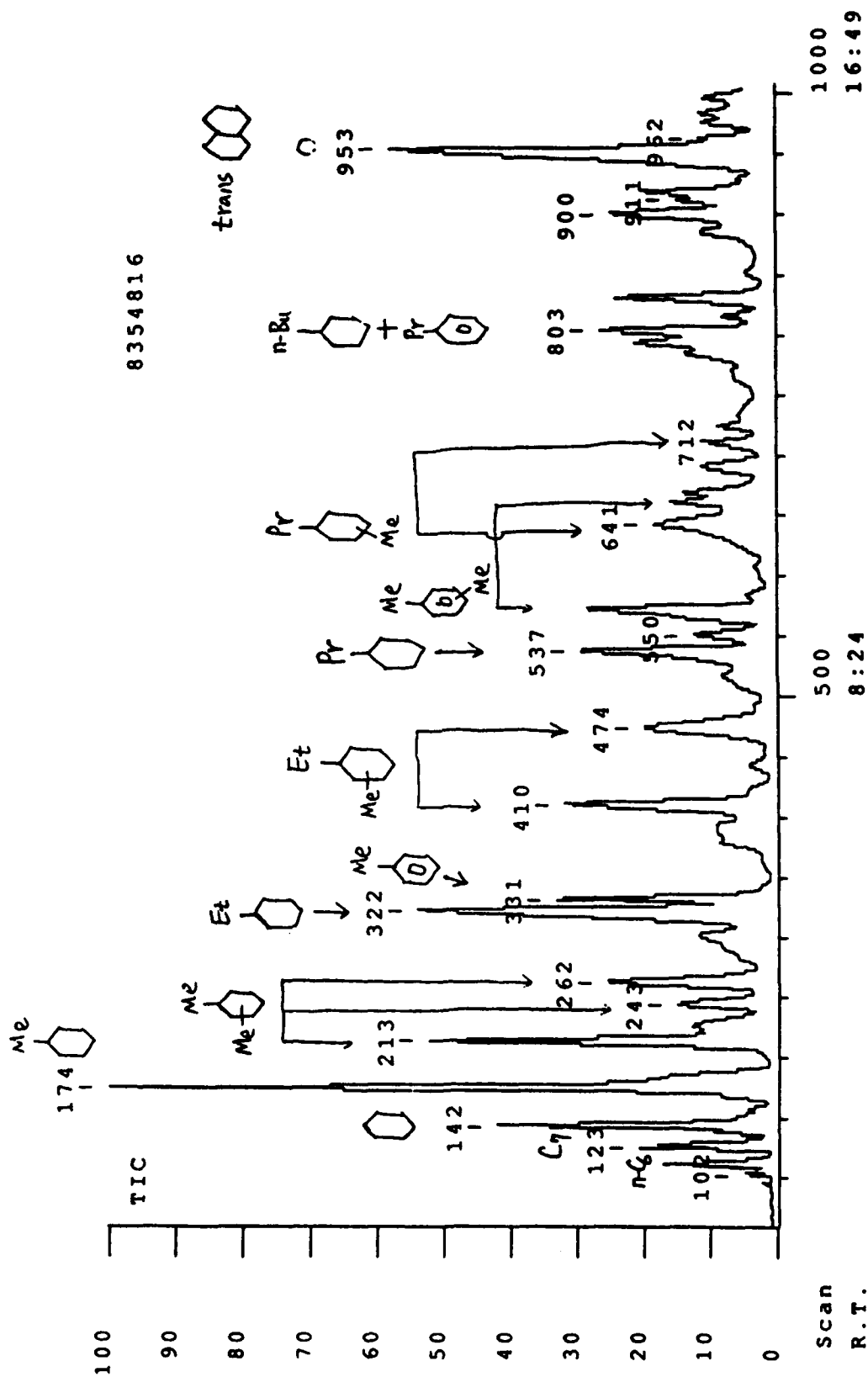


Figure 3a Retention time window I (1-16:53 min) of GC-MS profile for JP-8C using split injection of undiluted sample.

DS90 Chromatogram report Run: SONG660001, 17-Dec-90 20:15
 SONG JP-8C SPLIT 0.1 UL DB-17 40-5 TO 280-10 AT 4 KRA MS80

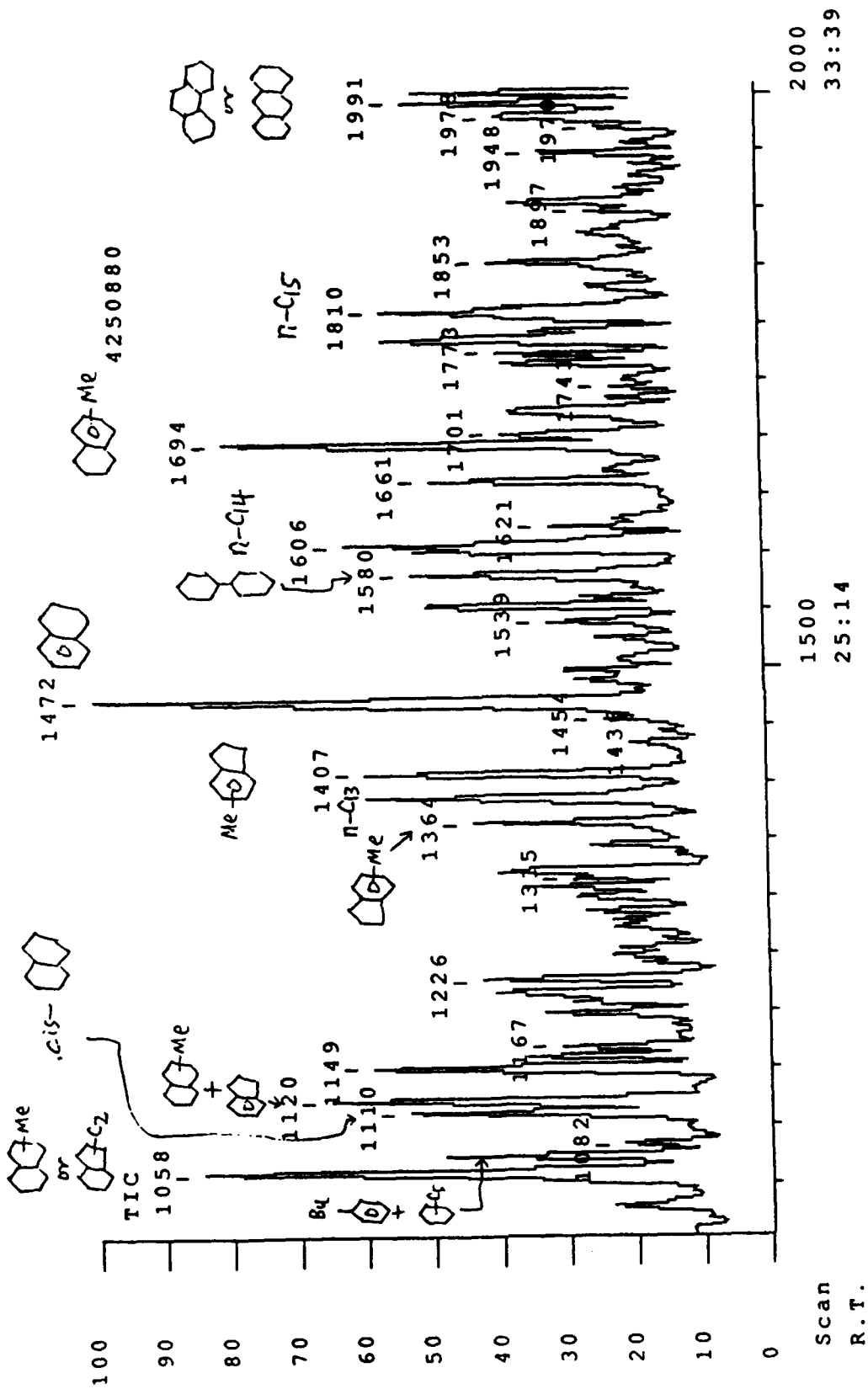


Figure 3b Retention time window II (16:54-33:43 min) of GC-MS profile for JP-8C.

DS90 Chromatogram report Run: SONG660001, 17-Dec-90 20:15
SONG JP-8C SPLIT 0.1 UL DB-17 40-5 TO 280-10 AT 4 KRA MS80

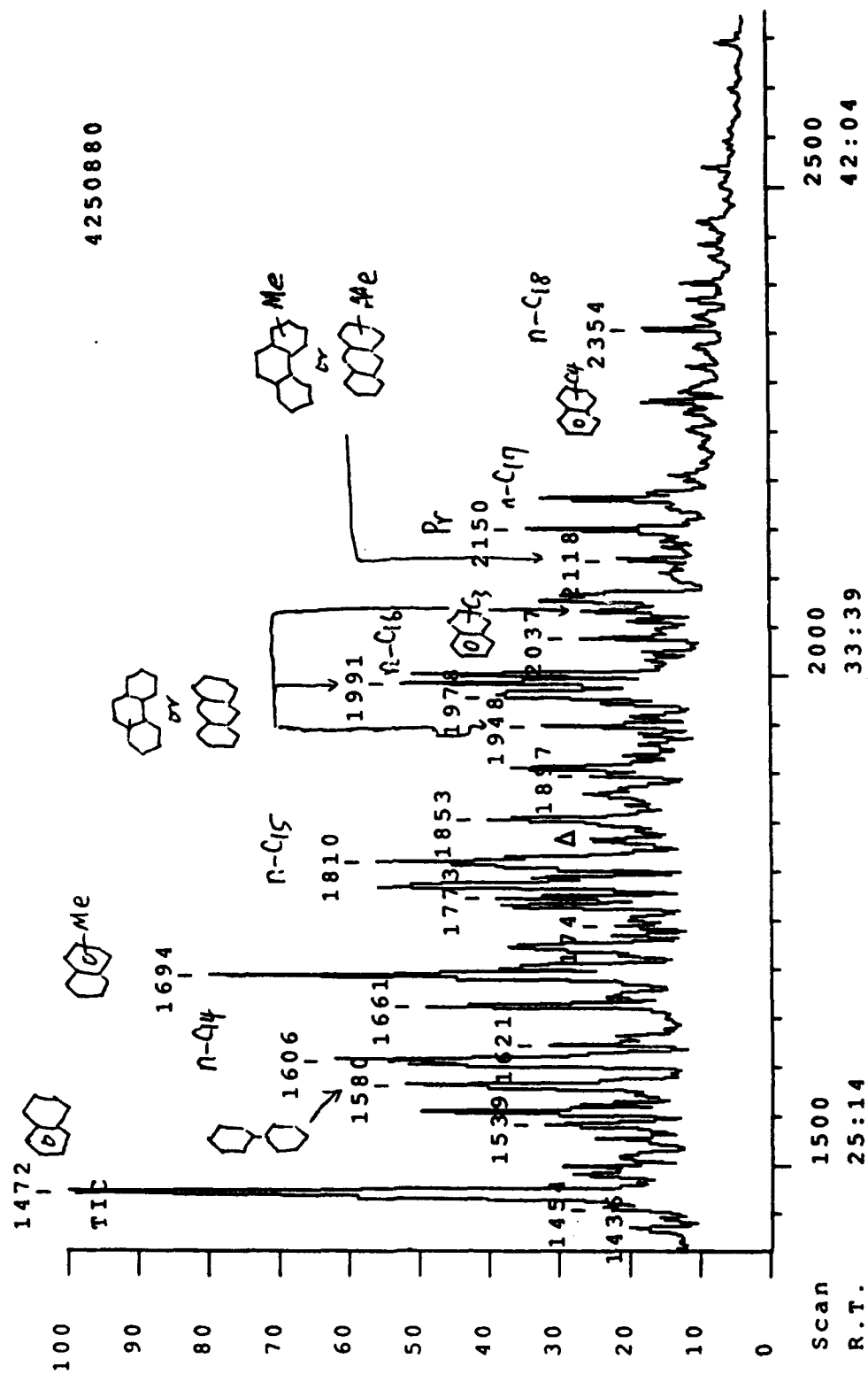


Figure 4 Retention time window III (24-45 min) of GC-MS profile for JP-8C.

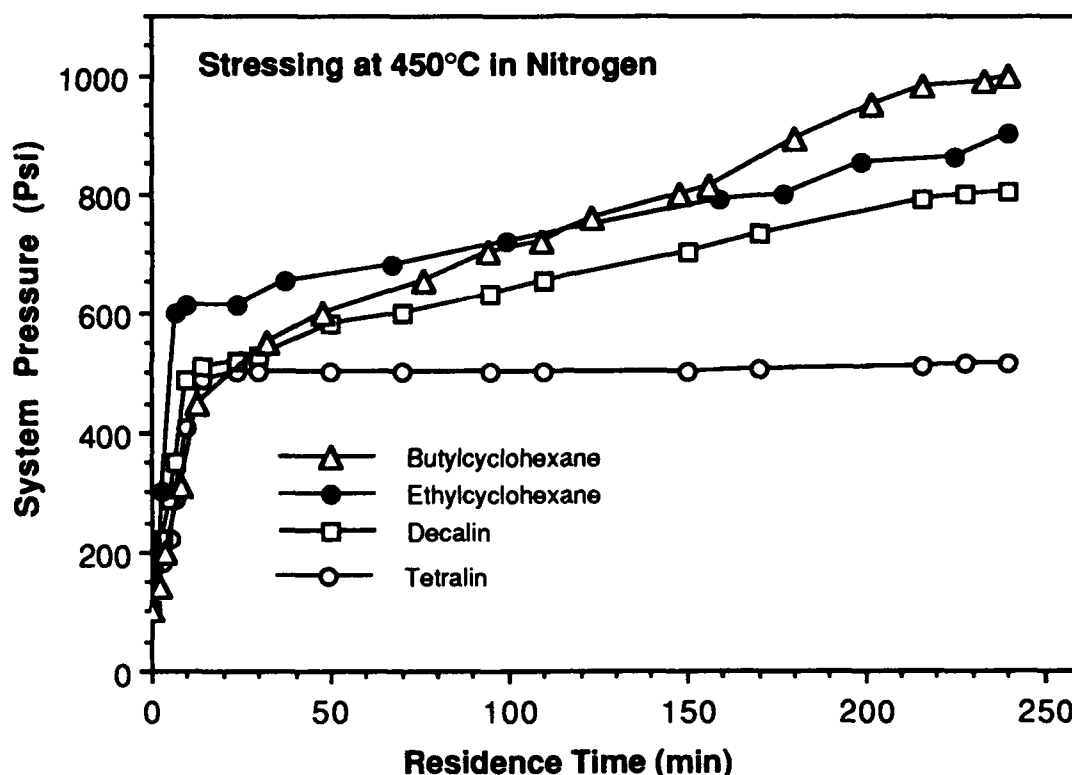


Figure 5. Time-pressure profiles for thermal stressing of model fuel components for coal-derived jet fuels

immersed into the fluidized sand-bath, the hydrocarbon liquids reach a equilibrium boiling state in about 10 min. When tetralin was heated under 100 psi nitrogen gas, the system pressure increased to about 500 psi in about 10 min, then the pressure maintained nearly constant. This reflects that there was no remarkable decomposition or dehydrogenation (to form gas products) during the four h period. The pressure increase for other three compounds indicates that the extent of decomposition and/or dehydrogenation increased with increasing residence time at 450°C. From Figure 3 and the results described in Task 3, it is likely that the thermal stability of the single compounds tested decreases in the order of tetralin > decalin > ethylcyclohexane > n-butylcyclohexane > decane > n-tetradecane.

The gaseous products from some typical model stressing experiments were analyzed by using the newly purchased Perkin Elmer AutoSystem gas chromatograph with flame ionization detector. This GC is connected to a Perkin Elmer Turbochrome II data processing system. A new

packed column SP-1700 (23% SP-1700 on 80/100 Chromosorb, 30 feet x 1/8 inch) from Supelco Co. was tested in the GC under different temperatures and flow rates of helium. From a number of preliminary tests, we found that the 30 feet SP-1700 column offered good separation of gas components but the retention time was too long at the oven temperature of 70°C. In addition, the recommended detector temperature of 110°C was too low, which caused the FID detection trouble in operating the AutoSystem GC because of the condensation of water vapor around the top cell of FID. Based on these tests, we separated the 30 feet column into two parts and increased the detector temperature. Satisfactory GC results were obtained by using the 15 feet SP-1700 column under the following conditions: carrier gas, He (about 25 ml/min); oven temperature, 60°C; injection port temperature, 100°C; detector temperature, 200°C.

For the purpose of identification of peaks in the gas chromatogram, the retention times of methane, ethane, propane, butane, pentane, ethylene, propylene, 1-butene and pentene were determined by using various gas standards purchased from Scott Specialty Gases Co. The other components in gases were tentatively identified according to the chromatogram report from Supelco Co. for the SP-1700 column. Table 1 shows the results of identification of the gas components, together with their area percent determined by the GC. The detected and identified gases ranged from methane to pentene (paraffinic and olefinic hydrocarbons). While ethane and ethylene do not separate on the SP-1700 column, it appears that the main products from thermal decomposition of the three model compounds are methane, ethane+ethylene, propane, propylene, butane and butene. The distribution patterns of the components in the gases from these three compounds are different from each other. In the case of n-butylcyclohexane, the concentration of the products appeared to be propane > ethane+ethylene > methane ≥ n-butane > propylene > 1-butene (Table 1). This order seems to suggest that beta-scission of the n-alkyl side-chain of cyclohexane is easier than the cleavage of other bonds, being similar to the case of n-alkylbenzene. On the other hand, the concentration of ethane+ethylene is higher than that of propane or methane in the gas from tetradecane, suggesting that beta-scission to form C₂ species was predominant in the initial stage of n-tetradecane cracking. In this case, the concentration (area%) of methane and propane was similar to each other. The formation C₁-C₄ hydrocarbon gases from decalin (Table 1) indicated that the ring opening and the subsequent cracking did occur, but the relative pressure increase (Figure 5) showed that this was not as remarkable as in the case of butylcyclohexane. The extent of pressure increase also suggested that the extent of gas formation was much smaller with cycloalkanes than with decane and tetradecane (Figure 5 and Task 3).

We also analyzed the liquids from n-butylcyclohexane, ethylcyclohexane and decalin by using GC-MS. It appears from product distribution that dealkylation and dehydrogenation are the major reactions occurring during the stressing of alkylcyclohexane. Cyclohexane and

Table 1. Gas products from thermal stressing of model compounds at 450°C for 4 h in N₂

Retention min ^{a)}	Compounds	Area %		
		Butylcyclohexane	Decalin	Tetradecane
1.4-1.6	Methane	12.71	23.03	25.09
1.7-1.9	Ethane + Ethylene	27.28	25.57	32.89
2.3-2.5	Propane	39.48	35.47	25.14
2.6-2.8	Propylene	4.08	4.54	3.82
3.1-3.5	iso-Butane	0.49	0.74	0.87
3.9-4.2	n-Butane	11.25	6.56	7.63
4.6-4.8	1-Butene	2.36	0.91	1.12
5.3-5.5	trans-2-Butene	0.85	0.38	0.40
5.9-6.1	cis-2-Butene	0.57	0.25	0.26
6.5-6.6	iso-Pentane	0.21	0.35	0.35
6.7-6.9	1,3-Butadiene ?	0.01	-	-
7.7-7.9	n-Pentane	0.43	1.61	1.80
8.9-9.1	1-Pentene	0.05	0.15	0.21

a) Analyzed by using Supelco SP-1700 column.

methylcyclohexane were formed as major products, and ethyl- and propylcyclohexane as minor products from dealkylation of n-butylcyclohexane at 450°C for 4 h. While toluene, ethylbenzene and benzene are the major dehydrogenation products, the partial dehydrogenation products such as methylcyclohexene and C₂-cyclohexene are also present in the liquids from stressed butylcyclohexane. Ethylcyclohexane is much more stable than butylcyclohexane, and it is still the most predominant peak after 4 h stressing. However, the stressed liquid also contains the dealkylation products such as cyclohexane and methylcyclohexane, and dehydrogenation products such as cyclohexene, methylcyclohexene, ethylcyclohexene and ethylbenzene. Detailed GC-MS results and the degradation mechanisms will be discussed in the next quarterly report.

n- and t-Butylbenzene

Characteristics of Solid Formation

n-Butylbenzene and t-butylbenzene were heat treated at different temperatures and times. These two isomers behave quite differently under similar experimental conditions. For t-butylbenzene, solid did not form even after 4 h at 450°C, while its isomer n-butylbenzene forms solid deposit after 1 h at the same temperature. It appears that the solid from t-butylbenzene deposits on the reactor wall as well as top and bottom of reactor homogeneously, while n-butylbenzene seems to form more solid on bottom.

Figure 6 shows the relationship between amount of solids produced from t-butylbenzene and residence time at three different temperatures. The amount of solid increases linearly with reaction time at relatively low treatment severity period, i.e., before 16 h at 450°C, before 12 h at 475°C and before 4 h at 500°C. This suggests a change in dominant reaction mechanism and/or differences in the solubility of solids in the accompanying liquids at high treatment severity.

Apparent Kinetic Analysis on Solid Formation

It is assumed that in linear portion of Figure 6, formation of solid obeys first-order reaction kinetics. Kinetic parameters can be obtained. The rate expression used can be written as:

$$dm / dt = k (1 - m / m_{\max})$$

where m is the mass of solids produced, m_{\max} is the maximum mass of solids that can be produced from t-butylbenzene, and t is the reaction time. For an apparent first-order behavior, the plot of $\ln(1-m/m_{\max})$ versus time at a given temperature should give a straight line with a slope equal to the reaction rate constant at that temperature. For practical purposes, the maximum amount of solids produced from t-butylbenzene was determined experimentally as the amount of solids produced at 500°C for 72 h. Because of deviations from apparent first-order kinetics for long reaction times, the data obtained for relatively short reaction times were used in kinetic analysis. Therefore, the calculated apparent kinetic parameters represent the initial degradation reactions. Figure 7 shows the apparent first-order plots for the formation of solids from t-butylbenzene, indicating good linear fits of the kinetic data. The Arrhenius plot in Figure 8 shows a perfect linear fit and yields an apparent activation energy of 47.1 kcal/mol and a preexponential factor of $3.22 \times 10^{12} \text{ h}^{-1}$ for the formation of solids from t-butylbenzene.

Head Space Gas Composition Analysis

Head space gas of t-butylbenzene stressed at 450°C for 30 min and 60 min has been analyzed using GC. As shown in Table 2, both 30 min and 60 min reaction produced gas

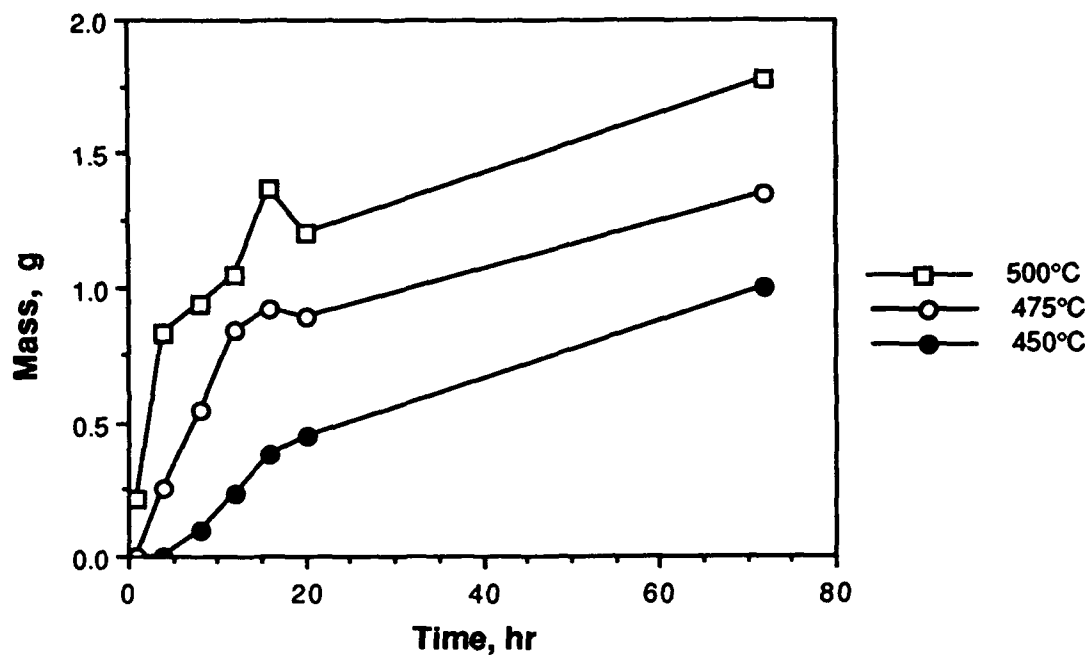


Figure 6. Formation of solids from t-butylbenzene as a function of time at 450, 475, and 500°C.

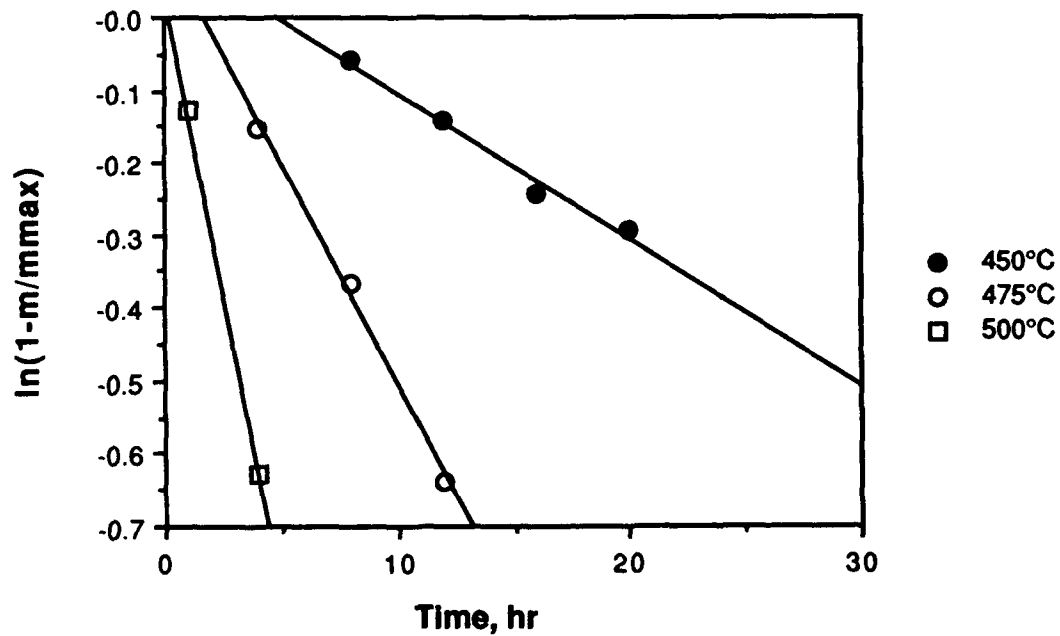


Figure 7. Apparent first-order plots for the formation of solids from t-butylbenzene.

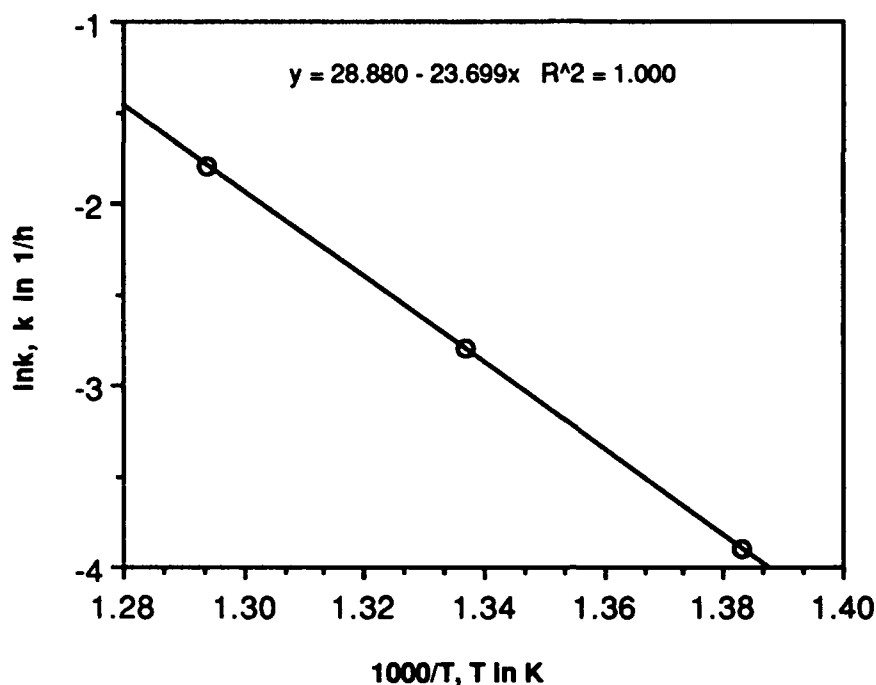


Figure 8. Apparent Arrhenius plot for the formation of solids from t-butylbenzene.

containing more than 64% methane. This is probably because the cleavage of methyl group from t-butylbenzene is the first step in chain reaction of t-butylbenzene. There is relatively high concentration of iso-butane (about 10%) which may be formed by direct cleavage of the aryl-alkyl bond in the substrate molecule.

In order to clarify if there is catalytic wall effect, we also conducted the stressing of t-butylbenzene in both regular tubing bomb (type A) and in the bomb with a quartz tube insert (type B). Capillary GC analysis indicated that the liquids from 15 min stressing of t-butylbenzene in both type-A reactor and type-B reactor are almost identical in view of the composition of the liquids. The differences between the two runs in the yields of isopropylbenzene, t-butylbenzene and isobutylbenzene are almost within experimental error. We also analyzed the gas products from t-butylbenzene after 30 and 60 min stressing by using GC with a packed column (Table 2). As we can see from Table 2 and the GC results of liquids shown in Figures 9-11, the liquids and gases from 30 min and 60 min stressing of t-butylbenzene in both type-A and type-B reactors are very similar to each other.

Table 2. Gas products from thermal stressing of t-butylbenzene at 450°C with and without quartz insert

	30min		60min	
	with quartz	without quartz	with quartz	without quartz
methane	65.22	64.23	67.60	69.20
C2	3.53	3.99	3.48	3.28
propane	4.51	2.89	1.98	2.27
propylene	9.08	11.13	10.56	9.97
isobutane	10.80	11.16	10.43	9.85
n-butane	0.59	0.33	0.21	0.22
neopentane	3.43	4.50	4.11	3.53
isopentane	0.00	0.00	0.09	0.07
n-pentane	0.11	0.04	----	---
C7	0.01	0.00	0.00	0.02
others	2.72	1.73	1.54	1.59

* Concentration of gas components is the area% of the peaks in GC by using a Chemipack C-18 packed column.

In the type-B stressing, t-butylbenzene was initially confined within the quartz tube without contact with stainless wall, and hence the effect of stainless wall in the initial period, if any, would be smaller than in the absence of the quartz tube. Nevertheless, the reaction products from 15-60 min stressing in both reactors are very similar. These facts seem to suggest that at 450°C (the stressing temperature), the thermally initiated homogeneous reactions of t-butylbenzene are the main reactions. However, these results are not conclusive.

Liquid Characterization by Capillary GC and GC-MS

Although n-butylbenzene exhibits higher reactivity than t-butylbenzene, the color of liquid products from both compounds changes with increasing severity from light yellow Æ light brown Æ dark brown Æ light brown. This sequence of color changes may be explained by processes leading to the formation of high molecular weight species (darkening color) and the depositions of solids pumping high molecular weight species into solid products and leaving behind low molecular weight species in liquids (light color).

Liquid products of thermally stressed n-butylbenzene and t-butylbenzene have been analyzed capillary GC. Figures 12-13 and 14-15 show the chromatograms of stressed

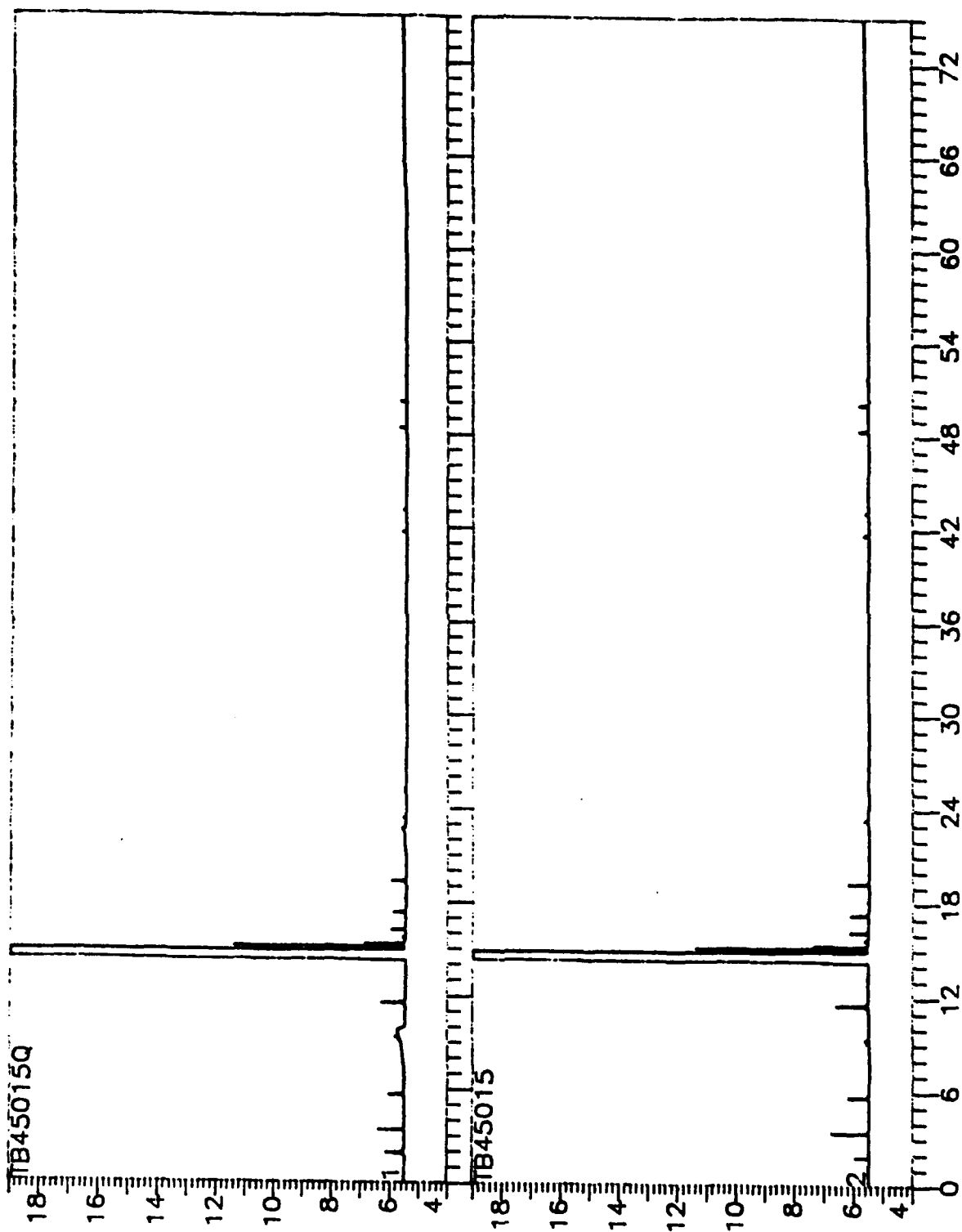


Figure 9. Capillary gas chromatograms of liquids from t-butylbenzene stressed at 450°C for 15 min with (top) and without quartz insert (bottom).

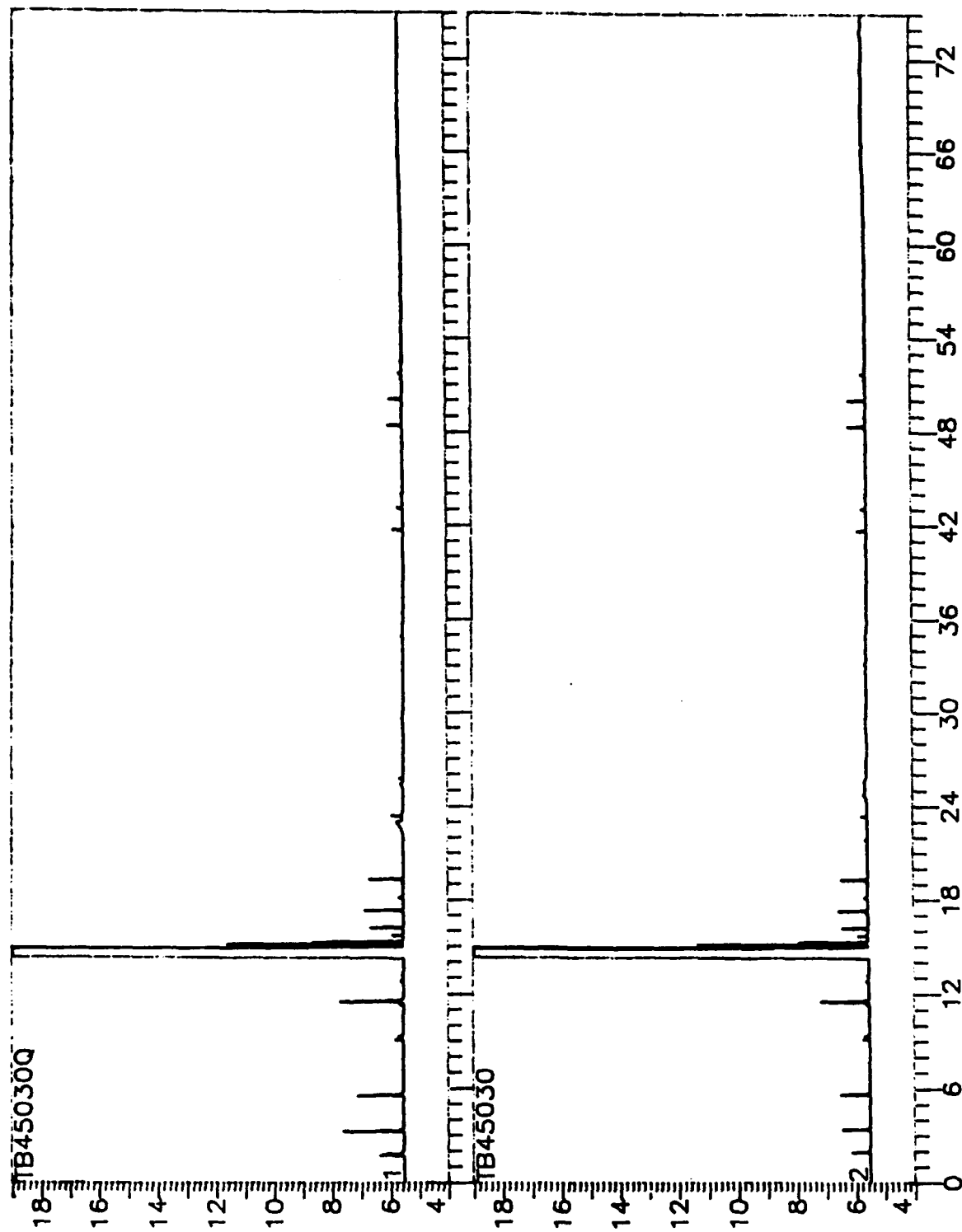


Figure 10. Capillary gas chromatograms of liquids from t-butylbenzene stressed at 450°C for 30 min with (top) and without quartz insert (bottom).

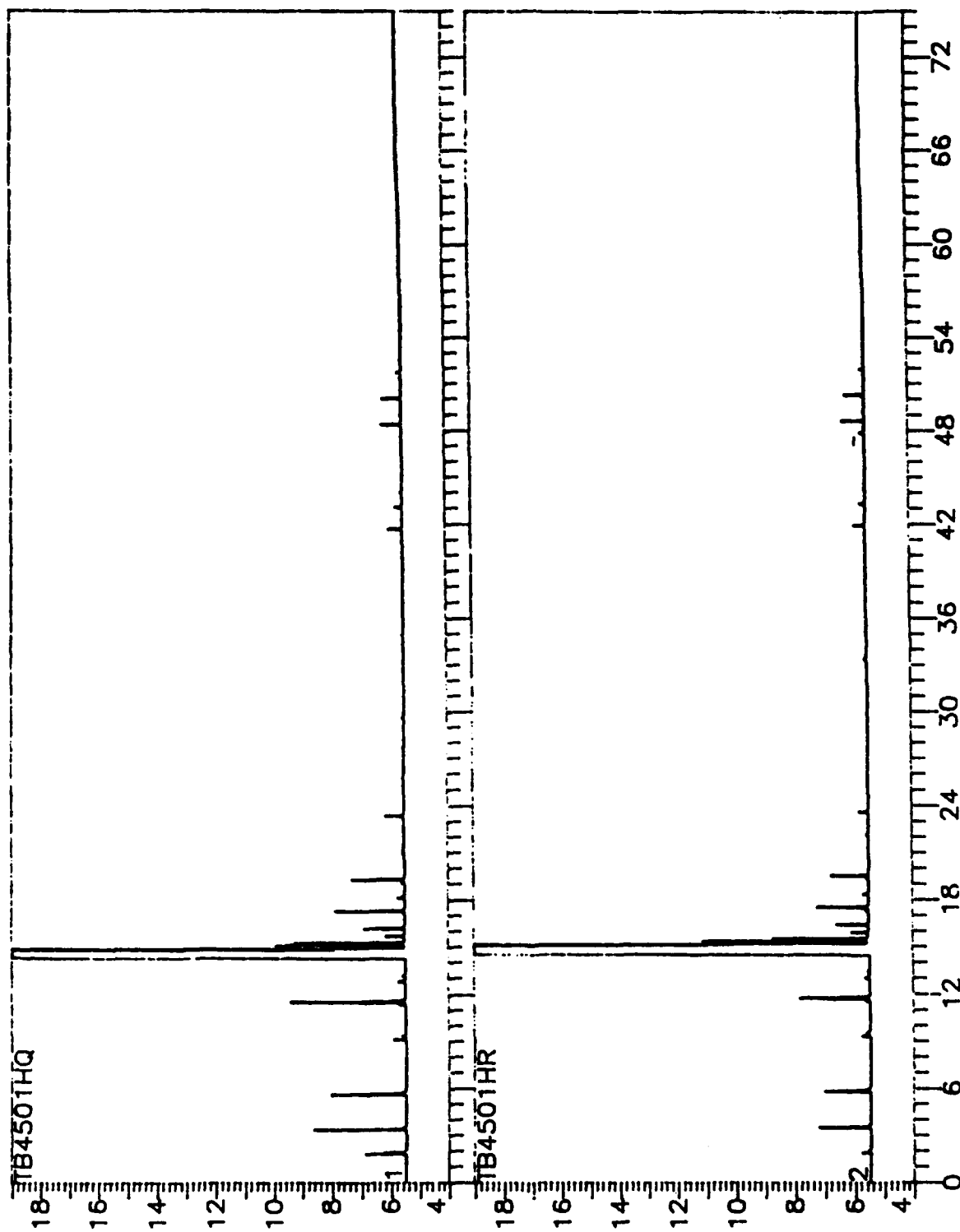


Figure 11. Capillary gas chromatograms of liquids from t-butylbenzene stressed at 450°C for 1 h min with (top) and without quartz insert (bottom).

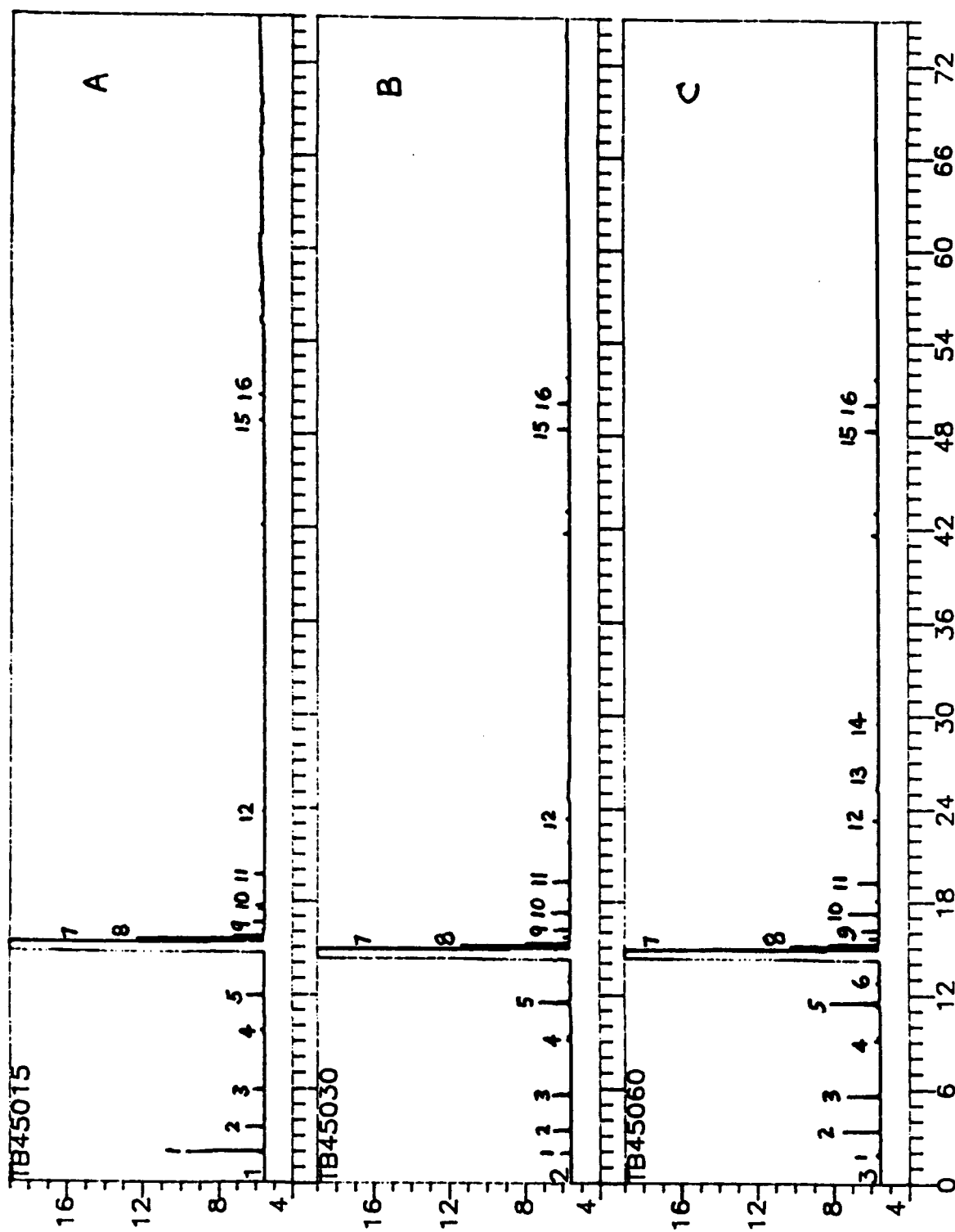


Figure 12. Capillary gas chromatograms of liquids from t-butylbenzene stressed at 450°C for 15 (A), 30 (B) and 60 minutes (C).

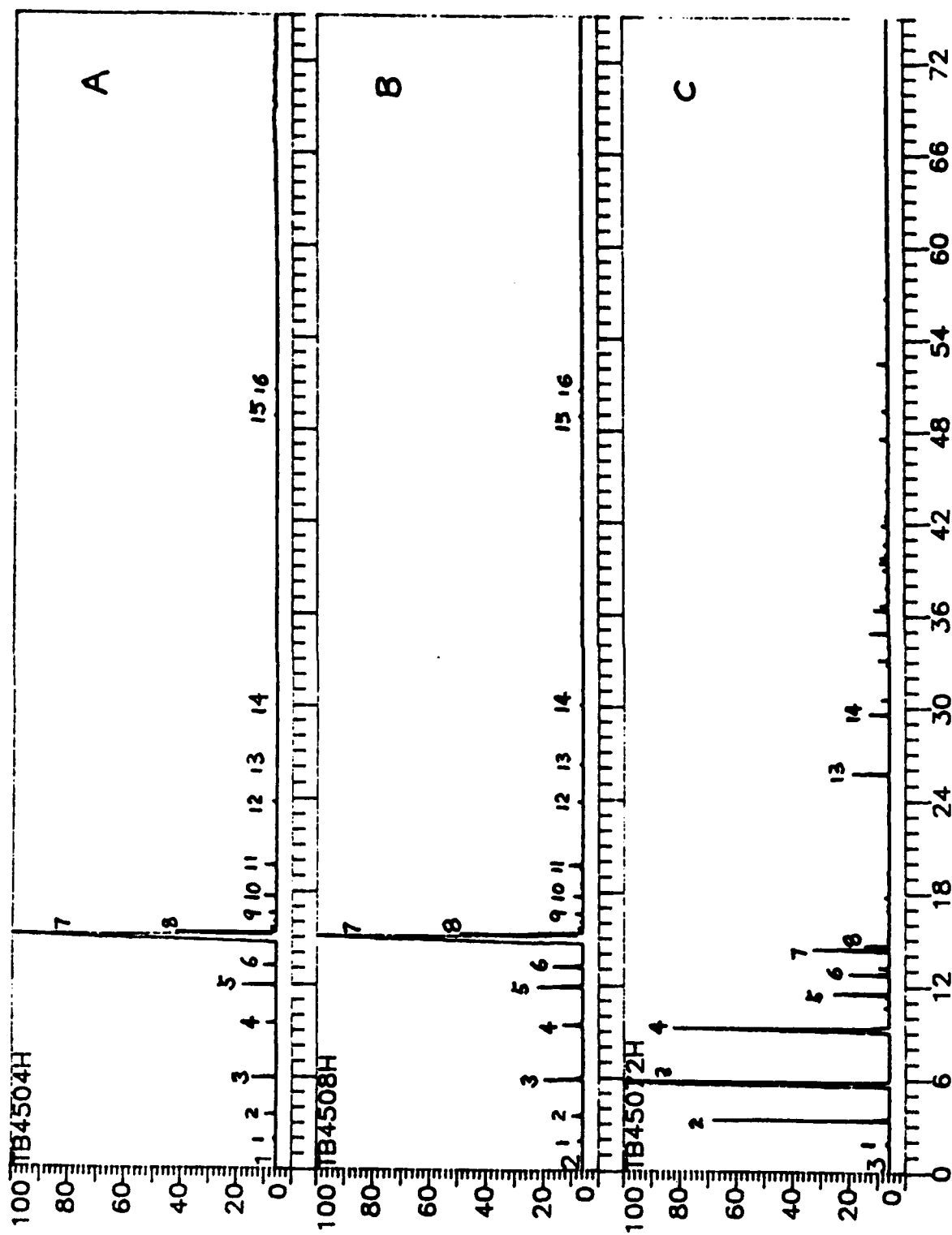


Figure 13. Capillary gas chromatograms of liquids from t-butylbenzene stressed at 450°C for 4 (A), 8 (B) and 72 h (C).

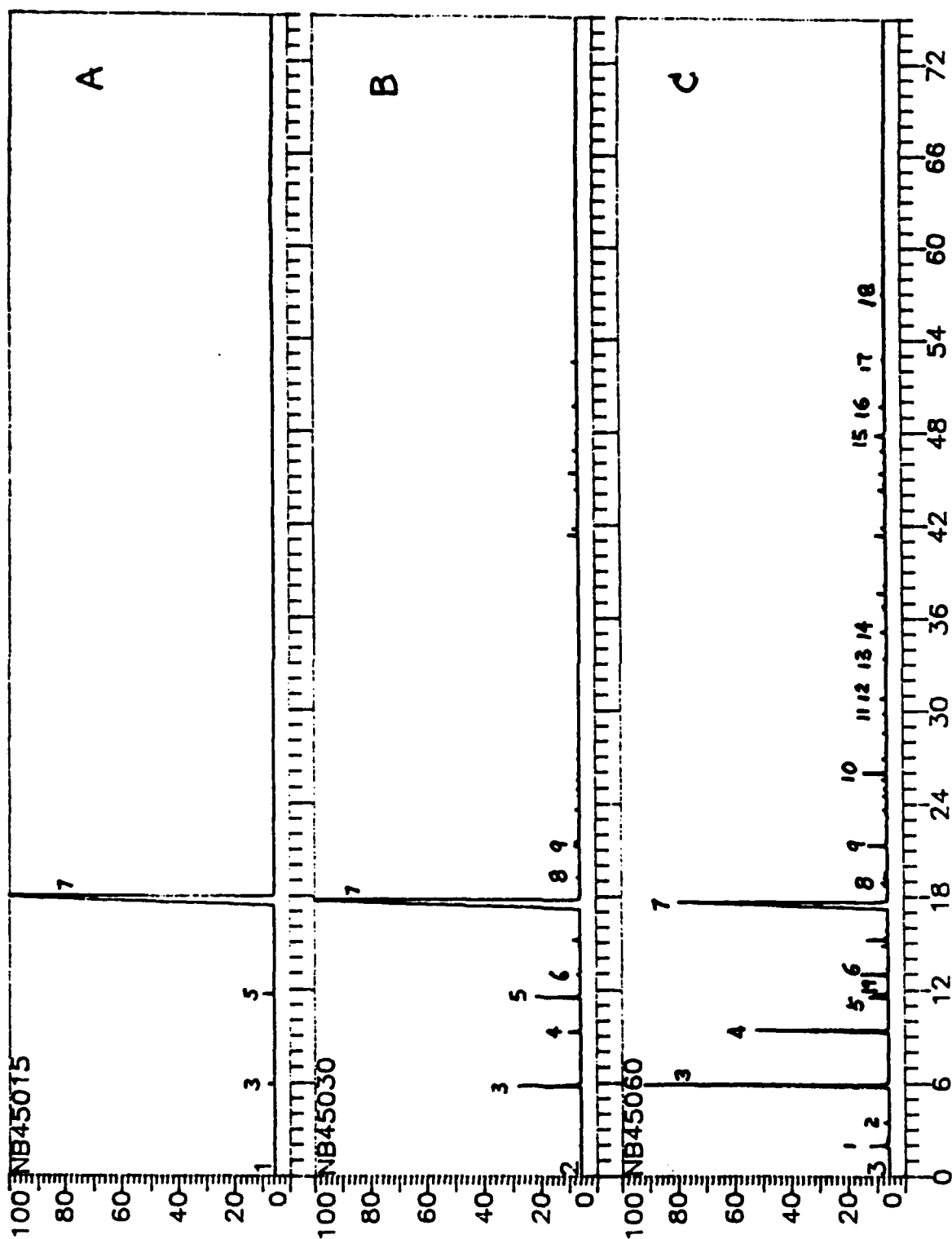


Figure 14. Capillary gas chromatograms of liquids from n-butylbenzene stressed at 450°C for 15 (A), 30 (B) and 60 min (C).

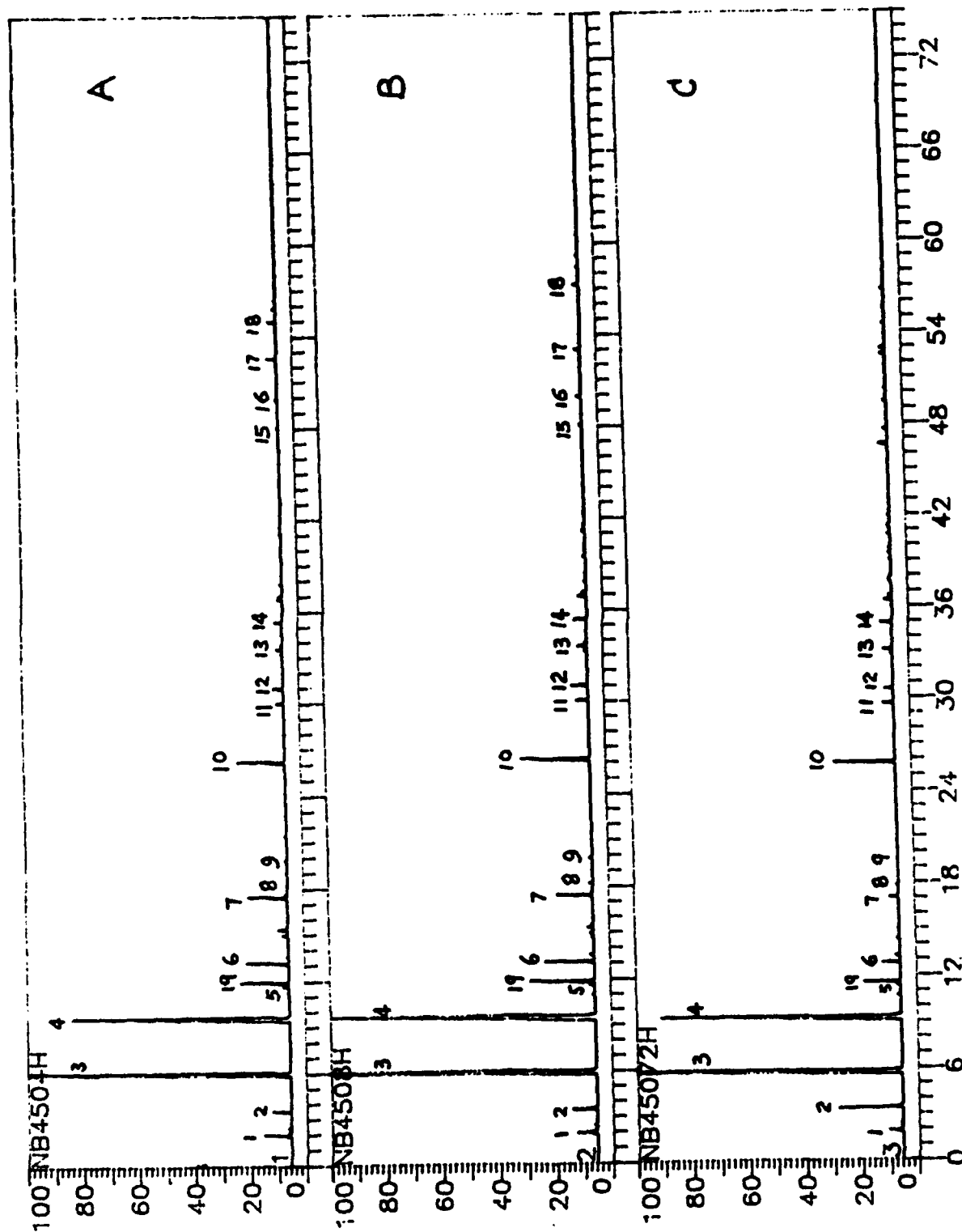


Figure 15. Capillary gas chromatograms of liquids from n-butylbenzene stressed at 450°C for 4 (A), 8 (B) and 72 h (C).

t-butylbenzene and n-butylbenzene respectively. The peaks designated by numbers in Figures 12-15 were identified by using Kratos GC-MS, and shown in Table 3.

It can be clearly seen from Figures 14 and 15 that area of substrate n-butylbenzene (peak 7) molecule decreases drastically from 15 min reaction to 8 h reaction. Initial products of n-butylbenzene thermal stressing are toluene (peak 3) and styrene (peak 5). High molecular weight products form after 30 min reaction and accompany the increasing amount of toluene and ethylbenzene (peak 4). Another trend is the progressive increase in intensity of naphthalene peak (peak 10) with time. As we have noticed previously, for most relatively high severity reactions, "cracking products" such as toluene and ethylbenzene become the dominant components in liquids (Table 3 and Figure 15).

As compared with n-butylbenzene (Figures 14-15), the chromatograms of stressed t-butylbenzene look quite different. Even after 72 h stressing, there is still some t-butylbenzene left in liquid (Figure 13). The decrease of substrate peak area (peak 7) is slow and accompanied by the formation of isobutylbenzene (2-methylpropylbenzene) (peak 8). There is only limited amount of naphthalene (peak 12) formed in the runs before 8 h, but it builds up to relatively high concentration in 72 h.

Fractionation of Liquid Products

From Figures 12-15, we can see that the major products elute within 24 min on the GC column. However, there are many heavy components (eluting after 24 min) responsible for the darkening of liquids and formation of solids, which seem to exist only in very small amount. Figure 16 shows a fractionation procedure which was developed to concentrate the higher molecular weight products. Table 4 shows the yields of the fractions.

GC-MS TICs of fraction 2 separated from the products of t- and n-butylbenzene are shown in Figures 17-19 and 20-22, respectively. Tables 5-10 list the compounds tentatively identified in fraction 2 of these liquid products. As we can see from Figures 17-19, butylbiphenyls and di-t-butylphenyls are the major compounds, implying that dimerization via the formation of biaryl bond is one of the initial stage reactions of t-butylbenzene. The existence of t-butylbiphenyl suggests that the reactions also involve dealkylation. As shown in these figures, fluorene, phenylnaphthalene and terphenyl are also detected in this fraction, but their concentrations are smaller than those mentioned above. In fraction 2 of 450°C-4hr liquid, t-butylbenzenes and di-t-butylbiphenyls are still major components, but the amount of fluorene, phenylnaphthalene and terphenyl increased. In fraction 2 of 450°C-8hr, phenylnaphthalene becomes one of the most abundant components. This trend shows that as the extent of thermal treatment increases, the degree of aromaticity and extent of condensation occurring in the liquid increases.

Table 3. Identified Compounds for Peaks Designated in Figures 12-15

Peak No.	Substrate	
	t-Butylbenzene	n-Butylbenzene
1	Pentane	Pentane
2	Benzene	Benzene
3	Toluene	Toluene
4	Ethylbenzene	Ethylbenzene
5	Isopropylbenzene	Styrene
6	n-Propylbenzene	n-Propylbenzene
7	t-Butylbenzene	n-Butylbenzene
8	Isobutylbenzene	Indane
9	Methylindane	C5-benzene
10	Indane	Naphthalene
11	Methylindane	Methylnaphthalene
12		Methylnaphthalene
13	Naphthalene	Biphenyl
14	Methylnaphthalene	Methylbiphenyl
15	Di-tert-butylbenzene	Ethylfluorene
16	Di-tert-butylbenzene	Phenathrene
17		Phenylnaphthalene
18		Terphenyl
19		Isopropylbenzene

In contrast to t-butylbenzene, we did not find dimers in fraction 2 of n-butylbenzene. Even in 400°C-1hr liquid, phenylnaphthalene and methylfluorene are formed, indicating that cyclization and condensation reactions of n-butylbenzene can take place under relatively milder conditions. Biphenyls and terphenyls are detected in 450°C-1hr reaction. There is a small amount of pyrene formed in fraction 2 of 450°C-8hr liquid. While there are many peaks remain to be identified, their mass spectra are characteristic of polyaromatic compounds.

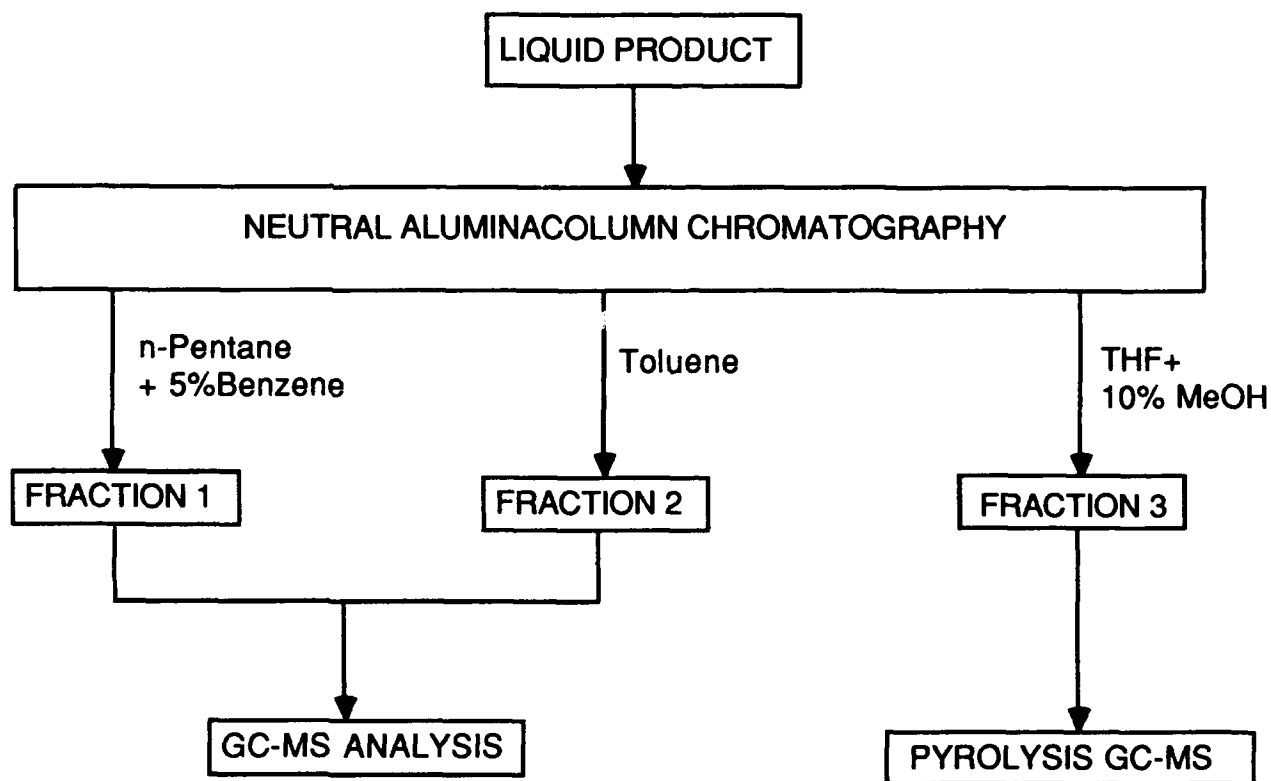


Figure 16. A separation scheme for concentrating minor components of liquid products.

Table 4. Fractional composition of liquid products from n- and t-butylbenzene.

Treatment in N ₂	Yield, % weight		
n-Butylbenzene	Fraction 1 ^a	Fraction 2	Fraction 3
400°C - 1 hr	98.28	0.35	1.37
450°C - 1 hr	92.50	3.77	3.73
450°C - 8 hr	93.35	4.65	2.00
t-Butylbenzene			
450°C - 1 hr	98.4	0.301	1.25
450°C - 4 hr	97.9	0.696	1.36
450°C - 8 hr	93.2	3.490	3.34
475°C - 1 hr	98.0	0.632	1.37
500°C - 1 hr	92.7	3.250	4.09

^a by difference.

DS90 Chromatogram report Run: YINGTB0026, 4-Jan-91 00:45
TB 450-1HR FRAC.2 40-280@4 IH=5, FH=10

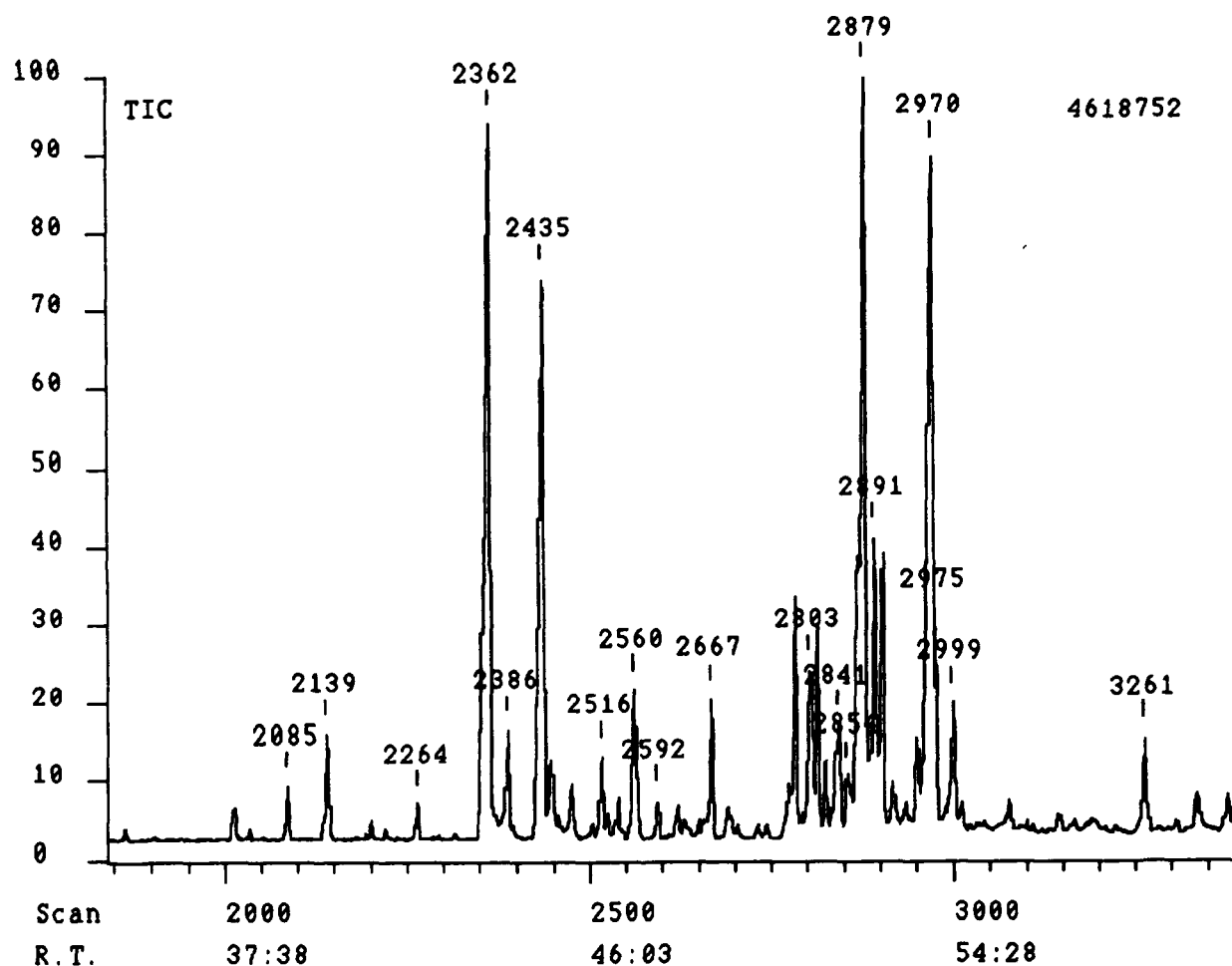


Figure 17. GC/MS total ion chromatogram of fraction 2 of the 450°C-1 h liquid product from t-butylbenzene.

DS90 Chromatogram report Run: YINGTB0024, 14-Dec-90 17:41
TB 450/4HR FRAC. 2 40-280@4 IH=5,FH=10

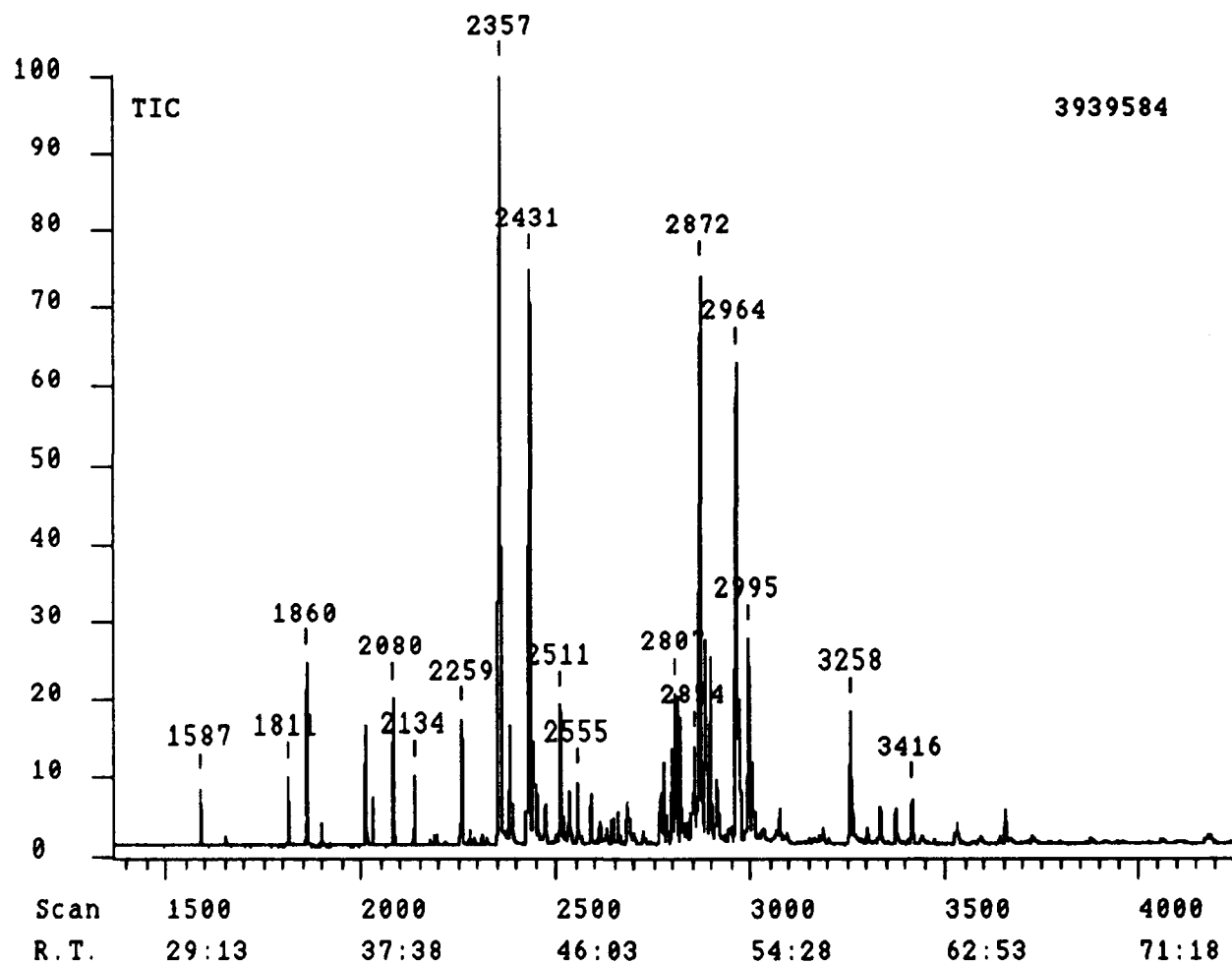


Figure 18. GC/MS total ion chromatogram of fraction 2 of the 450°C-4 h liquid product from *t*-butylbenzene.

DS90 Chromatogram report Run: YINGTB0025, 3-Jan-91 22:43
 TB 450-8HR FRAC.2 40-280@4 IH=5, FH=10

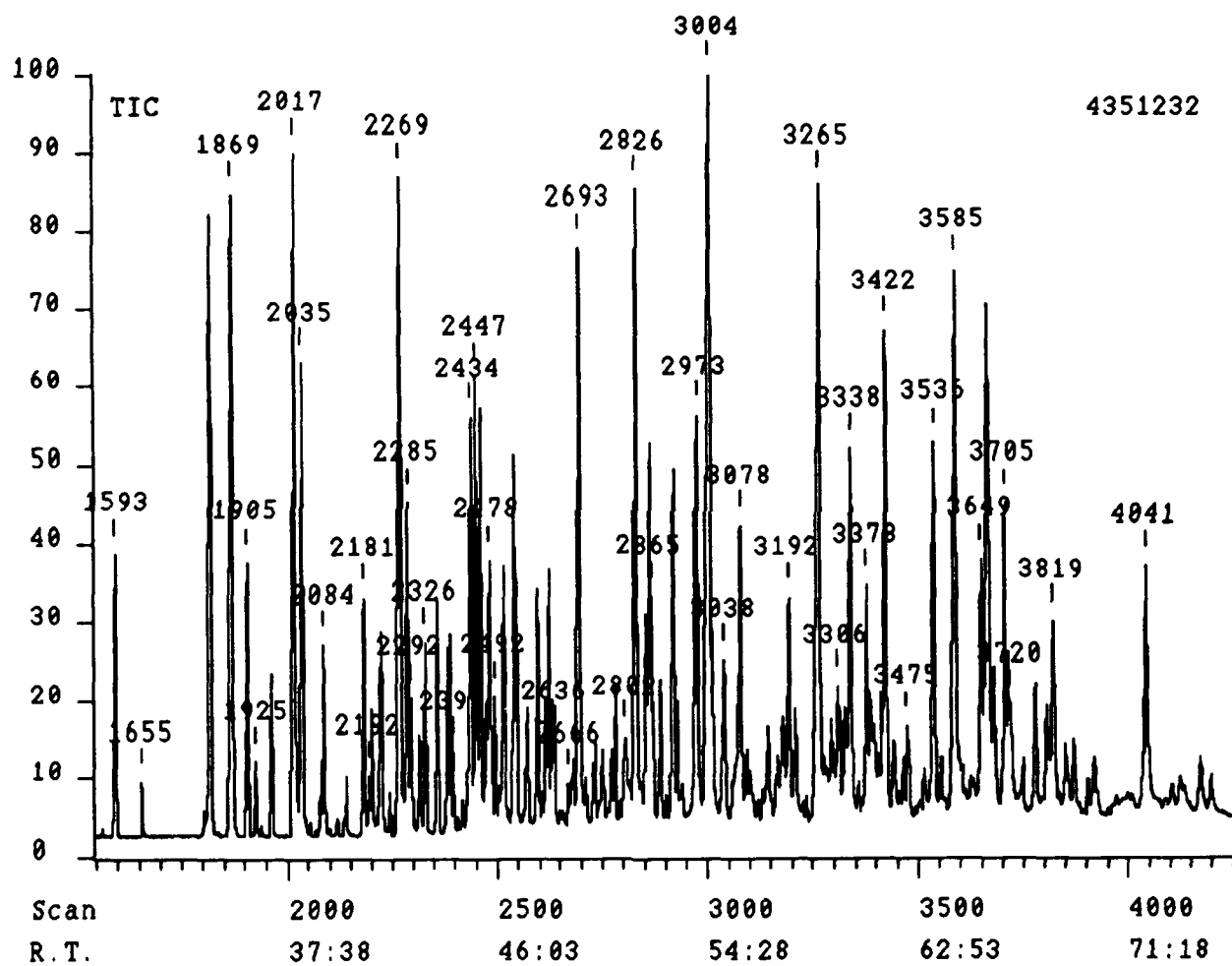


Figure 19. GC/MS total ion chromatogram of fraction 2 of the 450°C-8 h liquid product from t-butylbenzene.

DS90 Chromatogram report Run: YINGNB0005, 3-Jan-91 19:42
NB 400-1HR FRAC.2 40-28004 IH=5 FH=10

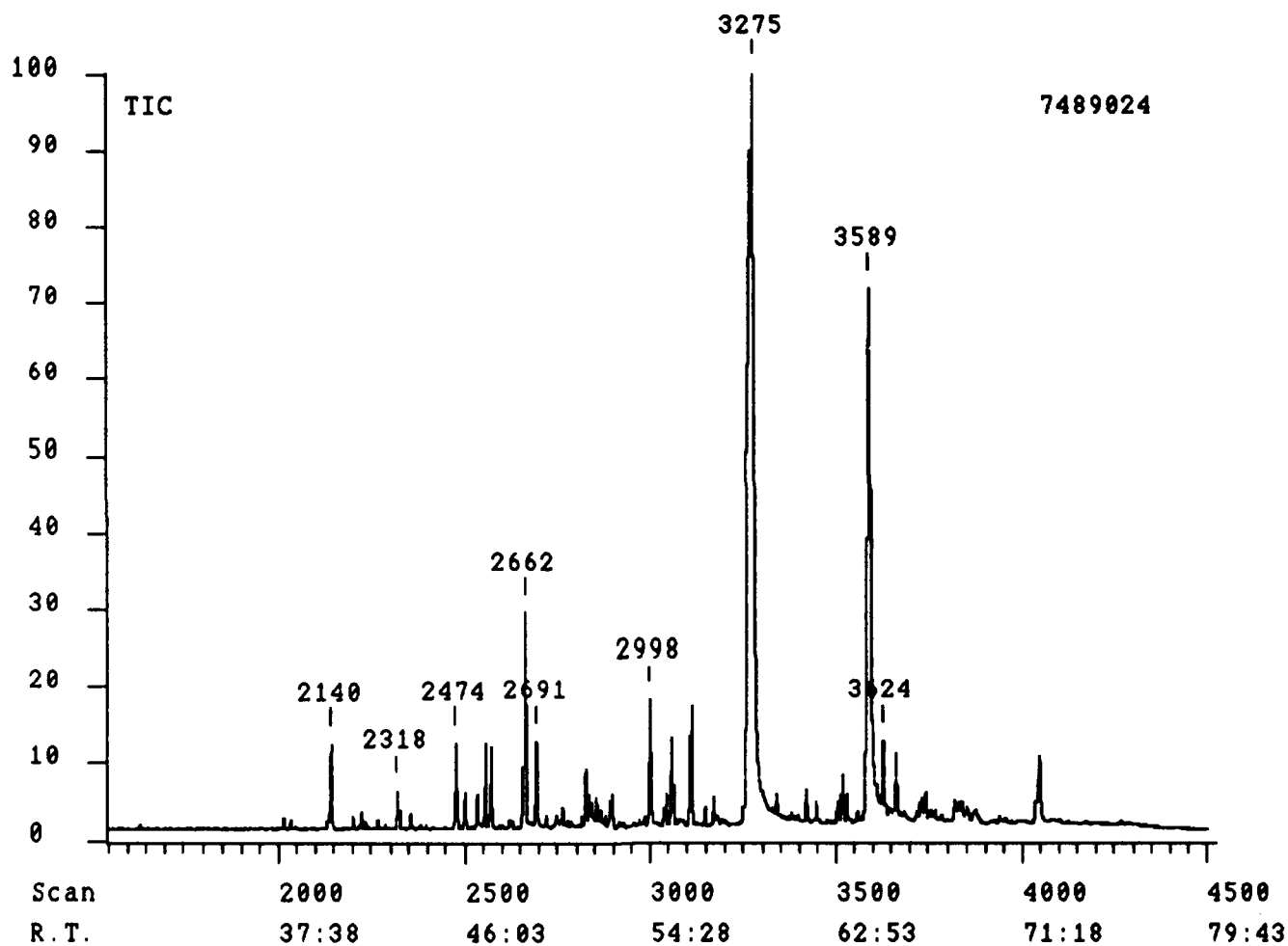


Figure 20. GC/MS total ion chromatogram of fraction 2 of the 400°C-1 h liquid product from n-butylbenzene.

DS90 Chromatogram report Run: YINGNB0003, 3-Jan-91 16:24
NB 450-1HR FRAC.2 40-280@4 IH=5, FH=10

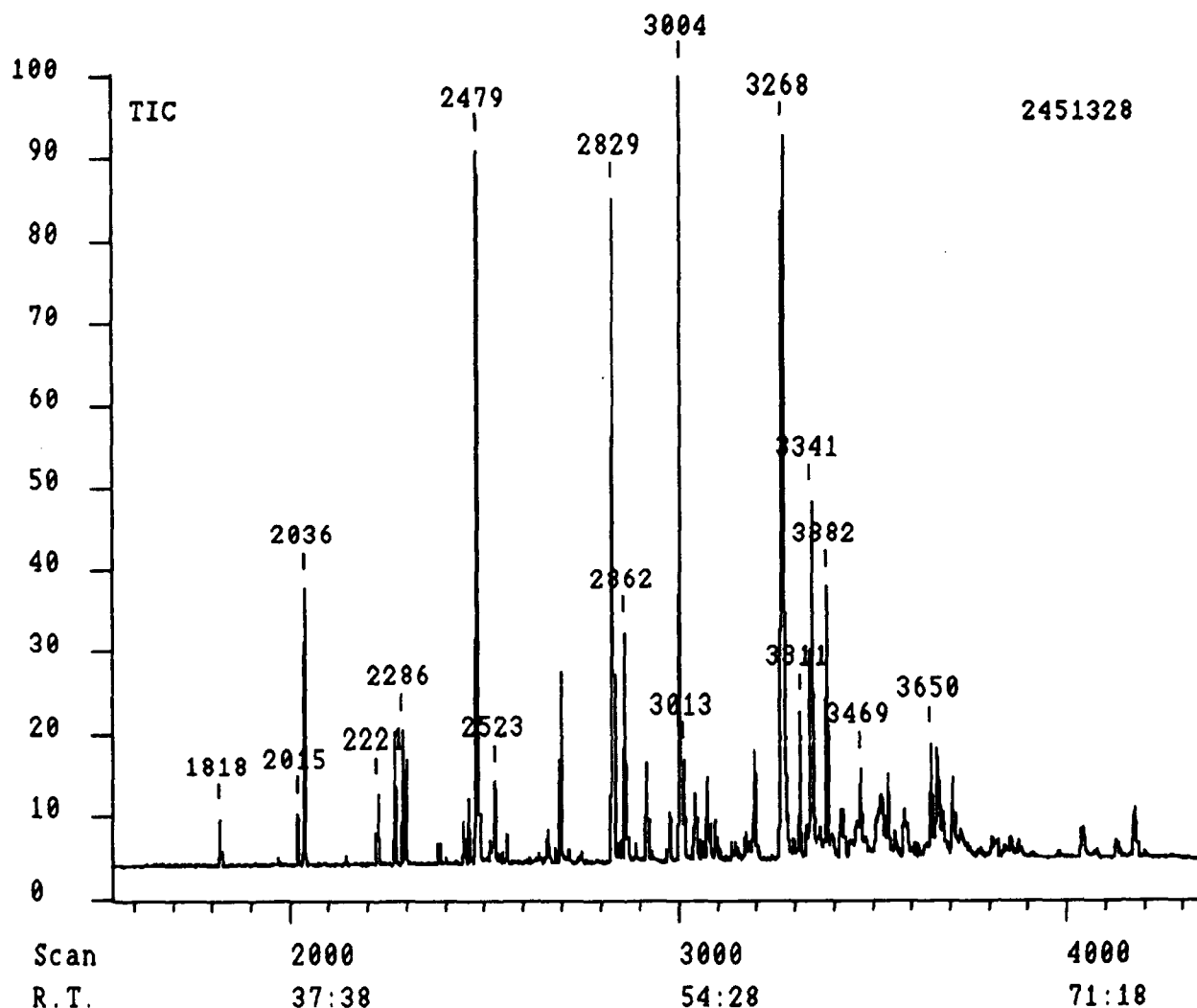


Figure 21. GC/MS total ion chromatogram of fraction 2 of the 450°C-1 h. liquid product from n-butylbenzene.

DS90 Chromatogram report Run: YINGNB0002, 2-Jan-91 15:53
NB 450-8HR FRAC. 2 40-280@4 IH=5, FH=10

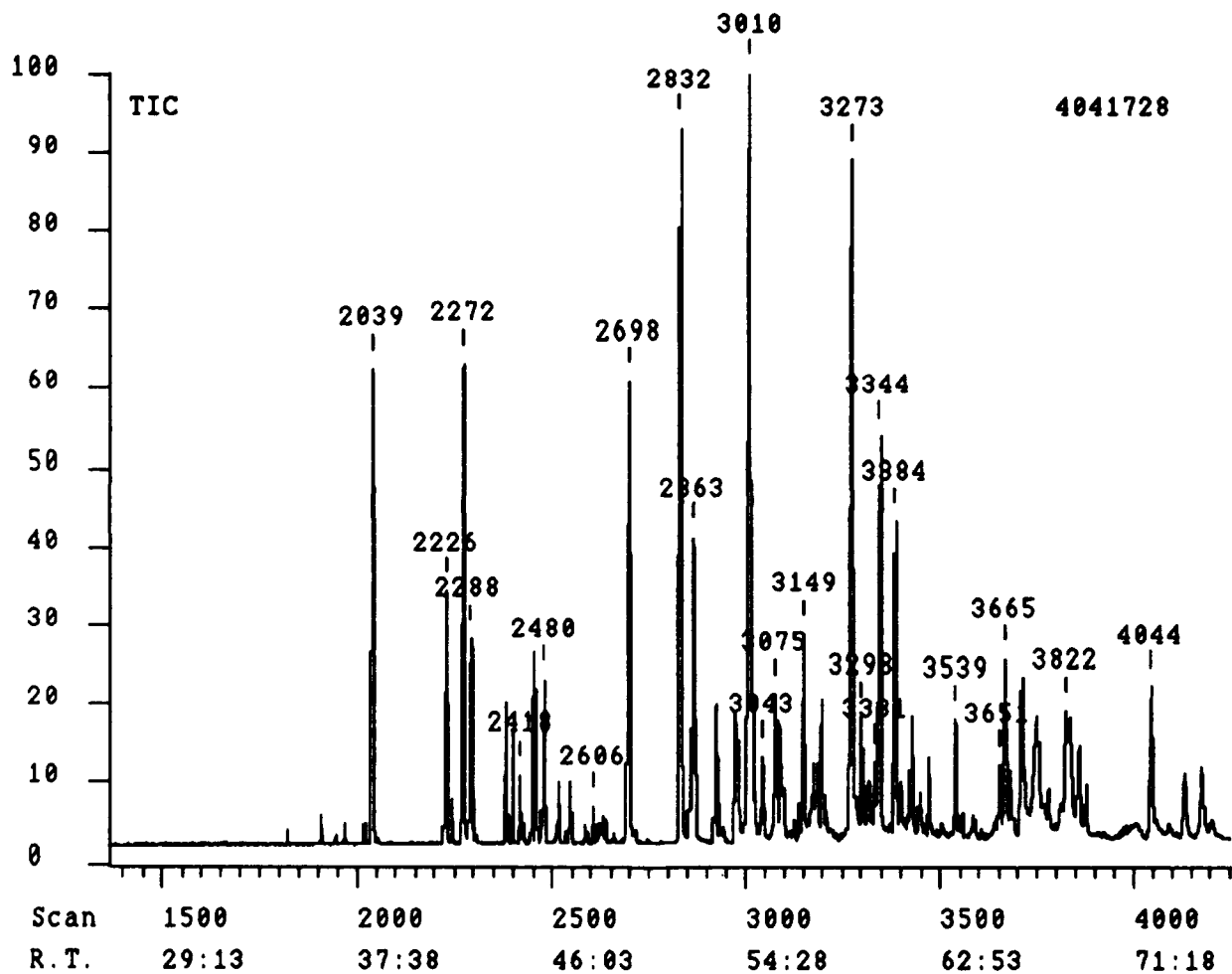


Figure 22. GC/MS total ion chromatogram of fraction 2 of the 450°C-8 h liquid product from n-butylbenzene.

Table 5. Identified compounds in fraction 2 of 450°C-1h liquid product of t-butylbenzene

Scan No.	Molecular Ion	Base Peak	Possible Compound
2085	182	91	Bibenzyl
2139	180	180	Methylfluorene
2264	166	166	Fluorene
2362	210	195	t-Butylbiphenyl
2386	210	167	sec-Butylbiphenyl
2435	210	195	t-butylbiphenyl
2516	224	209	Methyl-t-butylbiphenyl
2560	236	119	
2592	224	209	Methyl-t-butylbiphenyl
2667	238	91	
2803	236	117	
2803	266	251	di-t-Butylbiphenyl
2841	266	104	
2854	252	118	
2879	266	251	di-t-butylbiphenyl
2891	266	223	sec-t-di-butylbiphenyl
2975	266	251	di-t-Butylbiphenyl
2970	266	251	di-t-Butylbiphenyl
2999	204	204	Phenyl-naphalene
3261	230	230	Terphenyl

Table 6. Identified compounds in fraction 2 of 450°C-4 h liquid product of t-butylbenzene

Scan No.	Molecular Ion	Base Peak	Possible Compound
1587	142	142	Methylnaphthalene
1811	154	154	Biphenyl
1860	156	156	Dimethylnaphthalene
2080	182	91	Bibenzyl
2134	180	180	Methylfluorene
2259	166	166	Fluorene
2357	210	195	t-Butylbiphenyl
2431	210	195	t-Butylbiphenyl
2511	224	209	Methyl-t-butylbiphenyl
2555	236	119	
2807	266	251	di-t-Butylbiphenyl
2854	252	230	isopropyl-t-butyl-Biphenyl
2872	266	251	di-t-Butylbiphenyl
2964	266	251	di-t-Butylbiphenyl
2995	204	204	Phenylnaphthalene
3258	230	230	Terphenyl
3416	242	242	

Table 7. Identified compounds in fraction 2 of 450° C-8 h liquid product of t-butylbenzene

Scan No.	Molecular Ion	Base Peak	Possible Compound
1593	142	142	2-Methylnaphthalene
1655	142	142	1-Methylnaphthalene
1869	156	156	Dimethylnaphthalene
1905	156	156	Dimethylnaphthalene
1925	156	156	Dimethylnaphthalene
2017	168	168	Methylbiphenyl
2035	168	168	Methylbiphenyl
2084	182	91	Bibenzyl
2181	182	167	Ethylbiphenyl
2192	182	182	Ethylbiphenyl
2269	166	166	Fluorene
2285	180	165	Methylfluorene
2292	182	182	Ethylbiphenyl
2326	196	167	Propylbiphenyl
2395	196	181	Isopropylbiphenyl
2447	210	165	
2434	210	195	t-Butylbiphenyl
2478	180	180	Methylfluorene
2492	210	181	
2636	224	209	Methyl-t-butylbiphenyl
2636	194	179	
2666	224	91	Methyl-sec-butylbiphenyl
2693	238	223	Ethyl-t-butylbiphenyl
2693	178	178	Phenanthrene
2802	252	207	
2826	204	204	Phenylnaphthalene
2865	218	192	
2973	266	251	di-t-Butylbiphenyl
2973	218	218	
3004	204	204	Phenylnaphthalene
3038	218	218	
3078	218	218	

Table 7 (continued)

3192	218	218	
3265	230	230	Terphenyl
3306	244	244	
3338	230	230	Terphenyl
3378	244	244	
3422	242	242	
3475	256	256	
3536	242	242	
3585	178	149	
3649	256	256	
3705	242	242	
3720	256	256	
3819	228	228	
4041	254	254	

Table 8. Identified compounds in fraction 2 of 400°C-1 h liquid product of n-butylbenzene

Scan No.	Molecular Ion	Base Peak	Possible Compound
2140	180	180	Methylfluorene
2318	196	92	
2474	180	180	Methyluorene
2662	208	117	
2691	178	178	Phenanthrene
2998	204	204	Phenylnaphthalene
3624	196	91	
3275	260	129	Not identified
3589	300	149	Not identified

Table 9. Identified compounds in fraction 2 of 450°C-1 h liquid product of n-butylbenzene

Scan No.	Molecular Ion	Base Peak	Possible Compound
1818	154	154	Biphenyl
2015	168	168	Methylbiphenyl
2036	168	168	Methylbiphenyl
2221	182	167	Ethylbiphenyl or
2286	180	165	Methylfluorene
2479	180	179	Methylfluorene
2523	194	194	
2829	204	204	Phenylnaphthalene
2862	230	230	Terphenyl
3013	244	244	
3004	204	204	Phenylnaphthalene
3268	230	230	Terphenyl
3311	244	244	
3341	230	230	Terphenyl
3382	244	244	
3469	278	278	
3469	258	258	
3650	256	256	

Table 10. Identified compounds in fraction 2 of 450°C-8 h liquid product of n-butylbenzene

Scan No.	Molecular Ion	Base Peak	Possible Compounds
2039	168	168	Methylbiphenyl
2272	166	166	Fluorene
2226	168	166	Methylbiphenyl
2288	180	165	Methylfluorene
2418	196	181	
2480	180	165	Methylfluorene
2606	194	165	Ethylfluorene
2698	178	178	Phenanthrene
2832	204	204	Phenylnaphthalene
2863	230	230	Terphenyl
3010	204	204	Phenylnaphthalene
3043	218	218	
3075	218	218	
3149	218	218	
3273	230	230	Terphenyl
3298	202	202	Pyrene
3331	244	244	
3344	230	230	Terphenyl
3384	244	244	
3539	242	242	
3651	256	256	
3665	242	242	
3822	278	278	
3822	228	228	
4044	254	254	

Task 2. Identification and Characterization of Mixtures of Stable Hydrocarbon Species Present in Coal-Derived Fuels.

Task 2 is an extension of model compound testing in Task 1 to mixtures of hydrocarbon species such as real fuels and their fractions as well as mixtures of model compounds.

Activity 1. Fractionation of Jet Fuels

The GC-MS analysis of the whole (unfractionated) JP-8C using the modified GC-MS procedure indicated that methylcyclohexane is the most predominant component, although this was not detected by previous GC-MS analysis [1] due to the use of delay time to ionization. On the other hand, the analysis of the saturate fraction indicated that methylcyclohexane was lost in this fraction during the rotary evaporation. Therefore, the yield of saturate fraction from column chromatographic separation of JP-8C should be higher than reported previously [1]. In other words, the GC-MS results showed that the loss indicated by material balance of column separation is due to the evaporation of saturate materials, especially methylcyclohexane. Another analytical-scale chromatographic separation (run S-35) was conducted using 4 g JP-8C. To prevent the loss of light materials such as methylcyclohexane, the change in composition of saturates during evaporation was monitored by GC-MS. The yield of recovered saturates (fraction 1 of run S-35) is 77.9 wt%. Table 11 shows the results of chromatographic separation of JP-8C as well as those for JP-8P.

The saturate fraction (Fr.1) is predominant and constitutes about 78 % of JP-8C and 85 % of JP-8P. Aromatic fractions (Frs. 2 and 3) make up 20% of JP-8C and 12% of JP-8P. As reported previously, the LC fractions from the two jet fuels have distinctly different chemical constitutions [1]. Although some GC-MS results have been reported previously [1], the detailed identification results for the column fractions are summarized here in this report. The saturate fraction was analyzed by GC-MS using modified procedure (split injection of undiluted sample without delay to ionization). Figure 23 shows the TIC of the JP-8C saturates (from run S-35). The relative intensity of methylcyclohexane is lower in the saturate fraction than in the original JP-8C. Detailed identification results are shown in Table 12. Nearly 80 peaks in the TIC of JP-8C saturates were identified. Most of the major peaks are cycloalkanes, and some of them are long-chain paraffins. Although some aromatics are also present in this fraction, their concentrations are very low (trace amounts). Figure 24 and Table 13 give the GC-MS results for fraction 2, and Figure 25 and Table 14 for fraction 3 of JP-8C.

Table 11. Chromatographic separation of JP-8C and JP-8P jet fuels on neutral alumina

Fraction No.	Elution System	Yields (wt%)		Appearance (color)	Compounds Class
	Solvent	JP-8P	JP-8C		
1	n-Pentane	85.2	77.9	Colorless	Saturates
2	5% Benzene-Pentane	6.9	9.1	Colorless	Monoaromatics
3	Benzene	4.9	11.1	Yellowish	Aromatics
4	1% EtOH-Chloroform	0.7	0.5	Colorless	Polar-1+ Polyaromatics
5	10% EtOH-THF	1.0	1.0	Yellow	Polar-2 + Polyaromatics
Total		98.7	99.6		

** Average results of three chromatographic analytical-scale and two preparative-scale separation runs.

Activity 2. Thermal Stressing of JP-8C

In this task, the thermal stressing tests of JP-8C were conducted at 450°C for 0.5, 1, 4, 8, and 16 h using 5 ml sample in a microreactor with 100 psig UHP-grade N₂ (cold). The saturate fraction (Fr.1) from preparative chromatographic separation of JP-8C [1] was stressed at 450°C for 4 h. The microreactor (about 234 g in weight) consists of a single Swagelok port connector and two caps, and was used in a vertical mode with the upper cap connecting to a pressure gauge. The sealed reactor was purged with N₂ six times, pressurized and then placed into a fluidized sand bath preheated to 450°C. Immediately after the reaction, the reactor was quenched by cold water. The product work-up was carefully performed as follows. The liquid products were poured out into a 10 ml measuring cylinder. The reactor was then washed twice with 5 ml pentane and then dried. The amount of solid products was determined by measuring the weight gain of the reactor (after pouring out liquids, pentane-washing and drying) plus the solid taken from upper cap. The weights of the solids and the liquids actually recovered were also measured to confirm the solid yields obtained by measuring the weight gain of the reactors. The errors of measuring the reactor weight gain for determining the solids from JP-8C and from JP-8P at 450°C within four h might be relatively larger because of the small amounts of solids. In thermal stressing of fuel samples at 450°C for over 8 h, over 90% of the solid (indicated by weight gain of the reactor) was actually recovered.

DS90 Chromatogram report Run: SONG710001, 19-Jun-91 20:52
S-35 JP-8C FR.1/SH ORIG 40-5 TO 200-1004 SPLIT 0.05 UL

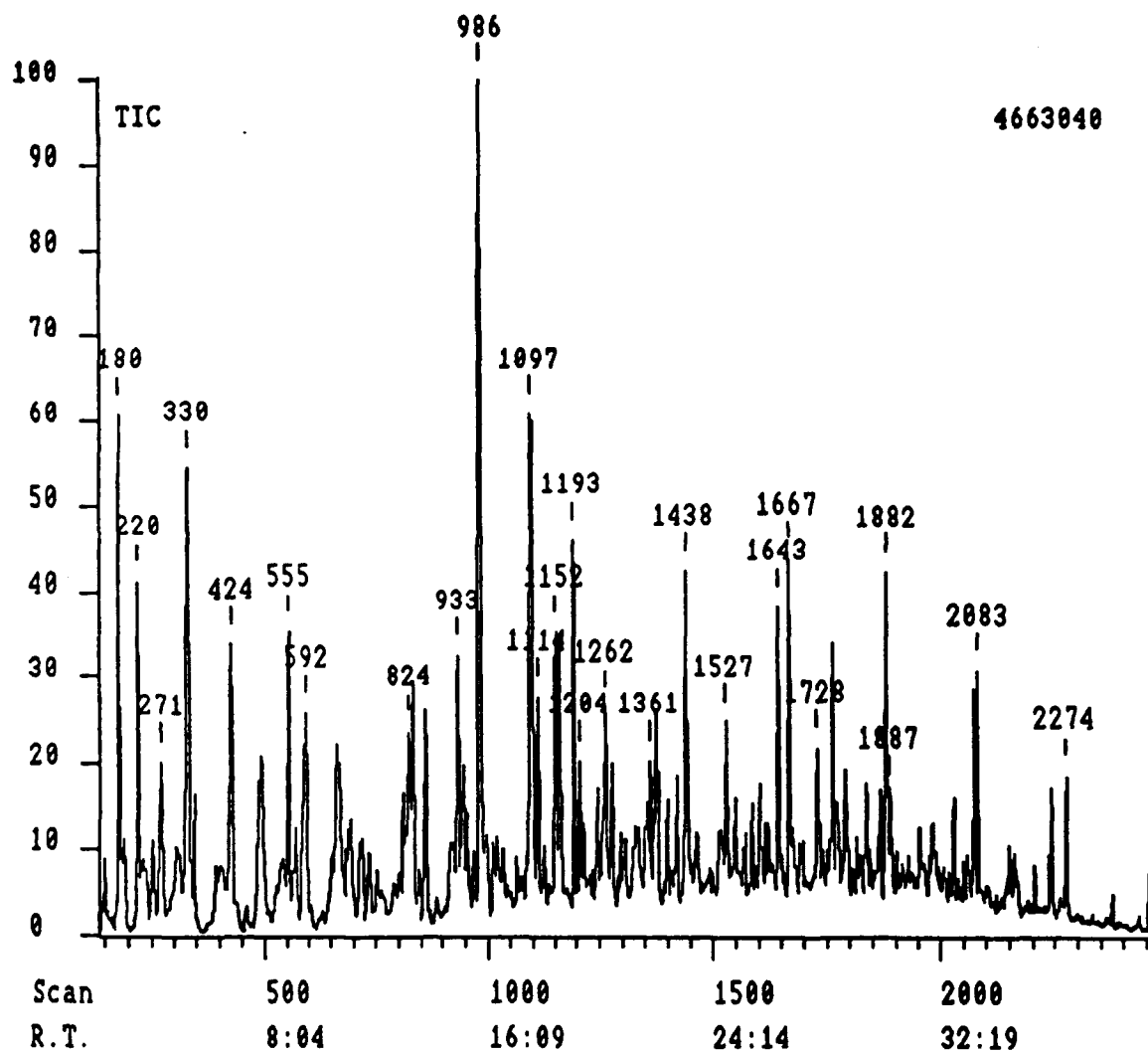


Figure 23. GC-MS TIC of saturate fraction (n-pentane elute) of JP-8C jet fuel (split injection of undiluted sample without delay to ionization)

Table 12. Identified compounds in saturate fraction of JP-8C jet fuel

Scan No.	Retention Time	Molecular Ion	Base Peak	Identified Compounds
100	1:38	72	43	n-Pentane (n-C5)
115	1:50	58	43	Acetone
149	2:23	84	56	Cyclohexane
		98		1-Heptene
180	2:54	98	83	Methylcyclohexane
190	3:03	114	43	iso-Octane
220	3:32	112	97	Dimethylcyclohexane
253	4:04	112	55	Dimethylcyclohexane
271	4:22	112	55	Dimethylcyclohexane
330	5:19	112	83	Ethylcyclohexane
343	5:32	92	91	Toluene
392	6:19	128	43	n-Nonane
		126		Nonene
424	6:50	126	97	Methylethylcyclohexane
491	7:55	126	55 or 97	Methylethylcyclohexane
555	8:57	126	83	Propylcyclohexane
571	9:13	140	55	Methylpropylcyclohexane
592	9:33	140	69	Diethylcyclohexane
		106	91	m- + p-Xylene
664	10:43	140	97	Methylpropylcyclohexane
693	11:11	124	67	trans-Hexahydroindan
717	11:34	140	55	C4-Cyclohexane
737	11:54	140	55 or 97	Methylpropylcyclohexane
813	13:08	138	81	Methylhexahydroindan (trans- ?)
824	13:18	124	81	cis-Hexahydroindan
		154	83	C5-Cyclohexane
834	13:28	140	83	n-Butylcyclohexane
		120	91	n-Propylbenzene
863	13:56	120	105	Methylethylbenzene
916	14:47	138	81	Methylhexahydroindan
		152		
933	15:04	138	81	Methylhexahydroindan (cis- ?)
946	15:17	154	55	Methylbutylcyclohexane
		138		Methylhexahydroindan
955	15:25	120	105	Trimethylbenzene
986	15:55	138	138	trans-Decalin
1036	16:44	152	81	Methyldecalin
1066	17:13	152	95	Methyldecalin
		168		C6-Cyclohexane
1090	17:36	152	81	Methyldecalin
1097	17:43	152	81	trans-2-Methyldecalin
1114	17:59	154	83	n-Pentylcyclohexane
		134	91	n-Butylbenzene

Table 12 (Continued)

1126	18:11	134	119	Dimethylethylbenzene
1152	18:36	138	67 or 81	cis-Decalin
1161	18:45	152	152	Methyldecalin (cis- ?)
1193	19:16	152	81	Methyldecalin
		170	57	n-Dodecane (n-C12)
1204	19:27	166	81	Dimethyldecalin
1213	19:36	168	97	C6-Cyclohexane
		152		Methyldecalin
		134	119	C4-Benzene
1245	20:07	152	95	Methyldecalin
1262	20:23	166	81	Dimethyldecalin
1276	20:37	152	95	Methyldecalin
		132	117	Methylindan
1297	20:57	166	81	Dimethyldecalin
1352	21:50	166	81	Dimethyldecalin
1361	21:59	166		C2-Decalin
		148	105	C4-Benzene
1375	22:13	168	83	n-Hexylcyclohexane
		166		C2-Decalin
		148	91	Pentylbenzene
1398	22:35	166	137	Ethyldecalin
1420	22:56	132	117	Methylindan
		180		C3-Decalin
1438	23:14	184	57	n-Tridecane (n-C13)
1464	23:29	180	55	C3-Decalin
		182		C7-Cyclohexane
		132	117	Methylindan
1527	24:40	180	95	C3-Decalin
		132	104	Tetralin
1549	25:01	166	55	Dimethyldecalin
		180	82 ?	
1569	25:21	166		C2-Decalin or C3-Hexahydroindan
		162	119	C6-Benzene
		180		
1602	25:53	162	105	C6-Benzene
1622	26:12	182	83	n-Heptylcyclohexane
		180		
1643	26:33	166	82	Bicyclohexyl
1667	26:56	198	57	n-Tetradecane
		146	131	Methyltetralin
1728	27:55	180	55	Methylbicyclohexyl
		176	106	Methylhexylbenzene
1761	28:27	146	131	Methyltetralin
1769	28:35	226	57	iso-Hexadecane
		194		
		180		
		176		
		160		

Table 12 (Continued)

1790	28:55	180 178	83	Dicyclohexylmethane Perhydrobenzoindan or Perhydrofluorene
1813	29:18	194 ?	55 43	Dimethylbicyclohexyl Long-chain paraffin
1835	29:39	178	67 or 97	Perhydrobenzoindan or Perhydrofluorene
1865	30:08	194 192 194	137 137	2-Butyldecalin Methylperhydrobenzoindan ? Butyldecalin n- ?
1882	30:24	212	57	n-Pentadecane
1887	30:29	194 160	81 or 55 145	C4-Decalin C2-Tetralin
1903	30:45	178	135	Perhydrobenzoindan or Perhydrofluorene
1956	31:36	176 178	119 97	C7-Benzene Perhydrofluorene or Perhydrobenzoindan
1983	32:02	160	131	2-Ethyltetralin
2028	32:46	192	192	Perhydroanthracene
2072	33:29	192	192	Perhydroanthracene
2083	33:39	226	57	n-Hexadecane
2150	34:44	192 206	135	Perhydrophenanthrene Methylperhydroanthracene ?
2160	34:54	192 206 188	135	Perhydrophenanthrene Methylperhydroanthracene or methylperhydrophenanthrene C4-Tetralin
2207	35:40	192 206	135	Perhydrophenanthrene Methylperhydroanthracene or methylperhydrophenanthrene
2240	36:12	268	57	2,6,10,14-Tetramethylpentadecane (Pristane)
2274	36:45	240	57	n-Heptadecane
2376	38:24	220 188	 145	C2-Perhydrophenanthrene ? C4-Tetralin
2455	39:40	254	57	n-Octadecane

* n-Pentane eluted fraction 1 from run S-35; GC-MS File: SONG710001

DS90 Chromatogram report Run: SONG20012, 20-Mar-90 15:26
SONG S01-A2 JP8-C 5%BENZENE-PENTANE ELU 40-5 TO 280-5 AT 4

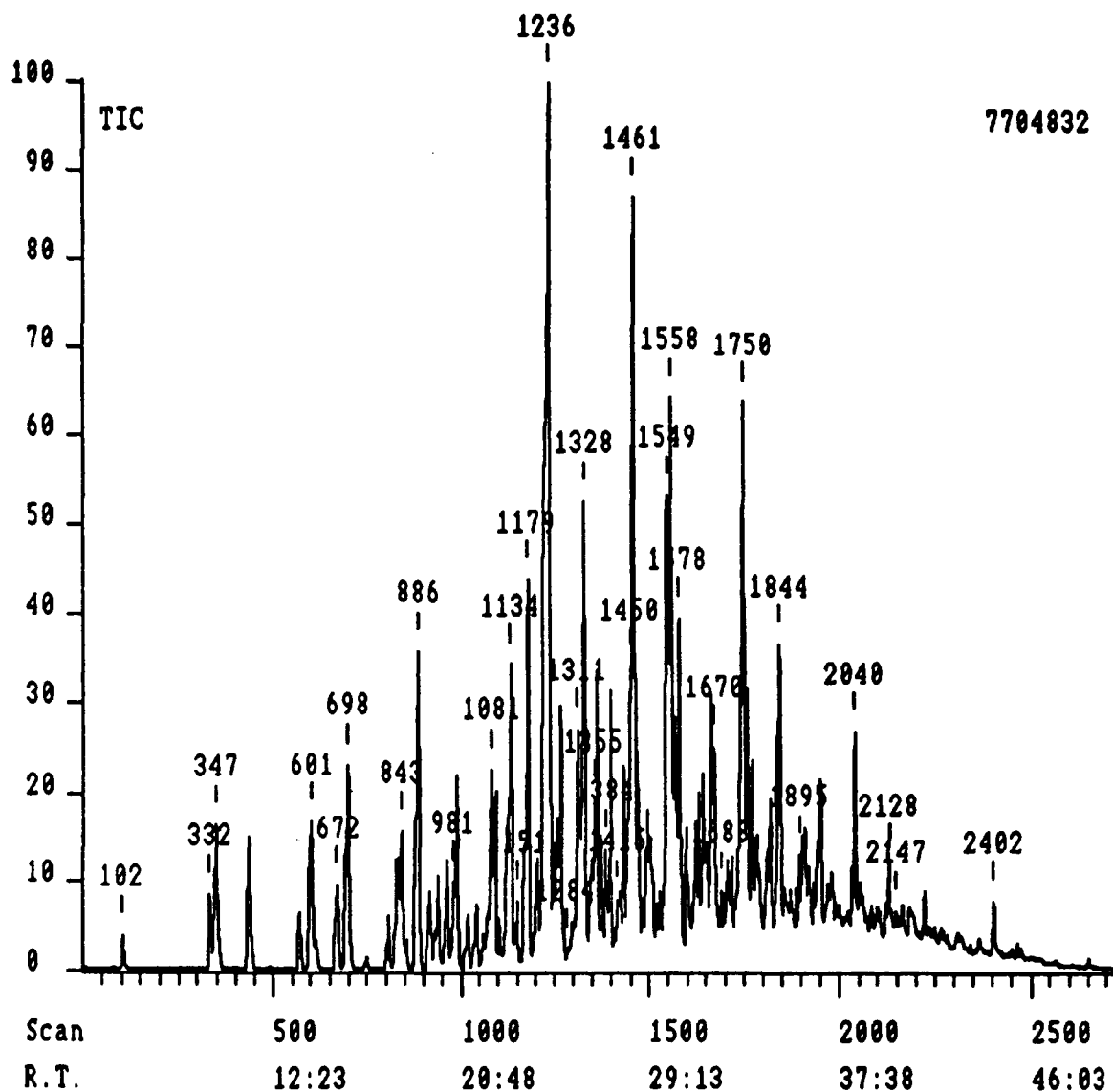


Figure 24. GC-MS TIC of monoaromatic fraction (5% benzene-pentane elute) of JP-8C jet fuel (splitless injection of diluted sample with 4 min delay to ionization)

Table 13. Identified compounds in monoaromatic fraction of JP-8C jet fuel

Scan No.	Retention Time	Molecular Ion	Base Peak	Identified Compounds
102	5:41	92	91	Toluene
332	9:93	106	91	Ethylbenzene
347	9:48	106	91	p- or m-Xylene
434	11:16	106	91	o-Xylene
573	13:37	120	91	n-Propylbenzene
601	14:05	120	105	Ethylmethylbenzene
618	14:22	120	105	1,3,5-Trimethylbenzene
674	15:19	120	105	Ethylmethylbenzene
698	15:43	120	105	1,2,4-Trimethylbenzene
807	17:33	120	105	1,2,3-Trimethylbenzene
829	17:55	134	105	Methylpropylbenzene
836	18:02	134	105	Methylpropylbenzene
843	18:09	134	91	n-Butylbenzene
856	18:22	134	119	Dimethylethylbenzene
886	18:53	118	117	Indan
922	19:29	134	119	Dimethylethylbenzene
931	19:38	134	119	Dimethylethylbenzene
940	19:47	134	119	Dimethylethylbenzene
964	20:11	132	117	1- or 2-Methylindan
989	20:37	132	117	1- or 2-Methylindan
1021	21:09	134	119	Tetramethylbenzene
1044	21:32	134	119	Tetramethylbenzene
1061	21:49	148	119	Dimethylpropylbenzene
1081	22:10	148	105	Methylbutylbenzene
1092	22:21	148	91	n-Pentylbenzene
1106	22:35	148	119	Dimethylpropylbenzene
1134	23:03	132	117	5- or 6-Methylindan
1152	23:21	148	119	Dimethylpropylbenzene
1179	23:49	132	117	6- or 5-Methylindan
1187	23:57	162	92	Hexylbenzene
1206	24:16	146	131	Dimethylindan
1236	24:46	132	104	Tetralin
		146	131	Dimethylindan
1249	24:59	146	117	Ethylindan
1256	25:06	146	131	Dimethylindan
1265	25:15	146	131	Dimethylindan
1311	26:02	162	105	Methylpentylbenzene
1328	26:19	146	104	2-Methyltetralin
1345	26:36	160	145	Trimethylindan
1355	26:46	162	105	Methylpentylbenzene
1363	26:54	146	131	1-Methyltetralin
1373	27:05	146	117	Ethylindan
1384	27:16	162	119	C ₆ -benzene
1398	27:30	146	131	Dimethylindan
1415	27:47	160	131	Methylethylindan
1430	28:02	176	106	Methylhexylbenzene
1450	28:22	160	145	Trimethylindan
1461	28:33	146	131	5- or 6-Methyltetralin

Table 13 (Continued)

1469	28:42	176	105	C7-Benzene
1494	29:07	146	131	Methyltetralin or or Dimethylindan
1503	29:16	160	131	Methylethylindan
1526	29:39	176	106	Methylhexylbenzene
1549	30:02	160	118	Dimethyltetralin
1558	30:11	160	104	Cyclohexylbenzene
1566	30:19	160	145	Dimethyltetralin or Trimethylindan
1578	30:32	160	145	Dimethyltetralin or Trimethylindan
1597	30:51	176	119	Dimethylhexylbenzene
1602	30:56	160	145	Methylethylindan
1619	31:13	160	145	Dimethyltetralin
		174		C3-tetralin or C4-Indan
1630	31:24	160	118	Dimethyltetralin
		174		C3-Tetralin or C4-Indan
1641	31:35	174	174	C3-tetralin
		190		C8-Benzene
1654	31:48	174	131	C3-tetralin
		190		C8-benzene
1663	31:57	160	131	5- or 6-Ethyltetralin
1670	32:05	160	145	C3-tetralin
		174		C3-Tetralin or C4-Indan
1688	32:23	174	145	Trimethyltetralin
1696	32:31	174	159	Trimethyltetralin
		190	106	C8-Benzene
1706	32:41	190	119	Dimethylhexylbenzene
1737	33:12	174	159	Methylethyltetralin
1750	33:25	190	119	Dimethylhexylbenzene
		160	145	Dimethyltetralin
1759	33:34	174	174	Cyclohexyltoluene
1770	33:46	174	131	Methylpropylindan
1782	33:58	174	145	C3-tetralin
1788	34:04	174	145	Methylethyltetralin
		188		C4-Tetralin
1819	34:45	174	159	Trimethyltetralin
1844	35:00	188	159 ?	C4-tetralin
		172	129 ?	Tetrahydrobenzoindan ?
1883	35:40	172	172	Tetrahydrobenzoindan ?
		188		C4-Tetralin
1895	35:52	188	145	C4-Tetralin
1904	36:01	188	145	C4-tetralin
1912	36:09	188	145	C4-tetralin
		172	157	Tetrahydrobenzoindan isomer ?
1949	36:46	188	159	C4-Tetralin
		186		Methyltetrahydrobenzoindan ?
		174		C3-Tetralin or C4-Indan
2032	38:10	186	143	Octahydrophenanthrene isomer ?
		188	145	C4-Tetralin
2040	38:18	188	145	5- or 6-Butyltetralin
2052	38:40	186	143	Octahydroanthracene isomer
2099	39:18	202	159	C5-Tetralin

Table 13 (Continued)

2106	39:25	202	159	C5-Tetralin
2128	39:47	202	145	C5-Tetralin
		172	172	Tetrahydrobenzoindan
2402	44:24	186	186	1,2,3,4,5,6,7,8-Octahydroanthracene
2464	45:26	200	200	2-Methyl-sym-octahydroanthracene
2472	45:35	186	186	1,2,3,4,5,6,7,8-Octahydrophenanthrene

* 5%benzene-pentane eluted fraction 2; GC-MS File: SONG20012

Figure 26 compares the results for the saturate fraction (Fr. 1) of JP-8C and the unfractionated (original) JP-8C. After 450°C for 4 h under a N₂ atmosphere, about 85% of these two samples remained as liquids, with the color changing from slightly yellowish to brown. The solid yields from both of them were well below 1wt%. The extent of gas formation from them was similar to each other. These results suggest that the two samples possess similar thermal stability. This is in contrast to the case of petroleum-derived JP-8P, where the saturates exhibited higher stability than the whole JP-8P (Task 4).

Figure 27 shows the liquid depletion and gas formation from JP-8C (whole) fuel as a function of residence time at 450°C in a N₂ atmosphere. In general, hydrocarbon pyrolysis is characterized by the production of lighter molecules on the one hand, and the formation of heavier materials on the other hand. The extent of liquid depletion and liquid darkening gradually increased, and the yields of gases progressively rose with increasing residence time. The stressing for 0.5 and 1 h caused gas formation and some change in the composition of liquid phase, but there was no solid formation. As shown in Figure 28, the deposit formation began to be observed when the stressing time was extended to 4 h. Increasing the residence time to over 4 h caused the marked solid formation, which appeared to be parallel with the gas formation. This trend reflects that the precursors to deposits were formed and accumulated from the first four h. This may be considered as an induction period for solid formation from JP-8C at 450°C in N₂. On the other hand, comparing the results for JP-8C and JP-8P given in Figure 29 revealed that both in short and long term stressing (as long as 16 h) at 450°C, the extents of gas formation and solid deposition are remarkably lower with the coal-derived JP-8C. These results again demonstrate that the chemical composition of fuels has a significant effect on their thermal degradation at high temperatures. As reported in the previous quarter, GC-MS analysis of liquid products (diluted with HPLC grade CH₂Cl₂, with 4 min delay) indicated that while there was a remarkable change in liquid composition after 4 h stressing at 450°C, a number of cycloalkanes including alkylcyclohexane, decalin and hexahydroindans still remained as the major components, as in the original JP-8C. However, the C₁₂-C₁₆ long-chain paraffins have disappeared from the liquid phase. The present results for both short and long term stressing (Figure 29) clearly showed that

DS90 Chromatogram report Run: SONG20014, 20-Mar-90 18:58
SONG S01-A3 JP8-C BENZENE ELUTE 40-5 TO 280-5 AT 4 HP-17 IU

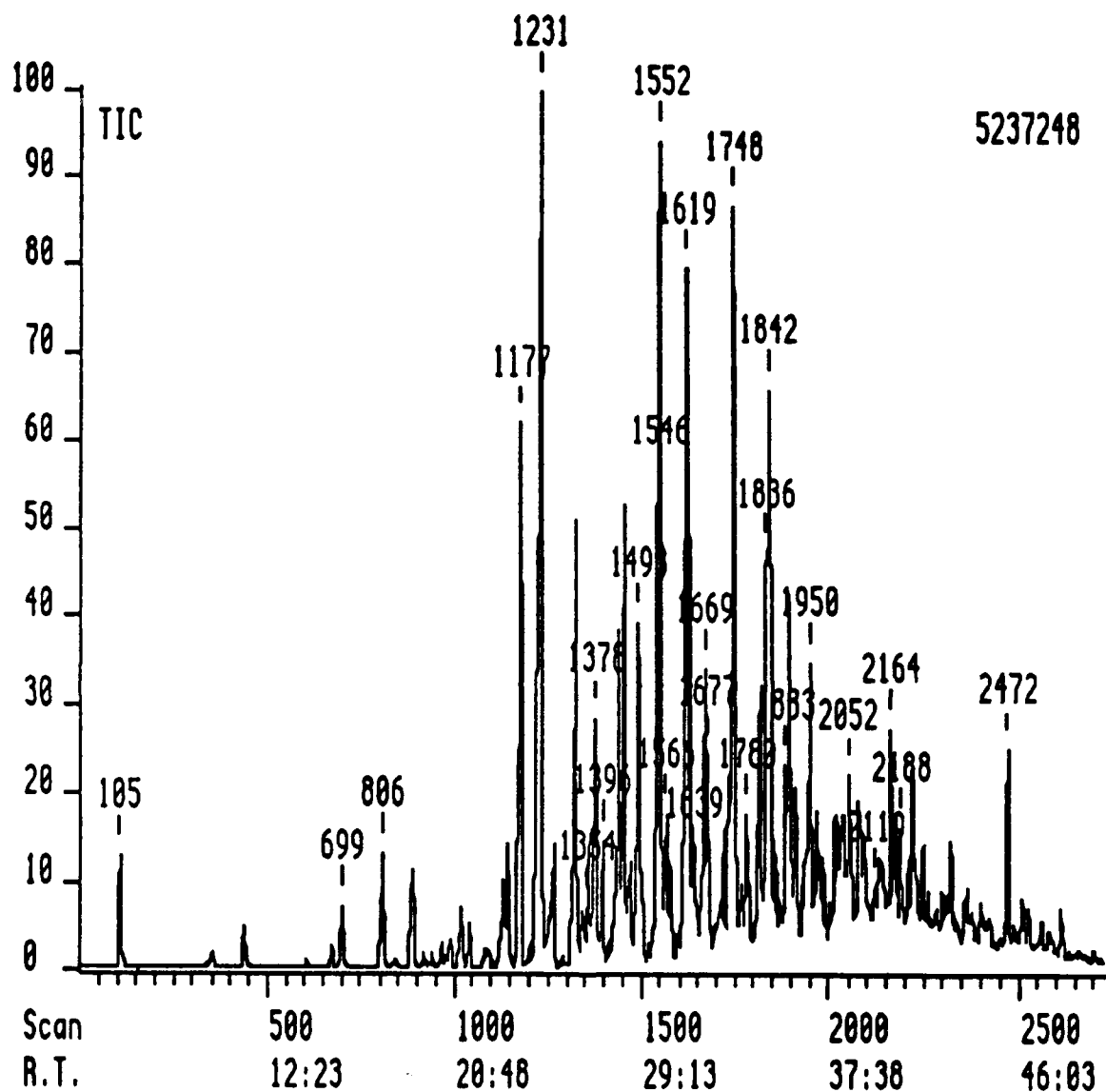


Figure 25. GC-MS TIC of aromatic fraction (benzene elute) of JP-8C jet fuel (splitless injection of diluted sample with 4 min delay to ionization)

Table 14. Identified compounds in aromatic fraction of JP-8C jet fuel

Peak Scan No.	Retention Time	Molecular Ion	Base Peak	Identified Compounds
105	5:44	92	91	Toluene
436	11:18	106	91	o-Xylene
699	15:44	120	105	Trimethylbenzene
806	17:32	120	105	Trimethylbenzene
886	18:53	118	117	Indan
942	19:49	134	119	Dimethylethylbenzene
964	20:12	132	117	Methylindan
988	20:36	132	117	Methylindan
1020	21:08	134	119	Dimethylethylbenzene
1043	21:31	134	119	Dimethylethylbenzene
1080	22:09	148	105	Methylbutylbenzene
1092	22:21	148	91	n-Pentylbenzene
1128	22:57	148	105	Methylbutylbenzene
1134	23:02	132	117	Methylindan
1145	23:14	134	119	Dimethylethylbenzene
1177	23:47	132	117	6- or 5-Methylindan
1231	24:41	132	104	Tetralin
1263	25:14	146	131	1-Methyltetralin or Dimethylindan
1325	26:16	146	104	2-Methyltetralin
1354	26:45	162	105	Methylpentylbenzene
1361	26:53	146	131	1-Methyltetralin or Dimethylindan
1378	27:10	128	128	Naphthalene
1396	27:28	146	131	Dimethylindan
1437	28:09	146	131	Dimethylindan
1456	28:28	146	131	5- or 6-Methyltetralin
1472	28:45	160	145	Dimethyltetralin
1493	29:06	146	131	Dimethylindan
1552	30:05	146	131	5- or 6-Methyltetralin
1566	30:20	160	145	Dimethyltetralin or Trimethylindan
1574	30:28	160	145	C2-Tetralin or C3-Indan
1581	30:35	160	104	Ethyltetralin
1619	31:13	142	142	2-Methylnaphthalene
		160	160	Dimethyltetralin
1630	31:24	160	118	2,6- or 2,7-Dimethyltetralin
1639	31:33	174	145	Methylethyltetralin
1644	31:38	176	119	Dimethylpentylbenzene
1669	32:04	160	145	Dimethyltetralin
1677	32:12	142	142	1-Methylnaphthalene
1715	32:50	160	131	5- or 6-Ethyltetralin
1723	32:58	160	145	Dimethyltetralin or Trimethylindan
1735	33:10	174	159	Methylethyltetralin
1741	33:16	160	145	5,6- or 5,7- or 6,7-Dimethyltetralin
		174		C3-Tetralin or C4-Indan
1748	33:23	190	119	Dimethylhexylbenzene
1768	33:44	174	145	C3-Tetralin or C4-Indan
1780	33:56	174	145	Methylethyltetralin
1810	34:26	174	159	Trimethyltetralin

Table 14 (continued)

1818	34:34	156	141	2-Ethyl-naphthalene
		174	159	Trimethyltetralin
1836	34:52	154	154	Biphenyl
1842	34:58	156	156	Dimethylnaphthalene
		172	129 ?	Tetrahydrobenzoindan ?
		160	145	Dimethyltetralin
1853	35:09	172	172	Tetrahydrobenzoindan isomer ?
1862	35:19	174	145	Methylethyltetralin
1869	35:26	174	145	2- or 1-Propyltetralin
1883	35:40	156	156	Dimethylnaphthalene
1895	35:52	156	156	Dimethylnaphthalene
1902	35:59	188	145	5- or 6-Butyltetralin
1913	36:10	174	159	Trimethyltetralin
1930	36:27	188	145	C4-Tetralin
		174		C3-Tetralin
1942	36:39	172	129	Tetrahydrobenzoindan isomer
		188		C4-Tetralin
		204		C9-Benzene
1950	36:47	174	159	Trimethyltetralin
1960	36:58	156	141	Dimethylnaphthalene
1969	37:07	172	144	Tetrahydrobenzoindan
1987	37:25	156	141	1-Ethyl-naphthalene ?
		188	145	C4-Tetralin
		174		C3-Tetralin
2027	38:05	170	155	Methylethyl-naphthalene
		188		
2037	38:15	168	168	Methylbiphenyl ?
		188	145	5- or 6-Butyltetralin
2052	38:30	186	186	Octahydroanthracene isomer ?
		172	144	Tetrahydrobenzoindan ?
2077	38:56	172	144	Tetrahydrobenzoindan ?
2093	39:12	170	170	Trimethylnaphthalene
2132	39:51	170	170	Trimethylnaphthalene
		200		C1-Octahydroanthracene ?
		188		C4-Tetralin
2138	39:57	170	155	Trimethylnaphthalene
2164	40:24	172	172	Tetrahydrobenzoindan ?
2175	40:05	170	155	Trimethylnaphthalene
		186	186	unsym-Octahydroanthracene
2188	40:48	170	141	C3-naphthalene
		186		
2219	41:19	186	186	Methyltetrahydrobenzoindan
2247	41:47	170	155	Trimethylnaphthalene
2300	42:41	166	166	Fluorene
2310	42:51	168	168	Methylbiphenyl

Table 14 (continued)

2321	43:02	168	168	Methylbiphenyl
2365		186	186	Octahydroanthracene
2399	44:21	186	186	1,2,3,4,5,6,7,8-Octahydroanthracene
2472	45:35	186	186	1,2,3,4,5,6,7,8-Octahydrophenanthrene
2486	45:49	180	180	Methylfluorene
2510	46:13	200	200	Methyloctahydroanthracene or Methyloctahydrophenanthrene
2527	46:30	200	200	Methyloctahydroanthracene or Methyloctahydrophenanthrene
2561	47:05	184	184	Tetramethylnaphthalene
2579	47:23	212	212	C6-Naphthalene
2615	47:58	182	182	Tetrahydroanthracene or Tetrahydrophenanthrene

* Benzene eluted fraction 3; GC-MS File: SONG20014

the cycloalkane-rich JP-8C has remarkably higher thermal stability than JP-8P which is rich in long-chain paraffins.

In order to gain some insight into general features of fuel degradation, we performed ^1H NMR analysis of the stressed as well as the original JP-8C jet fuel samples. The spectra were recorded on the Bruker NMR spectrometer at the Chemistry Department of Pennsylvania State University. Figures 30-33 present the NMR spectra of the original JP-8C and thermally stressed JP-8C at 450°C for 0.5, 4 and 8 h, respectively. Table 15 gives the tentative assignments of the signals observed in ^1H NMR spectra of jet fuels based on our knowledge on the composition of original and thermally stressed jet fuels and the available literature information on NMR analysis of liquid fuels [5,6,7]. The original JP-8C has a spectrum with high intensity of signals in the region of 0.2-1.05, 1.05-1.60, and 1.60-2.00 ppm. The signals in the 1.5-2.0 ppm region are characteristic of the coal-derived JP-8C fuel, and the original petroleum-derived JP-8P does not show a peak in this range of chemical shift (Task 4). It is possible that the signals in this region are due mainly to trans-decalin, since it shows a strong signal band in 1.4-2.0 ppm [7]. The spectrum of stressed JP-8C at 450°C for 0.5 h (Figure 31) is similar to that of the original fuel (Figure 30). Extending the stressing time from 0.5 to 4 h caused significant change of the NMR spectrum (Figure 32). The intensity of aromatic hydrogens (6.0-9.2 ppm), paraffinic methyl hydrogens (0.2-1.05 ppm) and alpha-methyl hydrogens (2.00-2.60 ppm) increased significantly. Probably these changes are due to the cracking of long-chain paraffins present in JP-8C which corresponds to the decrease in methylene hydrogens and increase in methyl hydrogens (relative to methylene), cyclization and aromatization which corresponds to the increase in aromatic hydrogens (6.0-9.2 ppm). The increase in methyl hydrogens alpha to an aromatic ring (2.0-2.6 ppm) may be a result

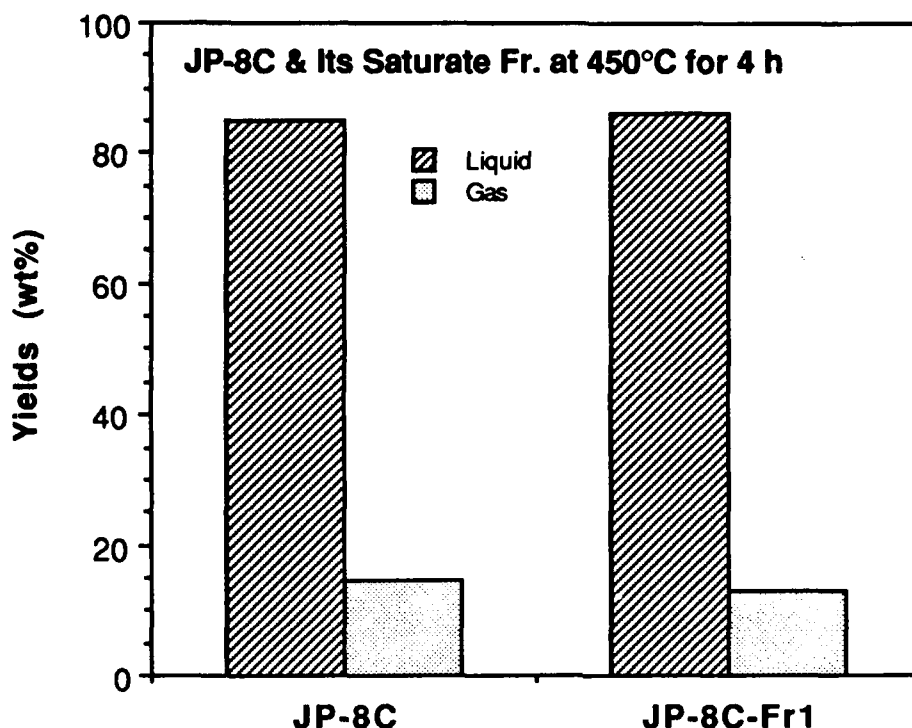


Figure 26. Liquid depletion and gas formation from JP-8C and its saturate fraction at 450°C.

of either dehydrogenation of methyl-substituted cycloalkanes or dealkylation of alkylaromatics. In fact, the intensity of alpha-methyl hydrogens further increased when the stressing time was extended to 8 h, as can be seen from Figure 32.

Clearly, the NMR spectra of the thermally stressed jet fuels show some progressive changes as a function of stressing time. These changes are related to the progressive changes observed from Figures 27 and 28. The extent of liquid depletion and liquid darkening gradually increased, and the yields of gases progressively rose with increasing residence time. The stressing for 0.5 and 1 h caused gas formation and some change in the composition of liquid phase, but there was no solid formation. The deposit formation began to be observed when the stressing time was extended to 4 h, where remarkable change in NMR spectrum of liquid products was observed. The precursors to deposits were formed and accumulated from the first four h. This may be considered as an induction period for solid formation from JP-8C at 450°C in N₂. Increasing the residence time to over 4 h caused the marked solid formation, which appeared to be parallel with the gas formation. This change from 4 to 8 h is accompanied by significant increase in

Table 14 (continued)

2321	43:02	168	168	Methylbiphenyl
2365		186	186	Octahydroanthracene
2399	44:21	186	186	1,2,3,4,5,6,7,8-Octahydroanthracene
2472	45:35	186	186	1,2,3,4,5,6,7,8-Octahydrophenanthrene
2486	45:49	180	180	Methylfluorene
2510	46:13	200	200	Methyloctahydroanthracene or Methyloctahydrophenanthrene
2527	46:30	200	200	Methyloctahydroanthracene or Methyloctahydrophenanthrene
2561	47:05	184	184	Tetramethylnaphthalene
2579	47:23	212	212	C6-Naphthalene
2615	47:58	182	182	Tetrahydroanthracene or Tetrahydrophenanthrene

* Benzene eluted fraction 3; GC-MS File: SONG20014

the cycloalkane-rich JP-8C has remarkably higher thermal stability than JP-8P which is rich in long-chain paraffins.

In order to gain some insight into general features of fuel degradation, we performed ^1H NMR analysis of the stressed as well as the original JP-8C jet fuel samples. The spectra were recorded on the Bruker NMR spectrometer at the Chemistry Department of Pennsylvania State University. Figures 30-33 present the NMR spectra of the original JP-8C and thermally stressed JP-8C at 450°C for 0.5, 4 and 8 h, respectively. Table 15 gives the tentative assignments of the signals observed in ^1H NMR spectra of jet fuels based on our knowledge on the composition of original and thermally stressed jet fuels and the available literature information on NMR analysis of liquid fuels [5,6,7]. The original JP-8C has a spectrum with high intensity of signals in the region of 0.2-1.05, 1.05-1.60, and 1.60-2.00 ppm. The signals in the 1.5-2.0 ppm region are characteristic of the coal-derived JP-8C fuel, and the original petroleum-derived JP-8P does not show a peak in this range of chemical shift (Task 4). It is possible that the signals in this region are due mainly to trans-decalin, since it shows a strong signal band in 1.4-2.0 ppm [7]. The spectrum of stressed JP-8C at 450°C for 0.5 h (Figure 31) is similar to that of the original fuel (Figure 30). Extending the stressing time from 0.5 to 4 h caused significant change of the NMR spectrum (Figure 32). The intensity of aromatic hydrogens (6.0-9.2 ppm), paraffinic methyl hydrogens (0.2-1.05 ppm) and alpha-methyl hydrogens (2.00-2.60 ppm) increased significantly. Probably these changes are due to the cracking of long-chain paraffins present in JP-8C which corresponds to the decrease in methylene hydrogens and increase in methyl hydrogens (relative to methylene), cyclization and aromatization which corresponds to the increase in aromatic hydrogens (6.0-9.2 ppm). The increase in methyl hydrogens alpha to an aromatic ring (2.0-2.6 ppm) may be a result

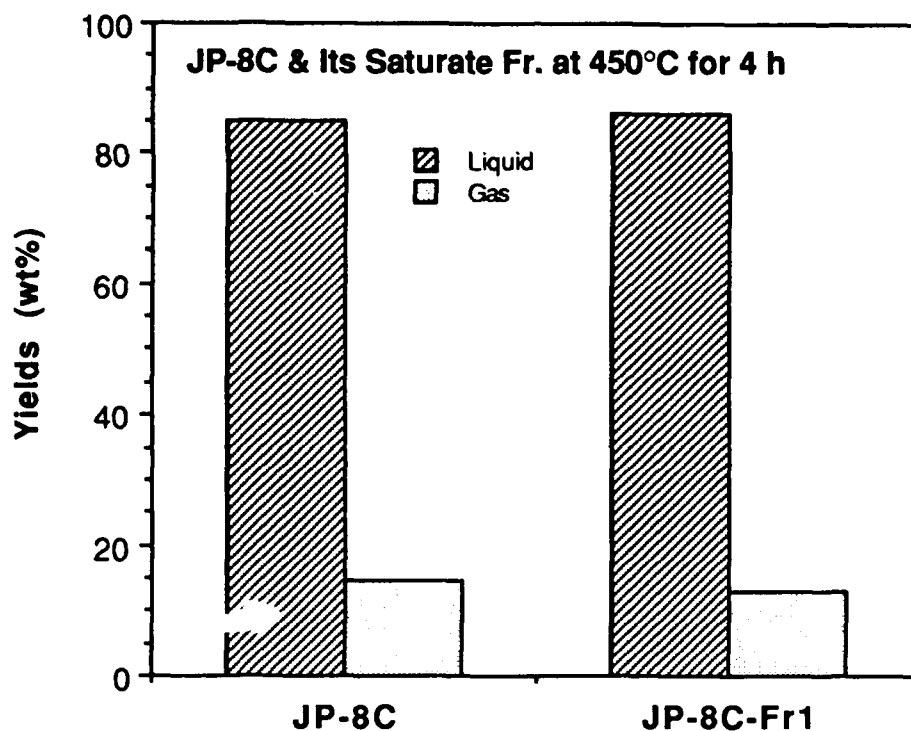


Figure 26. Liquid depletion and gas formation from JP-8C and its saturate fraction at 450°C.

of either dehydrogenation of methyl-substituted cycloalkanes or dealkylation of alkylaromatics. In fact, the intensity of alpha-methyl hydrogens further increased when the stressing time was extended to 8 h, as can be seen from Figure 32.

Clearly, the NMR spectra of the thermally stressed jet fuels show some progressive changes as a function of stressing time. These changes are related to the progressive changes observed from Figures 27 and 28. The extent of liquid depletion and liquid darkening gradually increased, and the yields of gases progressively rose with increasing residence time. The stressing for 0.5 and 1 h caused gas formation and some change in the composition of liquid phase, but there was no solid formation. The deposit formation began to be observed when the stressing time was extended to 4 h, where remarkable change in NMR spectrum of liquid products was observed. The precursors to deposits were formed and accumulated from the first four h. This may be considered as an induction period for solid formation from JP-8C at 450°C in N₂. Increasing the residence time to over 4 h caused the marked solid formation, which appeared to be parallel with the gas formation. This change from 4 to 8 h is accompanied by significant increase in

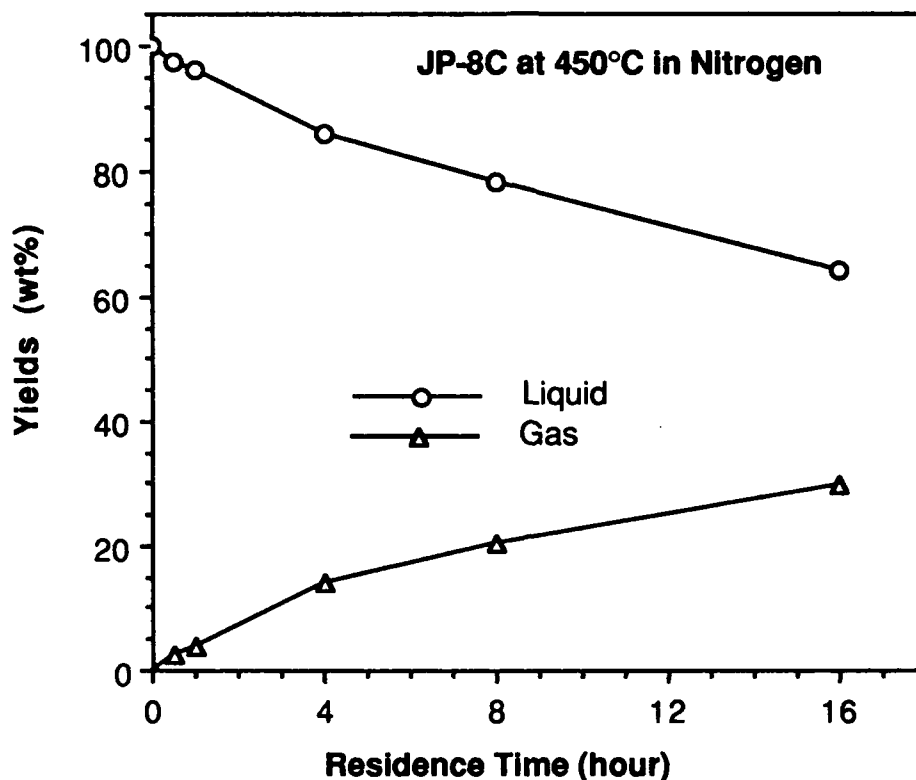


Figure 27. Liquid depletion and gas formation from coal-derived JP-8C versus the residence time at 450°C in a N₂ atmosphere

intensity of alpha methyl hydrogens (2.0-2.6 ppm) and aromatics (6.0-9.0 ppm) and decrease in paraffinic methyl and methylene hydrogens (0.5-1.6 ppm). At the present stage, the quantitative correlation between the NMR data and the above results is not yet found. However, while further detailed interpretation of the NMR spectra is needed, the NMR data revealed some features of molecular transformation of hydrocarbon components during the stressing of JP-8C fuel. More samples will be analyzed by NMR and quantitative calculations will be made in the future work.

In order to identify the thermally stable hydrocarbons, we analyzed the liquid products from JP-8C after stressing at 450°C for 0.5, 1 and 4 h, by GC-MS using split injection of undiluted sample. Figures 34-36 show the expanded retention time windows of the GC-MS profiles for the thermally stressed JP-8C. The window I in Figure 34 covers the compounds whose retention time is shorter than 16:53 min. The TIC in the top of Figure 13 is similar to that of

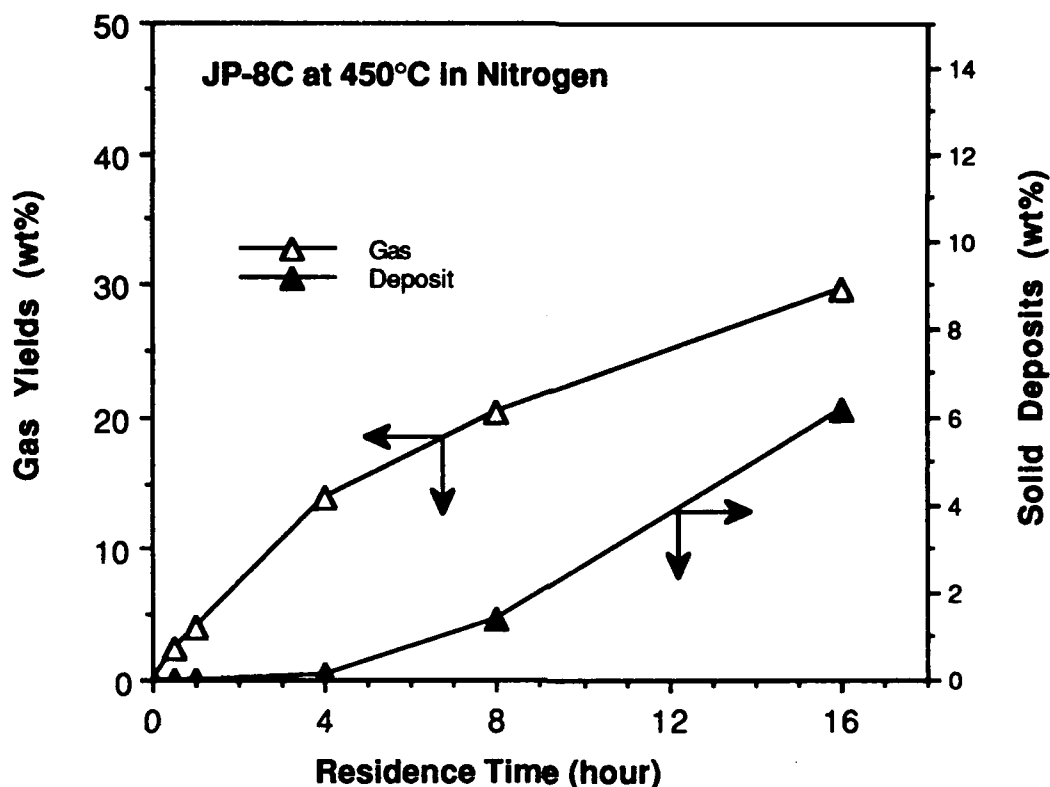


Figure 28. Thermal decomposition of coal-derived jet fuel JP-8C at 450°C to form gas and solid deposits.

the original JP-8C (Task 1). After 1 h stressing, the relative intensities of many peaks changed, and this trend becomes more remarkable after 4 h stressing.

The relative intensity of ethylcyclohexane (scan: 309, top TIC in Figure 34) decreased with increasing time from 0.5 to 4 h, as compared with dimethylcyclohexane (Scans: 206, 236 and 254). Similarly, relative to ethylmethylcyclohexane (scans: 399, 463, top TIC in Figure 34), the intensity of propylcyclohexane (scan: 524) progressively decreased. The same trend can be seen for the relative intensities of methylpropylcyclohexane and n-butylcyclohexane (this component is co-eluted with n-propylbenzene). Similarly, relative to methylcyclohexane, the intensity of ethyl- to butylcyclohexane decreased with increasing residence time. The concentration of trans-decalin also decreased with increasing time, as compared to methylcyclohexane. Although this suggests a lower stability of the former than the latter, it should be noted that the decreasing concentration of trans-decalin may be partly caused by dehydrogenation to form naphthalene. On the other hand, the

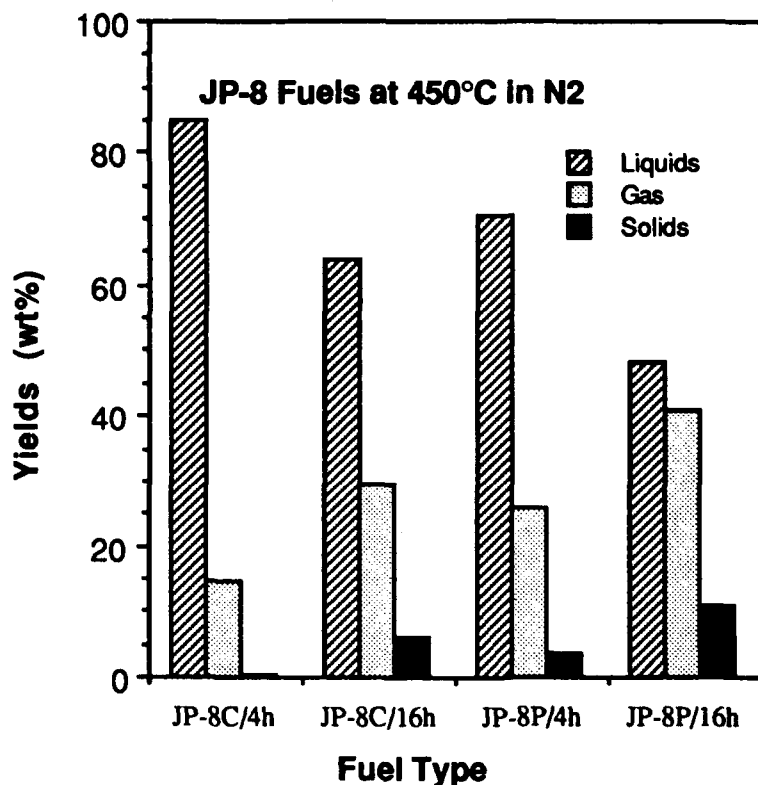


Figure 29. Thermal stability comparison between petroleum- and coal-derived JP-8 fuels.

stressing up to 4 h significantly increased the relative intensity of cyclohexane (Scan: 138), toluene (scan: 322), xylene (scans: 560, 650) and ethylmethyl or trimethylbenzene (scans: 820,908). It becomes clear from these results that at 450°C, the stability of alkylcyclohexanes decreases with increase in chain length, and multi-substituted cyclohexanes are more stable than the n-alkyl substituted cyclohexanes with the same carbon number.

Figures 35-36 covers the hydrocarbon components whose retention time is in the range of 16:54 to 33:43, and 24-45 min, respectively. The intensity of n-C₁₂ through n-C₁₇, cis-decalin, C₂-decalin, C₀ - to C₂-tetralins decreased with increasing residence time. After 1 h at 450°C, tetralin and 2-methyltetralin are still major peaks. However, they almost disappeared after 4 h. On the other hand, model compound studies using tetralin showed that it is quite stable when stressed



 BIOSERA

NAME STA
 DATE 6-3-91
 TS 302.134
 CI 5300.000
 C1 32765
 CO 32765
 CA 5300.000
 NZ/FT 305
 PW 17.0
 CD 5.000
 AD 3.277
 RB 8
 TS 16
 TE 297
 FM 5300
 G2 12100.000
 DE 10L P0
 LB 0.0
 LB 0.0
 LX 40.00
 LY 0.0
 F1 9.001P
 F2 9.999P
 MZ/CM 90.027
 PPM/CM 250
 SR 3981.00

JP 8C ORIGINAL

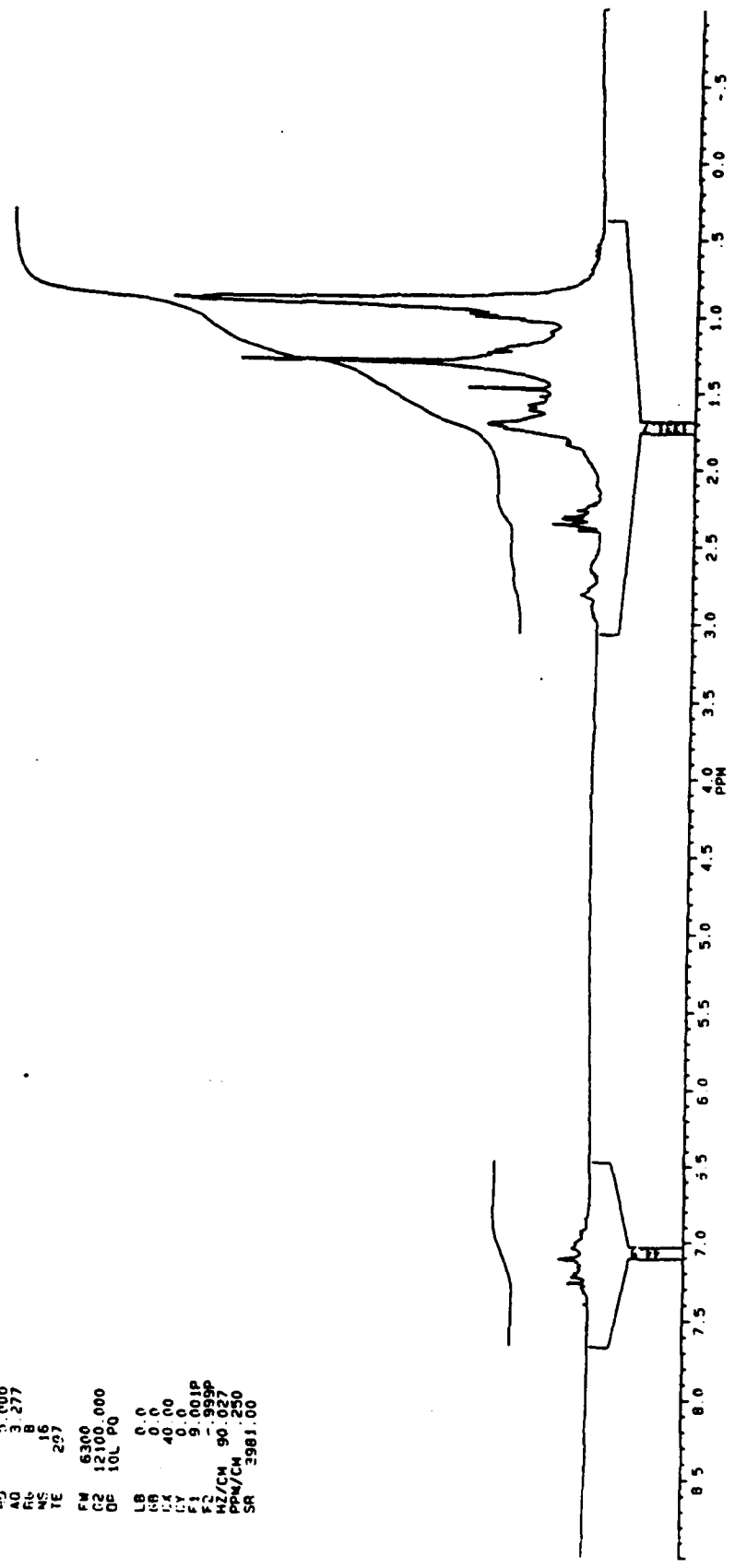


Figure 30 ¹H NMR spectrum of the original, coal-derived JP-8C fuel.

1	2	3	4	5	6	7	8	9	10	11	12	13	14	15	16	17	18	19	20	21	22	23	24	25	26	27	28	29	30	31	32	33	34	35	36	37	38	39	40	41	42	43	44	45	46	47	48	49	50	51	52	53	54	55	56	57	58	59	60	61	62	63	64	65	66	67	68	69	70	71	72	73	74	75	76	77	78	79	80	81	82	83	84	85	86	87	88	89	90	91	92	93	94	95	96	97	98	99	100
1	2	3	4	5	6	7	8	9	10	11	12	13	14	15	16	17	18	19	20	21	22	23	24	25	26	27	28	29	30	31	32	33	34	35	36	37	38	39	40	41	42	43	44	45	46	47	48	49	50	51	52	53	54	55	56	57	58	59	60	61	62	63	64	65	66	67	68	69	70	71	72	73	74	75	76	77	78	79	80	81	82	83	84	85	86	87	88	89	90	91	92	93	94	95	96	97	98	99	100

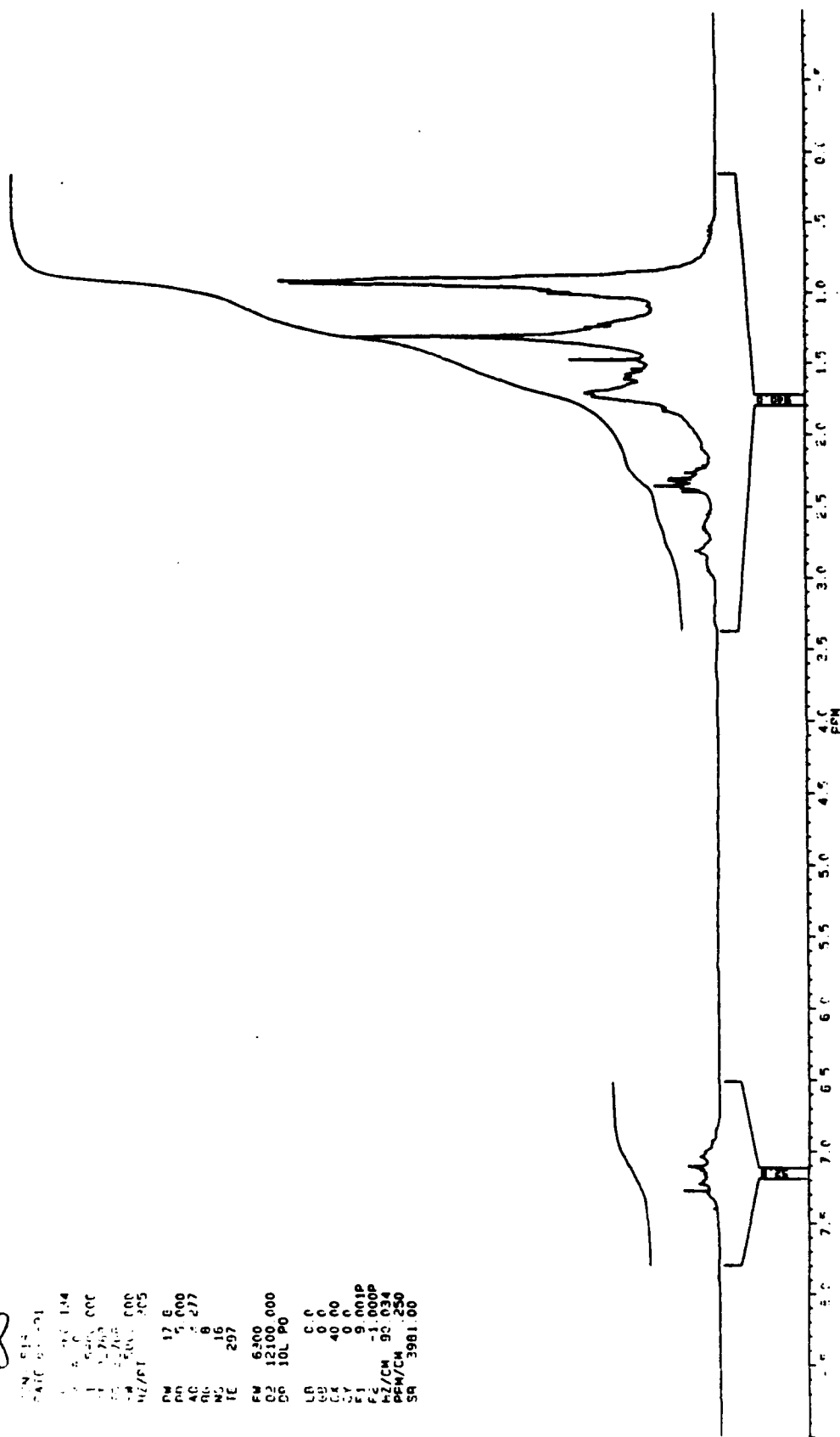


Figure 31 ^1H NMR spectrum of the thermally stressed JP-8C at 450°C for 0.5 h.

JP-8C 450 MHz

~~DP-8C~~
 NAME: JP-8C
 DATE: 05-01-71
 F1 124
 F2 5500.000
 F3 3269
 F4 3228
 F5 5500.000
 WZ/PI 305
 F4 17.6
 F5 5.000
 AC 3.277
 PC 8
 TE 16
 TE 297
 F4 5300.000
 F5 12100.000
 DP 10L P0
 LB 0.0
 CB 0.0
 CX 40.00
 CY 0.0
 F1 9.001P
 F2 -100P
 WZ/CM 81.932
 PH/CM 228
 SQ 3981.00

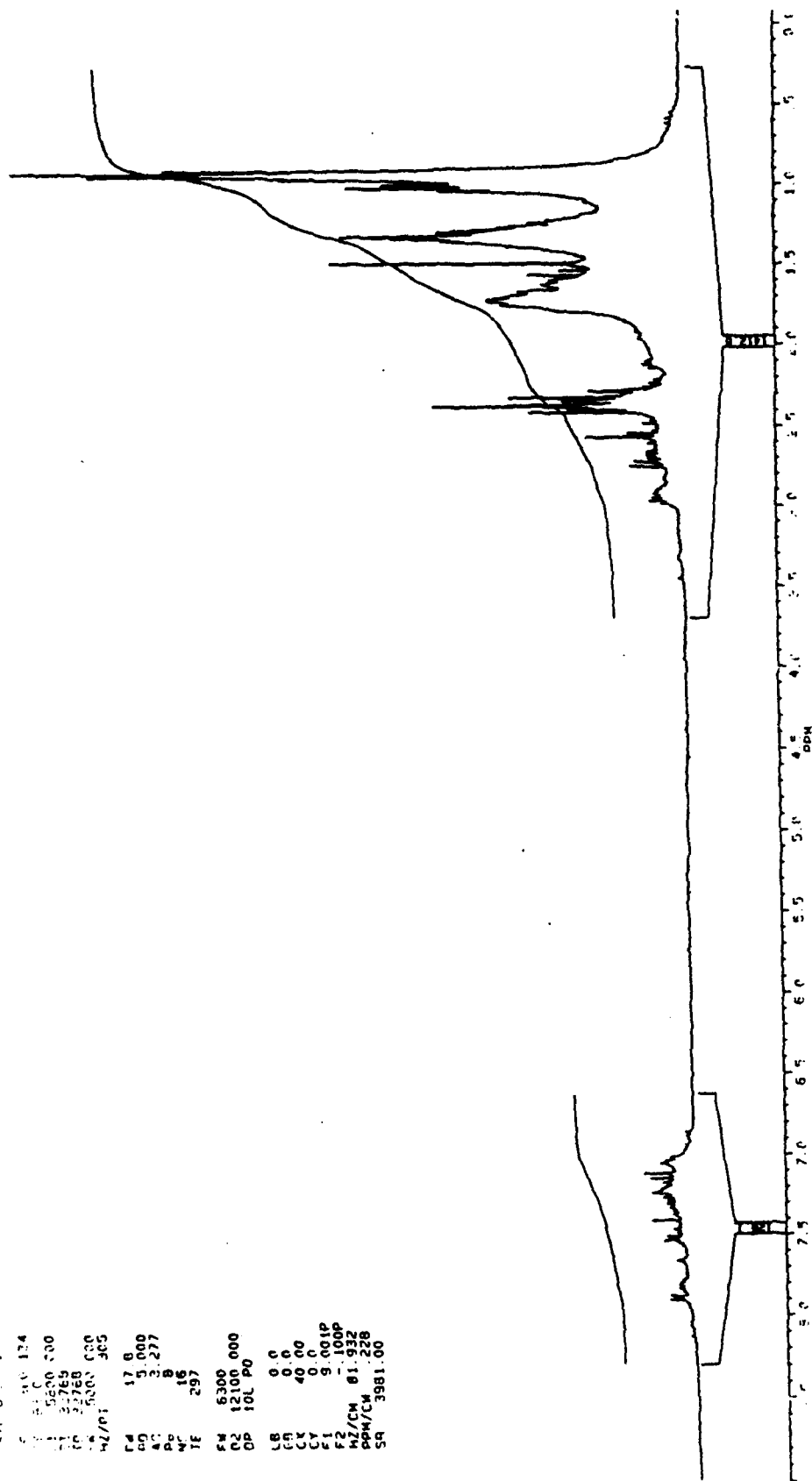


Figure 32 ^1H NMR spectrum of the thermally stressed JP-8C at 450°C for 4 h.

PM	17 B
PH	5 000
AD	8 277
MC	16
FE	297
FM	5 500
DZ	12100 000
OP	10L P0
L8	0 0
G0	0 0
C4	40 00
LY	0 0
F1	9 000P
M2	1 000P
FZ	90 R34
CM/CM	250
PQ	3981 00

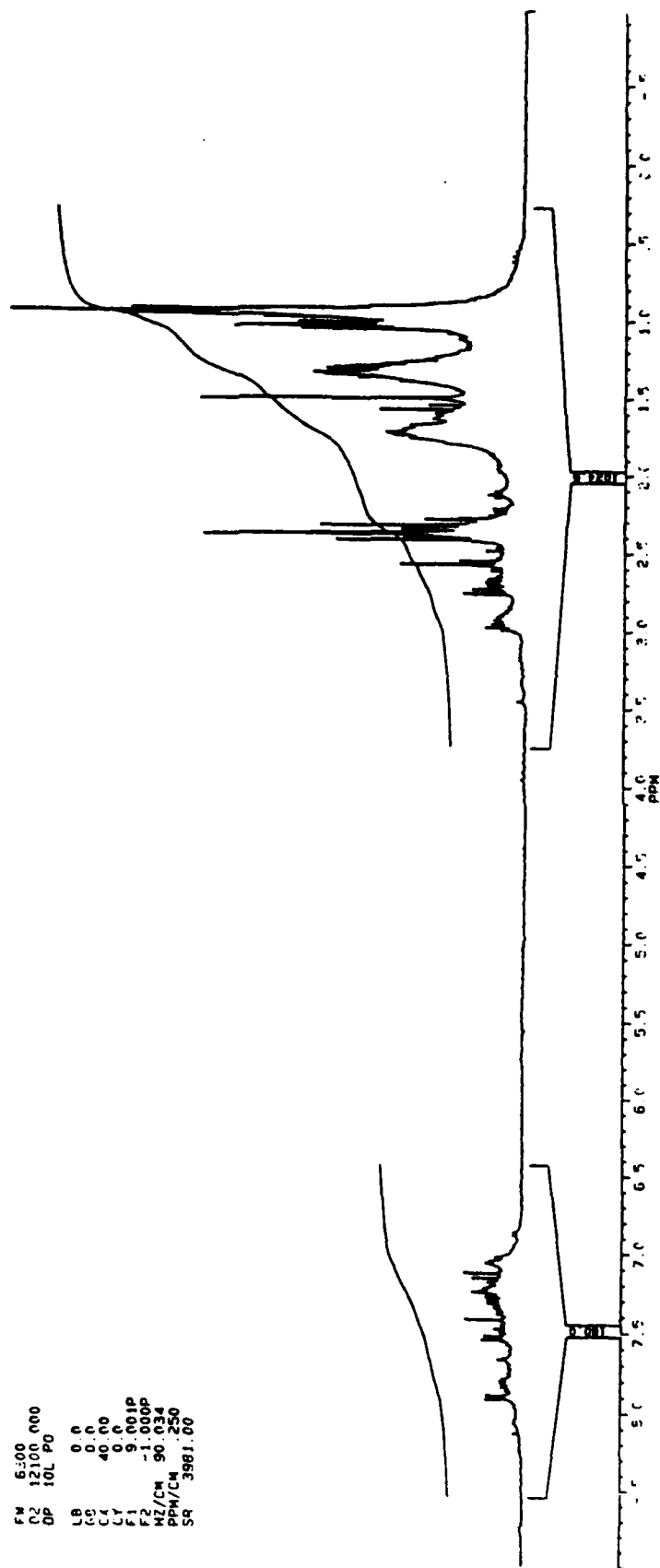


Figure 33 ^1H NMR spectrum of the thermally stressed JP-8C at 450°C for 8 h.

Table 15 Tentative assignments of ^1H NMR spectra of jet fuels

6.00-9.00	Ar-H*	Aromatics
5.55-6.00	R-CH*=CH ₂	External Olefin
5.30-5.55	R-CH*=CH*-R'	Internal Olefin
5.05-5.30	R(R')-C=CH*-R'	Internal Olefin
4.75-5.05	R-CH=CH ₂ *	External Olefin
4.50-4.75	R(R')-C=CH ₂ *	External Olefin
3.40-4.50	Ar-CH ₂ *-Ar	Alpha Methylene
2.60-3.40	Ar-CH ₂ *-R	Alpha Methylene
2.00-2.60	Ar-CH ₃ *	Alpha Methyl
1.05-2.00	R-CH ₂ *-R	Paraffinic Methylene
	Ar-CH ₂ -CH ₃ *	Beta Methyl ^{a)}
	Ar-(CH ₂) ₂ -(CH ₂) _n *-CH ₃	Gamma Methylene ^{a)}
	Ar-CH ₂ -CH ₂ *-R	Beta Methylene ^{b)}
0.50-1.05	R-(CH ₂) _n -CH ₃ *	Paraffinic Methyl
	Ar-(CH ₂) _n -CH ₃ *	Gamma or Terminal Methyl

a) Most beta-methyl and gamma-methylene hydrogens show signals in 1.05-1.60 ppm.

b) Most beta-methylene hydrogens show signals in 1.60-2.00 ppm.

alone [1]. Surprisingly, the intensity of bicyclohexyl also decreased with increasing residence time, and almost disappeared after 4 h. The intensity of octahydrophenanthrene or octahydroanthracene decreased with increasing time from 1 to 4 h. On the other hand, the concentration of aromatics in the liquid products continued to increase. It is clear from Figures 35-36 that after 4 h, naphthalene, 2-methylnaphthalene, 1-methylnaphthalene and dimethylnaphthalene become the major components in this retention time range. It is likely that naphthalenes were formed in part from tetralins. The reactive radicals can abstract hydrogens from tetralin, producing naphthalene. The H-donation by tetralin is considered to be an important reaction which may have contributed to

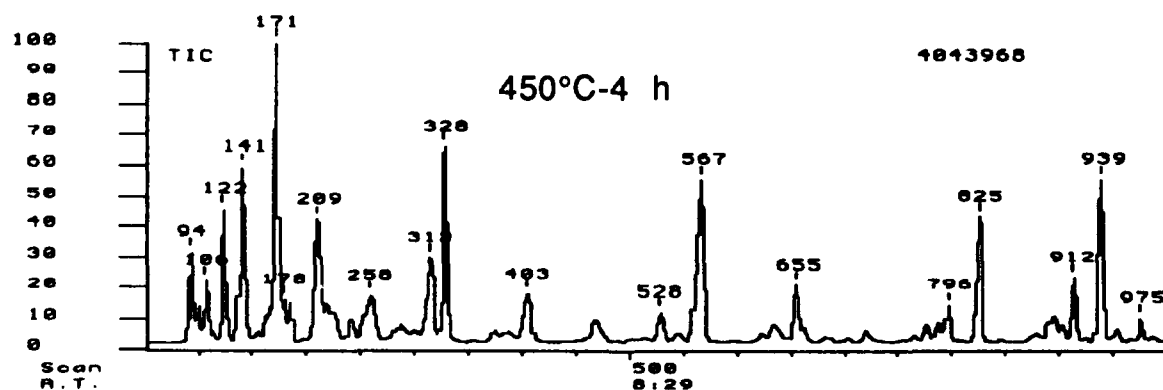
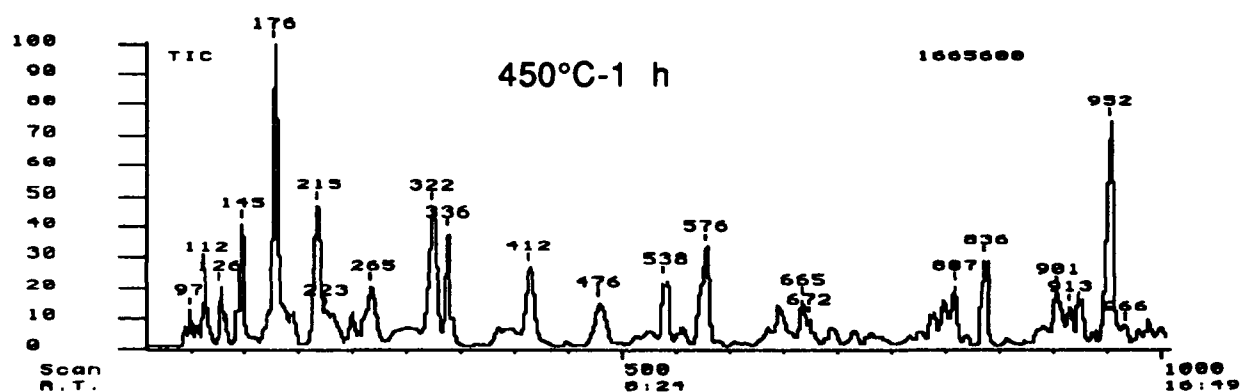
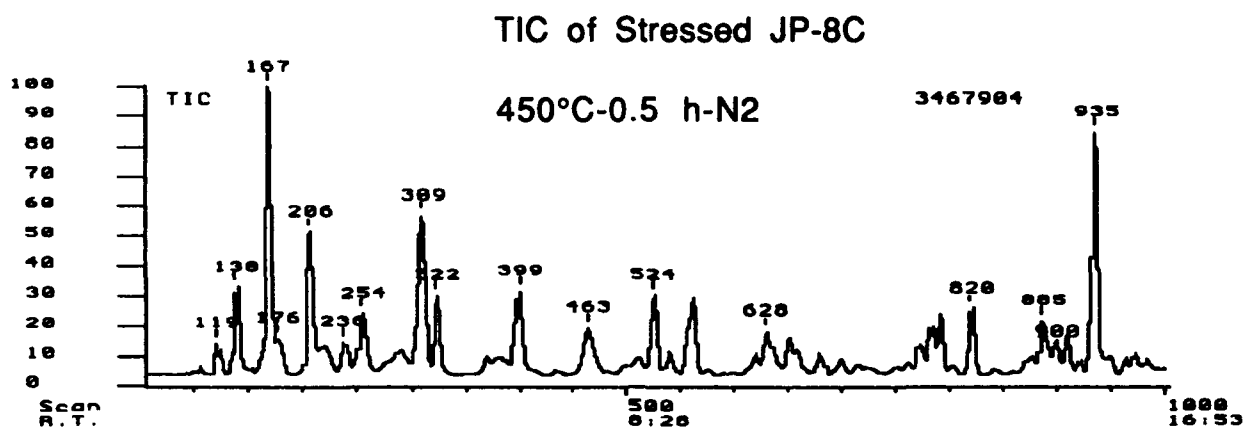


Figure 34 Retention time window I (1-16:53 min) of GC-MS profiles for thermally stressed, coal-derived JP-8C fuel for 0.5, 1 and 4 h.

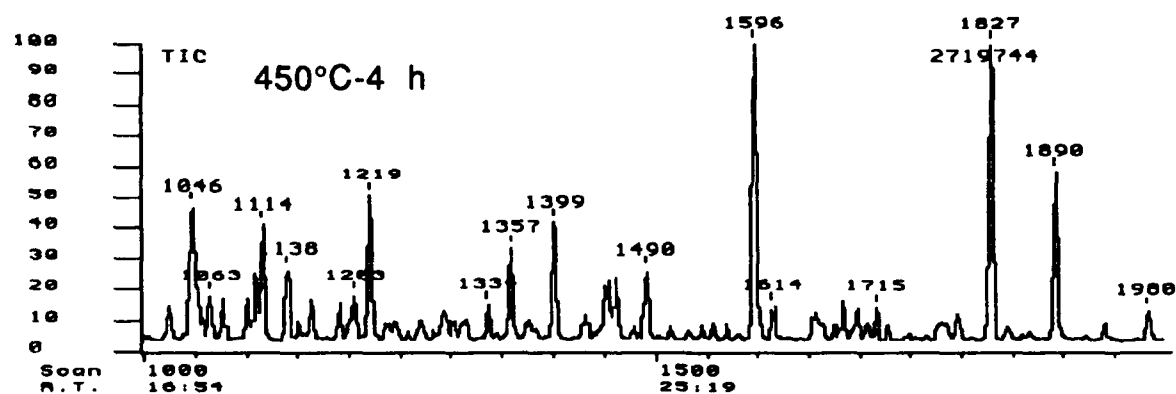
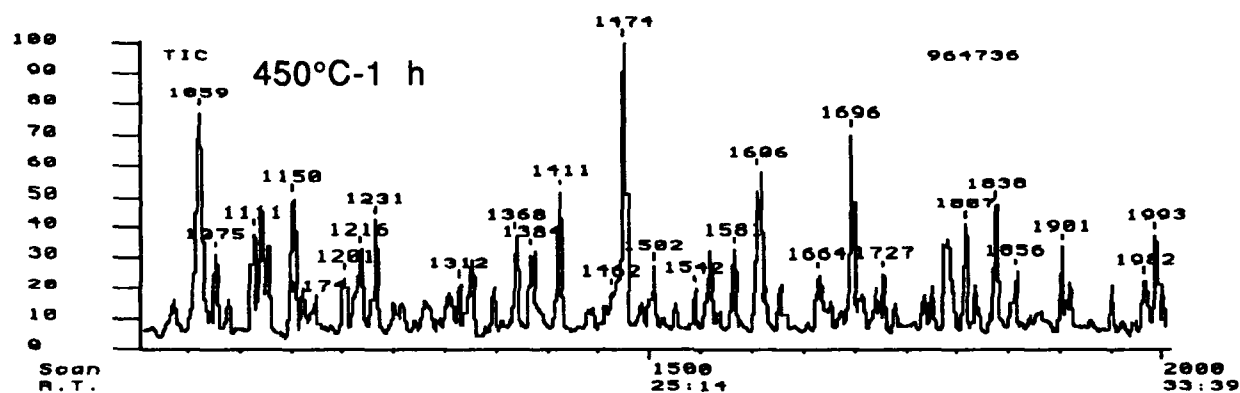
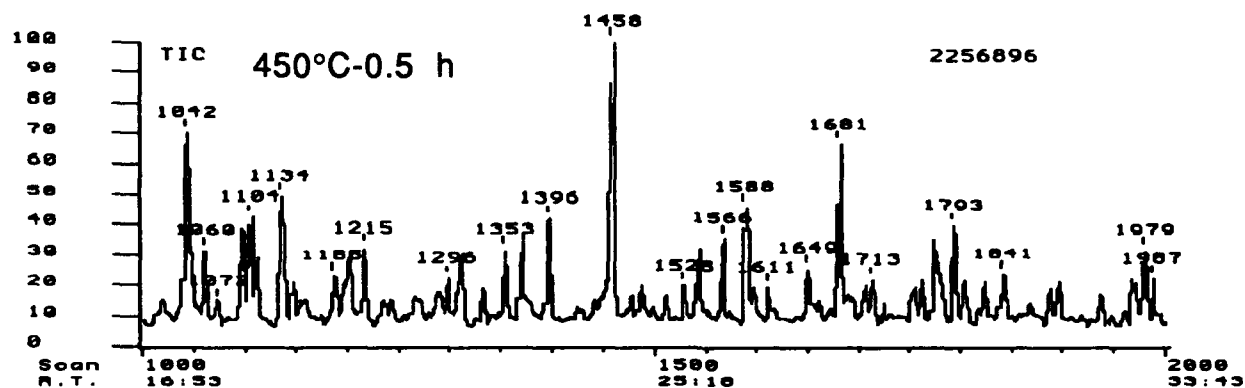


Figure 35 Retention time window II (16:54-33:43 min) of GC-MS profiles for thermally stressed, coal-derived JP-8C fuel for 0.5, 1 and 4 h.

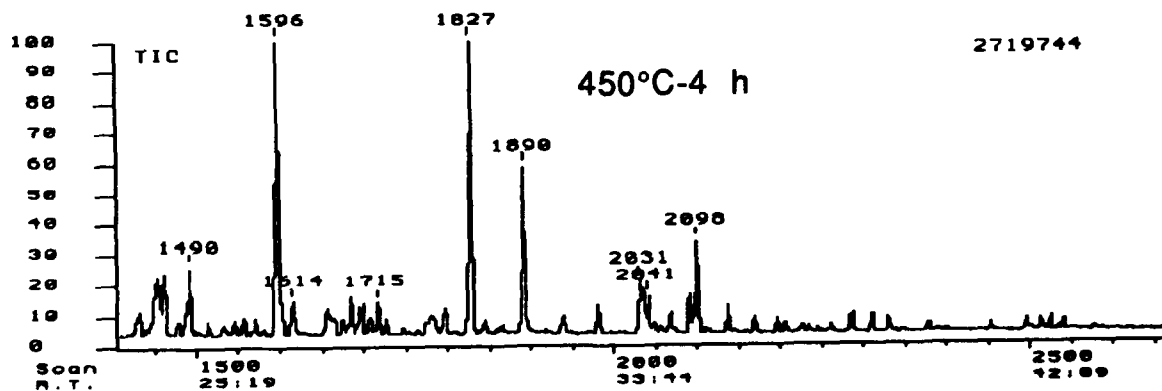
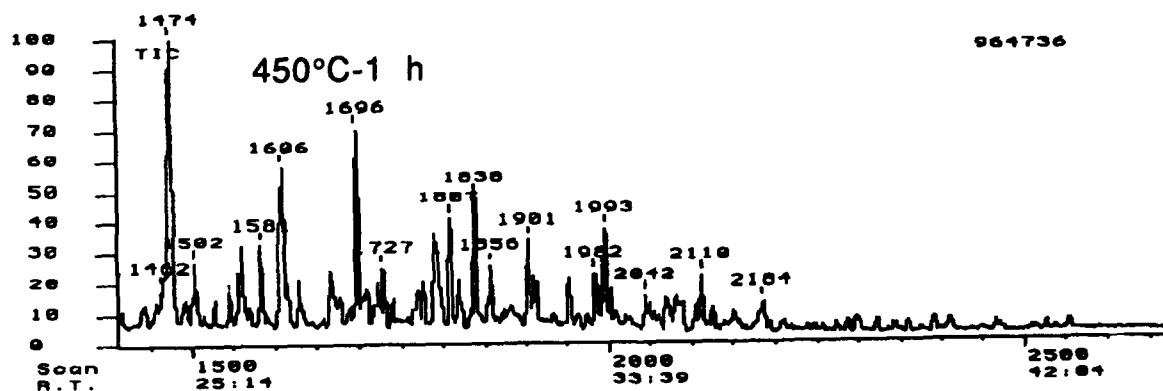
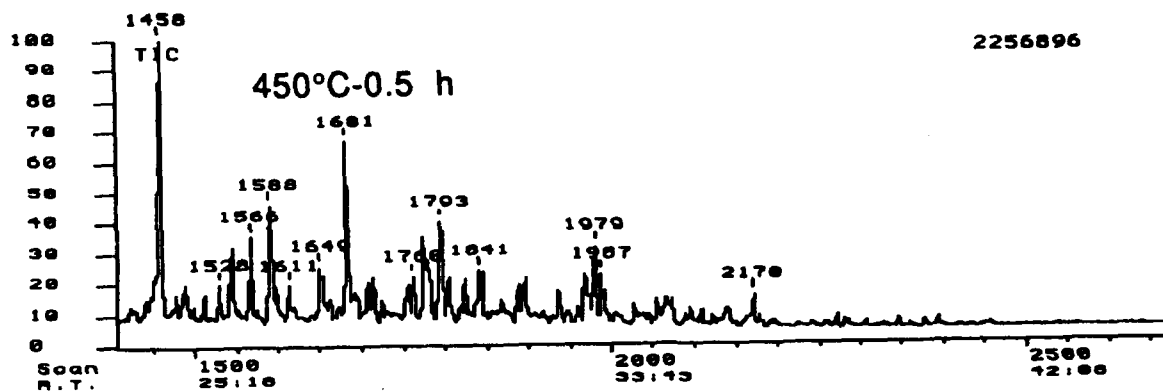


Figure 36 Retention time window III (24-45 min) of GC-MS profiles for thermally stressed, coal-derived JP-8C fuel for 0.5, 1 and 4 h.

suppressing solid formation from JP-8C fuel, as compared to petroleum-derived JP-8P which shows a higher solid-forming tendency under comparable conditions. Some additional changes can be seen from Figure 36 (24-45 min).

The comparative examination by GC-MS of stressed JP-8C using expanded retention time windows provided valuable information on the thermal stability ranking of hydrocarbon components in JP-8C. In general, the stability of the cycloalkanes is higher than long-chain paraffins present in JP-8C. Among the cycloalkanes, the most stable components are methylcyclohexane, dimethylcyclohexane, and trans-decalin (major components in JP-8C) as well as cyclohexane (present in JP-8C in much lower concentration relative to the above components). It also appears that the stability of cycloalkanes decreases with increase in ring-size, namely cyclohexane > decalin > octahydrophenanthrene or octahydroanthracene. Tetralin and methyltetralins are the major components in original and in stressed JP-8C at 450°C for 1 h, but they almost disappear after 4 h. This seems to be a result of their H-donation to some reactive radicals, which may have contributed to suppressing the undesirable reactions. The above results are for the stressing up to 4 h. For comparison, Figure 37 and Table 16 give the GC-MS results for the liquid products from JP-8C thermally stressed at 450°C for 16 h. Relative to the liquid products from 4 h stressing (Figures 34-36), there is remarkable change in the liquid composition, and the number of components in liquids became smaller after 16 h stressing. As would be expected, the liquid product from long time stressing is highly aromatic and contains many polyaromatic hydrocarbons. Among the aromatic products, the alkylbenzenes, indans, and naphthalenes are the major components. An apparent structural feature is that they are mainly multi-substituted when the carbon number in alkyl groups is equal to or larger than two, indicating that multi-substituted aromatics are more stable than the corresponding normal alkylaromatics, and the n-alkylaromatics with shorter chains are more stable than those with longer chains. In regard to the thermal stability of the aliphatic components, an important fact from Figure 37 and Table 16 is that cyclohexane, methylcyclohexane, dimethylcyclohexane and trans-decalin still exist, although their concentrations are lower than the aromatic products. All the other major components that were present in the original JP-8C have disappeared after 16 h.

DS90 Chromatogram report Run: SONG670006, 17-Jan-91 12:52
JP-8C 5ml 450oC-N2-16h SPLIT DB-17 40-5 TO 280-10e4 0.1 UL

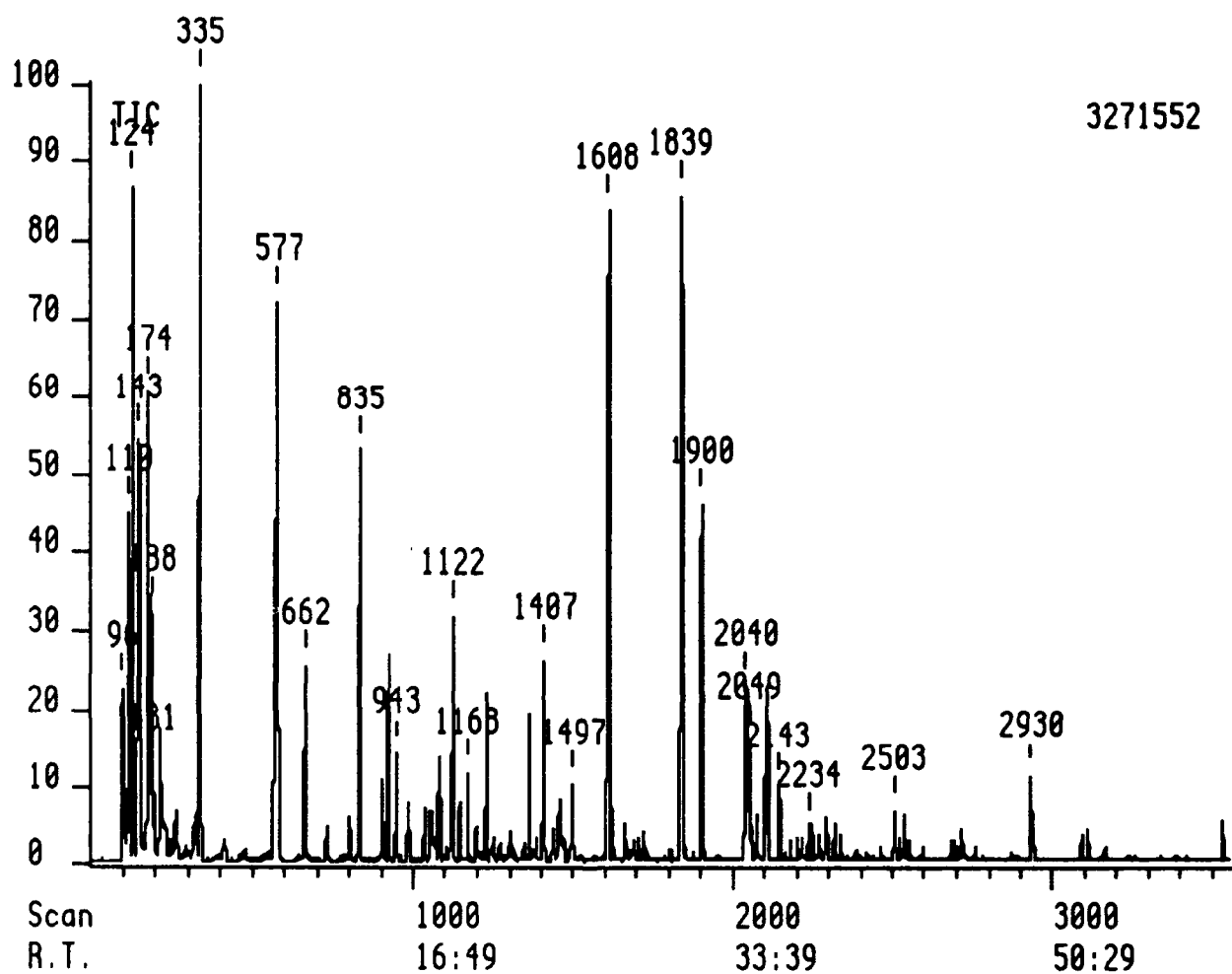


Figure 37. Total ion chromatogram of liquids from thermally treated whole JP-8C at 450°C for 16 h in N₂

Table 16. Identified compounds in thermally treated JP-8C at 450°C for 16 h. in N₂ by GC-MS using modified procedure

Scan No.	Retention Time	Molecular Ion	Base Peak	Compounds Identified
96	1:36	72	43	n-Pentane
124	2:04	84	56	Hexene
143	2:23	84	56	Cyclohexane
		98	56	1-Hexene
174	2:55	98	83	Methylocyclohexane
188	3:09	78	78	Benzene
213	3:34	112	97	Dimethylcyclohexane
335	5:37	92	91	Toluene
577	9:42	106	91	p-Xylene
662	11:07	106	91	o-Xylene
803	13:30	120	91	n-Propylbenzene
835	14:02	120	91	C3-benzene
902	15:10	120	91	C3-benzene
920	15:28	120	91	C3-benzene
943	15:51	138	138	trans-Decalin
982	16:31	134	119	C4-benzene
1030	17:19	120	105	C3-benzene
1057	17:46	134	105	C4-benzene
1062	17:51	134	105	C4-benzene
1069	17:58	134	119	C4-benzene
1082	18:12	134	119	C4-benzene
1122	18:52	118	117	Indan
1145	19:15	134	119	C4-benzene
1168	19:38	134	119	C4-benzene
1226	20:37	132	117	Methylindan
1364	22:56	132	117	Methylindan

Table 16 (continued)

1407	23:40	132	117	Methylindan
1460	24:33	146	131	C2-indan
1497	25:11	146	131	C2-indan
1608	27:03	128	128	Naphthalene
1621	27:16	146	131	C2-indan or Methyltetralin
1839	30:56	142	142	2-Methylnaphthalene
1900	31:58	142	142	1-Methylnaphthalene
2040	34:19	156	141	2-Ethylnaphthalene
2049	34:28	156	156	Dimethylnaphthalene
2055	34:34	154	154	Biphenyl
2074	34:54	156	141	1-Ethylnaphthalene
2098	35:18	156	156	Dimethylnaphthalene
2107	35:27	156	156	Dimethylnaphthalene
2143	36:03	170	155	C3-naphthalene
		156	156	Dimethylnaphthalene
2234	37:35	170	155	C3-naphthalene
2318	39:00	154	154	Acenaphthene
2503	42:07	166	166	Fluorene
2532	42:36	168	168	Methylacenaphthene ?
2930	49:18	178	178	Phenanthrene
3087	51:57	192	192	Methylphenanthrene
3106	52:16	192	192	Methylphenanthrene
3533	59:27	202	202	Pyrene

** GC-MS File: SONG670006, Split injection of undiluted sample without delay

Task 3. Identification and Characterization of Stable Hydrocarbon Species Present in Petroleum-derived Fuels.

The objective of Task 3 is to study the thermal stability of hydrocarbon species present in petroleum-derived jet fuels.

Activity 1. Identification of Hydrocarbon Species

In this task, three petroleum-derived jet fuels including Jet A-1, JP-7P and JP-8P were analyzed by GC-MS (Kratos MS80 system) using a modified procedure described in Task 1. The samples of JP-7P and Jet A-1, which contain no additives, were provided by WPAFB. Figures 38-40 show the specific ion chromatograms (SIC) of JP-8P, JP-7P and Jet A-1, respectively. The peaks in the SIC at m/z 71 correspond to all of the main peaks and many of the minor peaks in the TIC of JP-8P, JP-7P and Jet A-1. These results indicate that the major components in these petroleum-derived fuels are long-chain paraffins, while the coal-derived JP-8C is rich in cycloalkanes (Task 1). A number of minor peaks are those of cycloalkanes (SIC at m/z 81-83), alkylbenzenes (m/z 91-92) and alkylnaphthalenes (m/z 141-142). The aromatic components include C₁ - through C₈-benzenes and C₀- to C₃ -naphthalenes. The concentrations of these compounds in the petroleum-derived JP-8P are higher than in coal-derived JP-8C.

Figures 41-43 present the TIC together with the identity of major components of JP-8P, JP-7P and Jet A-1, respectively. It is clear from the TIC and SIC in Figures 38-43 that all these petroleum-derived jet fuels are composed mainly of long-chain paraffins, together with small concentrations of cycloalkanes, alkylbenzenes and alkylnaphthalenes. Identification of the mass spectra revealed that JP-8P has a wide C-number distribution of components ranging from C₈ to C₁₇. According to the literature [8], commercial Jet A-1 fuel is a kerosine fuel very similar to JP-8 (Nato F-34), and the properties of JP-8 are selected to be identical to those of commercial Jet A-1. However, comparison of Figure 43 with Figure 41 showed that there are apparent compositional differences between the JP-8P (received on 5-30-90) and Jet A-1 (dated 11-13-90, Tank S-7 in WPAFB) samples received from WPAFB. Relative to JP-8P, Jet A-1 has a narrow distribution of components ranging from C₁₀ (decane) to C₁₃ (tridecane). It is not yet clear that whether this sample is representative of all the commercial Jet A-1 fuels. The GC-MS results in Figure 42 showed that JP-7P is composed mainly of long-chain paraffins ranging from C₁₁ (undecane) to C₁₅ (pentadecane), in which the concentrations of aromatics are much lower than those in JP-8P (Figure 42). According to the summary report on military jet fuels [8], JP-7 is not a distillate fuel as are most other jet fuels but is composed of special blending stocks that have been subjected to special processes to remove aromatics. The comparative examination of Figure 43 with Figure 42 showed that JP-7P is relatively similar to Jet A-1, in that the components are distributed in a narrower C-

DS90 Chromatogram report Run: SONG660008, 19-Dec-90 17:34
SONG JP-8P SPLIT 0.04 UL DB-17 40-5 TO 280-10 AT 4 KRA MS80

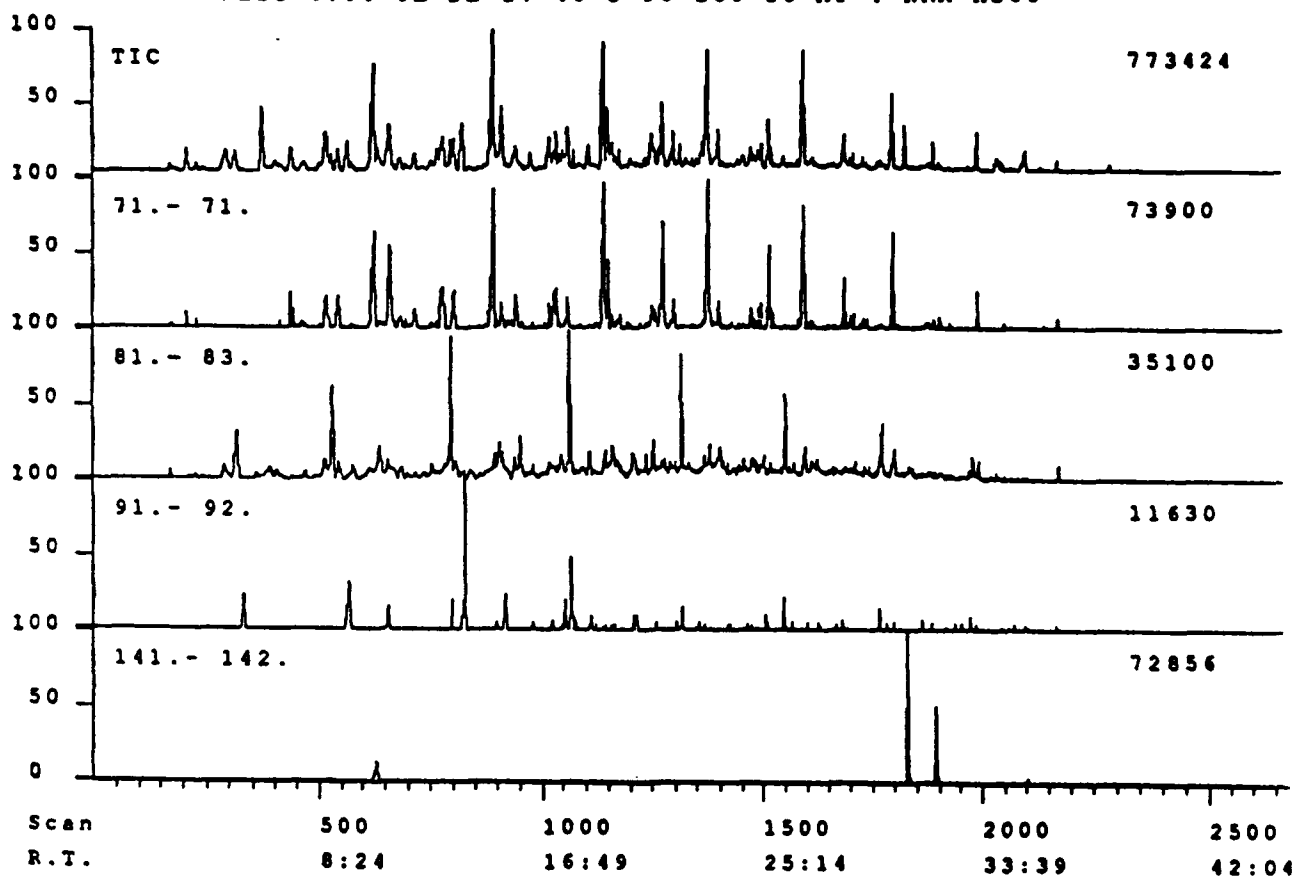


Figure 38. Specific ion chromatograms of petroleum-derived JP-8P from GC-MS using split injection of undiluted sample.

DS90 Chromatogram report Run: SONG660003, 18-Dec-90 13:05
SONG JP-7P SPLIT 0.04 UL DB-17 40-5 TO 280-10 AT 4 KRA MS80

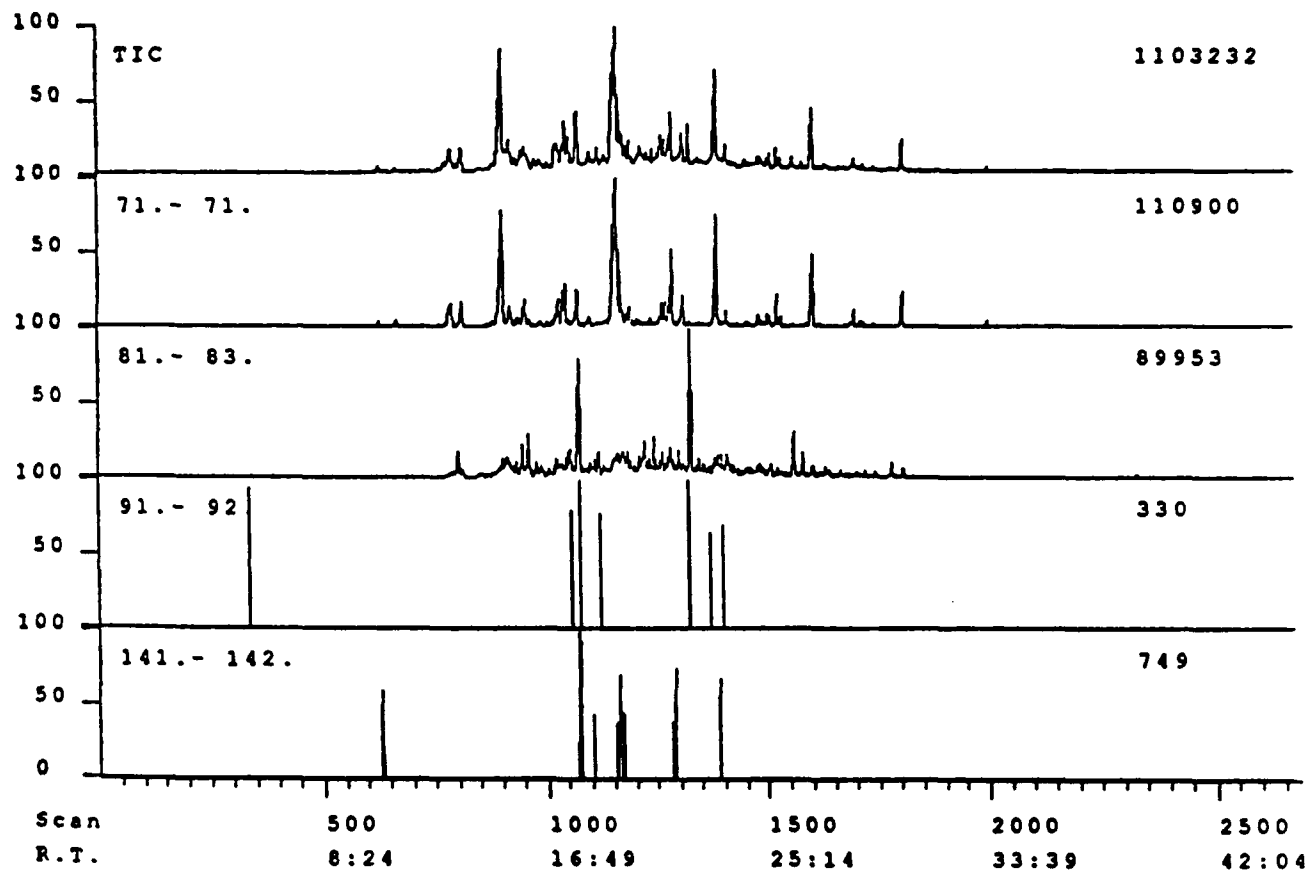


Figure 39. Specific ion chromatograms of petroleum-derived JP-7P from GC-MS using split injection of undiluted sample.

DS90 Chromatogram report Run: SONG660004, 18-Dec-90 14:41
SONG JET A-1/NEW SPLIT 0.04 UL DB-17 40-5 TO 280-10 AT 4 MS

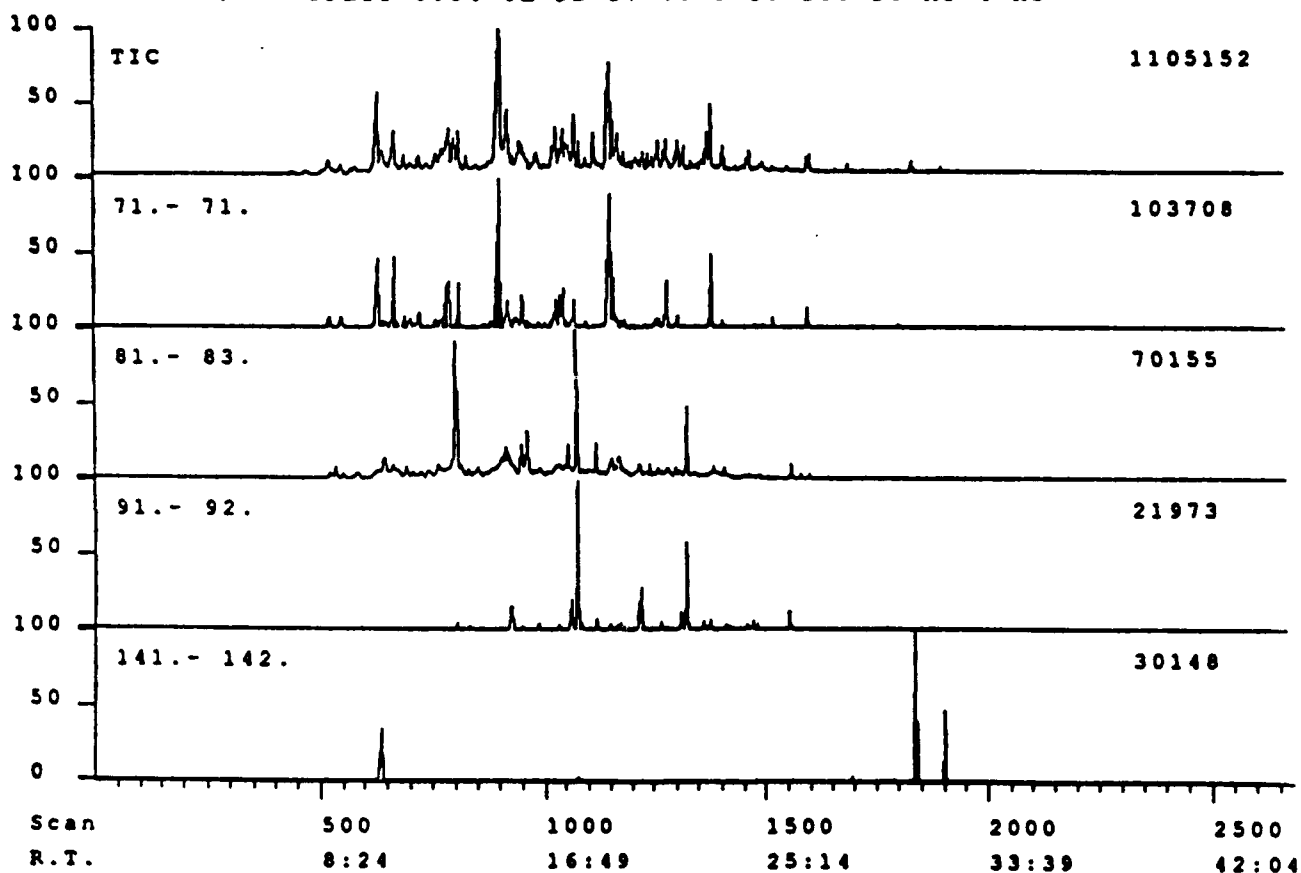


Figure 40. Specific ion chromatograms of petroleum-derived Jet A-1 from GC-MS using split injection of undiluted sample.

DS90 Chromatogram report Run: SONG660008, 19-Dec-90 17:34
SONG JP-8P SPLIT 0.04 UL DB-17 40-5 TO 280-10 AT 4 KRA MS80

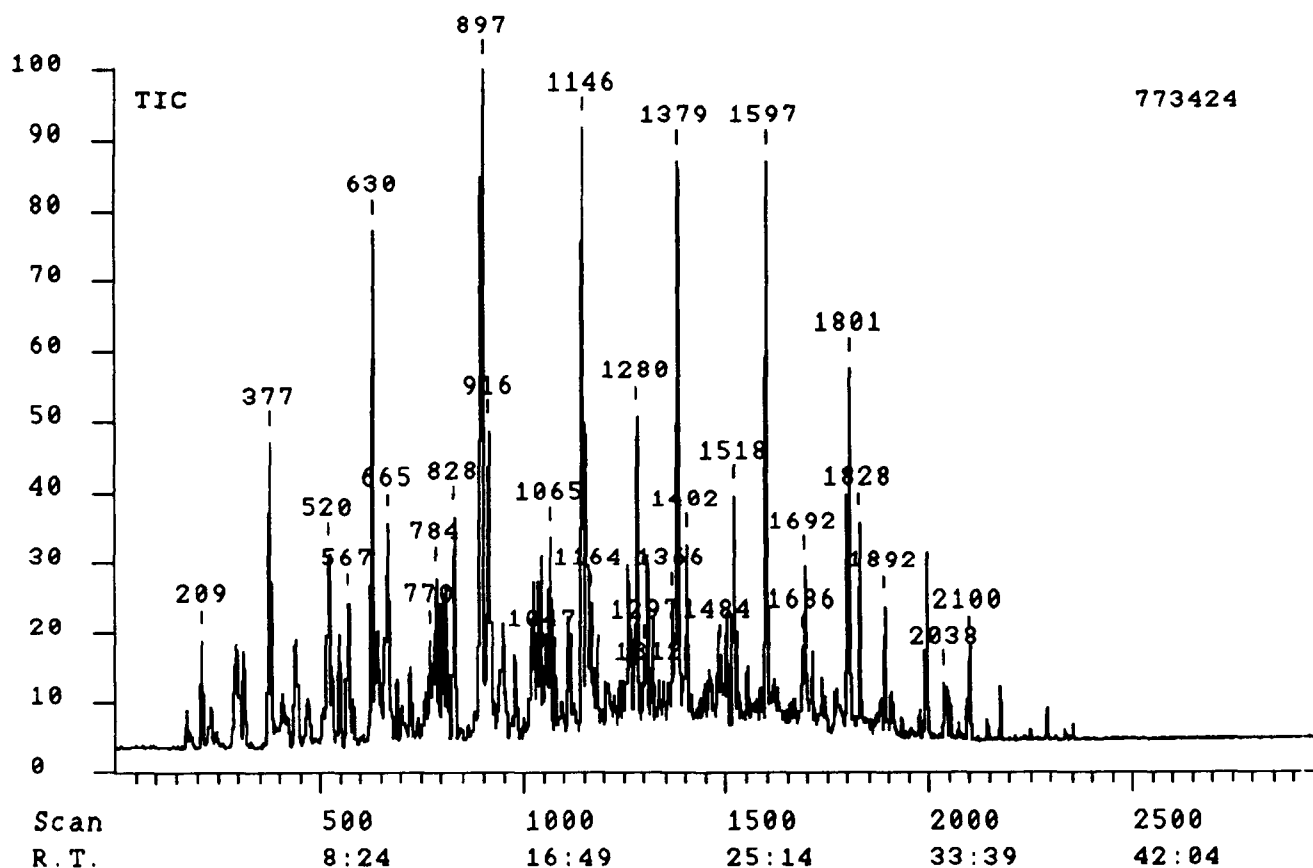


Figure 41. Total ion chromatograms of petroleum-derived JP-8P from GC-MS using split injection of undiluted sample.

DS90 Chromatogram report Run: SONG660003, 18-Dec-90 13:05
SONG JP-7P SPLIT 0.04 UL DB-17 40-5 TO 280-10 AT 4 KRA MS80

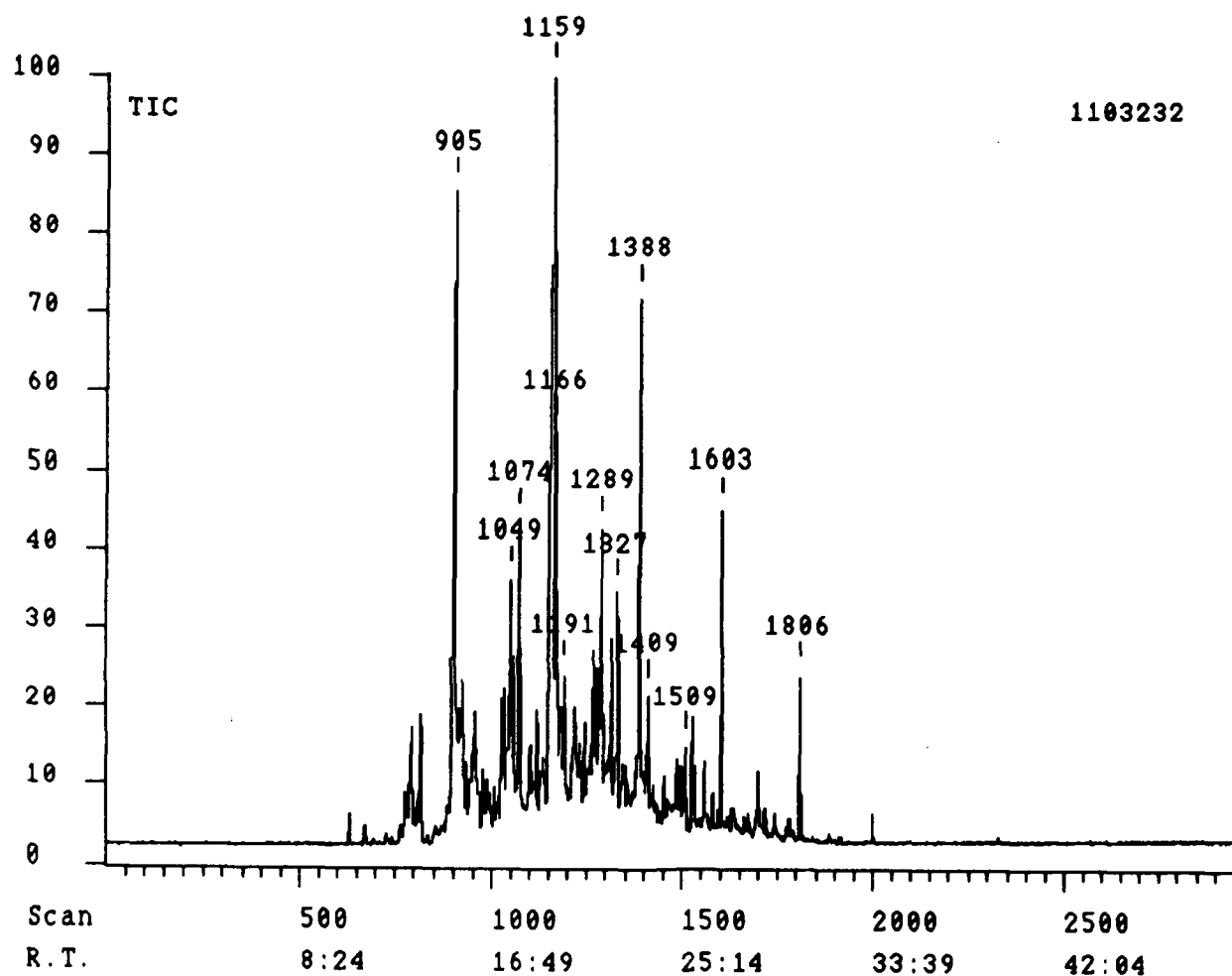


Figure 42. Total ion chromatograms of petroleum-derived JP-7P from GC-MS using split injection of undiluted sample.

DS90 Chromatogram report Run: SONG660004, 18-Dec-90 14:41
SONG JET A-1/NEW SPLIT 0.04 UL DB-17 40-5 TO 200-10 AT 4 MS

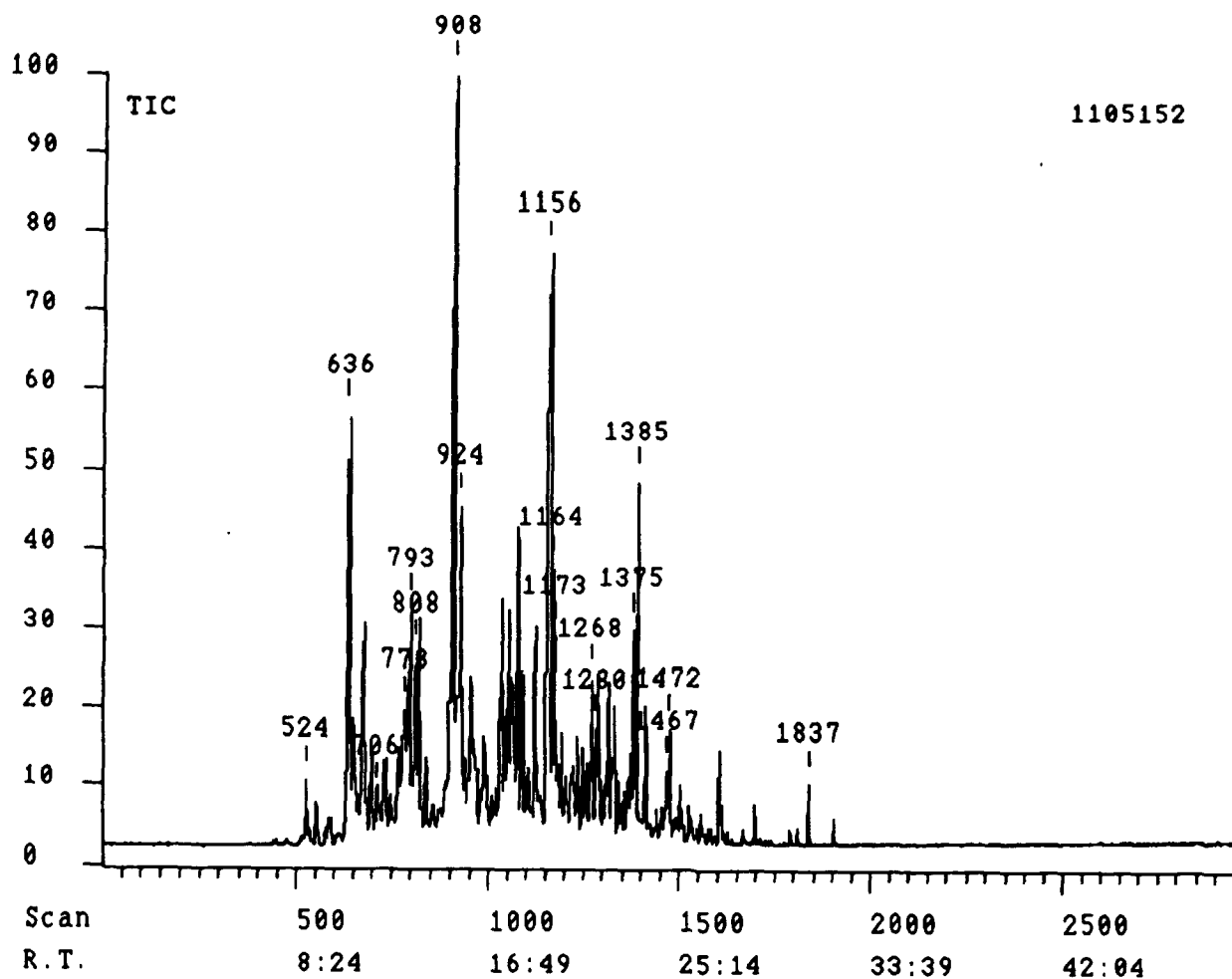


Figure 43. Total ion chromatograms of petroleum-derived Jet A-1 from GC-MS using split injection of undiluted sample.

number range (C₁₁-C₁₅ for JP-7P, and C₁₀-C₁₃ for Jet A-1), as compared to that of JP-8P (C₈-C₁₇). On the other hand, the Jet A-1 has higher aromatic content than JP-7P. Tetralin, naphthalene and methylnaphthalene are identified as some of the major aromatic components in Jet A-1.

Figures 44-46 shows the expanded retention time windows of GC-MS profile for the original JP-8P fuel, together with the structures of major peaks. The relative intensity in individual windows serves as baseline for evaluating thermal stability of hydrocarbon components in JP-8P, as described in Task 4. The GC-MS analysis for JP-8P and stressed JP-8P was conducted using the same temperature program, and their retention time windows are comparable. The NMR spectra of both the original and the stressed JP-8P were also measured, and the results are reported in Task 4.

Activity 2. Stressing of Model Compounds

Long-chain Paraffins

As we can see from the above GC-MS results, the studies on thermal stressing of long-chain paraffins are more pertinent to the petroleum-derived jet fuels. The detailed results for thermal stressing of dodecane and tetradecane at 400, 425, 450, and 475°C for time periods ranging from 1 h to 72 h, have been reported in the previous quarter [9]. A comparative examination of thermal stability of decane and tetradecane was performed at 450°C for 4 h in a N₂ atmosphere. As described in Task 1, the pressure increase during the stressing in a static reactor is indicative of the extent of thermal decomposition. Figure 47 shows the time-pressure profiles for decane and tetradecane, in which the profiles for decalin and tetralin are also shown for comparison. Upon immersing into the fluidized sand bath, tetralin, decalin and decane reached a equilibrium boiling state within about 10 minutes. At this point, the system pressure increased from 100 psi to about 500 psi. The further pressure increase is due to the decomposition (including cracking and dehydrogenation). The extent of the pressure increase within the first three hours suggests the decomposition extent to be tetradecane > decane > decalin. This observation in combination with previous GC-MS results [1] indicates that the stability of long-chain paraffins decreases with increase in the carbon number. Figure 28 shows the time-pressure profiles recorded for thermal stressing of JP-8P and JP-8C, which were derived from several stressing experiments using different reactors with the same configuration. While there are deviations between different runs due to the use of different pressure gauges, these profiles are indicative of the relative extent of thermal decomposition. The profiles for JP-8C and JP-8P are similar in trend to those of decalin and tetradecane, respectively. However, the difference in the system pressure between JP-8C and JP-8P at a given time (Figure 48) is smaller than that between pure decalin and tetradecane (Figure 47).

DS90 Chromatogram report Run: SONG660008, 19-Dec-90 17:34
 SONG JP-8P SPLIT 0.04 UL DB-17 40-5 TO 280-10 AT 4 KRA MS80

n-C₁₁

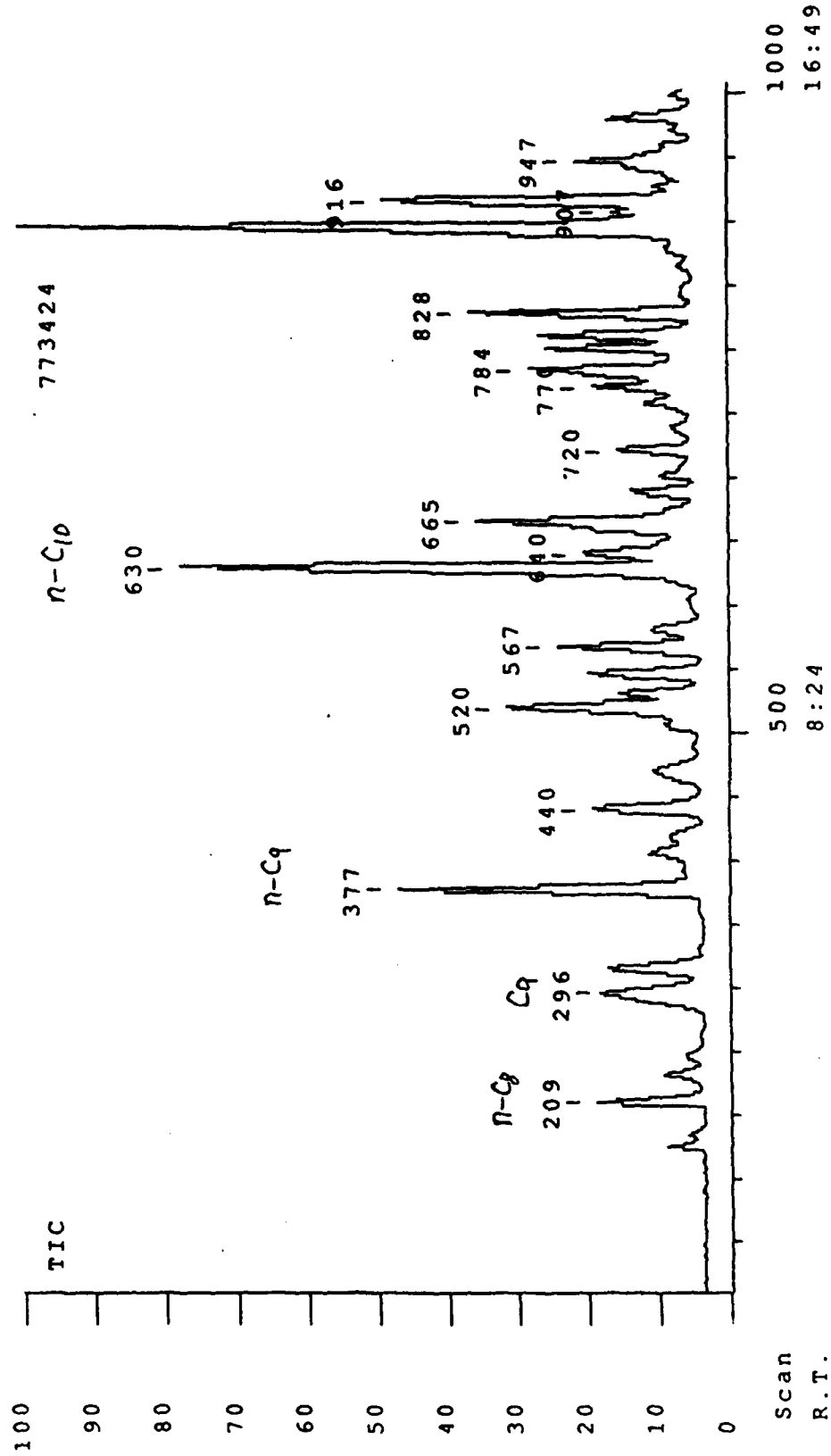


Figure 44 Retention time window I (1-16.53 minutes) of GC-MS profile for JP-8P using split injection of undiluted sample.

DS90 Chromatogram report Run: SONG660008, 19-Dec-90 17:34
 SONG JP-8P SPLIT 0.04 UL DB-17 40-5 TO 280-10 AT 4 KRA MS80

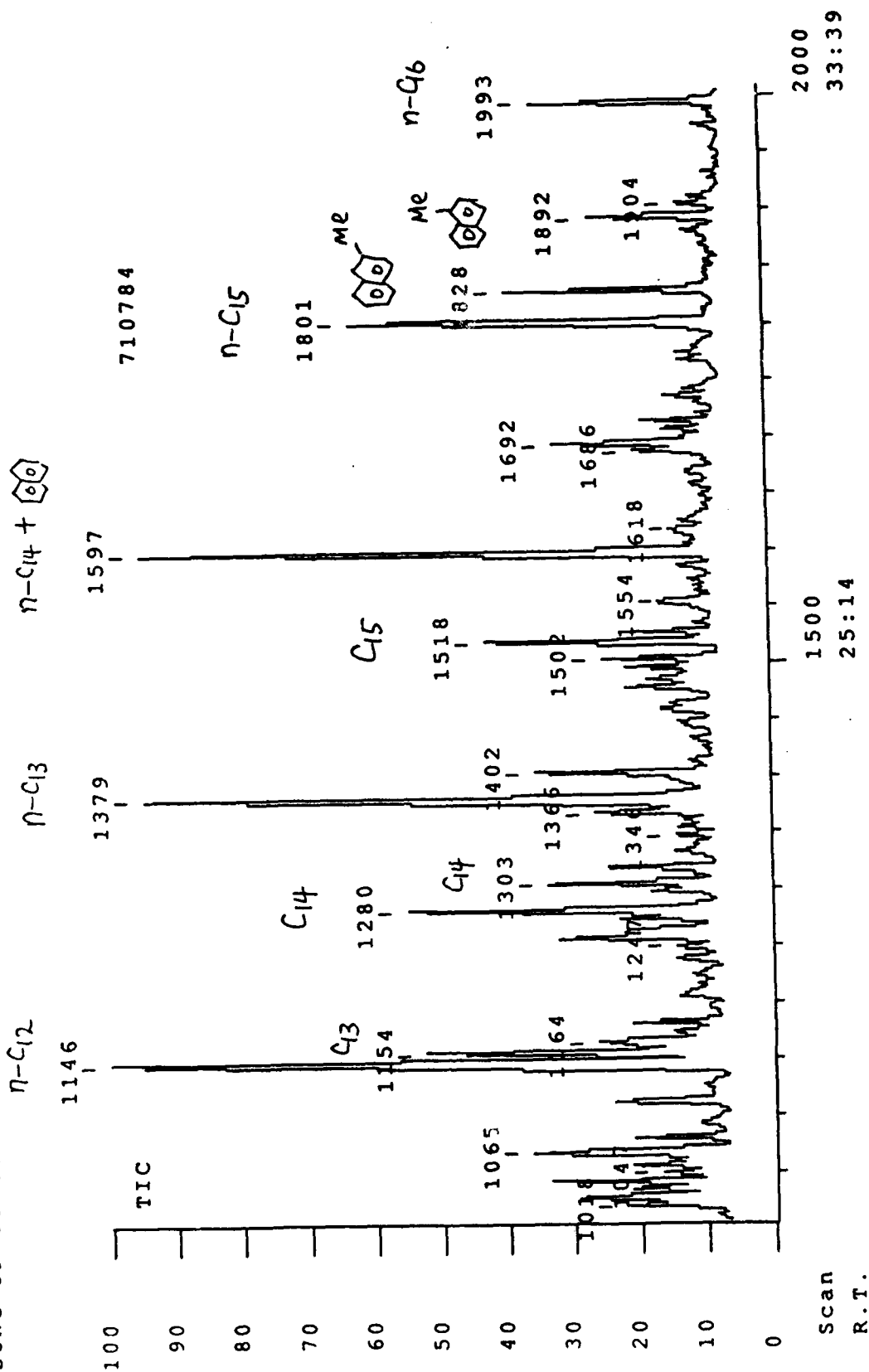


Figure 45 Retention time window II (16:54-33:43 minutes) of GC-MS profile for JP-8P.

DS90 Chromatogram report Run: SONG660008, 19-Dec-90 17:34
 SONG JP-8P SPLIT 0.04 UL DB-17 40-5 TO 280-10 AT 4 KRA MS80
 $n\text{-C}_{14} + \text{C}_{15}$

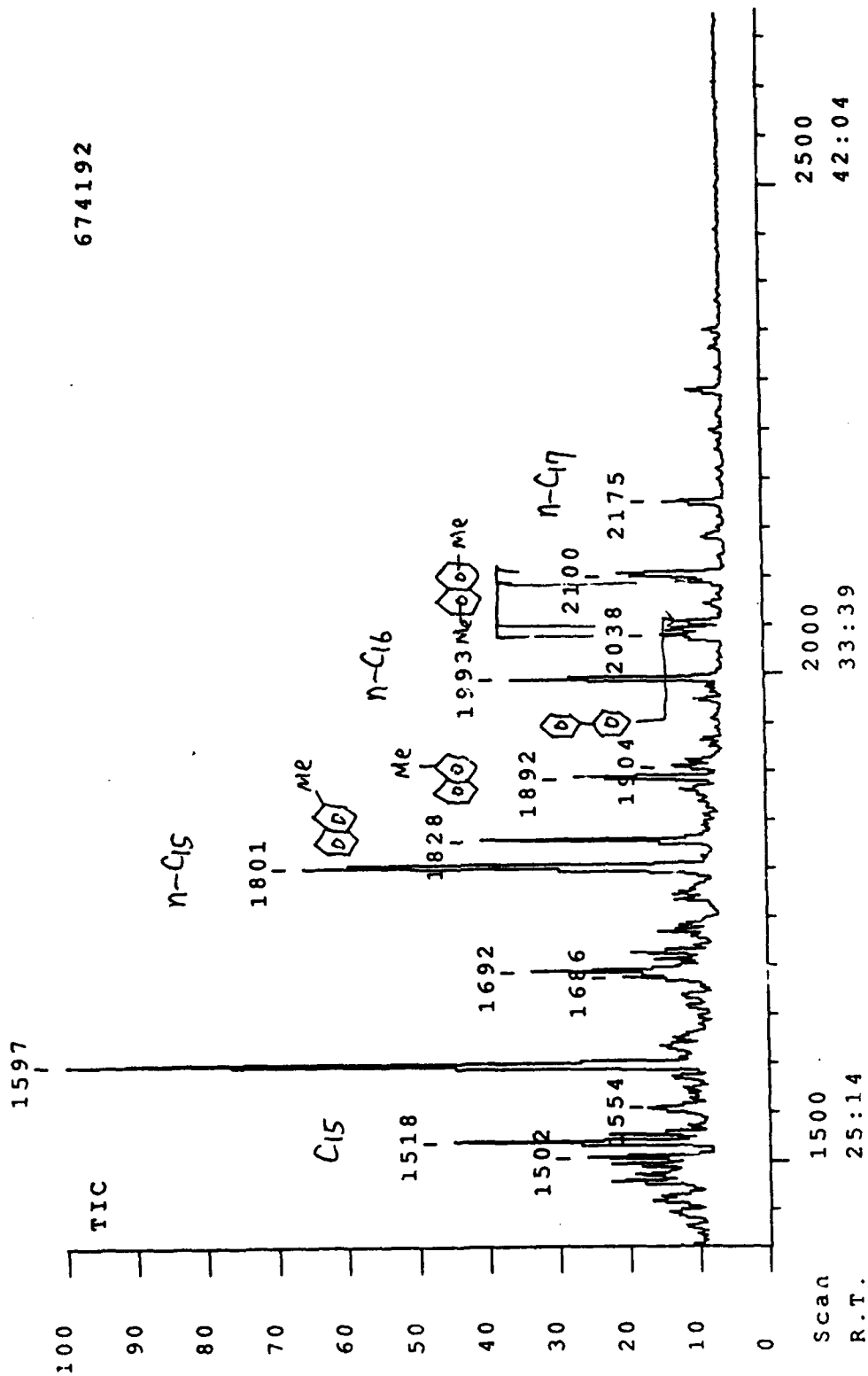


Figure 46 Retention time window III (24-45 minutes) of GC-MS profile for JP-8P.

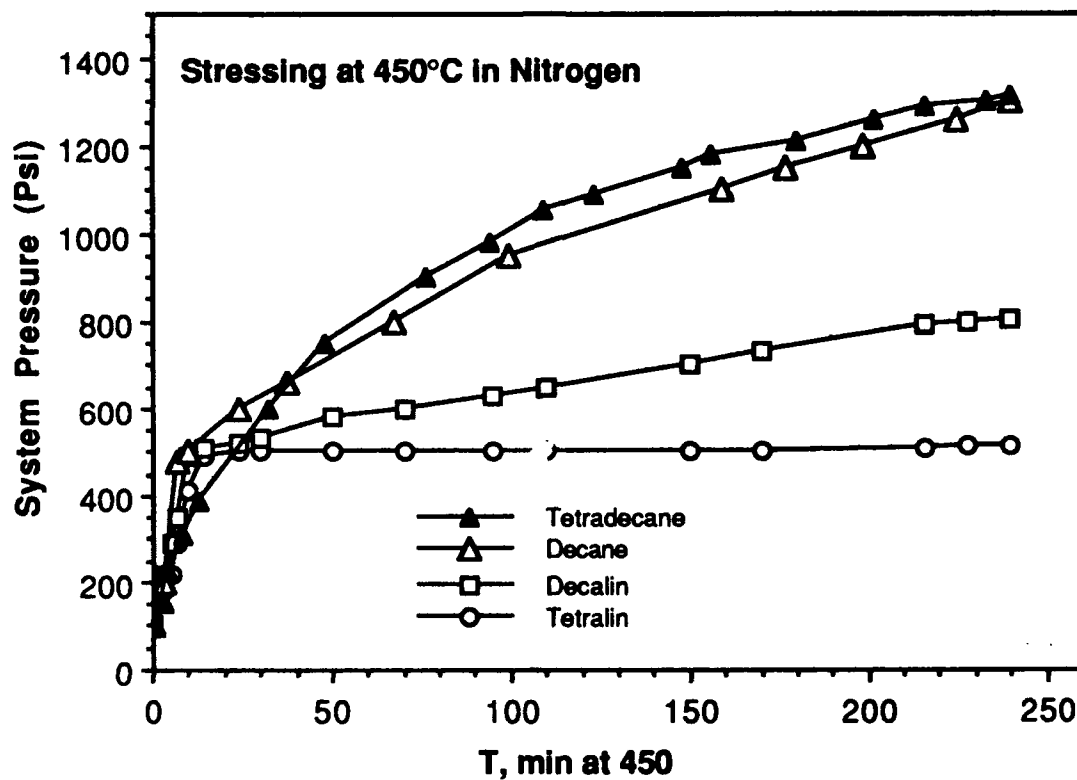


Figure 47. Time-pressure profiles for thermal stressing of model compounds at 450°C in N₂.

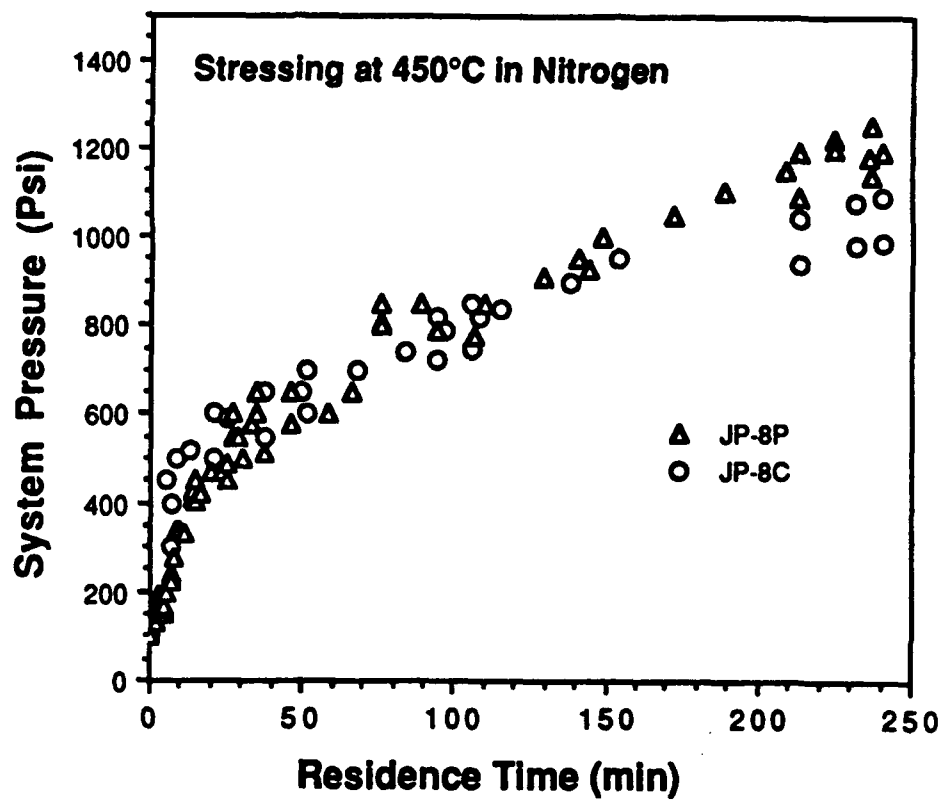


Figure 48. Time-pressure profiles for thermal stressing of JP-8P and JP-8C at 450°C.

Note that the maximum solid formation may not be directly proportional to the thermal stability of long-chain paraffins. Previous work [9] showed that the maximum amounts of deposits from n-decane, n-dodecane, and n-tetradecane are not always parallel with the order of their carbon number. The reaction conditions for determining the maximum amount of solids were selected as 72 h at 400°C, 24 h at 425°C and 450°C, and 6 h at 475°C. As shown in Figure 49, at 450°C, the amount of maximum solid deposit from dodecane appeared to be higher than that from tetradecane. Figure 50 shows the apparent first-order plots for the formation of solids from decane, dodecane and tetradecane at 450°C, indicating a reasonably linear relationships between the plotted parameters [9]. The rate constants were calculated from the slopes of the straight lines obtained by a least-squares fit of the data. Combining these previous results with the above results suggests that it is the precursor that determines the solid formation. The extent of initial decomposition, which depends upon the thermal stability of a given compound, is related to the later reaction but may not necessarily be proportional to the extent of solid formation. The chemical nature, such as structure and reactivity and the amounts of the precursor species, are probably the key factors controlling the solid-forming reactions. There may be some difference between the precursors from tetradecane, dodecane and decane, either in the amount/rate or in chemical nature.

The detailed results for thermal stressing tests of dodecane and tetradecane (conducted at 400, 425, 450, 475°C for time periods ranging from 1 h to 72 h) were presented in the previous quarter [9]. In addition to these two compounds, n-octane was also stressed at different temperatures. Some of the data for solid formation from octane are shown in Figure 51, together with the data for dodecane and tetradecane for comparison. At 400°C for 48 h solid deposition was first noted for dodecane, 20 mg, and tetradecane, 37 mg. At 400°C, 72 h dodecane produced 85 mg of solid and tetradecane 163 mg of solid deposit. At 400 and 425°C no solid deposition was noted for octane. This is to be expected since the short chain alkanes are more stable than the longer chain alkanes (Task 4). It is not until 450°C, 6 h stressing that deposits begin to form in appreciable amounts. It should be noted that the 450°C, 3 h stressing did blacken the wall of the reactor and produce a powdery deposit. The amount of this solid deposit was too small to be collected. Tests on octane at 475°C have not yet been conducted.

Analysis of Stressed Tetradecane

The thermal treated tetradecane samples stressed at 400, 425, 450, 475°C were examined by GC analysis. The chromatograms indicated that as the time is increased for each respective temperature, there is a significant degradation to form smaller compounds as can be seen in Figures 52 through 55. It was first thought from the predominant peaks that tetradecane was broken down into smaller chain alkanes and alkenes from C₅ on up. However when the retention times were compared with the standards, only a few peaks were compatible. These peaks were pentane,

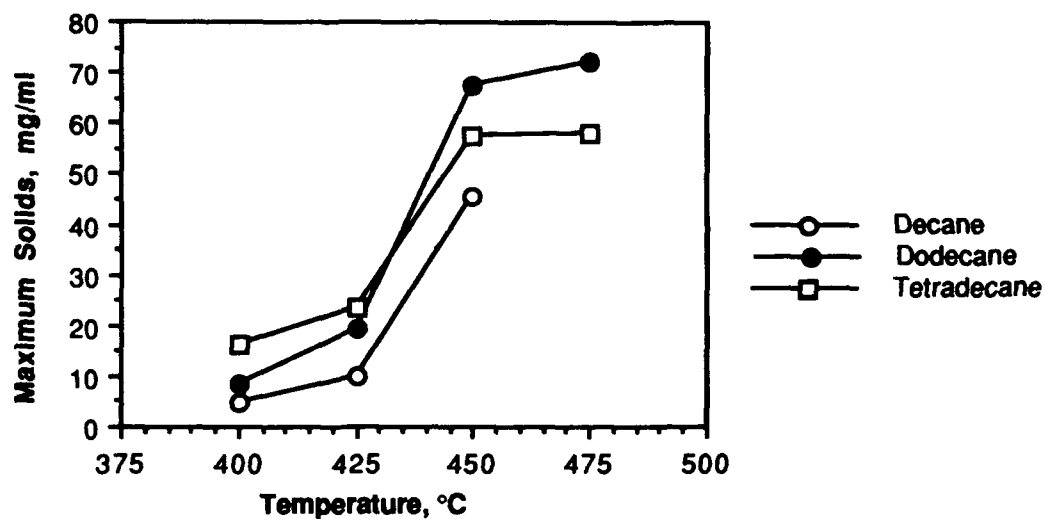


Figure 49. Maximum amount of solids produced by decane, dodecane, and tetradecane as a function of temperature.

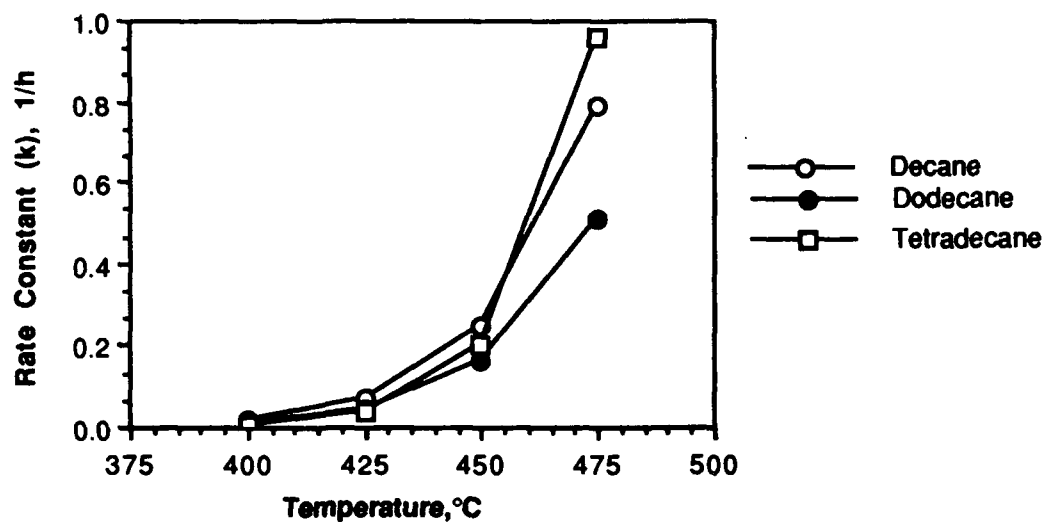


Figure 50. A comparison of the rate constants calculated for solid formation from decane, dodecane and tetradecane using a variable maximum conversion as a function of temperature (k for decane at 475°C by extrapolation).

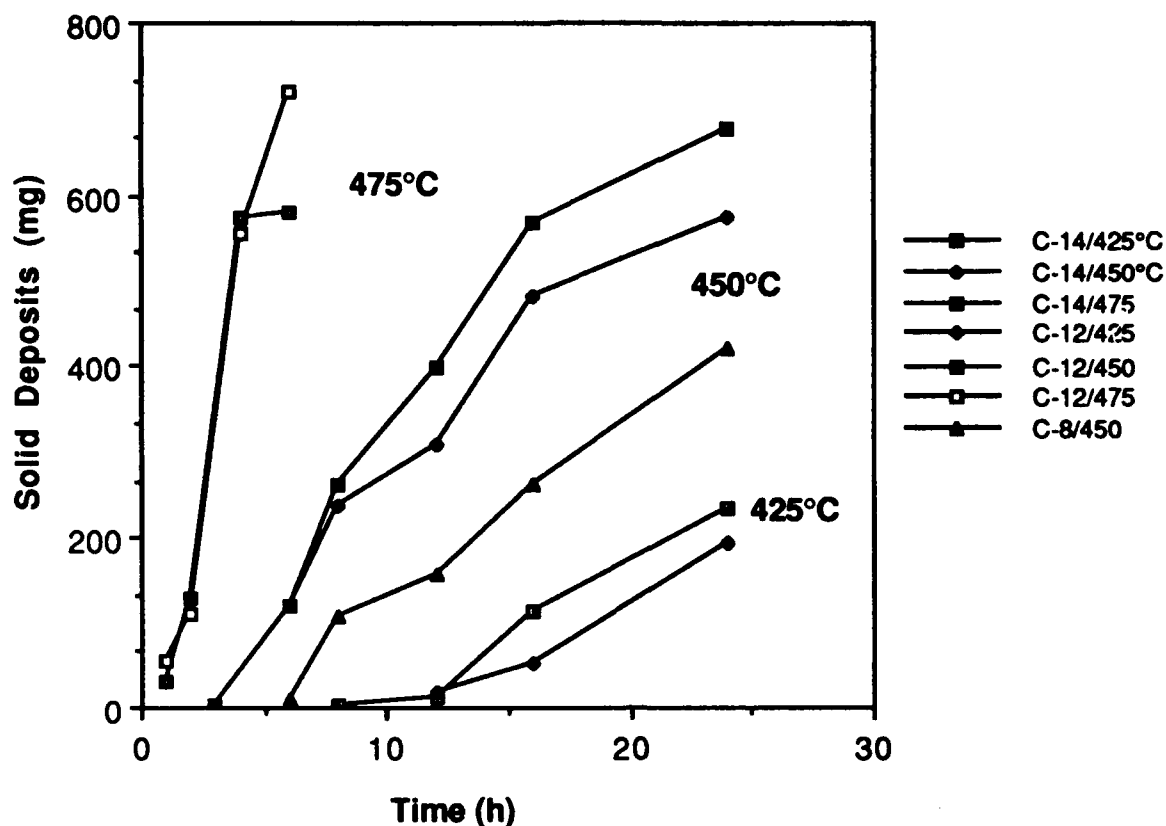


Figure 51. Formation of solids from octane, dodecane , and tetradecane at 400,425, 450, and 475°C as a function of time.

hexane, heptane, and decane. In order to determine the various types of compounds present, a GC-MS analysis was performed on a highly stressed tetradecane sample, 475°C for 6 h. Figure 56 shows the total ion chromatogram (TIC) and the identification results are given in Table 17. These results suggest that there are two main types of reactions occurring: hydrogen abstraction and ring condensation. As tetradecane is broken down, the smaller chain alkanes, alkenes, iso-alkanes, benzene, and methyl benzene (toluene) are formed. This can be seen on the 0-10 time scale. Once the benzene rings are formed substitutions on the ring begin to occur forming alkyl benzenes. This occurs in the 10-25 time region (retention time in chromatogram) and consists of C₂, C₃, and C₄-benzenes along with some larger chain alkanes. The next time region 25-45, naphthalene and substituted naphthalene begin to appear. This is the first appearance of ring closure or condensation. As shown in the latter portion of the TIC 45-70, ring condensation is occurring to a greater extent where compounds containing 3 rings, phenanthracene or anthracene, and 4 rings,

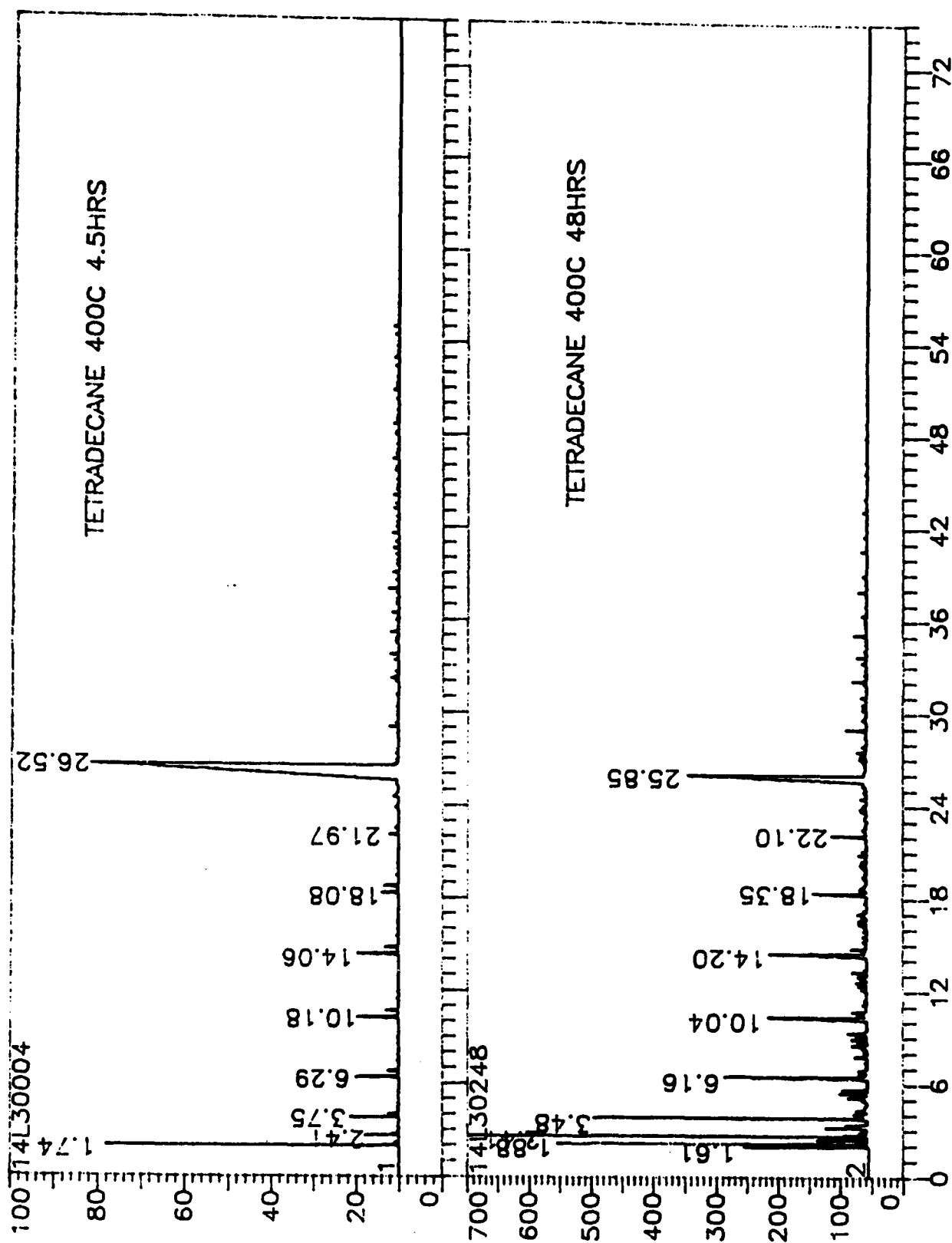


Figure 52. Chromatograms of thermally stressed n-tetradecane at 400 °C for 4.5 (top) and 48 (bottom) h in N₂.

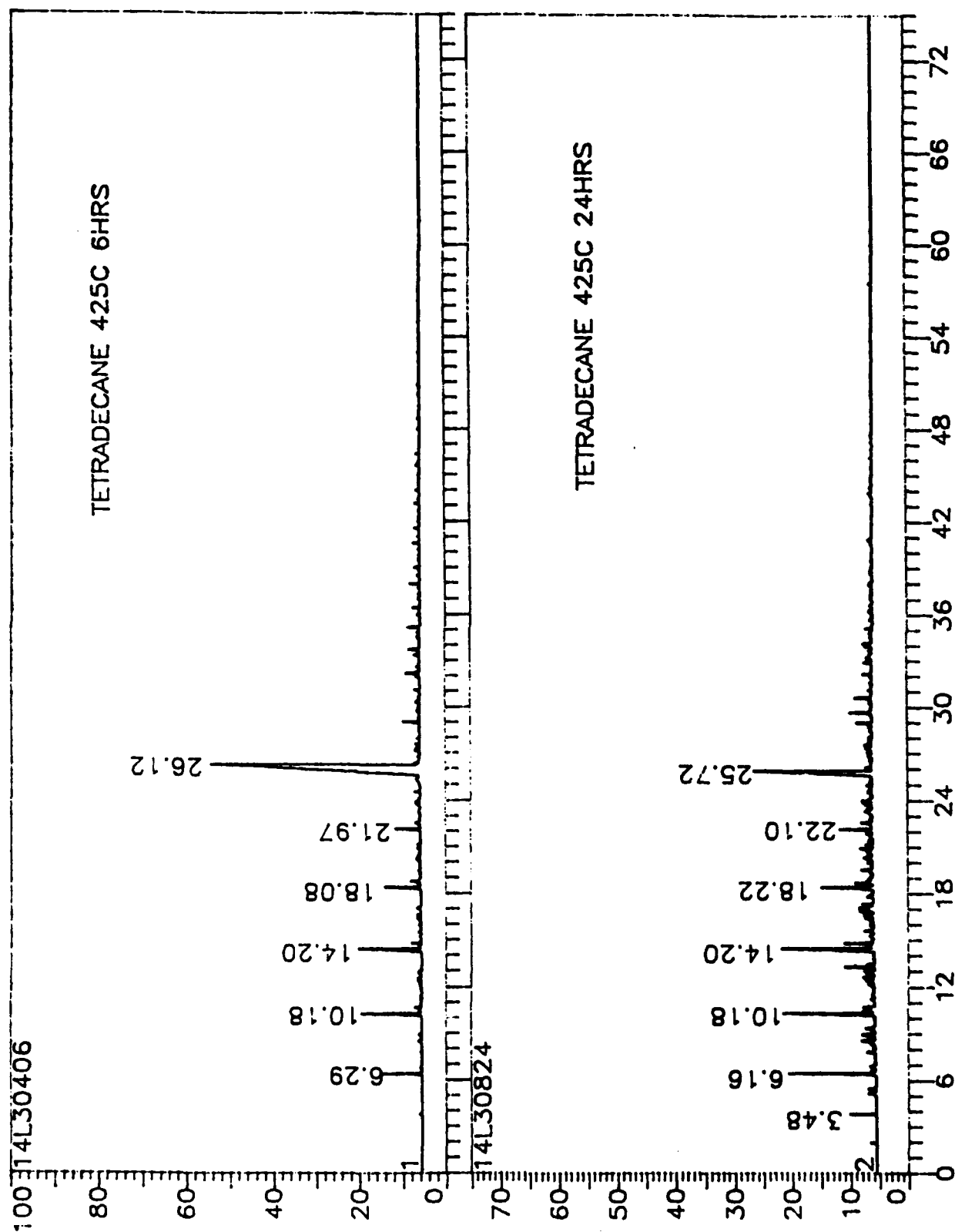


Figure 53. Chromatograms of thermally stressed n-tetradecane at 425 °C for 6 (top) and 24 (bottom) h in N₂.

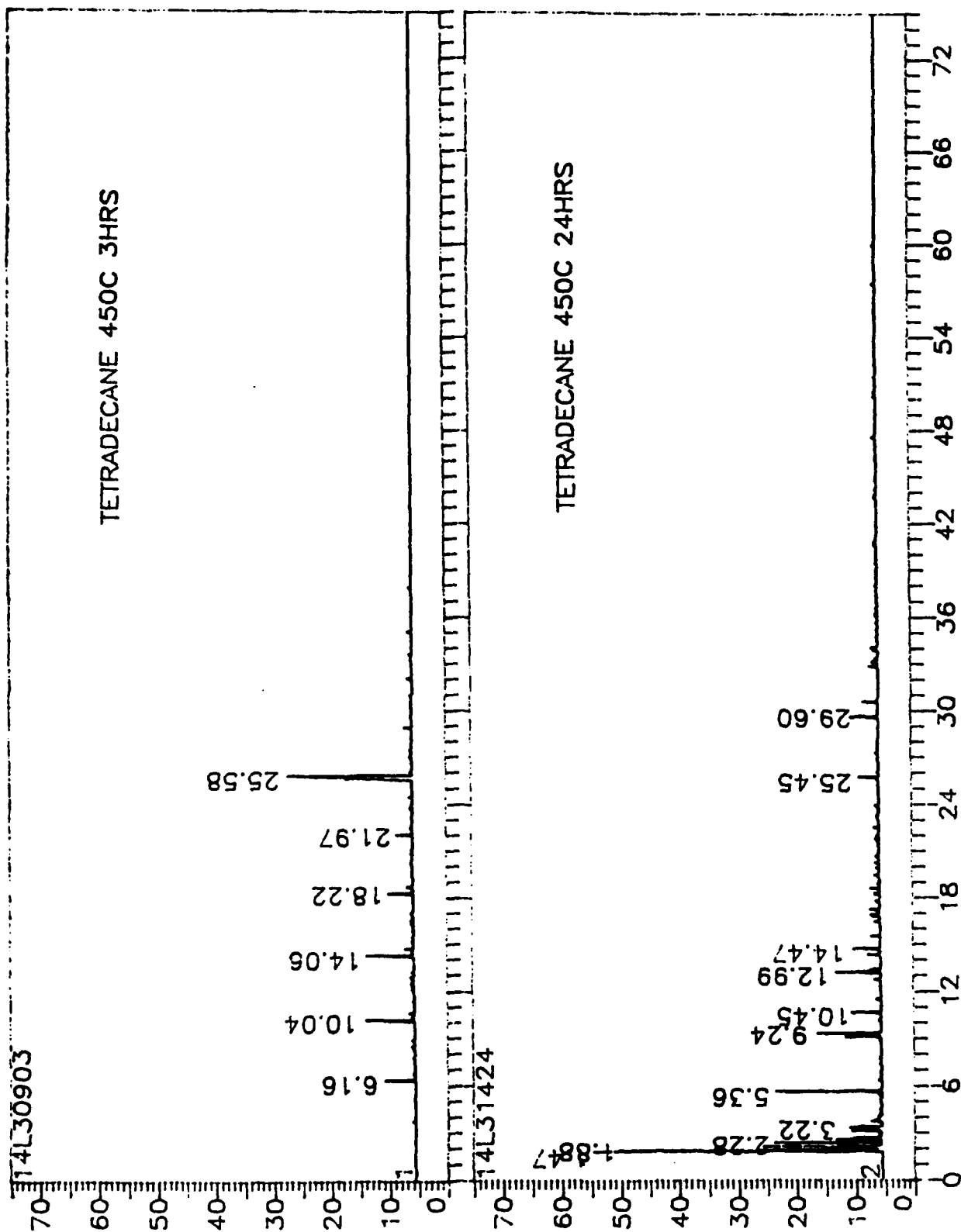


Figure 54. Chromatograms of thermally stressed n-tetradecane at 450 °C for 3 (top) and 24 (bottom) h in N₂.

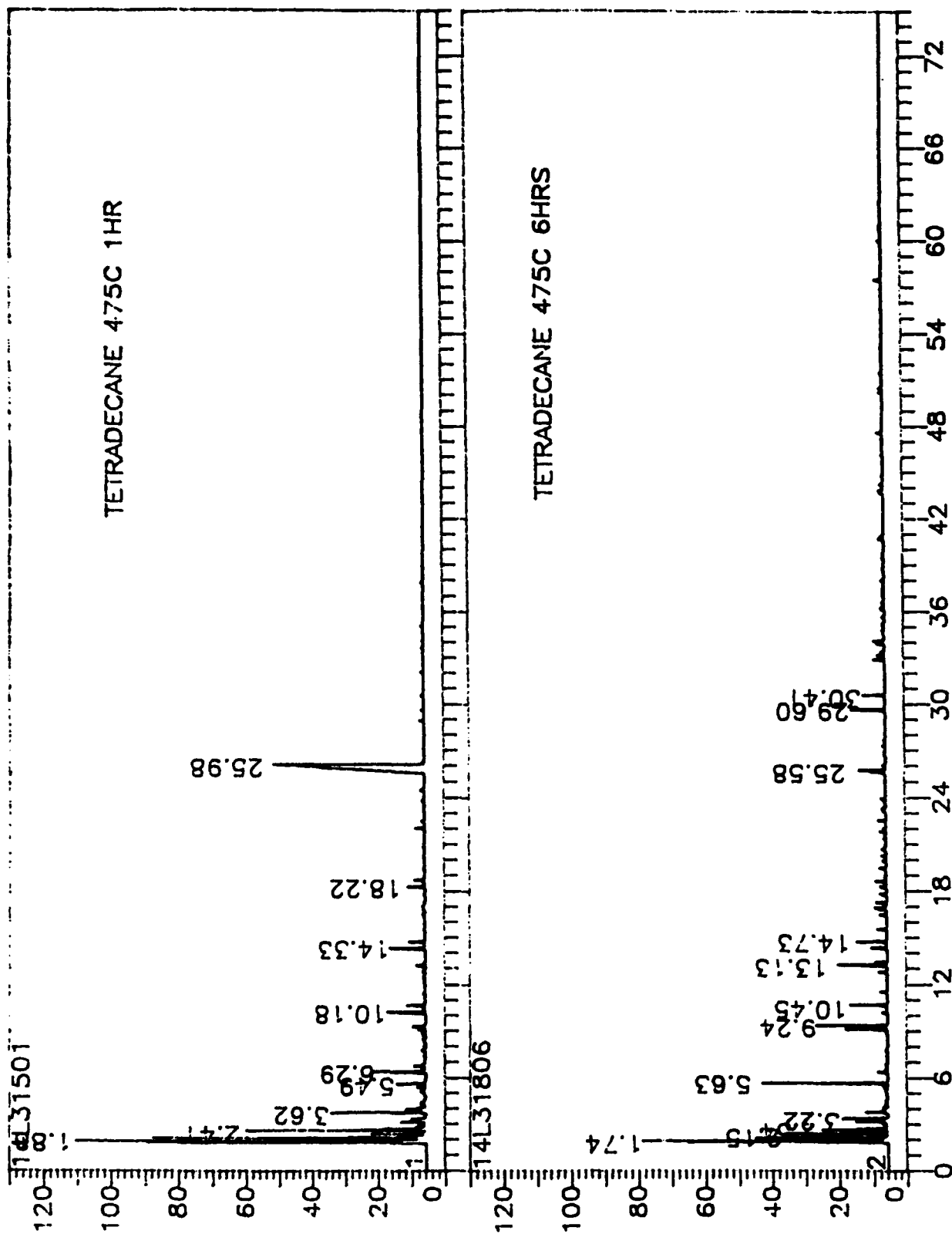


Figure 55. Chromatograms of thermally stressed n-tetradecane at 475 °C for 1 (top) and 6 (bottom) h in N₂.

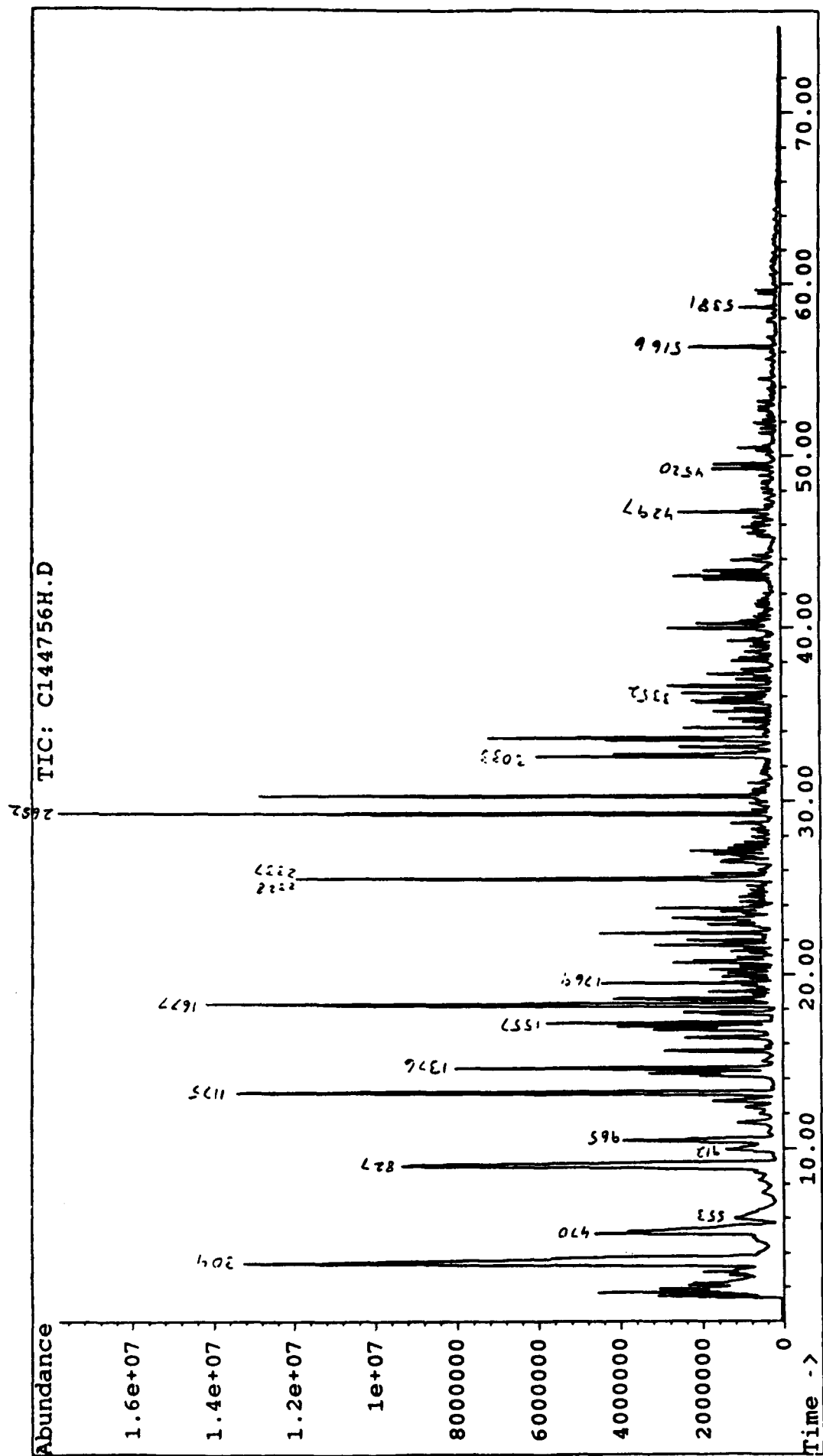


Figure 56. GC-MS TIC of thermally stressed n-tetradecane at 475 °C for 6 h in N₂.

Table 17: Identified compounds in thermally treated tetradecane at 475°C for 6 h in N₂.

Scan No.	Molecular Ion	Base Peak	Compound ID
134	72	43	n-Pentane
152	84	56	Hexane
304	114	43	Octane
470	92	91	Toluene
553	128	57	Nonane
827	106	91	C ₂ -benzene
912	142	57	n-Decane
965	106	91	C ₂ -benzene
1052	120	105	C ₃ -benzene
1055	120	105	C ₃ -benzene
1134	120	91	n-Propylbenzene
1291	156	57	Undecane
1376	134	105	Methylpropy benzene
1428	134	119	C ₄ -benzene
1498	120	105	C ₃ -benzene
1537	134	105	C ₄ -benzene
1557	134	105	C ₄ -benzene
1560	134	105	C ₄ -benzene
1677	170	57	Dodecane
1703	134	119	C ₄ -benzene
1745	148	133	C ₅ -benzene
1789	148	117	C ₄ -benzene
2328	198	57	Tetradecane
2337	198	128	Naphthalene
2682	142	142	Methylnaphthalene
3033	156	141	Dimethylnaphthalene
3352	170	155	C ₃ -Naphthalene
4297	178	178	Anthracene or Phenanthracene
4520	192	192	Methylantracene or Methylphenanthracene
4539	192	192	Methylantracene or Methylphenanthracene
5163	202	202	Pyrene
5381	216	216	Methylpyrene
5455	216	216	Methylpyre

pyrene, begin to appear. It is from the degradation of tetradecane into smaller compounds, the gradual building up to C₁-C₄-benzene, further ring closure and condensation to form 3 and 4 ring compounds that are believed to be the precursors to solid formation. The analysis of the solid deposits will be conducted in the future to obtain further information on how these deposits are formed.

Task 4. Identification and Characterization of Mixtures of Stable Hydrocarbon Species Present in Petroleum-derived Fuels.

Activity 1. Fractionation of Fuels

The scaled-up separation of a JP-8P using liquid chromatographic procedure has been completed. The separation results have been reported in Task 2. The results of detailed GC-MS analysis of the column fractions from JP-8P (using the modified procedure, Task 1) are presented in this report. It should be noted that unlike JP-8C, the low boiling components (retention time at 40°C: <4 minutes) are very limited in JP-8P and its saturates. Figure 57 and Table 18 give the detailed GC-MS results for the saturate fraction (n-pentane elute). JP-8P saturates contain many branched alkanes, which were identified only by their carbon number in the previous report [1]. In this report, the positions of branched chain are also indicated for many compounds, as shown in Table 18. Figure 58 and Table 19 show the detailed GC-MS results for fraction 2, and Figure 59 and Table 20 give the GC-MS results for fraction 3 from JP-8P. The GC-MS results for JP-8P saturates as well as JP-8C saturates were also reviewed by Dr. Jentaie Shiea, whose suggestions were most helpful. In particular, Dr. Shiea indicated the position of alkyl groups in many branched paraffins present in JP-8P saturates (fraction 1). It should be noted that trace amounts of aromatics were also found in the n-pentane elute of JP-8P, as shown in Table 18, and in many cases they were identified as impurities (co-eluted) with aliphatic peaks. For the aromatic fractions, the positions of alkyl groups for isomers of alkylaromatics were identified by comparison of their retention times with those of commercially available chemicals and/or by considering the difference in their boiling points.

Activity 2. Thermal Stressing of JP-8P and Its Saturate Fraction

The content of the saturate fraction of JP8-P is as high as 85 wt% (Task 2, Table 11). Figure 60 compares the liquid depletion and gas formation in the thermal stressing of the saturate fraction (Fr.1) as well as the whole JP8-P at 450°C for 4 h in N₂. As described in Task 2, the saturate fraction of JP-8C exhibited similar thermal stability as compared to the unfractionated (original) JP-8C. However, in the case of JP-8P, the extents of liquid depletion and gas formation are higher with the whole fuel than with its saturate fraction. This suggests that the intermolecular reactions between compounds in saturate fraction and those in other fractions play an important role in enhancing the decomposition during thermal stressing of whole JP8-P jet fuel.

In order to derive a general understanding of the degradation behavior, thermal stressing of the original JP-8P was conducted at 450°C for 0.5, 1, 2.5, 4, 8 and 16 h under 100 psi UHP-grade N₂. Figure 61 shows the liquid depletion and gas formation as a function of residence time.

DS90 Chromatogram report Run: SONG660005, 18-Dec-90 16:45
SONG JP-8P FR1 SATURATES 40-5 TO 200-10 AT 4 SPLIT 0.04 UL

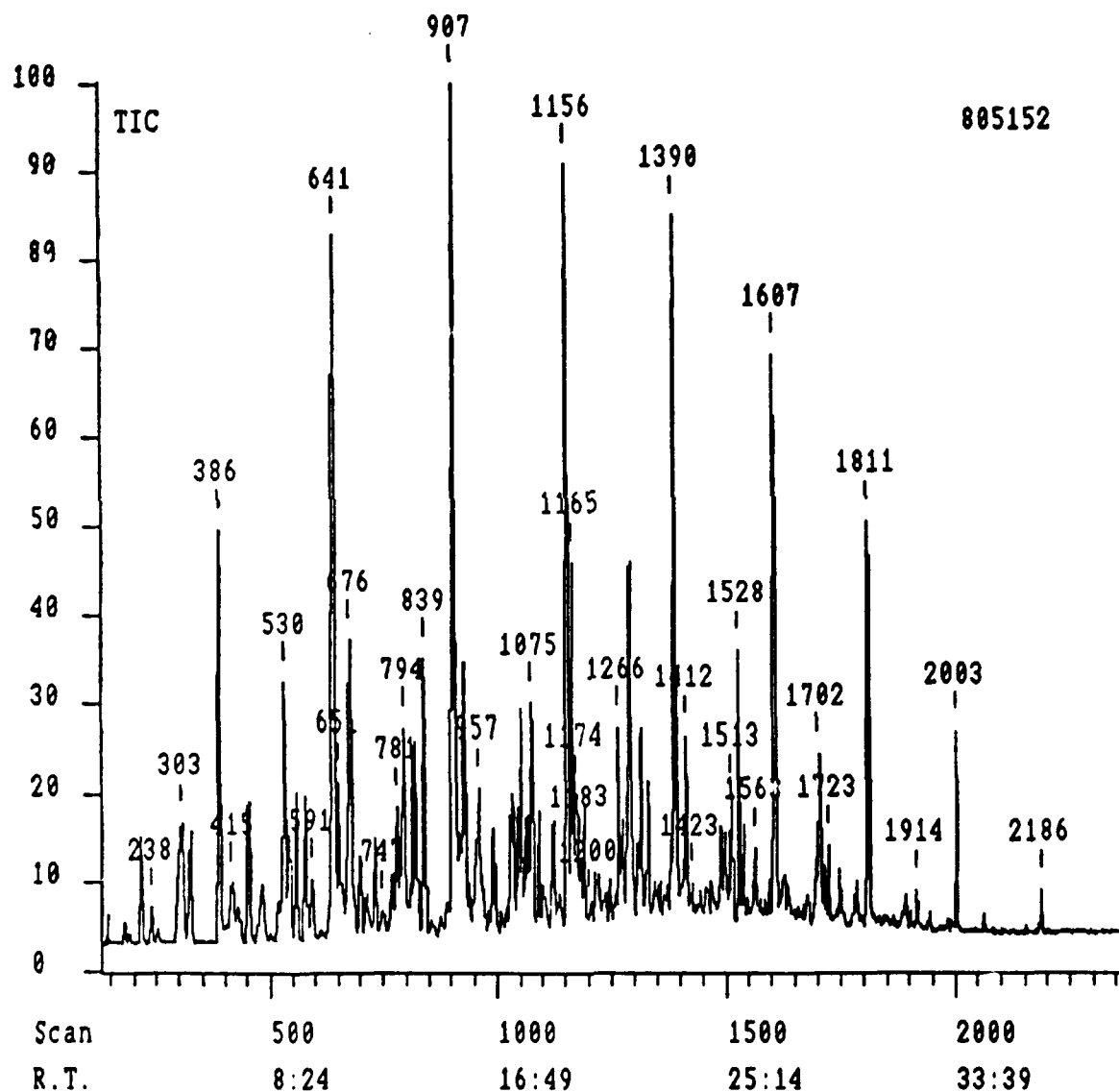


Figure 57. GC-MS TIC of saturate fraction (n-pentane elute) of JP-8P jet fuel (split injection of undiluted sample without delay to ionization)

Table 18. Identified compounds in saturate fraction of JP-8P jet fuel

Scan No.	Retention Time	Molecular Ion	Base Peak	Identified Compounds
99	1:39	72	43	n-Pentane (n-C5)
215	3:36	114	43	n-Octane (n-C8)
		112		iso-Octene
304	5:06	128	43	2-Methyloctane (C9)
		126		iso-Nonene ?
322	5:24	112	83	Ethylcyclohexane
		128 ?		3-Methyloctane ?
386	6:29	128	43	n-Nonane (n-C9)
450	7:33	142	57	2,6-Dimethyloctane (C10)
530	8:54	142	57	4-Methylnonane (C10)
541	9:05	126	83	n-Propylcyclohexane
556	9:20	142	57	3-Methylnonane
		140		iso-Nonene
578	9:43	140	69 or 111	C4-Cyclohexane
		106	91	p- + m-Xylene
641	10:06	142	57	n-Decane (n-C10)
651	10:56	140	55	Methylpropylcyclohexane
676	11:22	156	43	2,6-Dimethylnonane (C11)
698	11:44	140	55	Methylpropylcyclohexane
		138		
731	12:17	156	57	3,7-Dimethylnonane (C11)
		120	105	Isopropylbenzene
781	13:08	156	57	5-Methyldecane (C11)
794	13:21	156	43	4-Methyldecane (C11)
811	13:38	140	83	n-Butylcyclohexane
		120	91	n-Propylbenzene
820	13:47	156	57	3-Methyldecane (C11)
		154		
839	14:06	120	105	Methylethylbenzene
907	15:15	156	57	n-Undecane (n-C11)
917	15:25	154	55	C5-Cyclohexane
926	15:34	120	105	Trimethylbenzene
957	16:05	170	43	3,7-Dimethyldecane (C12)
990	16:39	134	119	Dimethylethylbenzene
1029	17:18	170	57	6-Methylundecane (C12)
1034	17:23	170	43	5-Methylundecane (C12)
1044	17:33	170	43	4-Methylundecane (C12)
1050	17:39	170	43	2-Methylundecane (C12)
1058	17:47	152	137	Methyldecalin
		170		iso-Decane (C12)
1065	17:54	134	119	Methylpropylbenzene
1075	18:05	168	83	C6-Cyclohexane
		154		
		134	119	Diethylbenzene

Table 18 (continued)

1089	18:19	134	119	Dimethylethylbenzene
1122	18:52	152	95	Methyldecalin
		134	105	Methylpropylbenzene
1156	19:26	170	57	n-Dodecane (n-C ₁₂)
1165	19:35	184	57	2,6-Dimethylundecane (iso-C ₁₃)
1176	19:47	134	119	Dimethylethylbenzene
		168		C ₆ -Cyclohexane
1191	20:02	148	119	C ₅ -Benzene
1214	20:05	168	55	C ₆ -Cyclohexane ?
		166		?
1266	21:17	184	57	6-Methyldodecane (C ₁₃)
		182		iso-Tridecene
1272	21:24	184 ?	43	5-Methyldodecane (C ₁₃) ?
1282	21:34	184 ?	43	4-Methyldodecane ?
		166		
		148	119	C ₅ -Benzene
1290	21:42	198	57	2,6,10-Trimethylundecane
1308	22:00	182	55	C ₇ -Cyclohexane
		148	119	C ₅ -Benzene
1314	22:06	198 ?	57	3-Methyldodecane ?
		148		C ₅ -Benzene
1328	22:20	168	83	n-Hexylcyclohexane
1382	23:15	184	43	iso-Tridecane
		196		C ₈ -Cyclohexane ?
		162	119	C ₆ -Benzene
1390	23:23	184	57	n-Tridecane (n-C ₁₃)
1412	23:45	198 ?	57	2,6-Dimethyldodecane ?
1487	25:01	198 ?	57	7-Methyltridecane & 6-Methyltridecane ?
1494	25:08	198 ?	43	5-Methyltridecane (C ₁₄) ?
		196		
1505	25:19	198 ?	43	4-Methyltridecane (C ₁₄) ?
1513	25:27	198 ?	43	2-Methyltridecane (C ₁₄) ?
1528	25:42	212	57	2,6,10-Trimethyldodecane (C ₁₅)
1536	25:50	198 ?	57	3-Methyltridecane (C ₁₄) ?
1564	26:18	182	83	n-Heptylcyclohexane
1607	27:02	198	57	n-Tetradecane (n-C ₁₄)
1702	28:38	226 ?	57	2,6,10-Trimethyltridecane (C ₁₆) ?
1715	28:51	212 ?	43	4-Methyltetradecane (C ₁₅) ?
1723	28:59	212 ?	57	2-Methyltetradecane (C ₁₅) ?
1811	30:28	212	57	n-Pentadecane (n-C ₁₅)
2003	33:42	226	57	n-Hexadecane (n-C ₁₆)
2186	36:47	240	57	n-Heptadecane (n-C ₁₇)

* n-Pentane eluted fraction 1; GC-MS File: SONG660005; Split

DS90 Chromatogram report Run: SONG620002, 22-Jun-90 13:51
SONG S03-A2 JP8-P 5%BENZENE-PENTANE 40-5 TO 280-5 AT 4 1UL

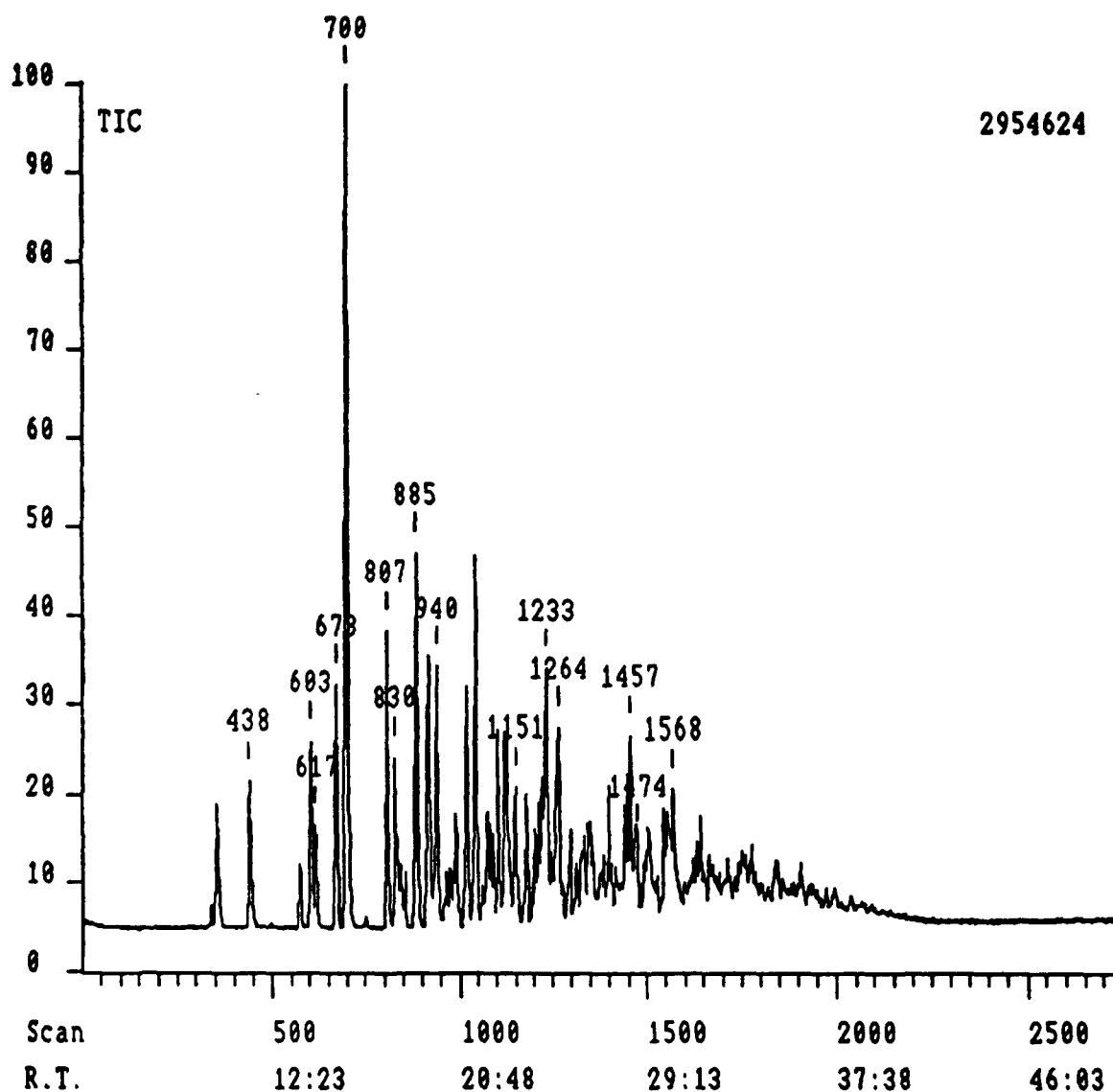


Figure 58. GC-MS TIC of monoaromatic fraction (5% benzene-pentane elute) of JP-8P jet fuel (splitless injection of diluted sample with 4 min delay to ionization)

Table 19. Identified compounds in monoaromatic fraction (fraction 2) of JP-8P jet fuel

Scan No.	Retention Time	Molecular Ion	Base Peak	Identified Compounds
339	9:40	106	91	Ethylbenzene
352	9:53	106	91	p-Xylene
438	11:20	106	91	o-Xylene
575	13:39	120	91	n-Propylbenzene
603	14:07	120	105	Methylethylbenzene
617	14:20	120	105	1,3,5-Trimethylbenzene
673	15:18	120	105	Methylethylbenzene
700	15:45	120	105	1,2,4-Trimethylbenzene
807	17:33	120	105	1,2,3-Trimethylbenzene
830	17:56	134	105	Methylpropylbenzene
843	18:09	134	91	n-Butylbenzene
857	18:23	134	119	Dimethylethylbenzene
885	18:52	134	105	Methylpropylbenzene
916	19:23	134	119	Dimethylethylbenzene
921	19:28	134	119	Dimethylethylbenzene
940	19:47	134	119	Dimethylethylbenzene
965	20:12	132	117	Methylindan
974	20:22	134	119	Dimethylethylbenzene
982	20:30	148	105	Methylbutylbenzene
989	20:37	132	117	Methylindan
1021	21:09	134	119	1,2,4,5-Tetramethylbenzene
1043	21:31	134	119	Tetramethylbenzene
1061	21:49	148	119	Dimethylpropylbenzene
1074	22:03	148	119	Dimethylpropylbenzene
1080	22:09	148	105	Methylbutylbenzene
1088	22:17	146	131	Dimethyltetralin
1105	22:34	148	119	Dimethylpropylbenzene
1122	22:51	148	119	Dimethylpropylbenzene
1128	22:57	148	105	Methylbutylbenzene
1134	23:03	132	117	5- or 6-Methylindan
		148	133	Trimethylethylbenzene
1146	23:15	148	119	Dimethylpropylbenzene
1151	23:20	148	119	Dimethylpropylbenzene
1197	24:07	148	133	Trimethylethylbenzene ?
1204	24:14	146	131	Dimethylindan
		160	145	C ₃ -Indan
1213	24:23	148	119	Dimethylpropylbenzene
1221	24:31	148	133	Trimethylethylbenzene ?
1233	24:43	146	131	Dimethylindan
1243	24:53	162	119	C ₆ -Benzene
		146	117	Ethylindan
1264	25:14	146	131	Dimethylindan
1278	25:29	162	133	Trimethylpropylbenzene
1296	25:47	162	119	Dimethylbutylbenzene

Table 19 (continued)

1312	26:03	160	145	Trimethylindan
1323	26:14	162	91	Hexylbenzene
1331	26:22	162	119	C ₆ -Benzene
1349	26:40	162	119	Dimethylbutylbenzene
1355	26:46	162	105	Methylpentylbenzene
1374	27:06	146	117	Ethylindan
1383	27:15	162	119	Dimethylbutylbenzene
1397	27:29	146	131	Dimethylindan
1404	27:36	162	133	Trimethylpropylbenzene
1423	27:55	174	159	C ₄ -Indan
		160	145	
1438	28:10	146	131	C ₂ -Indan
		176	119	C ₇ -Benzene
1448	28:20	160	145	C ₃ -Indan
		176	133	C ₇ -Benzene
1457	28:29	146	131	5- or 6-Methyltetralin
1467	28:39	160	145	C ₃ -Indan
		176	133	C ₇ -Benzene
1472	28:45	160	145	C ₃ -Indan or C ₂ -Tetralin
1493	29:06	176	119	C ₇ -Benzene
1502	29:15	160	145	C ₃ -Tetralin or C ₄ -Indan
1524	29:37	176	106	Methylhexylbenzene
1543	29:56	176	106	Methylhexylbenzene
1555	30:08	160	104	Cyclohexylbenzene
1568	30:21	176	105	Methylhexylbenzene
1640	31:34	174	159	C ₄ -Indan or C ₃ -Tetralin
1774	33:50	190	105	Methylheptylbenzene
1841	34:57	204	105	C ₉ -Benzene
		188	145	C ₄ -Tetralin or C ₅ -Indan
1906	36:03	204	119	C ₉ -Benzene
		188	145	C ₄ -Tetralin or C ₅ -Indan

* Fraction 2; GC-MS File: SONG620002; Splitless

DS90 Chromatogram report Run: SONG620003, 22-Jun-90 15:27
SONG S03-A3 JP8-P BENZENE ELUTE 40-5 TO 200-5 AT 4 HP-17 1U

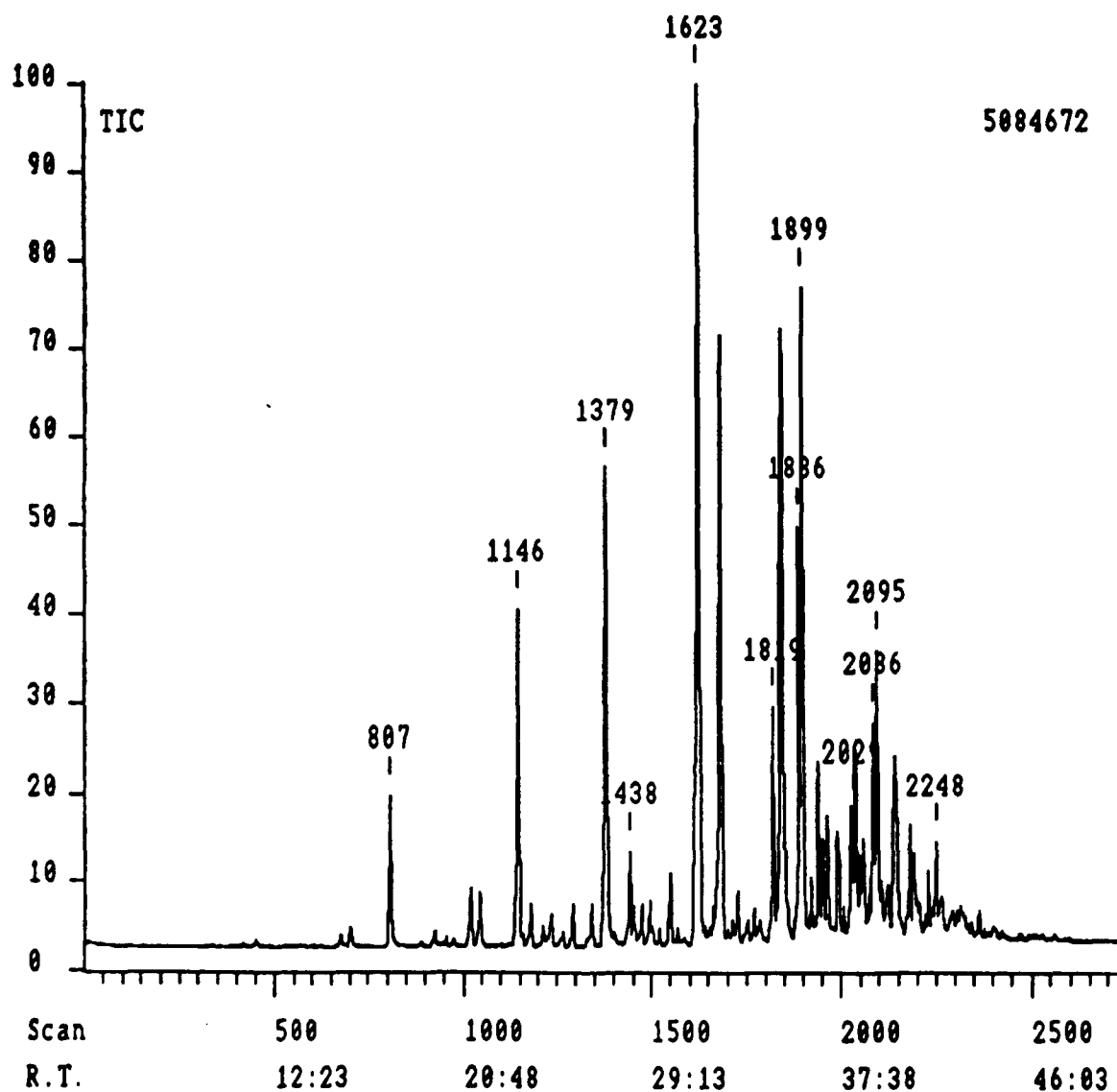


Figure 59. GC-MS TIC of aromatic fraction (benzene elute) of JP-8P jet fuel (splitless injection of diluted sample with 4 min delay to ionization)

Table 20. Identified compounds in aromatic fraction of JP-8P jet fuel

Scan No.	Retention Time	Molecular Ion	Base Peak	Identified Compounds
700	15:45	120	105	1,2,4-Trimethylbenzene
807	17:33	120	105	1,2,3-Trimethylbenzene
1021	21:09	134	119	Tetramethylbenzene
1043	21:31	134	119	Tetramethylbenzene
1146	23:15	134	119	Tetramethylbenzene
1178	23:48	132	117	6- or 5-Methylindan
1213	24:23	148	119	Dimethylpropylbenzene
1233	24:43	146	131	Dimethylindan
1291	25:42	148	133	Trimethylethylbenzene or Dimethylisopropylbenzene
1338	26:29	148	133	Trimethylethylbenzene or Dimethylisopropylbenzene
1379	27:11	128	128	Naphthalene
1438	28:10	146	131	Dimethylindan
1450	28:22	148	133	Trimethylethylbenzene
1473	28:46	160	145	Dimethyltetralin or Trimethylindan
1493	29:06	146	131	Methyltetralin or Dimethylindan
		176	119	C ₇ -Benzene
1518	29:31	162	133	Trimethylpropylbenzene
1541	29:54	160	145	Dimethyltetralin or Trimethylindan
1550	30:03	146	131	5- or 6-Methyltetralin
1623	31:17	142	142	2-Methylnaphthalene
1655	31:49	174	131	Propylnaphthalene
1661	31:55	176	133	Trimethylbutylbenzene
1680	32:15	142	142	1-Methylnaphthalene
1725	33:00	160	145	Dimethyltetralin or Trimethylindan
		176	133	Trimethylbutylbenzene
1752	33:27	174	159	Trimethyltetralin
1767	33:42	190	133	Trimethylpentylbenzene
1782	33:58	174	145	Methylethyltetralin or Diethylindan
1819	34:35	156	141	2-Ethylnaphthalene
1844	35:00	156	156	Dimethylnaphthalene
1886	35:43	156	156	Dimethylnaphthalene
1899	35:56	156	156	Dimethylnaphthalene
1919	36:16	170	155	Methylethylnaphthalene or Isopropylnaphthalene
1938	36:35	156	156	Dimethylnaphthalene
1950	36:47	156	156	Dimethylnaphthalene
1961	36:58	156	156	Dimethylnaphthalene
1990	37:28	156	141	1-Ethylnaphthalene
2006	37:44	170	141	Propylnaphthalene
2023	38:01	170	155	Methylethylnaphthalene
2029	38:07	170	155	Methylethylnaphthalene

Table 20 (continued)

2036	38:14	168	168	Methylbiphenyl
2048	38:26	170	155	Methylethynaphthalene
2056	38:34	168	168	Methylbiphenyl
2071	38:50	170	155	Methylethynaphthalene
2086	39:05	170	170	Trimethynaphthalene
2095	39:14	170	170	Trimethynaphthalene
2104	39:23	170	155	Methylethynaphthalene
2140	39:59	170	170	Trimethynaphthalene
2169	40:29	184	169	Dimethylethynaphthalene or Methylisopropylnaphthalene
2179	40:39	170	170	Trimethynaphthalene
2189	40:49	170	155	Trimethynaphthalene
2197	40:57	184	155	Methylpropylnaphthalene
2238	41:38	184	169	Dimethylethynaphthalene
2248	41:48	170	155	Trimethynaphthalene
2264	42:04	184	169	Dimethylethynaphthalene
2302	42:43	166	166	Fluorene
2362	43:43	184	184	Tetramethynaphthalene

* Fraction 3; GC-MS File: SONG620003; Splitless

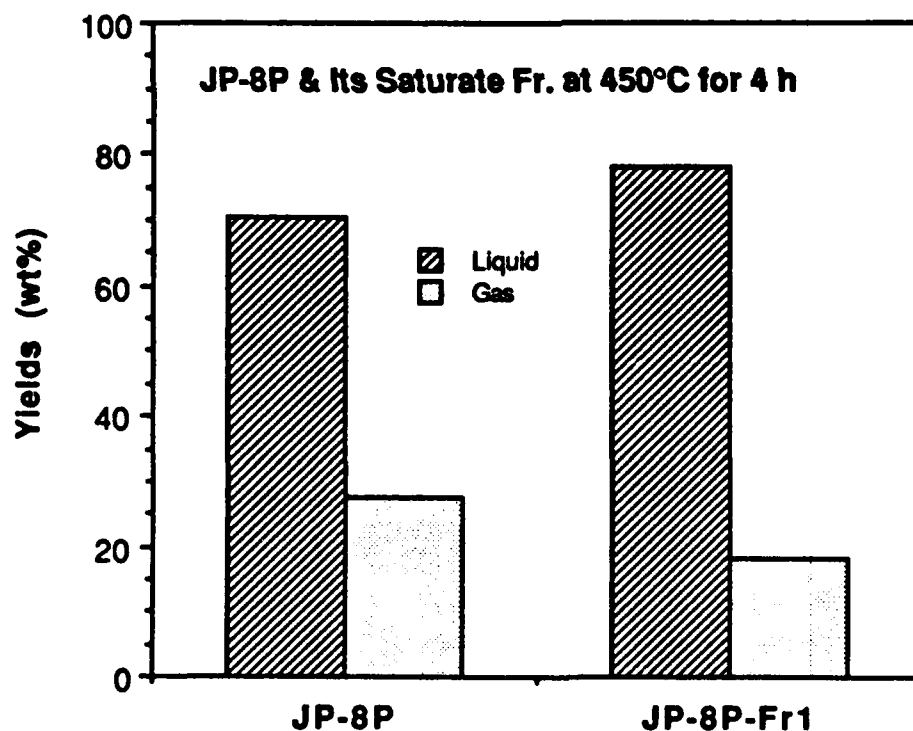


Figure 60. Liquid depletion and gas formation in the thermal stressing of the saturate fraction (Fr.1) as well as the whole fuel of JP8-P at 450°C for 4 h in N₂

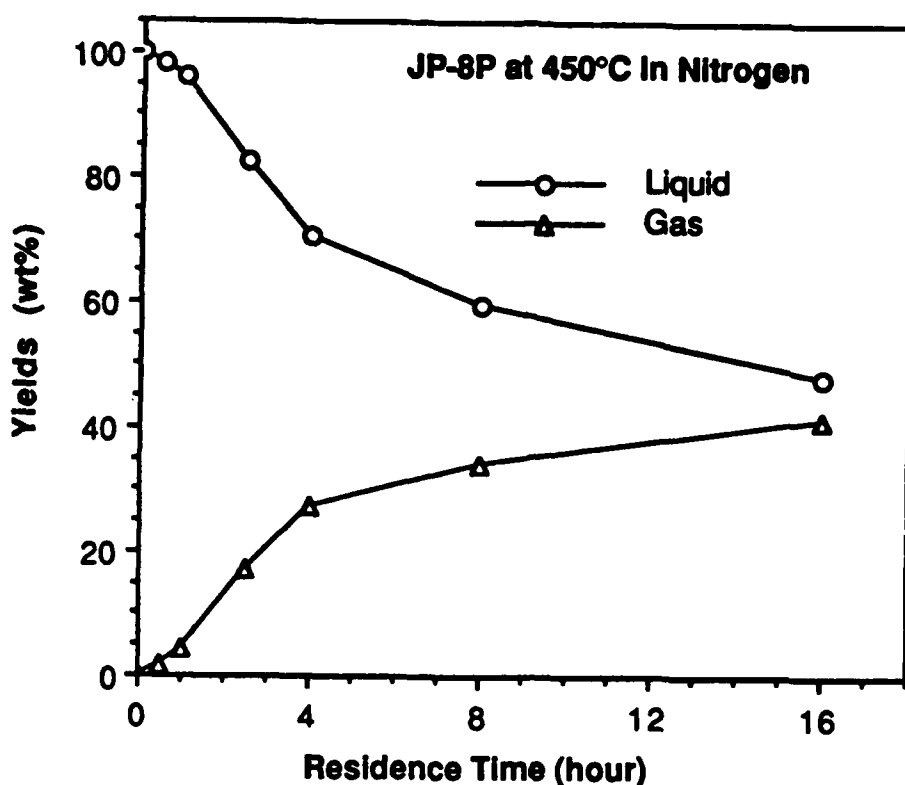


Figure 61. Liquid depletion and gas formation from petroleum-derived JP-8P versus residence time at 450°C under 100 psi N₂.

As we can see from Figure 61, the rapid liquid depletion and sharp increase in gas yield in the first 4 h of thermal stressing indicate that initial decomposition of JP-8P is faster, but the further increase in residence time has less effect in terms of depleting the liquids. This is probably because most of the less stable compounds have decomposed after 4 h. In the previous work [1], we have found from the GC-MS analysis of liquids (diluted with HPLC grade methylene chloride with 4 min delay to ionization) from the saturate fraction of JP8-P as well as the whole JP-8P that, nearly all the C₁₁ through C₁₆ long-chain paraffins, which are the predominant components of the original samples, have disappeared after 4 h at 450°C in N₂. The remaining long-chain paraffins are only nonane and decane. The products formed by thermal stressing include C₁- through C₃-cycloalkanes and C₁- to C₄-alkylbenzenes in high concentrations, and methylindan, naphthalene and 2-methylnaphthalene in small amounts.

Figure 62 shows the yields of solid deposits together with gas yields versus the residence time. There appeared an induction period in the process leading to solid formation. The solid formation was very limited in the first 2.5 h, while the liquid depletion (Figure 33) and gas

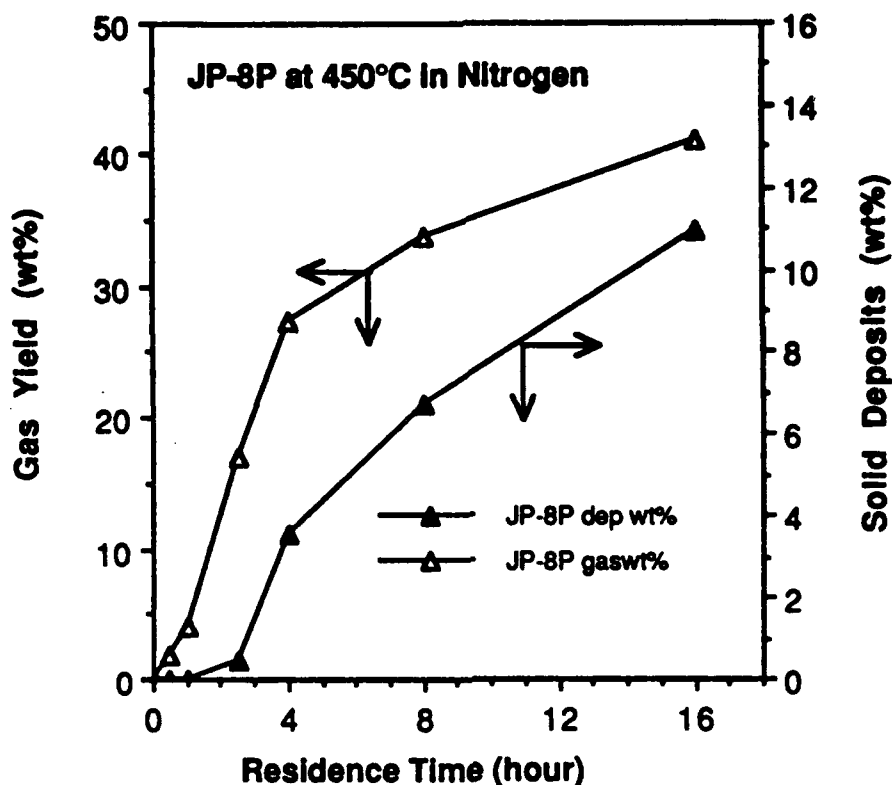


Figure 62. Thermal decomposition of petroleum-derived jet fuel JP-8P at 450°C to form gas and solid deposits.

formation were more remarkable within the first 4 h. In fact, there was not any solid after 0.5 and 1 hour stressing. The stressing over 2.5 h begin to cause remarkable solid formation, which is apparent from the results in Figure 33 for 4, 8, and 16 h stressing. The color of the liquid changed from colorless (original) to yellowish in 0.5 h, to yellow in 1 h, and to brown after 2.5 to 16 h stressing. These results indicate that the extent of decomposition of unstable components in JP-8P increases with increasing residence time for a certain period, and during this period the precursors to solid were formed and accumulated from the reactive intermediates. After this time/temperature threshold, the solid formation become much more remarkable.

The gas products from thermal stressing of JP-8P at 450°C for periods ranging from 0.5 to 16 h were analyzed by using AutoSystem gas chromatograph. Table 10 is a summary of the GC results. The gases included C₁-C₅ alkanes and C₂-C₅ olefins. The distribution pattern of gas components changed, and the total gas yields increased with increase in residence time. The major components in any case were the C₁-C₄ hydrocarbons. In the initial period (0.5 h), the concentration of ethane+ethylene in gas phase was remarkably higher than those of propane and

methane. The concentrations of propylene (about 14%) and 1-butene (about 6%) are also higher than those of other olefins. When the stressing time was extended to 1 h, the concentrations of propane (19.9 to 21%) and butane (5.9 to 8.1%) increased considerably, but those of methane and ethane+ethylene did not change to any significant extent. On the other hand, the concentrations of propylene and 1-butene decreased from 14.9 to 9.7% and from 6.4 to 3.0%, respectively. In fact, the concentrations of the C₃ and C₄ olefins in gases decreased with increasing residence time up to 8 h. Probably, this trend is also true for ethylene, although ethane and ethylene do not separate on the column used. The decrease in their concentrations may be due to either the in-situ H-transfer (to suppress the olefin formation or to convert the olefin to corresponding paraffin), or the increased amounts of other components, or both. The concentration of methane in gas increased from 17% in 1 hour to 29.3% in 4 hour. At the time of JP-8C stressing, the GC was not available. The gas products from JP-8C will also be analyzed by performing the duplicate thermal stressing experiments (see Table 21).

¹H NMR and GC-MS analyses of the liquid products from thermally stressed JP-8P at 450°C were performed in the work reported here. The tentative NMR assignments have been given in Task 2. Figure 63 shows the NMR spectrum of the original JP-8P. There are two major peaks in this spectrum, which are due to the resonance of paraffinic methylene and methyl hydrogens. This spectrum is different from that of coal-derived JP-8C, as mentioned above. Figures 64-67 present the NMR spectra of the liquid products from 1, 2.5, 4 and 8 h stressing of JP-8P, respectively. In general, the intensity of long-chain methylene hydrogens (1.05-1.60 ppm) decreases, and that of methyl hydrogens (0.5-1.05 ppm) increases with increasing time up to 4 h. This indicates the cracking of long-chain paraffins to form shorter-chain molecules, which increased the relative contents of methyl hydrogens. After 4 h at 450°C, the intensity of methyl hydrogens is almost as high as that of methylene hydrogens, as can be seen from Figure 27. It is interesting to note the progressive increase in the intensity of signals in the 1.5-2.0 ppm range from original JP-8P to that stressed for 4 h. Probably this is due to the formation of some cyclic hydrocarbons (not aromatic), whose methylene hydrogens show signals in this range. The formation of olefins from thermal cracking of long-chain paraffins is expected. In fact, there are also signals in the chemical shift range of 4.5 to 6.0 ppm in the NMR spectra of stressed samples (Figures 64-67), which can be attributed to olefins, but these signals are very low in intensity.

As we saw from Figures 24-28, the NMR spectra also revealed the progressive increase in the contents of aromatic compounds in the stressed JP-8P. The intensity of aromatic hydrogens (6.0-9.0 ppm) and methyl hydrogens alpha to an aromatic ring (2.0-2.6 ppm) increased monotonically with the increase in stressing time from 0 (original JP-8P, Figure 63) to 8 h (Figure 67). After 8 h, the alpha methyl hydrogens show very strong signals (Figure 67). This indicates that most of the alkylaromatics (formed and remained unchanged) are methyl-substituted ones. These results are consistent with the GC-MS analysis, as described below. The advantage of NMR

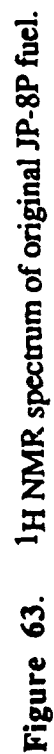
Table 21. Gas products from thermal stressing of JP-8P at 450°C for 0.5-16 h in N₂

Retention min	Compounds	Area%					
		0.5 h	1 h	2.5 h	4 h	8 h	16 h
1.4-1.6	Methane	17.49	16.96	23.01	29.31	24.48	23.93
1.7-1.9	Ethane + Ethylene	30.81	31.14	30.80	32.72	34.79	30.43
2.3-2.5	Propane	19.85	29.10	28.15	21.78	33.01	27.93
2.6-2.8	Propylene	14.39	9.67	4.98	2.75	0.02	1.66
3.1-3.5	iso-Butane	1.33	1.87	2.93	2.93	1.94	4.91
3.9-4.2	n-Butane	5.89	8.02	7.86	5.85	5.78	7.70
4.6-4.8	1-Butene	6.41	3.04	1.49	1.30	-	0.76
5.3-5.5	trans-2-Butene	0.55	-	-	0.33	-	0.22
5.9-6.1	cis-2-Butene	0.31	-	-	0.22	-	0.13
6.5-6.6	iso-Pentane	0.71	-	0.36	1.00	-	1.03
6.7-6.9	1,3-Butadiene ?	0.26	-	-	0.03	-	-
7.7-7.9	n-Pentane	1.02	0.20	0.63	1.18	-	1.06
8.9-9.1	1-Pentene	0.70	-	-	0.10	-	0.03


analysis is that it is simple and can provide information on the general feature of thermal degradation process of jet fuels. Although GC-MS analysis is time-consuming, and the spectra interpretation is much more difficult, it is GC-MS that can provide clear and important information on the change in contents of specific hydrocarbon components of jet fuels during thermal stressing.

We now turn to the identification of hydrocarbons in thermally stressed JP-8P. Figures 68-70 show the expanded retention time windows in the range of 1-16:53, 16:54-33:43 and 24-45 minutes, respectively. It is clear from Figures 68-70 that the extent of decomposition of n-C₈ through n-C₁₇ increased with increasing residence time at 450°C up to 4 h. This is accompanied by the progressive increase in the contents of lower alkanes and olefins (C₅-C₈) and those of alkylbenzenes (Figure 68), methylnaphthalenes (Figure 69) and dimethylnaphthalenes as well as other polyaromatic compounds (Figure 70). While long-chain paraffins are still the major components after 1 hour, all the C₁₁ to C₁₇ components almost disappear after 4 h. The present results unambiguously demonstrated that the long-chain paraffinic components in petroleum-derived jet fuels undergo significant decomposition reactions at high temperatures and most of them decompose completely at 450°C for 4 h. While the comparable GC-MS data for model compounds are not available at the present stage, it seems that the decomposition of the long-chain paraffins is faster in the stressing of real fuel than in the stressing of pure model compounds. This is considered

1961, 1962, 1963, 1964, 1965, 1966, 1967, 1968, 1969, 1970, 1971, 1972, 1973, 1974, 1975, 1976, 1977, 1978, 1979, 1980, 1981, 1982, 1983, 1984, 1985, 1986, 1987, 1988, 1989, 1990, 1991, 1992, 1993, 1994, 1995, 1996, 1997, 1998, 1999, 2000, 2001, 2002, 2003, 2004, 2005, 2006, 2007, 2008, 2009, 2010, 2011, 2012, 2013, 2014, 2015, 2016, 2017, 2018, 2019, 2020, 2021, 2022, 2023, 2024, 2025, 2026, 2027, 2028, 2029, 2030, 2031, 2032, 2033, 2034, 2035, 2036, 2037, 2038, 2039, 2040, 2041, 2042, 2043, 2044, 2045, 2046, 2047, 2048, 2049, 2050, 2051, 2052, 2053, 2054, 2055, 2056, 2057, 2058, 2059, 2060, 2061, 2062, 2063, 2064, 2065, 2066, 2067, 2068, 2069, 2070, 2071, 2072, 2073, 2074, 2075, 2076, 2077, 2078, 2079, 2080, 2081, 2082, 2083, 2084, 2085, 2086, 2087, 2088, 2089, 2090, 2091, 2092, 2093, 2094, 2095, 2096, 2097, 2098, 2099, 2100, 2101, 2102, 2103, 2104, 2105, 2106, 2107, 2108, 2109, 2110, 2111, 2112, 2113, 2114, 2115, 2116, 2117, 2118, 2119, 2120, 2121, 2122, 2123, 2124, 2125, 2126, 2127, 2128, 2129, 2130, 2131, 2132, 2133, 2134, 2135, 2136, 2137, 2138, 2139, 2140, 2141, 2142, 2143, 2144, 2145, 2146, 2147, 2148, 2149, 2150, 2151, 2152, 2153, 2154, 2155, 2156, 2157, 2158, 2159, 2160, 2161, 2162, 2163, 2164, 2165, 2166, 2167, 2168, 2169, 2170, 2171, 2172, 2173, 2174, 2175, 2176, 2177, 2178, 2179, 2180, 2181, 2182, 2183, 2184, 2185, 2186, 2187, 2188, 2189, 2190, 2191, 2192, 2193, 2194, 2195, 2196, 2197, 2198, 2199, 2200, 2201, 2202, 2203, 2204, 2205, 2206, 2207, 2208, 2209, 2210, 2211, 2212, 2213, 2214, 2215, 2216, 2217, 2218, 2219, 2220, 2221, 2222, 2223, 2224, 2225, 2226, 2227, 2228, 2229, 2230, 2231, 2232, 2233, 2234, 2235, 2236, 2237, 2238, 2239, 2240, 2241, 2242, 2243, 2244, 2245, 2246, 2247, 2248, 2249, 2250, 2251, 2252, 2253, 2254, 2255, 2256, 2257, 2258, 2259, 2260, 2261, 2262, 2263, 2264, 2265, 2266, 2267, 2268, 2269, 2270, 2271, 2272, 2273, 2274, 2275, 2276, 2277, 2278, 2279, 2280, 2281, 2282, 2283, 2284, 2285, 2286, 2287, 2288, 2289, 2290, 2291, 2292, 2293, 2294, 2295, 2296, 2297, 2298, 2299, 2300, 2301, 2302, 2303, 2304, 2305, 2306, 2307, 2308, 2309, 2310, 2311, 2312, 2313, 2314, 2315, 2316, 2317, 2318, 2319, 2320, 2321, 2322, 2323, 2324, 2325, 2326, 2327, 2328, 2329, 2330, 2331, 2332, 2333, 2334, 2335, 2336, 2337, 2338, 2339, 2340, 2341, 2342, 2343, 2344, 2345, 2346, 2347, 2348, 2349, 2350, 2351, 2352, 2353, 2354, 2355, 2356, 2357, 2358, 2359, 2360, 2361, 2362, 2363, 2364, 2365, 2366, 2367, 2368, 2369, 2370, 2371, 2372, 2373, 2374, 2375, 2376, 2377, 2378, 2379, 2380, 2381, 2382, 2383, 2384, 2385, 2386, 2387, 2388, 2389, 2390, 2391, 2392, 2393, 2394, 2395, 2396, 2397, 2398, 2399, 2400, 2401, 2402, 2403, 2404, 2405, 2406, 2407, 2408, 2409, 2410, 2411, 2412, 2413, 2414, 2415, 2416, 2417, 2418, 2419, 2420, 2421, 2422, 2423, 2424, 2425, 2426, 2427, 2428, 2429, 2430, 2431, 2432, 2433, 2434, 2435, 2436, 2437, 2438, 2439, 2440, 2441, 2442, 2443, 2444, 2445, 2446, 2447, 2448, 2449, 2450, 2451, 2452, 2453, 2454, 2455, 2456, 2457, 2458, 2459, 2460, 2461, 2462, 2463, 2464, 2465, 2466, 2467, 2468, 2469, 2470, 2471, 2472, 2473, 2474, 2475, 2476, 2477, 2478, 2479, 2480, 2481, 2482, 2483, 2484, 2485, 2486, 2487, 2488, 2489, 2490, 2491, 2492, 2493, 2494, 2495, 2496, 2497, 2498, 2499, 2500, 2501, 2502, 2503, 2504, 2505, 2506, 2507, 2508, 2509, 2510, 2511, 2512, 2513, 2514, 2515, 2516, 2517, 2518, 2519, 2520, 2521, 2522, 2523, 2524, 2525, 2526, 2527, 2528, 2529, 2530, 2531, 2532, 2533, 2534, 2535, 2536, 2537, 2538, 2539, 2540, 2541, 2542, 2543, 2544, 2545, 2546, 2547, 2548, 2549, 2550, 2551, 2552, 2553, 2554, 2555, 2556, 2557, 2558, 2559, 2560, 2561, 2562, 2563, 2564, 2565, 2566, 2567, 2568, 2569, 2570, 2571, 2572, 2573, 2574, 2575, 2576, 2577, 2578, 2579, 2580, 2581, 2582, 2583, 2584, 2585, 2586, 2587, 2588, 2589, 2590, 2591, 2592, 2593, 2594, 2595, 2596, 2597, 2598, 2599, 2600, 2601, 2602, 2603, 2604, 2605, 2606, 2607, 2608, 2609, 2610, 2611, 2612, 2613, 2614, 2615, 2616, 2617, 2618, 2619, 2620, 2621, 2622, 2623, 2624, 2625, 2626, 2627, 2628, 2629, 2630, 2631, 2632, 2633, 2634, 2635, 2636, 2637, 2638, 2639, 2640, 2641, 2642, 26



1H 0P 450 1144


 SONG S30
 GATE 6.3-91
 SF 360 134
 SY 83.0
 O1 5400.000
 S1 32760
 FO 32768
 MW 3000.000
 HZ/PT 365
 PW 17.8
 PG 5.000
 AG 3.277
 NG 8
 MS 16
 TE 297
 FM 6300
 O2 12100.000
 DP 101.00
 LB 0.0
 GB 0.0
 CY 40.00
 F1 0.001P
 F2 -1.000P
 HZ/CM 90.034
 PPM/CM 250
 SR 3981.00

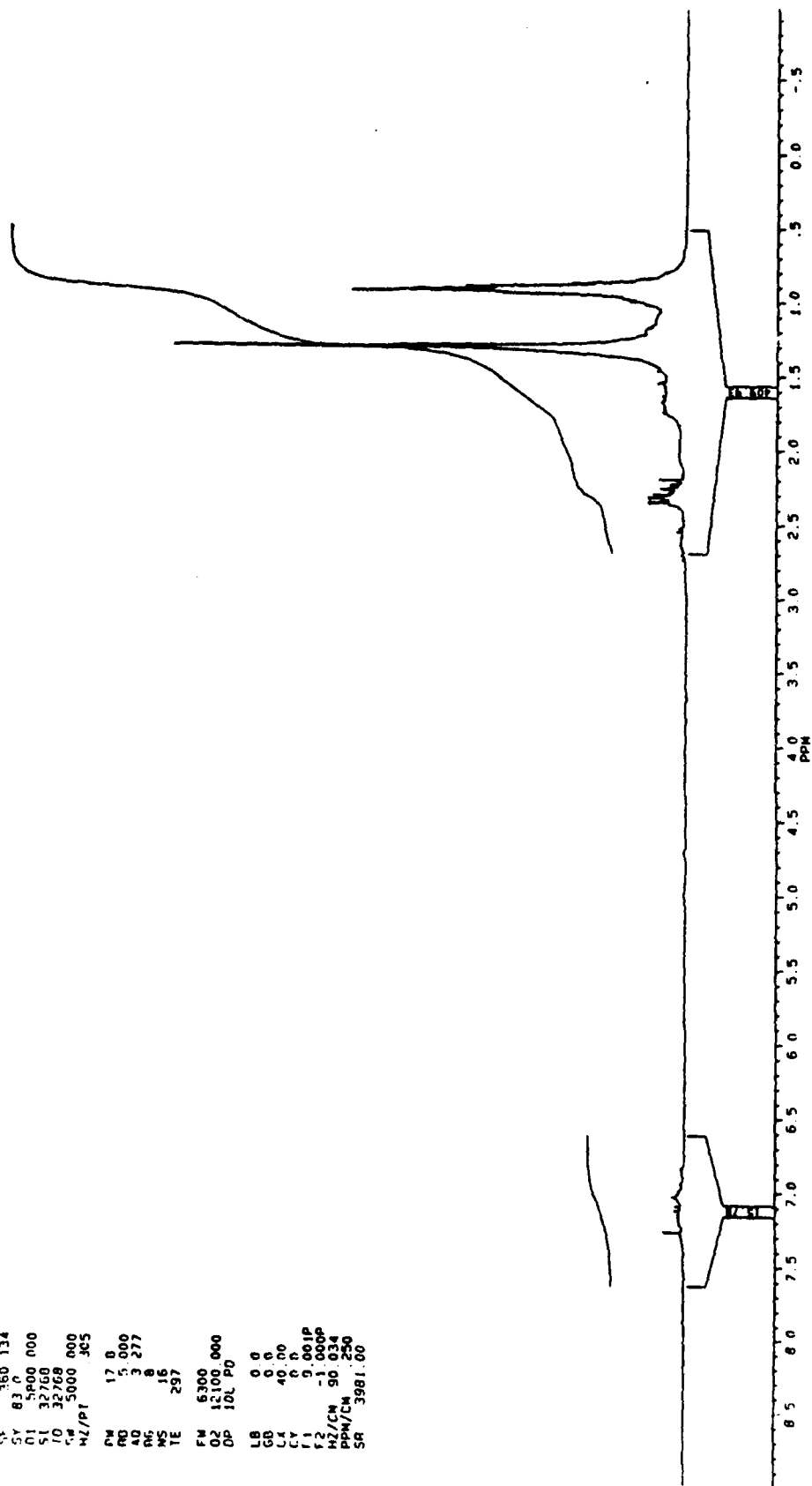



Figure 64. ¹H NMR spectrum of thermally stressed JP-8P at 450°C for 1 h.

 **BRUKER**
 SONG S31
 DATE 6-3-91
 CF 360.134
 CY 6300.000
 SI 5000.000
 FI 32768
 DI 32768
 SD 5000.000
 HZ/PT 305
 PW 17.8
 NO 5.000
 AQ 3.277
 RG 8
 NS 16
 TE 297
 FW 6300.000
 NZ 12100.000
 DP 10L PQ
 LB 0.0
 GB 0.0
 CY 40.00
 CY 0.0
 F1 9.001P
 F2 -1.000P
 HZ/CM 90.034
 PPM/CM 250
 SR 3981.00

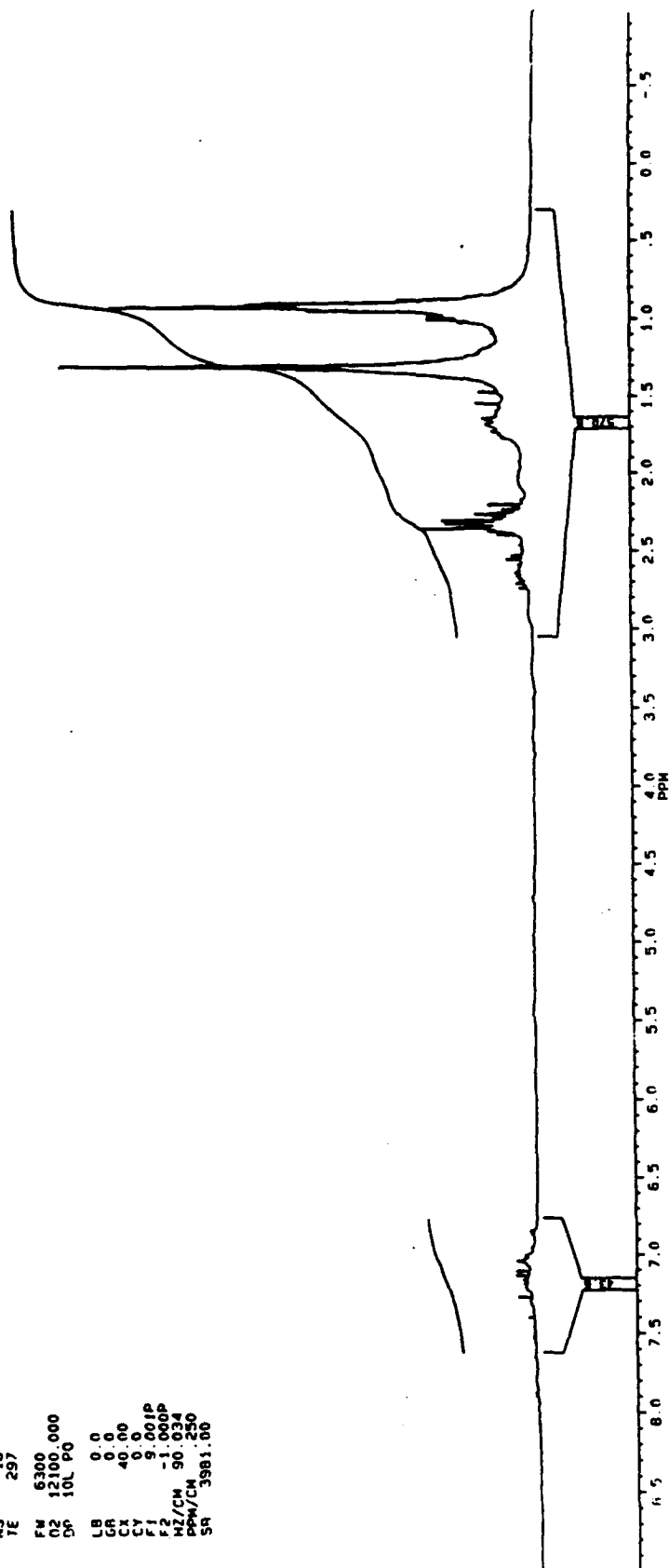


Figure 65. ¹H NMR spectrum of thermally stressed JP-8P at 450°C for 2.5 h.

OXIR

SONG S33
DATE 6-3-91

SF 360 134
SY 83.0
O1 5800.000
SI 32768
TD 32768
SW 5000.000
WZ/PT 305

PW 17.8
AQ 5.000
RG 3.277
RG 16
TE 297

FW 5300
D2 12100.000
D6 10L P0

LB 0.0
GB 0.0
CX 40.00
CY 0.0
F1 9.001P
F2 -9999
WZ/CM 90.027
PPM/CM 250
SA 3981.00

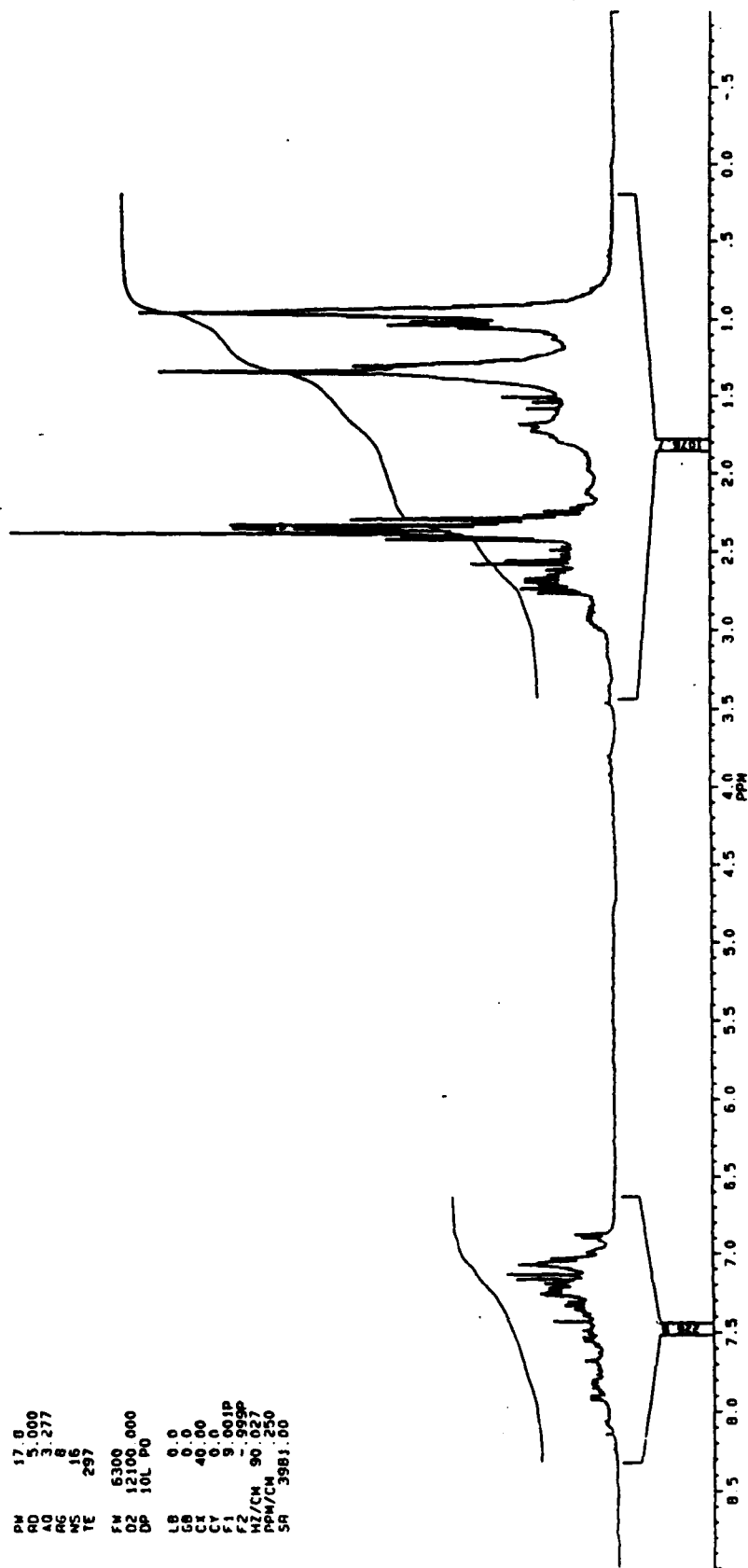


Figure 67. ^1H NMR spectrum of thermally stressed JP-8P at 450°C for 8 h.

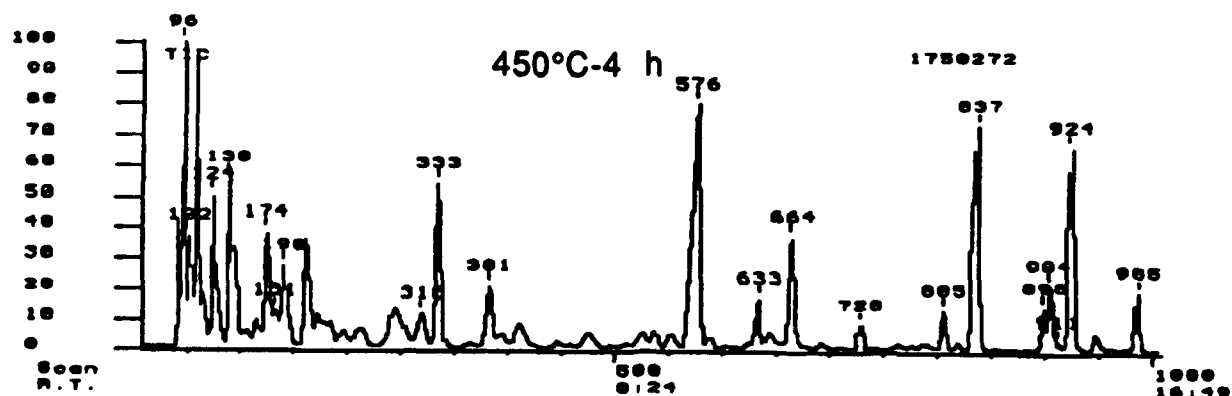
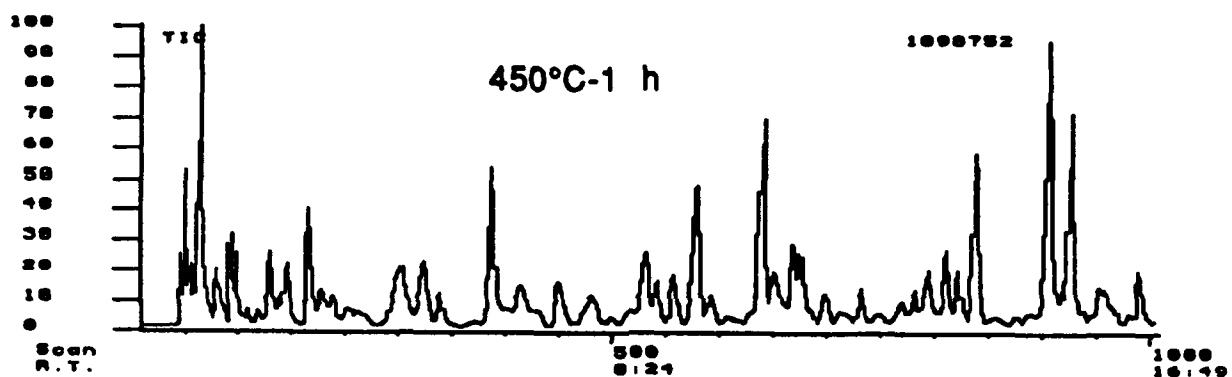
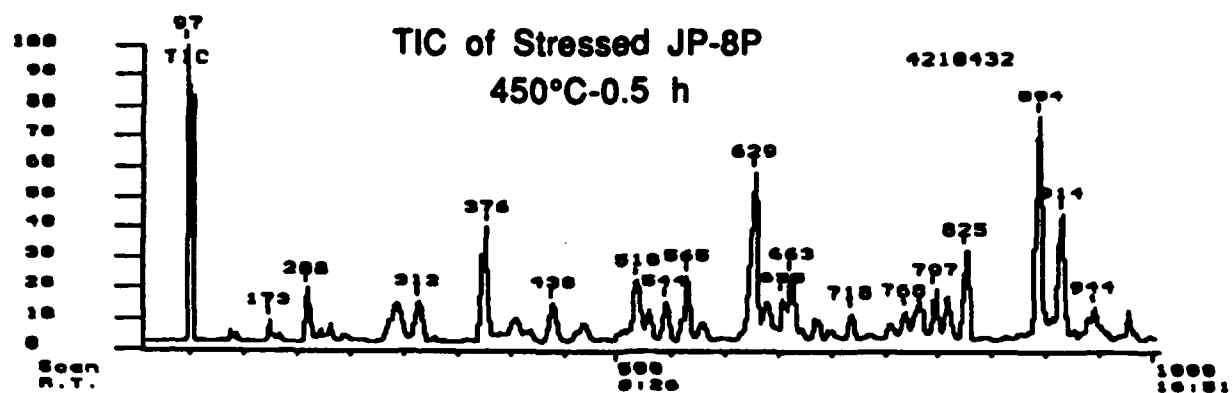


Figure 68. Retention time window I (1-16:53 min) of GC-MS profiles for thermally stressed, petroleum-derived JP-8C fuel for 0.5, 1 and 4 h. The peak with scan number of 97 in the top TIC is due to solvent contamination.

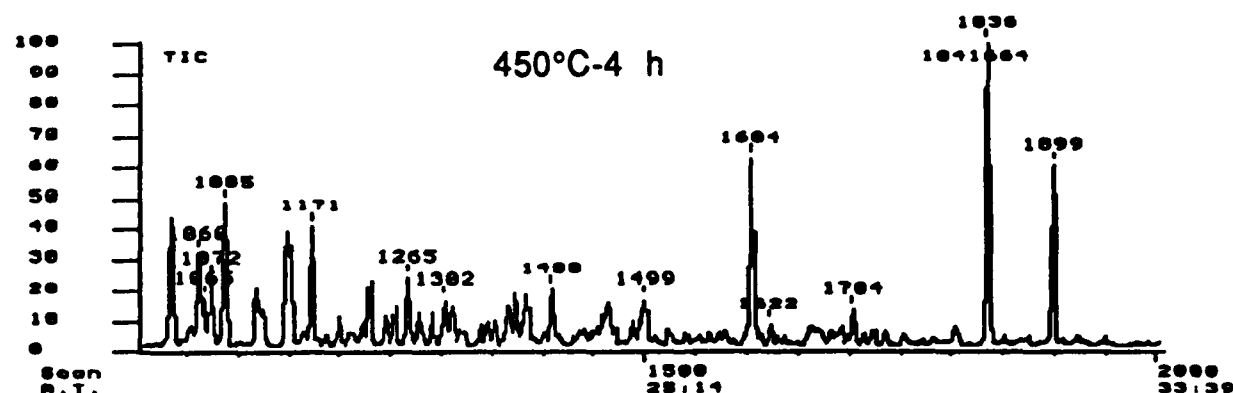
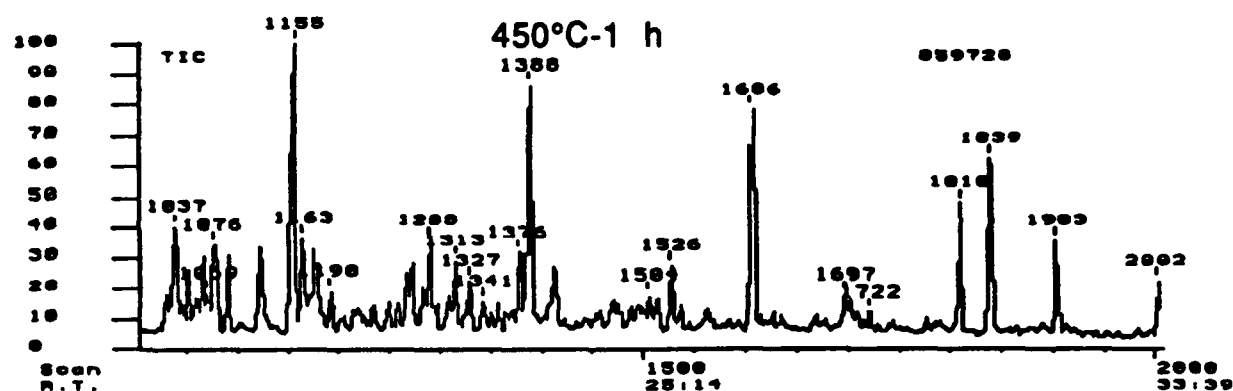
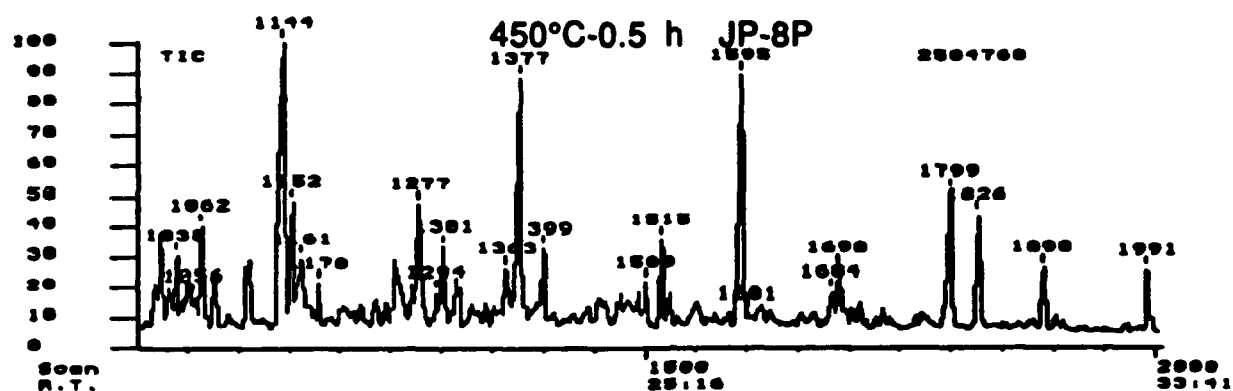


Figure 69. Retention time window II (16:54-33:43 min) of GC-MS profiles for thermally stressed, petroleum-derived JP-8C fuel for 0.5, 1 and 4 h.

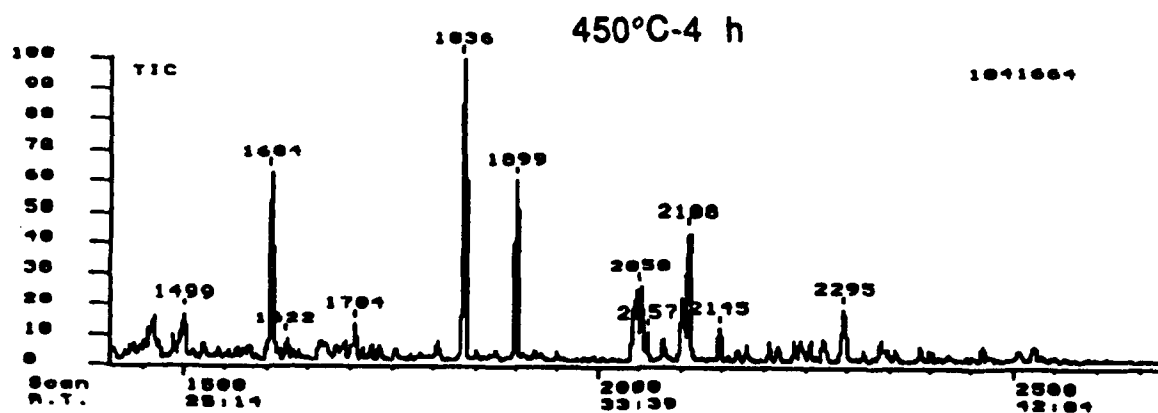
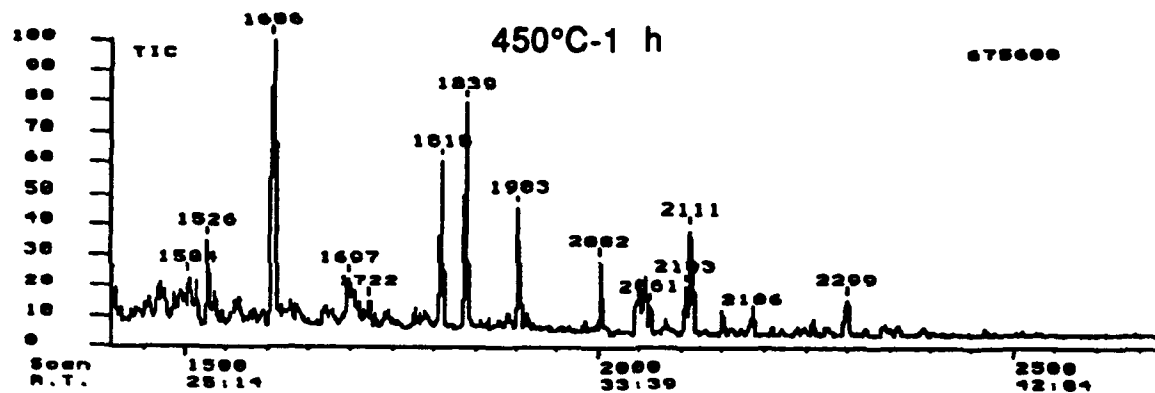
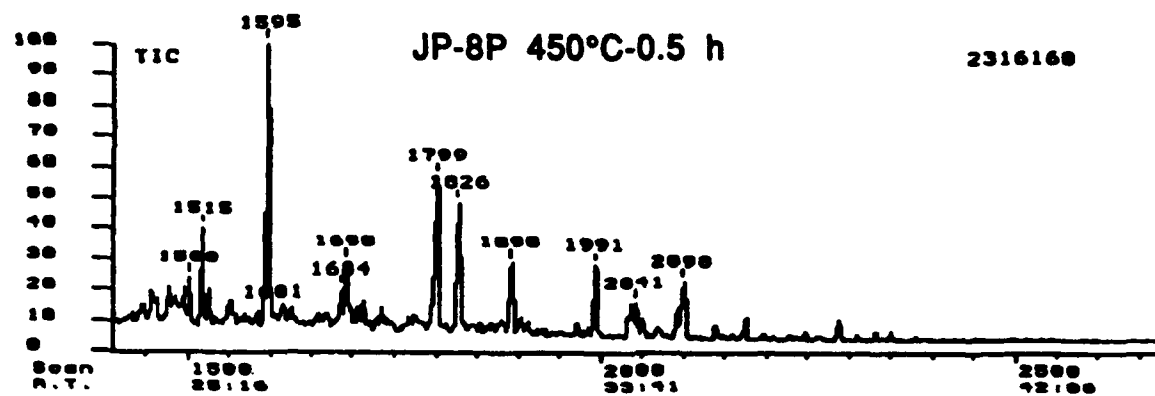


Figure 70. Retention time window III (24-45 min) of GC-MS profiles for thermally stressed, petroleum-derived JP-8C fuel for 0.5, 1 and 4 h.

to be due to intermolecular interactions. Our previous results for stressing of saturate fraction and whole JP-8P have shown that intermolecular interactions between different compounds or radicals play an important role in the thermal degradation process. Comparison of these GC-MS results with those for coal-derived fuel (Task 2) reinforces our earlier conclusion [1] that the higher thermal stability of JP-8C is due mainly to its higher contents of relatively stable cycloalkanes. The presence of unstable long-chain paraffins in JP-8C is offset by the presence of hydroaromatics such as tetralins, which can stabilize the radicals generated from unstable compounds through H-donation.

The liquid products from 450°C-16 h stressing of JP-8P were analyzed by GC-MS. Figure 71 and Table 22 show the GC-MS results for the liquid products. As we can see from the GC-MS results, all the long-chain paraffins with C-chain longer than 9, which were the major components in the original JP-8P, have completely disappeared. Apparently, they were decomposed and transformed into gases and other liquid products as well as solid deposits. There exist both lighter and heavier components in the liquids from the JP-8P after 16 h at 450°C. The lighter components are n-C₅ to n-C₈ paraffins, C₆ and C₇ olefins and cyclohexanes. All the other products are 1-ring to 4-ring aromatics (Table 22). The relatively lighter products are benzene, toluene and C₂-benzenes. The heavier products are C₃- to C₅-substituted benzenes, alkylnaphthalenes, biphenyl, fluorenes and pyrenes. Unlike the liquids from short time stressing, there are some similarities between the liquids from long time (450°C-16 h) stressing of JP-8P (Table 22) and JP-9C (Table 16), in that many aromatic products are the same, but their relative concentrations (Figures 37 and 71) as well as the yield of liquids (Figures 27 and 61) are different.

Mechanistic Considerations

The mechanisms for the formation of many products identified in the liquids formed from JP-8P and JP-8C and their saturates have been discussed in the previous quarters [9]. Here in this section, we will discuss the mechanistic aspects of fuel degradation and solid formation, based on the results described in Task 1 to Task 4. It is considered that the degradation of hydrocarbon jet fuels at high temperatures proceeds through many parallel and consecutive reactions, and the chemistry is extremely complex. First of all, we will try to discuss some chemistry related to the initial decomposition of straight-chain paraffins which are the major components of petroleum-derived jet fuel and also present in coal-derived jet fuel. The GC results of gas products from JP-8P and from n-tetradecane suggest that the preference for the formation of gas products during initial decomposition of paraffinic components was $C_2 \geq C_3 > C_1 > C_4$. The initial C₂-C₅ gas species included both paraffin and olefin, but the concentration of the latter decreased with increasing residence time. The C₁-C₄ paraffins may derive from the thermal cracking of long-chain paraffin C_mH_{2m+2}, which could give C_{m-n}H_{2(m-n)} olefin and gaseous product C_nH_{2n+2} (m: the carbon number of a given long-chain paraffinic component in jet fuels, $m \geq 8$; n: the carbon number of the

DS90 Chromatogram report Run: SONG670005, 17-Jan-91 11:07
 JP-8P/5ml 450oC-16h-N2 SPLIT DB-17 40-5 TO 280-10e4 0.1UI

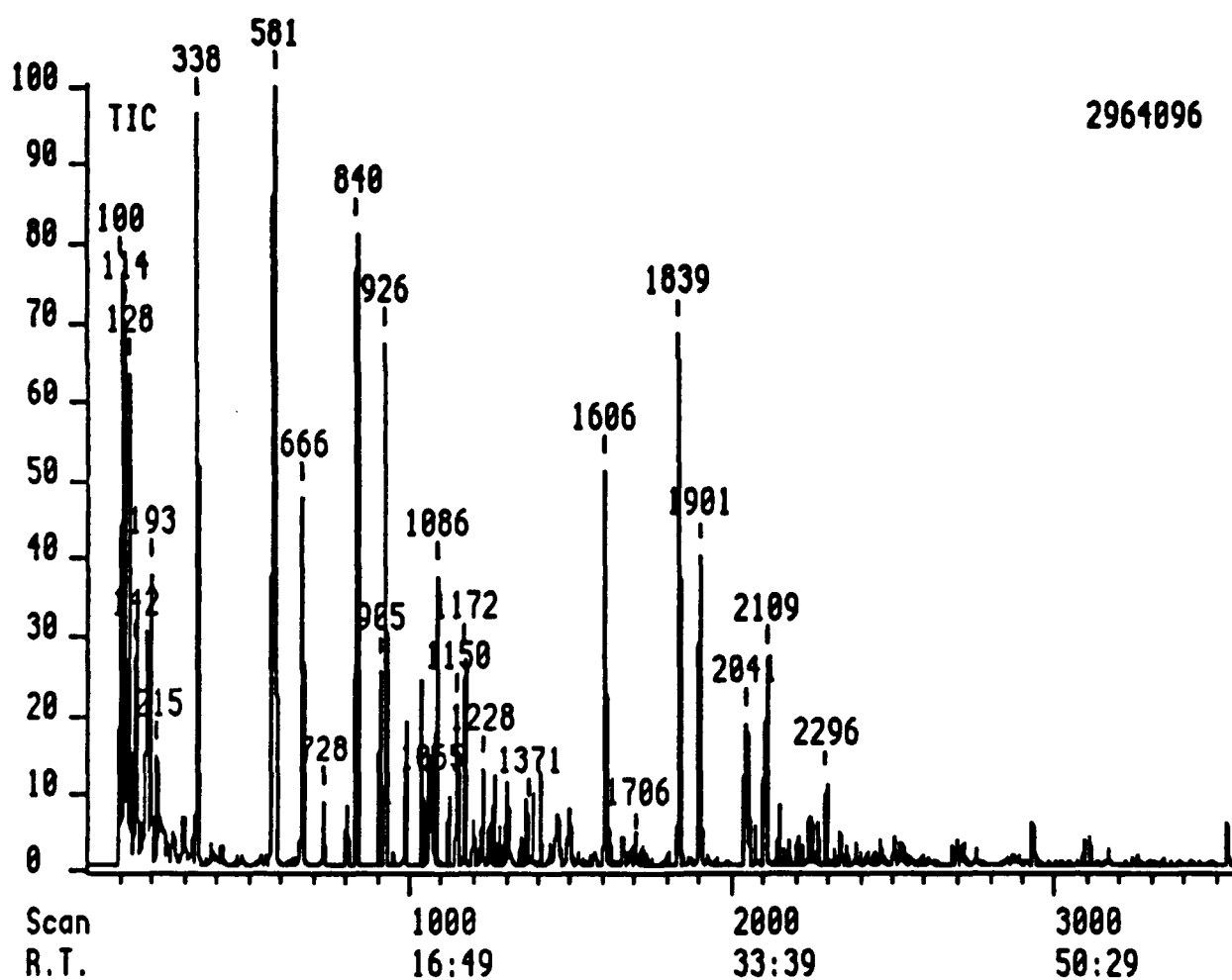


Figure 71. Total ion chromatogram of thermally treated whole JP-8P at 450°C for 16 h in N₂.

Table 22. Identified compounds in thermally treated JP-8P at 450°C for
16 h in N₂ by GC-MS using modified procedure

Scan No.	Retention Time	Molecular Ion	Base Peak	Compounds Identified
100	1:40	72	43	n-Pentane
114	1:54	86	57	n-Hexane
128	2:08	84	56	Hexane
142	2:22	100	43	n-Heptane
147	2:27	84	56	Cyclohexane
		98	56	1-Heptane
168	2:49	96	81	Methylcyclohexene ?
185	3:06	98	69	Ethylcyclopentane ?
193	3:14	78	78	Benzene
215	3:36	112	97	C ₂ -cyclohexane
		114	43	n-Octane
338	5:40	92	91	Toluene
581	9:46	106	91	p- or m-Xylene
666	11:11	106	91	o-Xylene
728	12:14	120	105	iso-Propylbenzene
806	13:33	120	91	n-Propylbenzene
840	14:07	120	105	Methylethylbenzene
905	15:13	120	105	Methylethylbenzene
926	15:34	120	105	C ₃ -Benzene
986	16:34	134	119	C ₄ -Benzene
1034	17:49	1340	105	C ₃ -Benzene
1060	17:49	1340	105	C ₄ -Benzene
1060	17:54	134	105	C ₄ -Benzene
1072	18:02	134	119	C ₄ -Benzene
1086	18:16	134	119	C ₄ -Benzene
1117	18:47	134	105	C ₄ -Benzene
1150	19:20	134	119	C ₄ -Benzene
1172	19:43	134	119	C ₄ -Benzene
1198	20:09	148	133	C ₅ -Benzene
1228	20:39	132	117	Methylindan
1244	20:55	134	119	C ₄ -Benzene
1252	21:03	134	119	C ₄ -Benzene
1265	21:16	134	119	C ₄ -Benzene

Table 22 (continued)

1277	21:29	148	119	C ₅ -Benzene
1289	21:41	148	119	C ₅ -Benzene
1303	21:55	148	199	C ₅ -Benzene
1308	22:00	148	133	C ₅ -Benzene
1371	23:04	134	119	C ₄ -Benzene
1383	23:16	148	119	C ₅ -Benzene
1408	23:41	132	117	Methylindan
1464	24:37	148	133	C ₅ -Benzene
		146	131	Methylindan
1500	25:14	146	131	Methylindan
1606	27:01	128	128	Naphthalene
1706	28:42	160	145	C ₃ -indan ?
1839	30:56	142	142	2-Methylnaphthalene
1901	31:59	142	142	1-Methylnaphthalene
2041	34:20	156	141	2-Ethylnaphthalene
2046	34:25	156	156	Dimethylnaphthalene
2051	34:30	156	156	Dimethylnaphthalene
2057	34:36	154	154	Biphenyl
2100	35:20	156	141	1-Ethylnaphthalene
2109	35:29	156	156	Dimethylnaphthalene
2145	36:05	156	156	Dimethylnaphthalene
		170	155	C ₃ -naphthalene
2235	37:36	170	155	C ₃ -naphthalene
2296	38:38	170	170	Trimethylnaphthalene
2502	42:06	166	166	Fluorene
		184	169	C ₄ -naphthalene ?
2524	42:28	180	165f	Methylfluorene ?
2532	42:36	168	167	Methylbiphenyl ?
2682	45:08	180	165	Methylfuroene ?
2698	45:24	180	180	Methylfluorene ?
		194		
2717	45:43	180	180	Methylfluorene ?
2758	46:24	180	165	Methylfluorene
		182		
2932	49:20	178	178	Phenanthrene
3093	52:03	192	192	Methylphenanthrene

Table 22. (continued)

3106	52:16	192	192	Methylphenanthrene
3166	53:16	192	192	Methylphenanthrene
3256	54:47	206	206	Dimethylphenanthrene ?
3335	56:07	206	206	Dimethylphenanthrene ?
3536	59:30	202	202	Pyrene
3681	61:57	216	216	Methylpyrene ?
3735	62:51	216	216	Methylpyrene ?
3743	7259	216	216	Methylpyrene ?

products, $n \leq 5$). This path could rationalize the the formation of C_6 - C_{11} olefins from short time stressing of JP-8P (see below). The decomposition of C_mH_{2m+2} can also produce $C_{m-n}H_{2(m-n)+2}$ paraffin and olefinic gaseous product C_nH_{2n} , which accounts for the formation of C_2 - C_4 olefins from JP-8P.

These two paths are generalized by formulas 1 and 2. A more complex case is shown by formula 3, which is the decomposition of one large molecule to form several smaller molecules. The source of the initial radical intermediates in path 1 and path 2 are essentially the same, homolytic C-C bond cleavage as shown in formula 4. If the reactive radicals can be hydrogenated, they will be stabilized and become the corresponding paraffins. However, since there is no external hydrogen source in the initial reaction stage, these two radicals must be stabilized by the following reactions: H-abstraction, radical coupling, and dehydrogenation. Formulas 5-8 indicates the possible reactions of the initial radical intermediates including H-abstraction (5-6) and radical decomposition (7-8). Another reaction that could take place in competition to the H-abstraction reactions is the radical coupling of two radicals, as shown in formula 9. Some examples of the reactions 1 and 2 are given by formulas 10-11. The radical coupling may be a considerable reaction when the above H-abstraction paths are not readily available for the radicals. Because of this, there is uncertainty about whether all the products obtained from thermal stressing were formed directly from the decomposition of long-chain paraffins.

The above discussion aims at developing a fundamental understanding of the initial decomposition process. Our preliminary GC-MS analysis of liquid products and GC of gas products provided some supporting evidence for the proposed reaction paths shown by formulas 1-3. For example, we have identified C_6 - C_{11} olefins, and C_5 - C_{17} paraffins in the liquid products, and C_1 - C_5 paraffins as well as C_2 - C_4 olefins in the gas products from thermal stressing of JP-8P at 450°C for 1 hour. These appeared to be consistent with the reaction paths shown by formulas 1-3. Some other products including C_1 - to C_4 -cyclohexanes, benzene to C_5 -benzenes, and alkylindans were also identified.

Scheme I. Initial Decomposition of n-Alkane C_mH_{2m+2}

Possible Decomposition Reactions

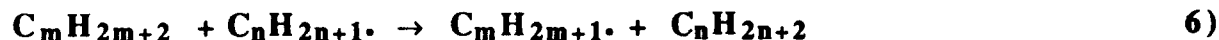


Possible Mechanisms

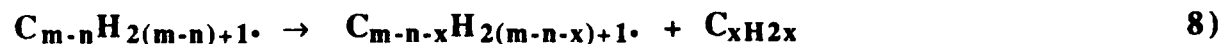
Initial Radical Generation



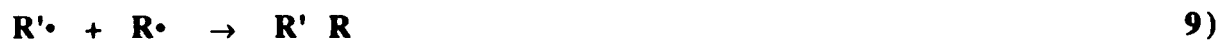
Attacking of Radical to Paraffin



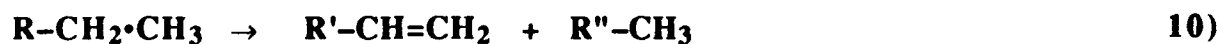
Radical Decomposition



Radical Coupling



Examples of 1-2) given by 10-11)



(R' = Alkyl group; R'' = alkyl or hydrogen)

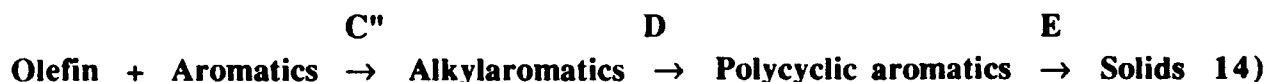
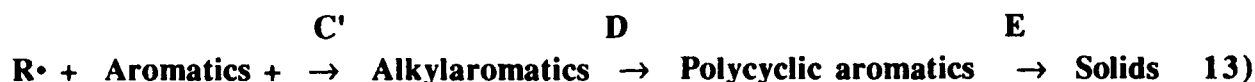
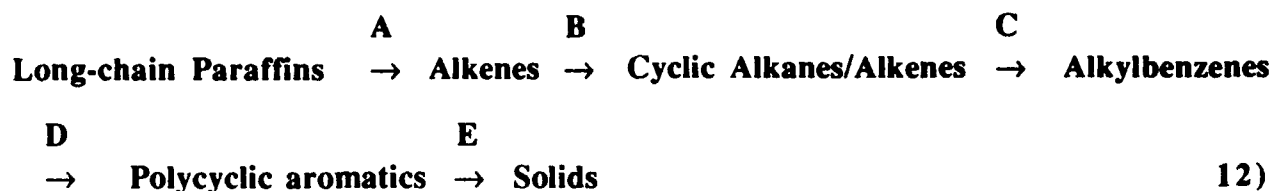
We now turn to the 'solid-forming' reactions. Two facts should be mentioned first before discussing the reactions for solid formation. First, there is an induction period for deposit formation from both JP-8C and JP-8P at 450°C under 100 psi N₂ (Task 2 and Task 4). This period, within which there was no solid formation or solids were not detectable, appeared to be longer with JP-8C than with JP-8P. Under the conditions tested, the amounts of the deposits were remarkably lower with JP-8C and its saturate fraction than with JP-8P and its saturate fraction. Second, solid state ¹³C NMR and FT-IR analyses clearly showed that the deposits from thermal stressing of a number of model compounds and jet fuel samples, are polyaromatic in nature.

The overall reaction sequences for solid formation from long-chain paraffins under the conditions used may be step-by-step in process, as shown in Scheme II. A number of alkenes, cyclic alkanes and alkylbenzenes have been found in the liquid product from JP-8P stressing at 450°C for 1 h, where no solid was formed. Based on this fact, the chemical reactions occurring during the observed induction period may be those shown in Steps A to D in formula 12 of Scheme II. When there is considerable amount of aromatics formed, the following two reactions may begin to occur: the attack of radical (formula 13) and olefin (formula 14) to form alkylaromatics (Steps C' and C'' in Scheme II), which undergo further condensation and/or coupling reactions to form polyaromatics.

The questions as to what are the structure and reactivity of the initially formed (may not necessarily be those mentioned above) species written as 'Cyclic Alkanes/Alkenes', remain to be answered. As reported in previous quarter [1], we also observed the formation of cyclohexanes and alkylbenzenes from the JP-8P saturate fraction which originally consists mainly of long-chain paraffins. Undoubtedly, the above-mentioned products were formed mainly at the expense of long-chain paraffins. Another related fact is that in the model compound studies, thermal stressing of long-chain paraffins such as decane, dodecane and tetradecane produced remarkably higher amounts of solids than cycloalkanes such as decalin [1]. Probably, the decomposition of long-chain paraffins to form alkylaromatics is a major reaction process in the induction period leading to solid formation from JP-8P in later stage. This process involves some very reactive intermediates which ultimately lead to a higher rate of solid formation. If the 'Cyclic Alkanes/Alkenes' in Scheme II are the key intermediates to the precursors (to solids), they must have higher reactivity than the identified major cycloalkane components in coal-derived JP-8C and its saturate fraction, because the amounts of solid formed from JP-8P saturates and whole fuel samples are remarkably higher than the corresponding JP-8C samples. Such intermediates need to be identified in the future work.

Apparently the so-called precursors to solids are formed and/or accumulated during the induction period. One of the key questions is what are the precursors? At the present stage, there is no clear answer to this question. However, based on the preliminary results of spectroscopic characterization of solids formed from jet fuels and model compounds, it is likely that the two- to

Scheme II. Possible Processes for Solid Formation from n-Paraffins



four-ring aromatic compounds can be precursors to the solids. In fact, such aromatics have been found in the liquids from JP-8C and JP-8P treated at 450°C for 4 h and for 16 h. In the previous report [1], we noted that although solid formation and decomposition of liquid components were significant with JP-8P samples, there are no remarkable amounts of three-ring and larger polycyclic aromatics in the treated liquid products, and concentrations of alkylnaphthalenes in these liquids are also lower than those in treated JP-8C samples. These results, however, do not suggest a major reaction process for solid formation without involving these polycyclic aromatics.

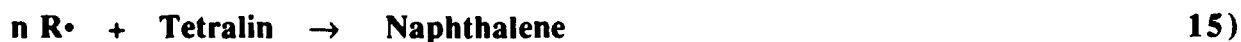
It seems reasonable to consider the two- to four-ring aromatic compounds as some of the precursors to the solids, although we still do not know the specific compounds. First, the deposits obtained are polyaromatic in nature and at the time just before they were formed, they were no longer soluble. Second, the coupling of the larger than two-ring aromatics will give polycondensed aromatics whose size is equal to or larger than four rings. Such polycondensed aromatics have very limited solubility, hence they could 'precipitate' onto the reactor wall and undergo further condensation reaction. The agglomeration of such species will give large-sized deposits.

In fact, we have found that there are also species in the treated JP-8P and JP-8C and their saturate fractions (450°C for over 4 h) which are soluble in the treated jet fuel samples but precipitate when n-pentane was added. The solubility of the saturates of jet fuels is similar to that of pentane, but the thermally treated jet fuels have higher solubility because of their higher contents of alkylbenzenes, as compared to the original fuel. These pentane-insoluble species might fall into the category of gum, rather than the solid deposits. However, this observation at least indicates that when the condensation degree of aromatics formed in the liquid phase becomes sufficiently high, they can hardly be solubilized in the liquid phase and/or gas phase and tend to 'precipitate' and adhere to the reactor wall. This is apparently the beginning of the solid deposition. On the other hand, the exact state of the reaction system under the solid-forming conditions is not clear, and there may be a

continuous change of the state between liquid, gas and supercritical state due to the continuous chemical reactions.

When one compares the thermal stability of coal- and petroleum-derived jet fuels, a question that arise is why the JP-8C is more stable than JP-8P ? At the present stage, the most unambiguous answer is that JP-8C has higher contents of thermally stable cycloalkanes. Its relatively higher contents of hydroaromatics such as tetralins is also a good reason for less solid formation, because the weak benzylic C-H bonds in tetralin-type compounds provide a pool for H-abstraction which will stabilize the reactive radicals, as shown in Scheme III [5]. On the other hand, there are several long-chain paraffins present in the original JP-8C in relatively high (but much lower than those in JP-8P) concentrations. They disappeared after 4 h at 450°C. The questions that arise are what was their transformation process, and why they did not cause remarkable solid formation in this case ? If we consider the fuel degradation and solid formation processes according to the proposed sequences shown by the above formulas 1-11, two things become apparent. First, if the radicals from initial C-C bond cleavage (formula 4) can be stabilized, further degradation can be reduced by preventing the secondary reactions induced by the primary decomposition. The H-donation from hydroaromatics present in JP-8C can stabilize the thermally generated radicals (formula 15), thus preventing other compounds from their attack [5]. If the hydroaromatics are not readily available as in the case of saturate fraction or in the later reaction stage of whole JP-8C, the cycloalkanes such as decalin can also act as H-donors, as shown in formula 16. Second, if the coupling of the aromatics formed from dehydrogenation of cycloalkanes begin to take place, the hydroaromatics and/or cycloalkanes (when they are still present) may suppress such coupling/condensation reactions by stabilizing the radical intermediates through H-donation. In addition, it should be mentioned that the reason we used the term 'thermally stable cycloalkanes' to represent the major cycloalkane components contained in JP-8C, is that there may be thermally unstable cycloalkanes. The cyclohexanes substituted with long alkyl side-chain are less stable than those with shorter side-chain. For example, n-butylcyclohexane is less stable than ethylcyclohexane. Fortunately, there are not considerable amounts of long-chain (longer than n-C5 side-chain) substituted cycloalkanes in JP-8C. It is not yet clear whether such less stable species are formed during the decomposition of long-chain paraffins.

Scheme III. Possible H-Transfer Reactions During JP-8C Stressing



Finally, it should be noted that the above mechanistic considerations for fuel degradation and solid formation processes are still in the hypothetical stage. We seek to derive more detailed information by identifying and quantifying the initial and later reaction products. The systematic analysis of the liquid and gas products from jet fuels as well as those from model compounds stressed under various reaction conditions will be performed using GC-MS and GC. The results and modified mechanisms will be reported in the future.

Task 5. Characterization of Solid Deposits

The principal objective of this task is to characterize solid deposits formed in aircraft fuel systems and in microautoclaves to shed light on the mechanisms of solid formation and deposition. Solids deposits were analyzed by using various spectroscopic techniques, optical and electron microscopy, and x-ray diffraction.

A sample of actual aircraft fuel system deposits, identified as "afterburner component B" was analyzed by using solid state CPMAS ^{13}C NMR, FTIR, optical microscopy, XRD and SEM. Solid samples produced from jet fuels and model compounds in tubing reactors were also analyzed by NMR, FTIR and optical microscopy. The results of these analyses on actual fuel system deposits and solids produced in laboratory experiments are summarized below. A more detailed discussion of the data on solid samples can be found in the quarterly reports [9-11].

Aircraft Fuel System Deposits

The deposit sample (approximately 140 mg) contains solids with two distinctly different morphologies; visibly porous, black globular particles and thin flakes with a gray luster. The globular particles and flakes were analyzed separately, except for the NMR analysis in which the whole sample was placed in the spinner because of the small sample size.

Solid-State CPMAS ^{13}C NMR

A Chemagnetics M-100 solid-state ^{13}C NMR spectrometer was used for analyzing the whole deposit sample. No meaningful signal could be obtained from the sample during the CPMAS ^{13}C NMR analysis, because the sample caused severe detuning of the probe. This is probably due to the high electrical conductivity of the sample because of the graphitic nature of the deposits and/or metal contamination. Alternatively, the presence of paramagnetic substances can cause similar behavior. A preliminary examination of the deposits by scanning electron microscopy (SEM) equipped with an energy-dispersive x-ray detector did not show any detectable level of metal (including titanium) contamination. Presumably, it is the graphitic nature of the flakes resulting in the high conductivity which interferes with NMR measurements. As will be discussed later, FTIR data suggest that the flakes consist of highly condensed polyaromatic sheets and optical micrographs of these solids indicate a high degree of crystallite alignment in thin flakes. Altogether, these observations suggest that the flakes are composed of large planar molecules with some degree of alignment, similar, in essence, to the structure of graphite. SEM analyses and x-ray diffraction data presented below confirm that the flakes consist of large sheets of crystallites with two-dimensional alignment, as found in turbostratic carbons [12].

Fourier Transform Infrared Spectroscopy

FTIR spectra of the solids were obtained by using a Digilab FTS 60 instrument in the Polymer Science Program at Penn State University. Standard KBr pellets of the solid samples were prepared by grinding 1 mg sample with 150 mg KBr. Sixteen scans of the pellets were coadded at a resolution of 2 cm^{-1} to obtain the FTIR spectra. Some of the spectra were subjected to baseline corrections using standard software.

Figure 72 shows the spectrum obtained from the globular particles of the deposits. The broad band between 3350 and 3550 cm^{-1} is OH stretch due to water adsorbed on KBr pellets. This is a commonly encountered problem with pellet preparation. The strong bands at 3050 cm^{-1} (aromatic C-H stretch), 1600 cm^{-1} (aromatic ring stretch) and at $700\text{--}900\text{ cm}^{-1}$ (aromatic H out-of-plane bend) indicate the highly aromatic nature of the solid sample. The bands between 2850 and 2970 cm^{-1} are assigned to CH_3 and CH_2 groups, indicating alkyl substitution on the aromatic rings. Relatively high intensity of the absorption at 750 cm^{-1} (assigned to four adjacent aromatic H) compared to the other bending modes (near 815 , 833 , and 860 cm^{-1} assigned to three adjacent aromatic H, two adjacent aromatic H, and isolated aromatic H, respectively) suggest that the aromatic ring systems are not heavily substituted. The broad band between 1000 and 1300 cm^{-1} and the sharp shoulder at 1700 cm^{-1} may be attributed to C-O groups. These observations suggest that the globular particles in actual fuel system deposits consist of polynuclear aromatic hydrocarbons with a low degree of alkyl substitution and a low degree of aromatic condensation or conjugation. There are oxygen functional groups (most probably carbonyls) in the structure of these solids. The FTIR spectrum in Figure 72 is similar, in many respects, to the spectra obtained from the solids produced in microautoclaves from model compounds and jet fuels [9,10].

The FTIR spectrum of the flakes was found to be quite different from that of the globular particles, indicating that the thin flakes consist primarily of highly condensed aromatic rings of carbon atoms with very low concentrations of aromatic hydrogen [10]. This structure is distinctly different from that of the globular particles. It is clear that the flakes were formed under more severe thermal stressing conditions than the globular particles.

Optical Microscopy

The globular particles and flakes were separately embedded in epoxy resin to prepare polished sections for microscopic examination. A brief description of the microscope system and the interpretation of the optical image is given below.

A Zeiss microscope (Model GFL) with a rotating stage was used to examine the polished specimens in incident plane-polarized light obtained by placing a polarizer between the light source and the specimen surface. Another polarizer was inserted in the path of the reflected light. With the incorporation of a retardation plate (phase-sensitive plate, red-quartz, $1/4$ -wave in this case), an

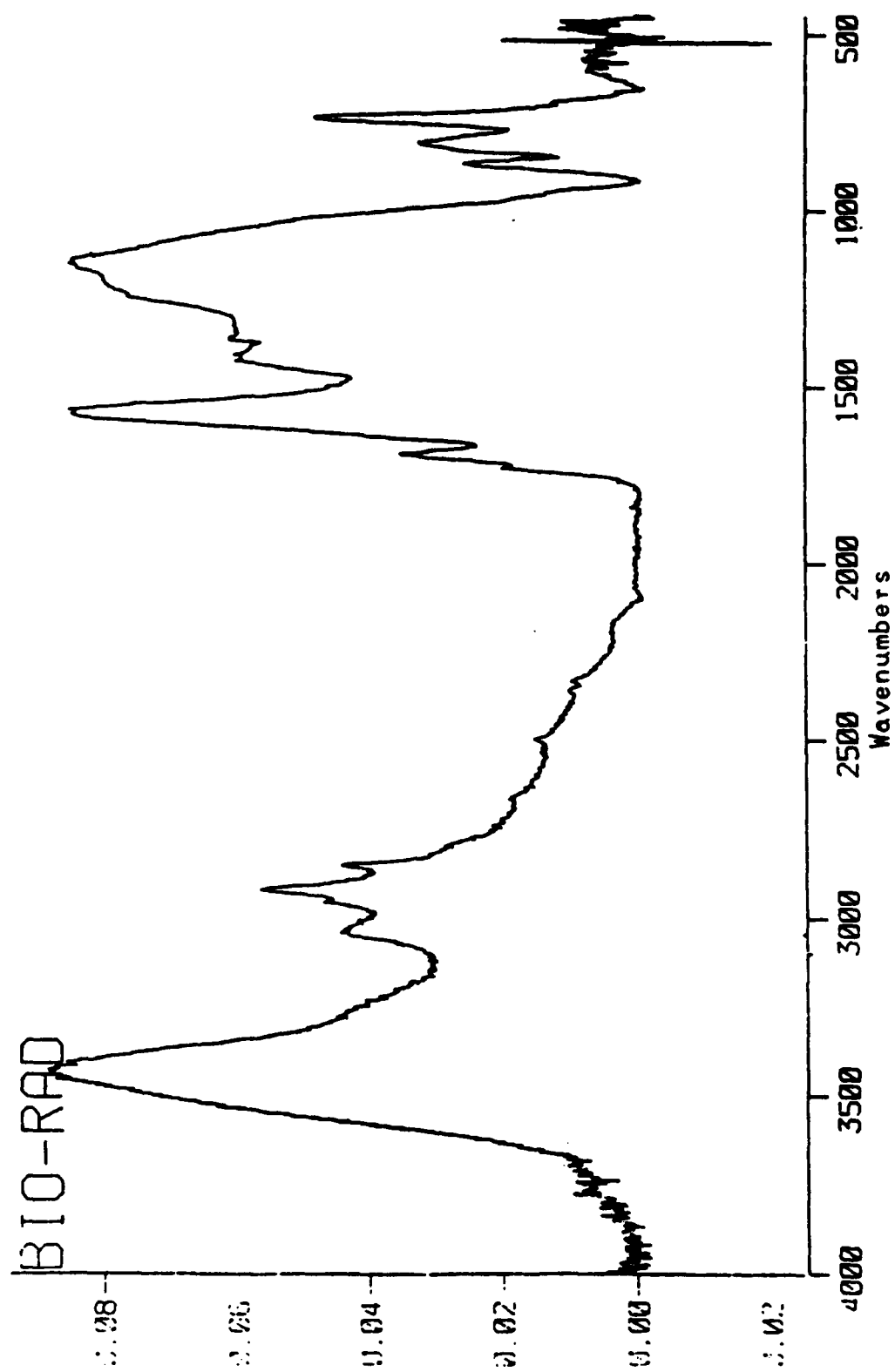
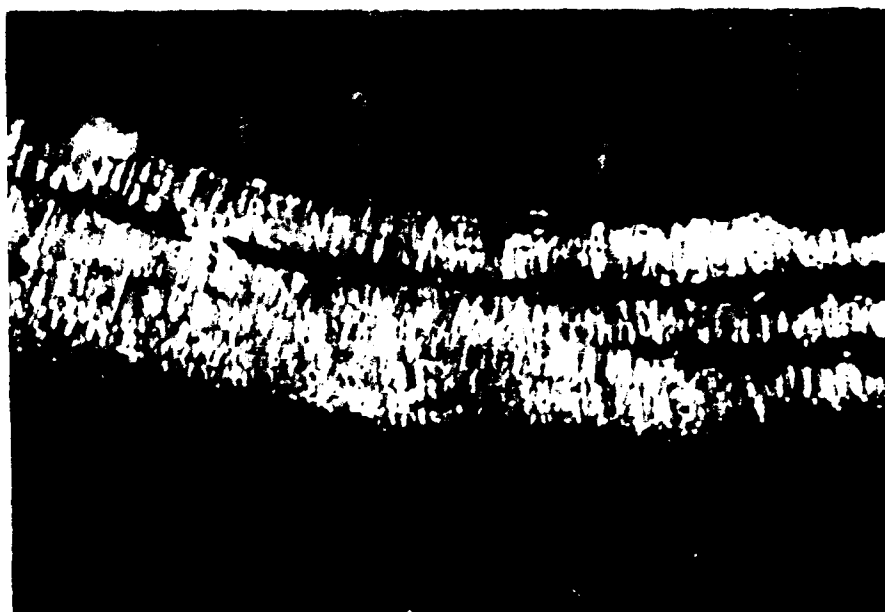
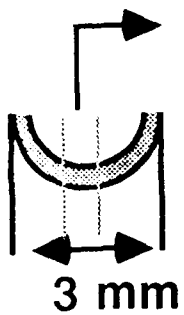


Figure 72. FTIR absorbance spectrum of globular particles from actual fuel system deposits.

anisotropic coke or carbon exhibits from its surface yellow, blue and dark purple areas [13]. After viewing each specimen, selected areas were photographed by using 400 ASA 35 mm color film and a Nikon camera attached to the microscope. A more detailed description of the examination method is given in the quarterly reports. The colored micrographs of the solid deposits are contained in files in the Fuel Science Program [10,11]. For this report, some micrographs are reproduced in black and white. Different shades of gray in these micrographs represent different orientations of basal planes in anisotropic carbons. The size and shape of the areas with the same gray levels represent the degree of microstructural order in the carbon deposits and provide information about the phase (liquid or gas) in which they were formed.

The flakes and globular particles showed distinctly different microstructures under reflected polarized-light. Figure 73 shows the micrographs of a tube deposit in the shape of a halved cylindrical shell with a diameter of approximately 3 mm. This type of deposits formed the flakes upon gentle grinding. As indicated in the diagram on the left-hand side of Figure 73, the micrographs show the texture of the cross-sectional area perpendicular to the cylinder axis. The convex surface of the deposits in the micrographs shows the tube side of the deposits. The magnification of the micrographs is shown by the scale given in the figure. The microstructures observed in the micrographs of Figure 73 closely resemble those of pyrolytic carbons deposited during the pyrolysis of small gaseous hydrocarbons at relatively high temperatures (above 700°C) [14]. A clearly visible feature of the deposit is the presence of distinct layers separated either by slit-shaped pores (filled with epoxy resin seen as featureless dark regions) or by boundaries reflecting different growth patterns across the deposit. Higher magnification micrographs of the deposit in Figure 74 more clearly show the discontinuities in the growth patterns which separate the different layers. Microstructures of the layers are made up of columnar grains of layer planes perpendicular to the growth direction. In other words, the layer planes are stacked parallel to the tube surface with a rather high degree of alignment, as shown by the uniform shades of gray seen in the micrographs. The conical structures seen in the micrographs are commonly encountered features of pyrolytic carbons, the tips of the cones indicating the nucleating sites. You can see in the micrographs of Figure 74 that the new growth cones originate at different layers throughout the deposit. This structure is termed as the "regenerative" or "continuous" nucleation in contrast to "singular" or "substrate" nucleation where all the cones in a deposit originate on the substrate [12]. This observation suggests that the nucleation of the deposits takes place in the gas phase or on the previously formed carbonaceous deposits. The lack of singular, or substrate nucleation and the layered nature of the deposits suggest that the presence of a metallic surface (i.e., tube surface) may not play a critical role in deposit formation other than providing a hot surface for the initial deposition. The observed microstructures of the tube deposits imply orderly growth of solids,



a

80 μm




b

Figure 73. Polarized-light micrographs of the actual engine deposits in the form of flakes.



a


20 μm



b

ACTUAL ENGINE DEPOSITS (FLAKES)

Figure 74. Polarized-light micrographs of the actual engine deposits in the form of flakes.

known to be favored by large temperature and/or concentration gradients with a low degree of supersaturation in the gas phase [14].

Many mechanisms have been proposed to explain the formation of pyrolytic carbons [12,14]. The proposed mechanisms differ in terms of the intermediate species and the sequences of aggregation involved in the formation of carbons from relatively small molecules. The models which involve polymerization reactions to form large molecules of carbon atoms arranged in hexagonal arrays are probably most relevant to the formation of deposits from jet fuels. The growth cones and the overall order present in the tube deposits suggest that the deposition involved large complexes formed in the gas phase before condensation on the tube surface or on the surface of the previously formed carbonaceous layer. Although the reactions in the gas phase appear to govern the formation of tube deposits (flakes), formation of an intermediate liquid phase on the substrate surfaces cannot be ruled out. The presence of "inverted" cones and other fine structures between the layers of deposits indicate that rather complex processes are involved in the formation of tube deposits. It is clear, however, that the tube deposits shown in Figures 73 and 74 represent pyrolytic carbon structures with a relatively high degree of preferred orientation, as evidenced by the fragmentation of these deposits in the form of flakes. This observation supports the FTIR data on the flakes and suggests that the flakes can have high electrical and thermal conductivities in the direction parallel to the basal planes. Based on the FTIR data and the observed microstructures of the tube deposits, it can, further, be inferred that these deposits were formed upon exposure of fuel (or degraded fuel components) to relatively high temperatures. The presence of distinct layers of deposits may actually represent temperature cycles (or aircraft flights) in the history of formation of these solids.

In contrast to the pyrolytic carbon structures observed in the flakes, the globular particles found in the fuel system deposits exhibit an isotropic texture containing anisotropic regions of "carbonaceous mesophase" development. These microstructures suggest that the formation of the globular particles is controlled, at least in the final stages of aggregation, by liquid phase reactions. Figure 75 shows the isotropic regions of the particles as (dark gray in micrograph a) as well as the anisotropic structures (light gray in micrographs a and b) formed by carbonaceous mesophase development. Carbonaceous mesophase is a plastic, anisotropic phase which is formed during carbonization of a range of materials including petroleum feedstocks, thermoplastic polymers, and polynuclear aromatic compounds. Mesophase is considered as a unique ordered fluid consisting of essentially planar molecules which are aligned roughly parallel to each other without any order of stacking sequence [15]. Some properties of carbonaceous mesophase resemble those of nematic liquid crystals.

The formation of mesophase starts with the nucleation of anisotropic spheres (consisting of aligned planar molecules) in an isotropic phase, followed by the growth of these spheres at the



a

20 μm



b

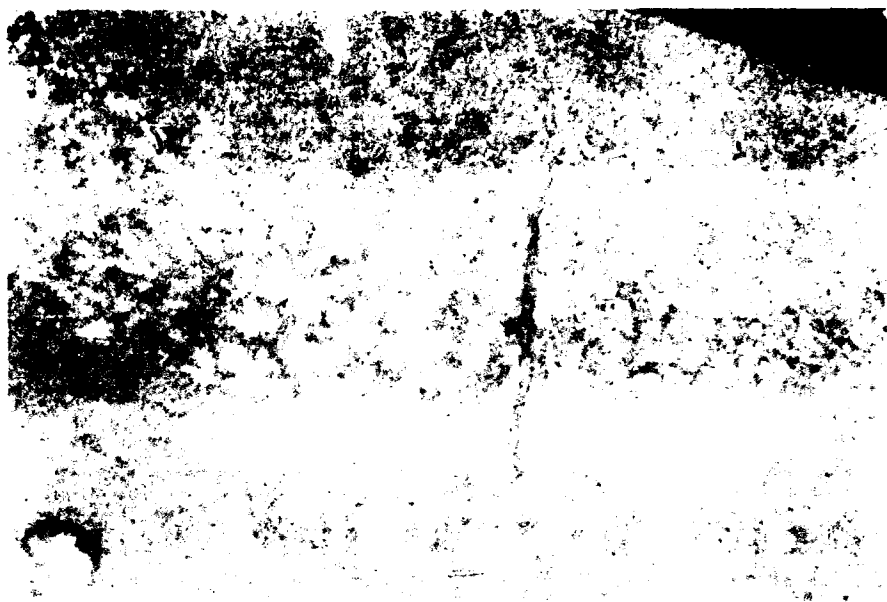
Figure 75. Polarized-light micrographs of the actual engine deposits in the form of globules.

expense of isotropic phase and their coalescence lead eventually to all anisotropic coke. The nucleation of mesophase spheres and the growth of anisotropic regions can be followed by examining the interference colors of anisotropic carbons, as explained above. Figure 76 shows a localized anisotropic region formed by rapid coalescence of mesophase spheres in an isotropic matrix (micrograph a) and anisotropic structures (flow domains) between two pores (micrograph b) elongated by the evolution of volatiles during pyrolysis. It appears that, unlike in the structure of the flakes, the process of solid formation has not reached completion. Upon further stressing, the whole texture would probably be converted into anisotropic coke. The microstructures shown in Figures 75 and 76 closely resemble those seen in petroleum cokes produced from heavy residua by prolonged heat treatment. The presence of an isotropic pitch phase together with mesophase indicates the highly aromatic nature of the globular solids as well as high concentrations of aliphatic functionalities. This inference is in agreement with the FTIR data on the globular solids.

It is clear from microscopic examination of the samples that the two types of macroscopically different solids (the flakes and globular particles) found in the actual fuel system deposits were formed via different mechanisms. probably at different locations in the fuel system. The flakes were formed primarily by gas (or vapor) phase reactions leading to a pyrolytic carbon texture under severe thermal stress conditions. On the other hand, the porous globular particles were formed in the liquid phase involving the mesophase development from an isotropic pitch which had been formed via cracking and polymerization of fuel components. These conclusions suggest that the both gas phase and liquid phase reactions are important in studying the solid formation from jet fuels.

X- Ray Diffraction

A sample of flakes was ground in an agate mortar and pestle and a thin film of solids was bound to a glass slide using an adhesive mixed with acetone. A Rigaku Geiger-Flex X-ray diffractometer and DMAX control panel with monochromatic (40 kV, 20 mA) $\text{CuK}\alpha$ radiation was used to obtain the diffraction profile. An NBS Standard Reference standard silicon and a sample of single crystal graphite (SP-1) were used as external standards. Figure 77 shows the diffraction profiles of the solid flakes and the standards. A very broad 002 peak obtained from the flakes indicates the turbostratic nature (presence of large aromatic sheets with some alignment, but lack of three dimensional order) of these solids. Using the Bragg equation, $\lambda = 2d\sin\theta$, where d is the interlayer spacing, θ is the angle of incidence for $\text{CuK}\alpha$ radiation with a wavelength λ of 0.15418 nm, one can calculate an average interlayer spacing of 0.344 nm for a 2θ of 26° . This interlayer spacing is also consistent with the value frequently observed for turbostratic carbons [12].



a

20 μm



b

Figure 76. Polarized-light micrographs of the actual engine deposits in the form of globules.

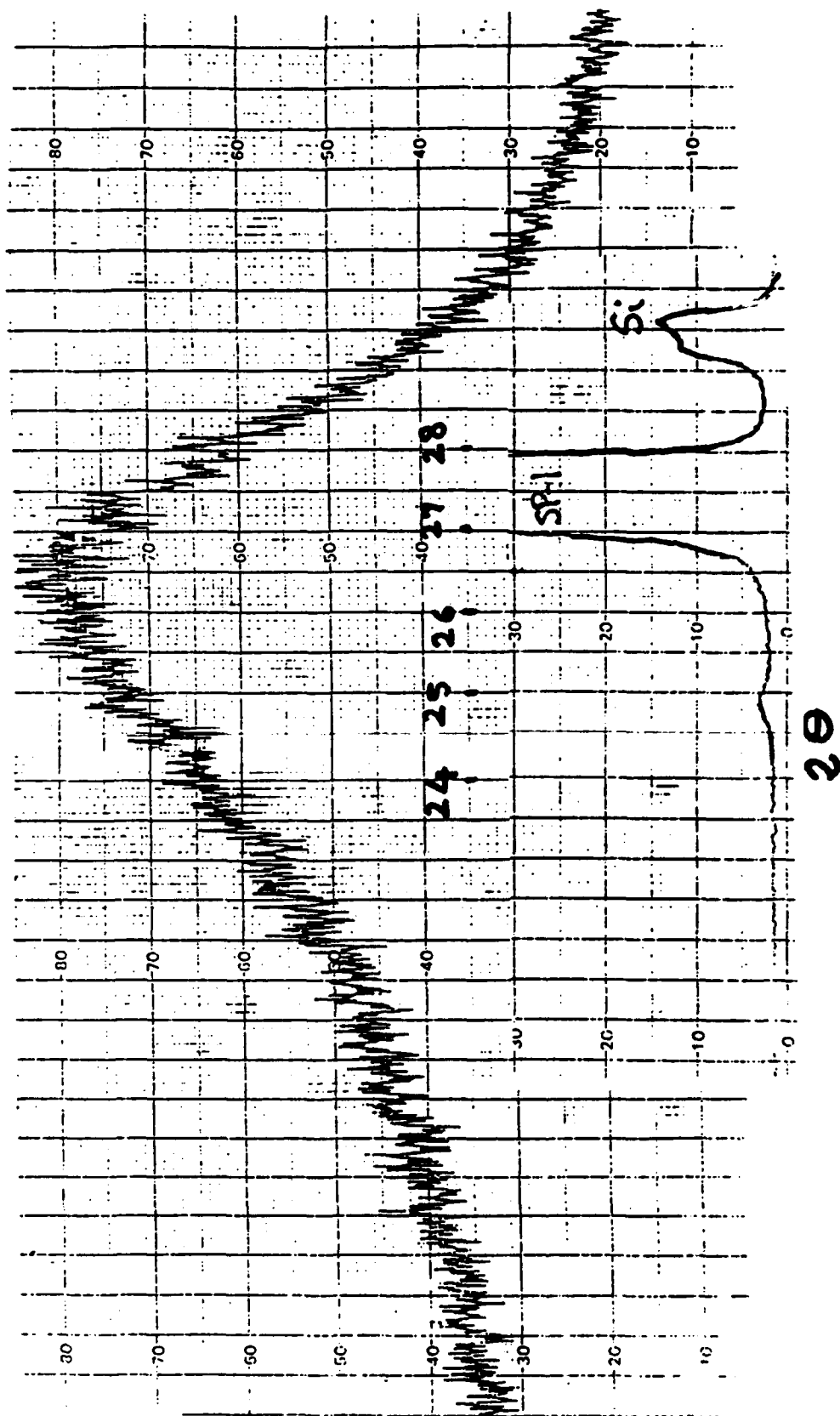


Figure 77. X-Ray Diffraction profiles of flake deposits found in actual fuel system deposits and those of Si and SP-1 single crystal graphite.

Scanning Electron Microscopy

Figure 78 shows the scanning electron micrographs of flakes and globules mounted in epoxy resin pellets. The layered microstructure of flakes is clearly shown in micrograph a. The globules, on the other hand, show mosaic regions without much order (micrograph b).

XRD and SEM analyses of the fuel system deposits, thus, confirmed the differences observed between the flakes and globules and the associated formation mechanisms.

Solids Produced in Laboratory Microautoclaves

Solids produced from jet fuel samples and model compounds have also been characterized by using various methods and the results of these analysis have been presented in the previous quarterly reports [9-11]. In this report, we summarize the NMR data on t-butylbenzene solids and FTIR data obtained for the solids produced from Jet-A1 sample in nitrogen and air atmospheres as well as optical micrographic examination of the solids produced from a sample of petroleum and coal-derived JP8 fuels and some model compounds.

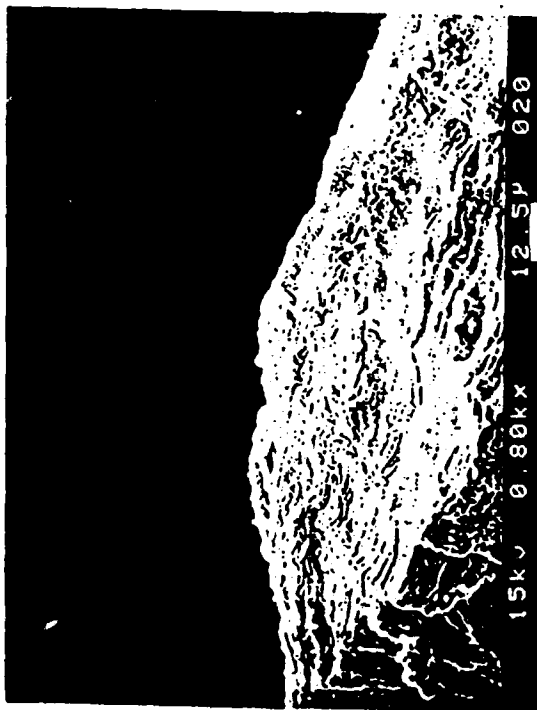
Nuclear Magnetic Resonance Spectroscopy

Figure 79 and 80 shows CPMAS ^{13}C NMR spectra of the solids produced from t-butylbenzene in 8 and 20 h reactions at 450°C, indicating that the solid carbons are highly aromatic. The spectrum shows weak peaks for CH_2 and CH_3 groups around 20 and 30 ppm, compared to a very strong aromatic carbon peak around 140 ppm. Table 23 lists the aromaticity of the t-butylbenzene solids as a function of reaction time. Note that the aromaticity of the solids does not change significantly with the reaction time between 8 h and 20 h at 450°C.

Fourier Transform Infrared Spectroscopy

The FTIR spectra on the Jet A-1 solids were obtained using the same instrument and conditions described above. Figure 81 shows a baseline-corrected spectrum for the solids produced from 10 ml Jet-A1 heated at 425°C for 18 h under 100 psi cold air overpressure. In many respects, this spectrum is comparable to that of globular fuel system deposits shown in Figure 72. Based on the comparable intensity ratios of aromatic to aliphatic C-H stretch bands, Jet A-1 solids and globular solids were produced probably under similar extents of thermal stress, assuming that the fuel precursor to globular solids is comparable to Jet A-1. There are two major differences between the spectra of these solids: 1) The intensity of aromatic C-H out-of-plane bending modes for four adjacent aromatic hydrogens is comparatively high in the spectrum of the globular solids. This observation indicates that the aromatic ring systems constituting the globular solids of actual fuels system deposits are less heavily substituted by alkyl groups than those in Jet

Figure 78. Scanning electron micrographs of the flakes and the globules found in actual deposits.



(a)



(b)

Figure 78. Scanning electron micrographs of the flakes and the globules found in actual engine deposits.

PENN STATE UNIVERSITY M100-0301

COM: SOLID 1-8 450 MHz 100PS1 CPMAS 7-5-90

FNA: T645084.Y00

NUC: 13C

F085: 25.035000

NA: 20000

AL: 512

DL: 4056

TLB: 19.865

TIME: 18.41.18 0188/90

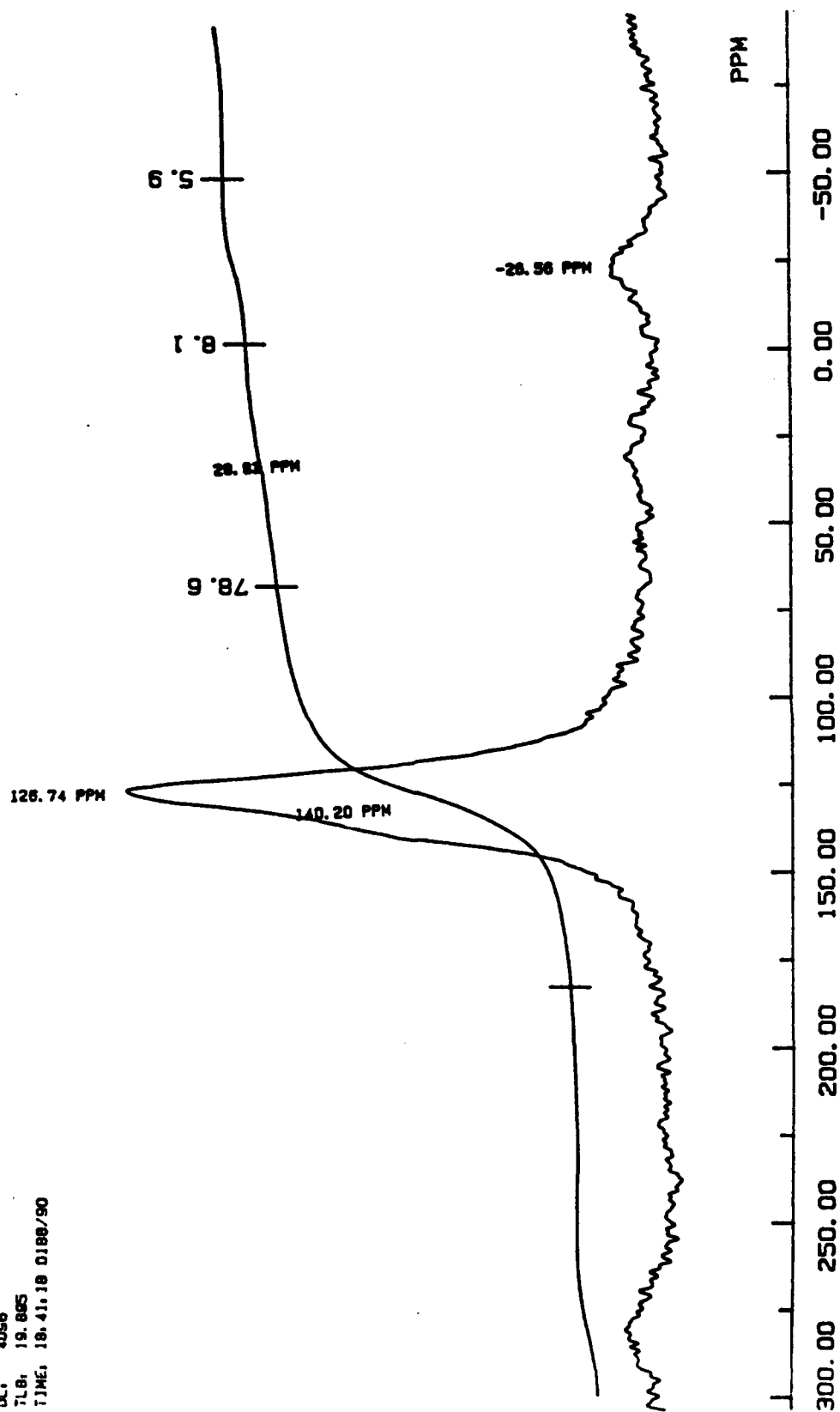


Figure 79. CPMAS ^{13}C NMR spectrum of the solids produced from t-butylbenzene in 8 h at 450°C .

PENN STATE UNIVERSITY M100-0301

CON: SOLID OF T-B AT 450 204R 100PS1 94L CPMAS 7-5-80

FNA: 78450204L Y00
 NUC: 13C
 F0BS: 25.035000
 NA: 10000
 AL: S12
 DL: 4096
 TLB: 18.885
 TIME: 18.34.35 0188/90

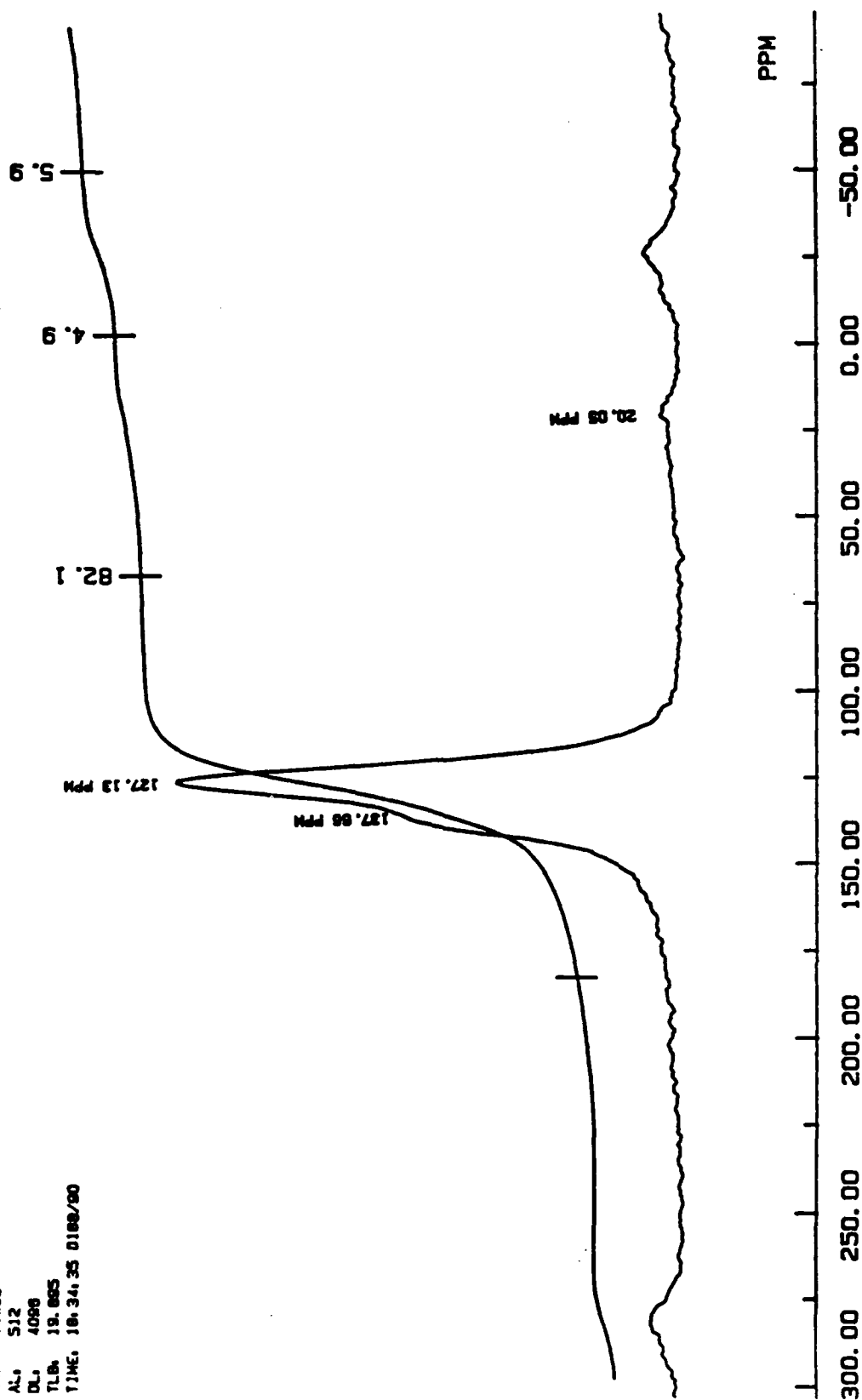


Figure 80. CPMAS ¹³C NMR spectrum of the solids produced from t-butylbenzene in 20 h at 450°C.

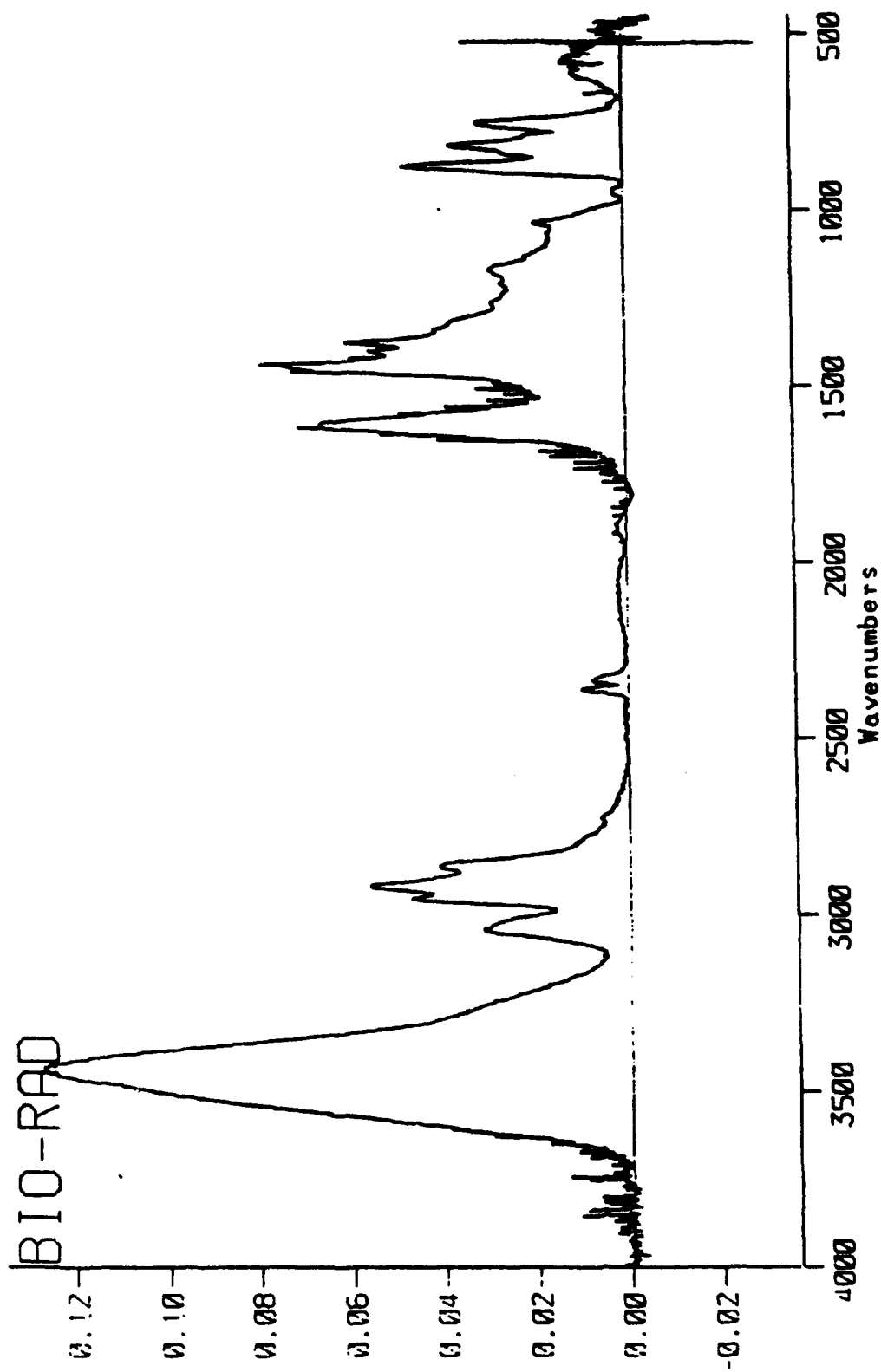


Figure 81. FTIR absorbance spectrum of solids produced from Jet A-1 at 425°C for 18 h under 100 psi air pressure.

Table 23. Aromaticity of the solids from the reactions of t-butylbenzene as a function of reaction time at 450°C.

	8 h	12 h	16 h	20 h
C _{ar} (%C)	90.4	89.1	93.5	93.9

A-1 solids produced at 425°C in 18 h. 2) There are no oxygen functional groups present in the structure of Jet A-1 solids.

Figure 82 compares the FTIR spectra for the solids produced from Jet A-1 in air and nitrogen overpressures under the same conditions (425°C, 18 h). One can see that the two spectra are almost identical, indicating that the change in atmosphere did not affect the structure of the solids under the conditions used. There is no doubt that the presence of oxygen at reaction temperatures has a significant influence on the kinetics of solid formation. However, the apparent lack of oxygen functional groups in the solids produced under an air atmosphere suggests that oxygen may be involved only in the formation of reactive intermediates and does not end up in the final solid under the conditions used. Further, the close similarities of the structures of the solids formed under different atmospheres further suggest that the reaction mechanisms leading to the solid formation were probably the same under nitrogen or air atmospheres. A longer reaction time at the same temperature (24 h at 425°C) did not show any significant structural differences, either, between the solids formed in inert and oxidative atmospheres.

Optical Microscopy

The microstructures of solids produced in microautoclaves from JP8 fuels and model compounds showed signs of both gas phase and liquid phase deposition processes. Similar to the actual tube deposit flakes, there is preferred orientation of planar molecules in thin flakes of solids formed in microautoclaves by gas phase reactions. Clear signs of carbonaceous mesophase development in the solid products indicated also the presence of liquid-phase carbonization reactions. Microscopic observations indicate the extremely complex and heterogeneous nature of the processes leading to the formation of solids in a microautoclave, including, presumably, the

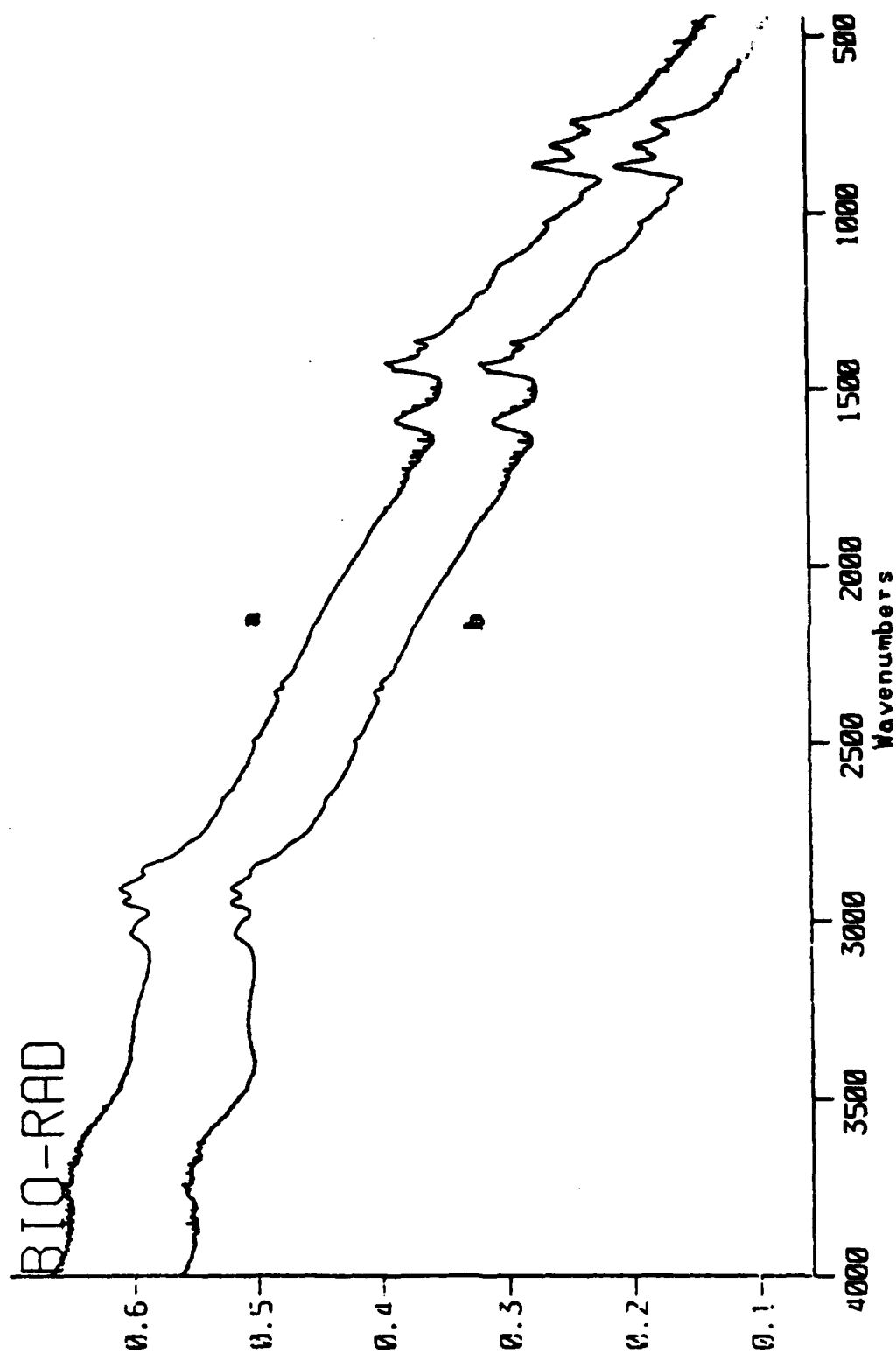


Figure 82. FTIR absorbance spectrum of solids produced from Jet A-1 at 425°C for 18 h under 100 psi air (a) and nitrogen (b) pressure.

presence of a supercritical phase, condensation of high-molecular weight species on reactor walls, and vapor phase cracking of reaction intermediates in pores created by previously formed solids.

Solids from JP8 Fuel Samples

The microstructures of the solids produced from the samples of petroleum- and coal-derived JP8 were described in detail in the quarterly reports [10,11]. In both petroleum-derived JP8 (JP8-P) and coal-derived JP8 (JP8-C) solids produced at 450°C, we observed particles showing the nucleation of mesophase spheres in an isotropic matrix, the initial stage of mesophase development [9]. Gas-phase deposits, in the form of flakes with pyrolytic carbon microstructures were also common to the solids produced by JP8-P and JP8-C at 450°C. JP8-P produced more gas-phase carbons than JP8-C under comparable conditions. In general, the solids produced from JP8-C exhibit a higher degree of mesophase development preceding the formation of solids than those obtained from JP8-P. This observation suggests that the reaction intermediates, or solid precursors, produced during the thermal stressing of JP8-C are more planar and less reactive, in other words, more aromatic, than those involved in solid formation from JP8-P. Also, hydrogen transfer reactions involving hydroaromatic compounds as hydrogen donors, which are present in high concentrations in JP8-C, promote mesophase development via stabilizing the nascent free radicals [10].

It appears that, in addition to the temperature, the stressing pressure and/or the concentration of volatile reaction products also have a significant effect on the microstructure of the solids produced from jet fuels. For example, the doubling of the sample volume of JP8-C (from 5 to 10 ml) changed the solid formation mechanisms from predominantly liquid-phase reactions (carbonaceous mesophase) to predominantly gas-phase reactions (pyrolytic carbons). This effect can be explained by increased stressing pressure and the attendant changes in phase equilibrium and/or formation of a supercritical phase.

Solids from Model Compounds

Rather thick flakes (80-200 μm) were produced upon thermal treatment of decane at 450°C. A high degree of preferred orientation was, again, clearly visible. In addition, more randomly ordered, large mesophase structures and finer structures in flakes were also present in decane solids.

The deposits recovered from the top of the microautoclaves after the treatment of dodecane at 475°C showed flakes with typical pyrolytic carbon texture, whereas the solids formed at the bottom of the reactors showed signs of mesophase development and porous structures. This observation again points out the simultaneous occurrence of gas-phase and liquid-phase reactions leading to solid formation.

Thermal stressing of n-butylbenzene at 450°C produced a range of mesophase structures (from mosaics to flow domains) in the solids, whereas t-butylbenzene produced isotropic and fine

mosaic structures in the solids produced by both gas- and liquid-phase reactions. It is clear that the reaction intermediates leading to the formation of solids from these two isomers are different, in addition to the difference in relative thermal stability of these compounds.

One particular feature of the flakes found in actual aircraft fuel system deposits was its layered nature, which was attributed to temperature cycles as effected by the flights of the aircraft. A series of experiments was planned to consist of multiple stressing of 10 ml of tetradecane at 450°C for 8 h with quenching and making up the depleted liquid volume to 10 ml after each stressing. The thermal stressing was carried out three times, and the solids were recovered only after the third stressing.

Figure 83 shows the solids obtained from tetradecane by multiple stressing, indicating layered structures somewhat similar to those observed in the flakes found in actual engine deposits, with a significantly lower degree of crystallite alignment. These structures indicate that principally the gas-phase reactions were responsible for the formation of solids during multiple stressing of tetradecane. The presence of layered microstructures indicates that the surface of the solid deposits initially produced can act as a substrate for further solid deposition (i.e., regenerative nucleation, as found in the flakes from actual engine deposits).

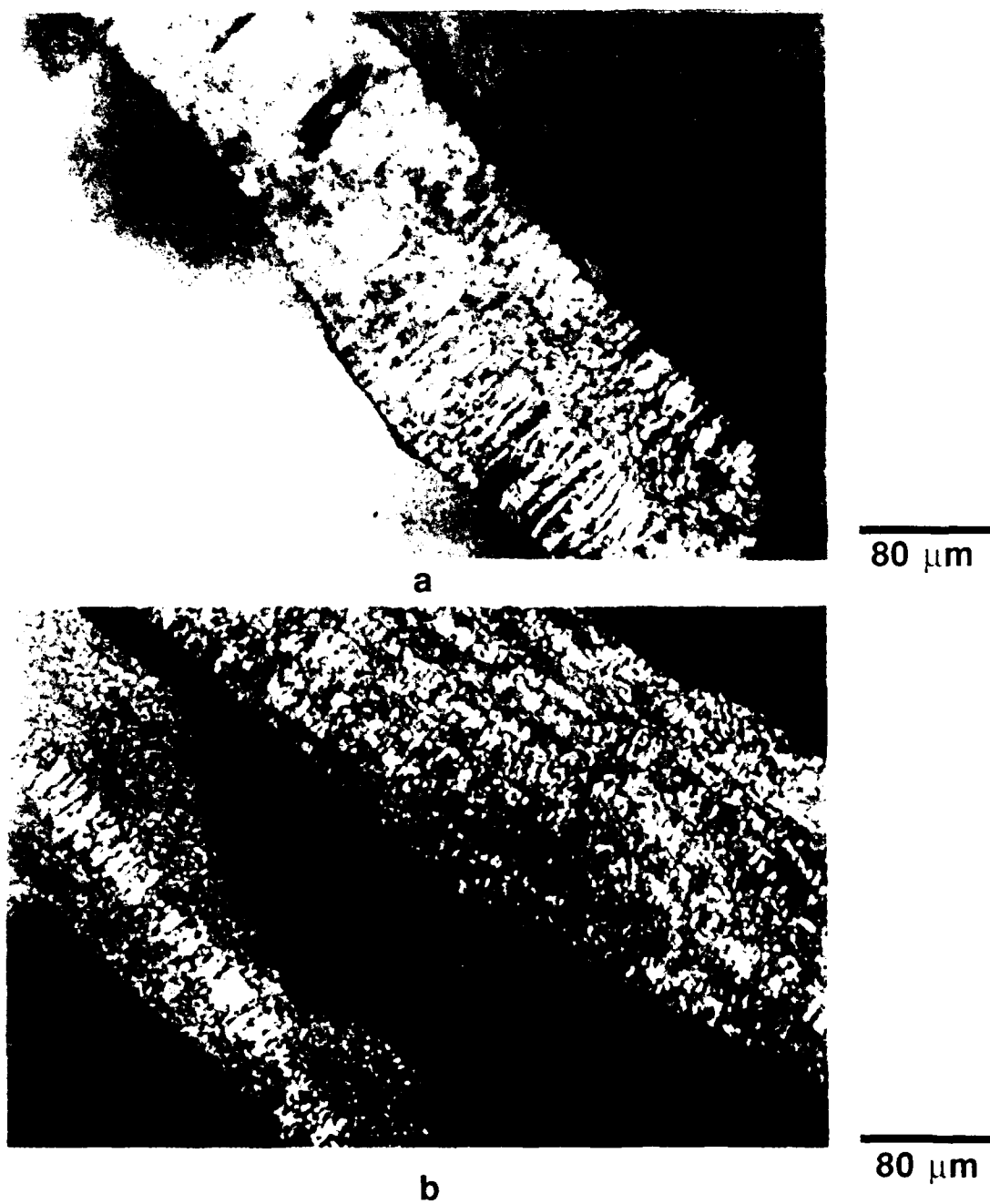


Figure 83. Polarized-light micrographs of solids from triple stressing of tetradecane at 450°C for 8 h in nitrogen.

Task 6. Exploratory Studies for Fuel Thermal Stability Enhancement.

The objective of this task is to identify suitable additives which can prevent solid formation and enhance the thermal stability of the jet fuels in the temperature region of 400 to 450°C. An extensive literature survey has been done on antioxidants and their effects on jet fuel thermal stability. From our literature survey, we find that there is hardly any report on the effect of antioxidant behaviors on the stability of jet fuels at such high temperatures. We selected 2,6-di-*tert*-butyl-4-methylphenol as one of the antioxidants for our preliminary experimental studies.

Stressing experiments were performed on two different jet fuel samples, JP-8 neat and jet A-1, mixed with varying concentrations of the antioxidant 2,6-di-*tert*-butyl-4-methylphenol. The results of stressing experiments on these fuels, which were described in detail in the quarterly reports [10,11], are summarized below. JP-8 neat contains additives in the fuel and does not represent a good starting material for degradation studies. Jet A-1 fuel is considered to be a better starting material, since it contains less additives than JP-8 neat does. Apparently, it is very difficult to obtain additive free jet fuel samples.

A preliminary study on the effect of adding 2,4,6-tri-*tert*-butylphenol and 2,4,6-trimethylphenol to JP-8 neat has also been conducted. The results of this study are presented separately in the next section.

Stressing experiments were performed using tubing bombs of 15 ml capacity in a fluidized sand bath. Ten ml of fuel was mixed with different concentrations of A.O. The reactor was purged with UHP grade nitrogen five times (i.e., each time pressurized with 1000 psi nitrogen, followed by gradually depressurizing of the tubing bomb). It was finally pressurized with 100 psi of either nitrogen or air, and was placed in a preheated sand bath for the required reaction time. The heat treated tubing bomb was removed from the sand bath and quenched immediately in cold water, followed by depressurization to remove the head space gases. The quantity of stressed fuel and the solids present were determined.

Upon a suggestion of Dr. Elmer Klavetter, another set of experiments was performed in which the time duration of thermal stress was kept constant (4 h) and the degradation of Jet A-1 fuel was studied as a function of temperature (190, 220, 250, 280 and 310°C). The infrared spectra obtained from this set of experiments were compared with the infrared spectra obtained from fuel with 0.3% A.O. stressed at 425°C for various time duration (0, 1, 3, 6, 12, 18 and 24 h).

FTIR spectra of the unstressed and stressed fuels with and without antioxidant were obtained using a Digilab FTS 60 instrument in the Polymer Science Program. A KBr sealed cell with path length of 0.015 mm was used throughout the study.

Addition of 2,6-di-tert-butyl-4-methylphenol to JP 8 Neat Fuel

Experiments were conducted to study the effect of temperature on the solid formation from JP8 neat fuel (a petroleum derived fuel) under 100 psi nitrogen or air overpressure (cold) for different time duration. We performed experiments at 350,400,425 and 450°C for 1,3,6,12,18 and 24 h. We observed that the degradation was more extensive in air than in nitrogen. Solid deposit formation was observed only at 425°C and 450°C. Hence we chose 425°C to study the effect of the antioxidant, 2,6-di-tert-butyl-4-methylphenol on solid formation from JP 8 neat fuel.

Figures 84 and 85 show the formation of solids at 425°C from 10 ml of JP-8 neat mixed with 0.02 g of antioxidant under nitrogen and air atmospheres, respectively. It is interesting to note that the addition of the antioxidant increases the amount of solids formed in a nitrogen atmosphere (Figure 84), whereas a reduction in solid formation is observed under an air overpressure (Figure 85). Clearly, the behavior of the antioxidant is different in nitrogen and air atmospheres.

In order to determine the optimum amount of antioxidant (A.O.) 2,6-di-tert-butyl-4-methylphenol necessary to minimize solid formation, thermal stressing experiments were

Figures 86 and 87 show the solid formation in JP8 neat under nitrogen and air, respectively, at 425°C. It is observed that 0.005 g is the optimum amount of antioxidant required for 10.0 ml of JP8 neat fuel in an overpressure of nitrogen as well as air. Figures 86 and 87 indicate how critical is the effect of concentration of antioxidant on solid formation in JP-8 neat fuel. It is important to emphasize that JP8 neat already contains an unknown quantity of an unidentified antioxidant. Similar stressing experiments were carried out on a sample of Jet A-1 fuel which has been supplied without additives. It is, however, known that Jet A-1 also contains some antioxidant and antistatic additives.

Addition of 2,6-di-tert-butyl-4-methylphenol to Jet A-1 Fuel

A series of experiments were conducted to establish the optimum amount of A.O. required to minimize formation of solids in the Jet A-1 fuel which had been thermally stressed at 425°C for 24 h. Figure 88 shows the amount of solids formed under 100 psi of air and nitrogen with different concentrations of antioxidant. The effect of the antioxidant as measured by the mass of solid formed under an atmosphere of nitrogen, is greater than that compared to an air atmosphere. In fact it could be argued that under air the effect is minimal at its best. The optimum concentration of antioxidant for Jet A-1 is in the range of 0.02 -0.03 g / 10.0 ml of fuel.

Fourier Transform Infrared (FTIR) Spectroscopic Analysis

Figure 89 represents the infrared spectra in the region of 3720-3480 cm^{-1} of the Jet A-1 fuel mixed with 0.3% A.O. stressed for 4 h in nitrogen at different temperatures ranging from 190

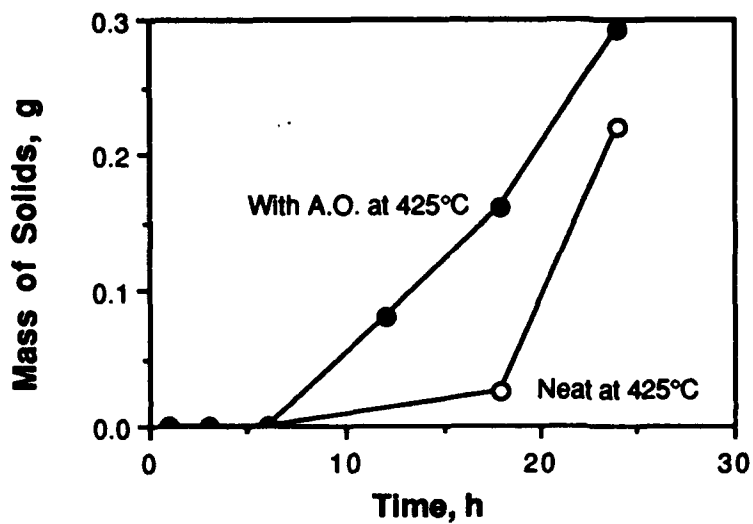


Figure 84. Effects of adding 2,4-di-tert-butyl-4-methylphenol on solid formation from JP8 at 425°C in 100 psi N₂ (cold).

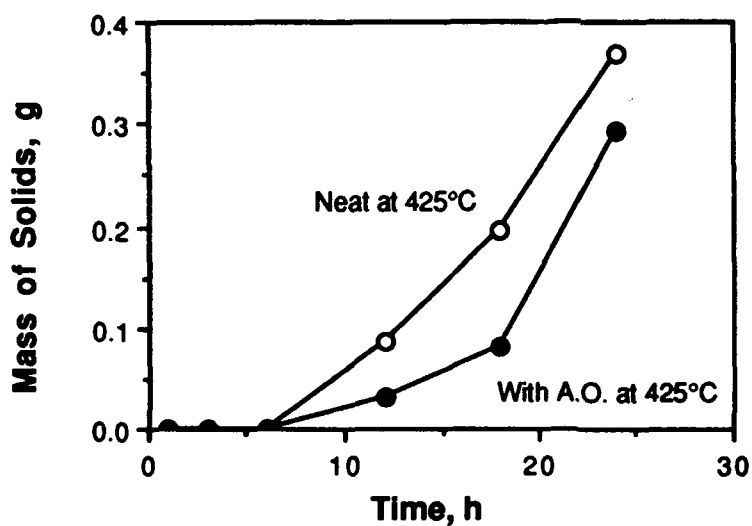


Figure 85. Effects of adding 2,4-di-tert-butyl-4-methylphenol on solid formation from JP8 Neat at 425°C in 100 psi air (cold).

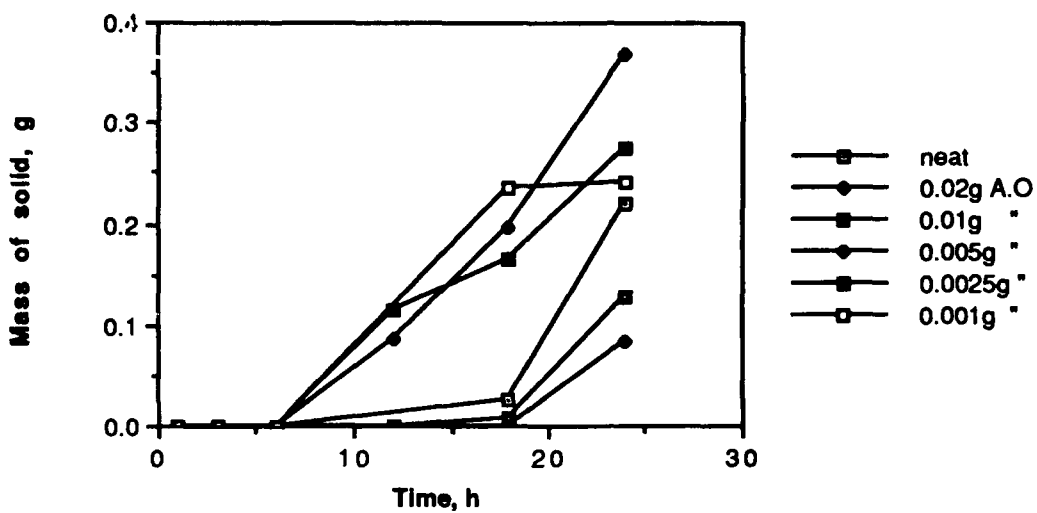


Figure 86. Solid formation at 425°C under 100 psi nitrogen pressure from JP8 neat mixed with 2,6-di-tert-butyl-4-methylphenol.

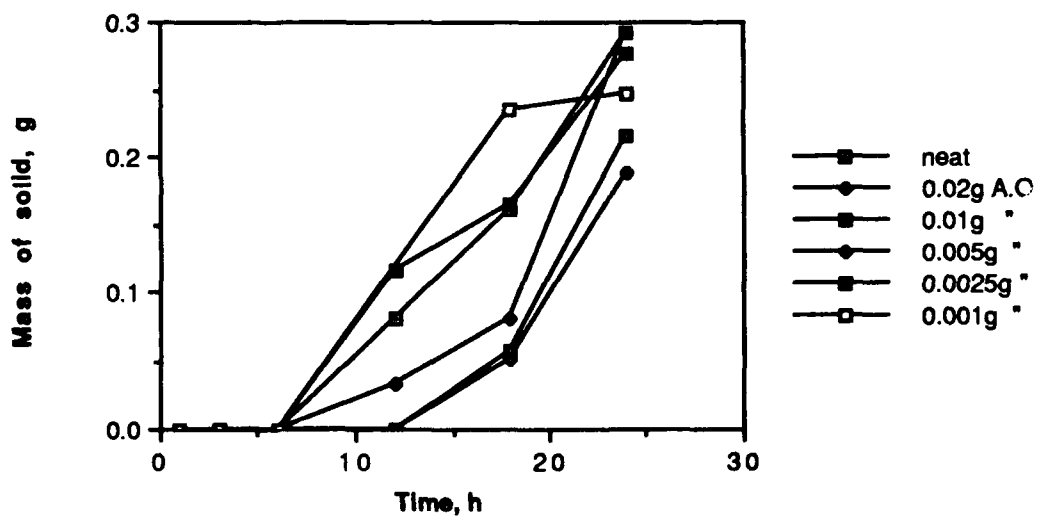


Figure 87. Solid formation at 425°C under 100 psi air pressure from JP8 neat mixed with 2,6-di-tert-butyl-4-methylphenol.

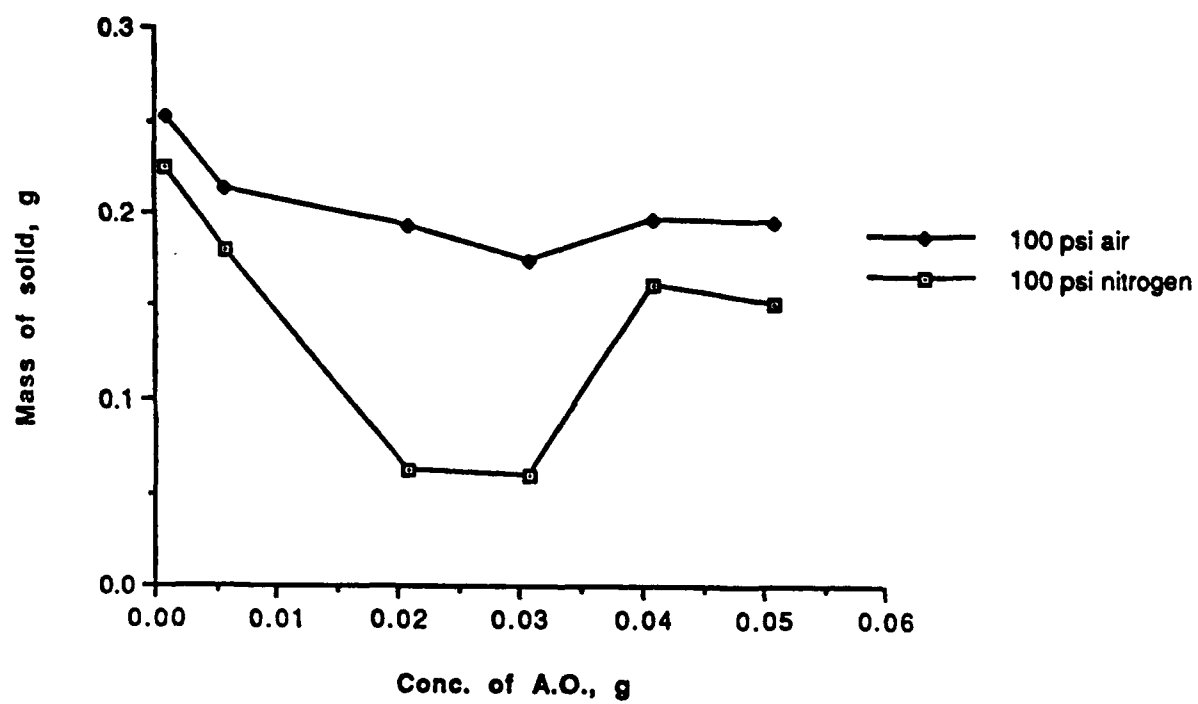


Figure 88. Effect of A.O. concentration on formation of solids from Jet A-1 at 425°C for 24 h.

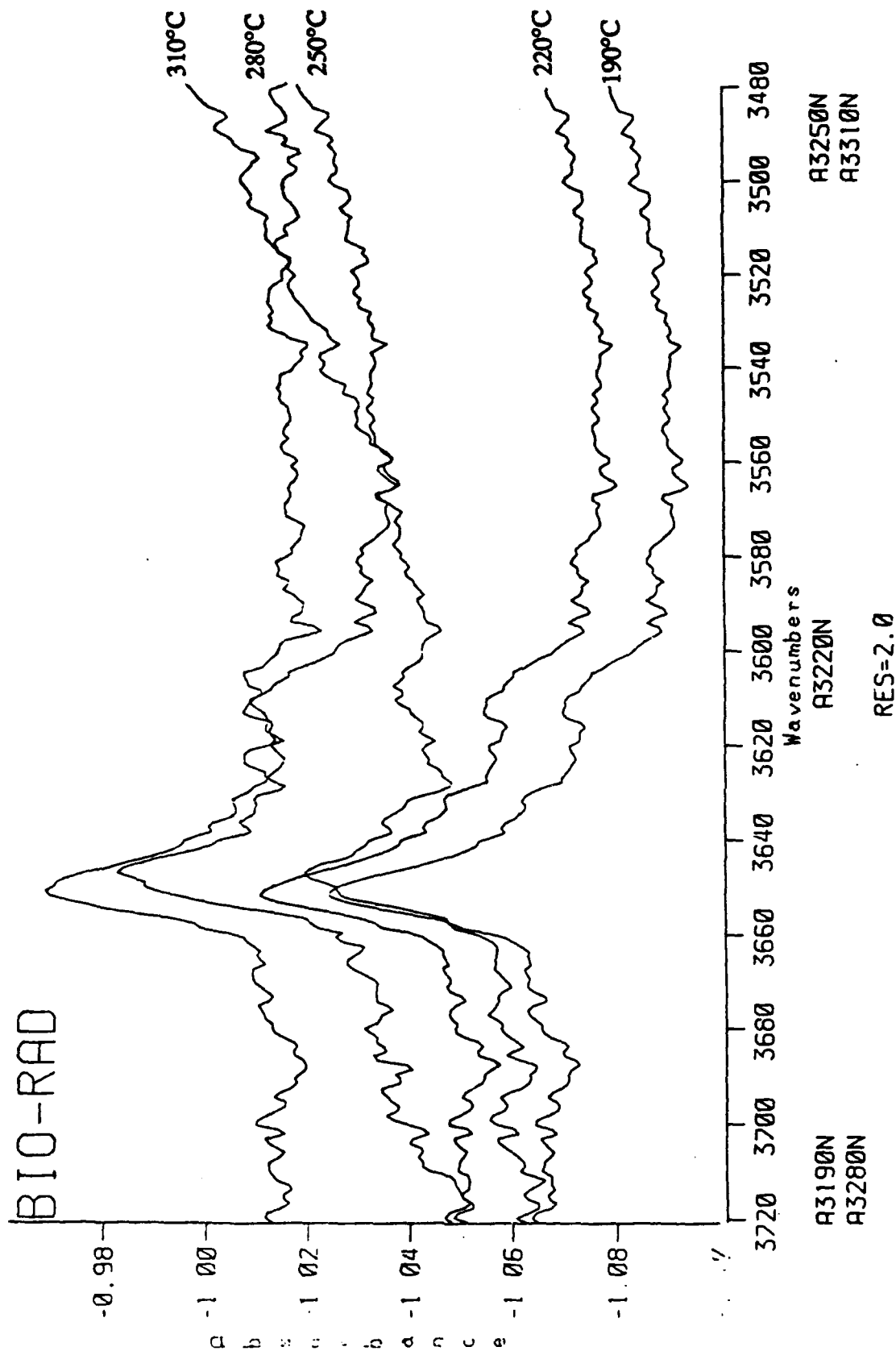


Figure 89. FTIR absorbance spectra of the liquid products obtained from reactions of Jet A-1 + 0.3% A. O. at temperatures 190°C-310°C for 4 h in nitrogen.

to 310°C. In this region, only one peak is detected at 3650 cm⁻¹ which may be attributed to the -OH stretching vibration of 2,6-di-*tert*-butyl-4-methylphenol. Around 310°C, in air overpressure, under similar conditions, we observe the development of another peak at ~ 3620 cm⁻¹ (Figure 90). Figure 91 shows the infrared spectra in the region of 3720-3480 cm⁻¹ of the Jet A-1 fuel stressed at 425°C for various time periods under nitrogen. As reported earlier for the unstressed fuel we observe only one peak at 3650 cm⁻¹. On thermal stressing for 1 h, the peak intensity at 3650 cm⁻¹ decreases and another peak appears at 3624 cm⁻¹. We also observe that at times in excess of 1 h of thermal stressing the peak at 3650 cm⁻¹ disappears and the new peak at 3624 cm⁻¹ dominates. In air overpressure, under similar conditions (Figure 92), we note the following differences. The disappearance of the peak at 3650 cm⁻¹ and the appearance of the peak at 3624 cm⁻¹ is faster for fuels stressed for 1 h under air than under nitrogen. This suggests that the antioxidant is more stable in nitrogen atmosphere than in air. In the spectra of fuel stressed at 425°C for periods in excess of 12 h under air a new peak appears at 3550 cm⁻¹. We are currently in the process of attempting to assign the infrared bands at 3624 and 3550 cm⁻¹ using model compounds. The former band is most probably associated with a degradation reaction of the antioxidant molecule (cleavage of the tertiary butyl group ?) while the latter may be a oxidation product formed at long reaction periods (hydroxyl containing group ?).

Figures 93 and 94 show the infrared spectra in the region 1550-2300 cm⁻¹ of the Jet A-1 fuel stressed for 4 h at different temperatures varying from 190°C to 310°C, under nitrogen and air respectively. In this region of the spectra no noticeable change is detected as compared to the infrared spectra of the unstressed Jet A-1 fuel with A.O. Figures 95 and 96 show the infrared spectra in the region 1660-1540 cm⁻¹ of Jet A-1 fuel stressed at 425°C for various time durations in under nitrogen and air respectively. On thermal stressing for 1 h at 425°C we note the appearance of the peaks at 1642 and 1652 cm⁻¹. This band can barely be detected on thermal stressing for 12 and 18 h under nitrogen and air overpressure respectively. Absorptions in the 1660-1640 cm⁻¹ range may be assigned to the C=C stretching vibration. The appearance of these peaks may well correspond to the thermal cracking of the fuel to produce olefins. Their disappearance can probably be related to the cyclization of these olefins which later form ring structures leading to the formation of carbonaceous solids. The disappearance of these absorptions in fact corresponds to the appearance of solids. This region of the spectrum offers considerable potential for mechanistic studies. It should be mentioned that if the primary route to carbonaceous deposits is indeed the formation of olefins and subsequent cyclization, then the role of oxygen at high temperatures (> 400°C) may well be to catalyze the formation double bonds. Additives that retard this process will then have to be found and this may well dictate our future research direction.

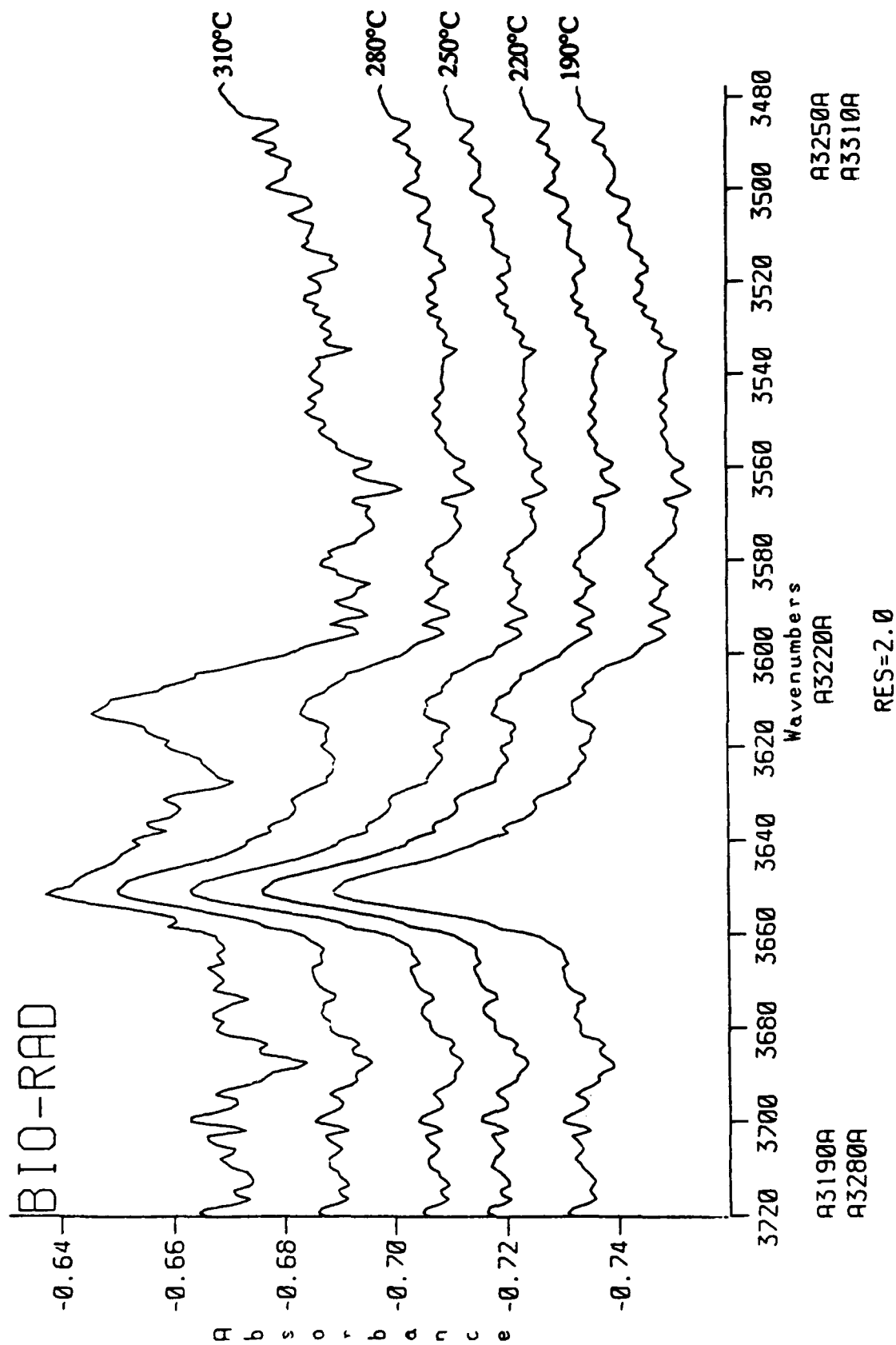


Figure 90. FTIR absorbance spectra of the liquid products obtained from reactions of Jet A-1 + 0.3% A. O. at temperatures 190°C-310°C for 4 h in air.

Jet A-1 + 0.3% A.O. under 100psi nitrogen at 425°C

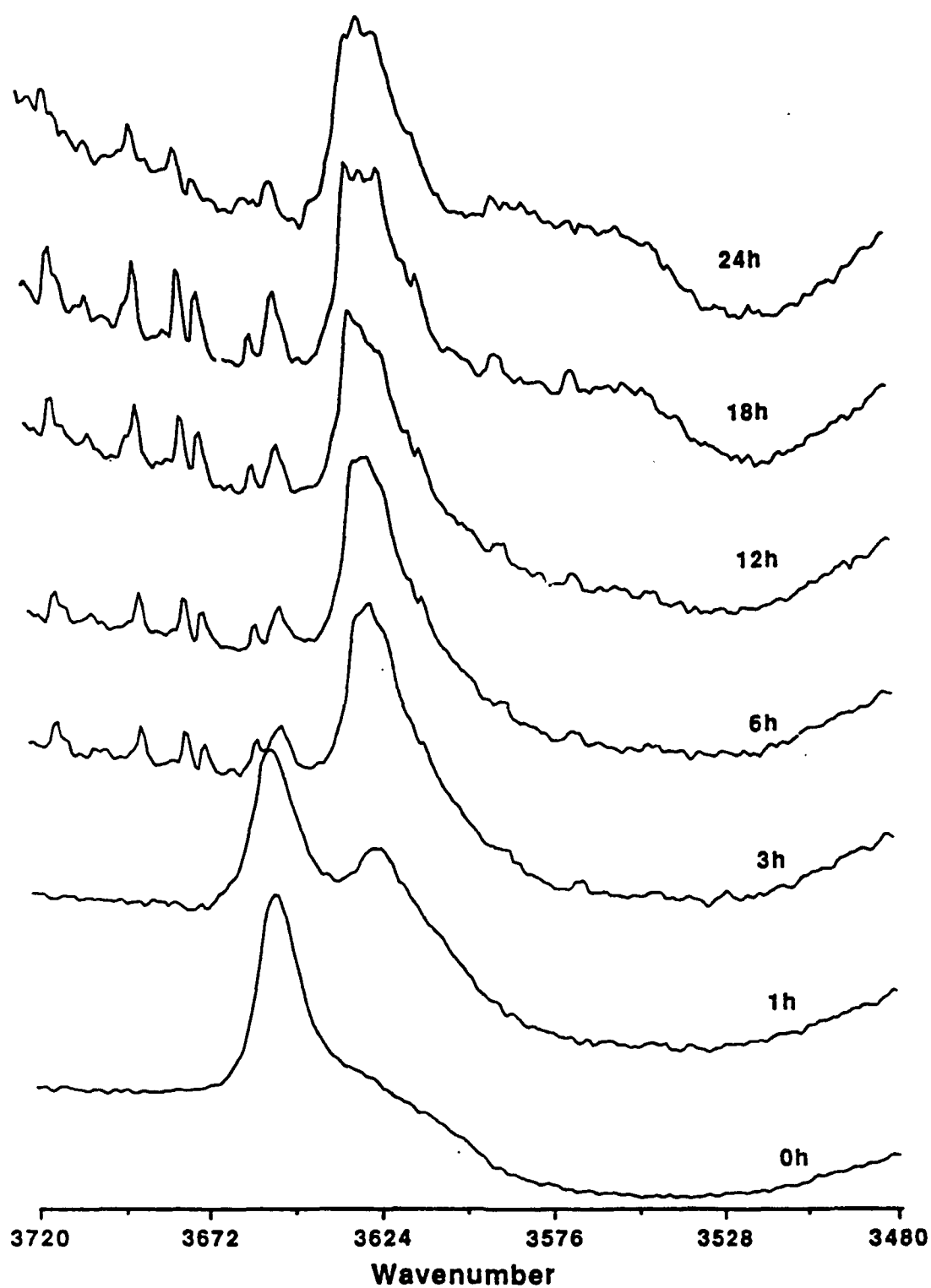


Figure 91. FTIR absorbance spectra of the liquid products obtained from reactions of Jet A-1 + 0.3% A. O. at 425°C for 0-24 h in nitrogen.

Jet A-1 + 0.3% A.O. under 100psi air at 425°C

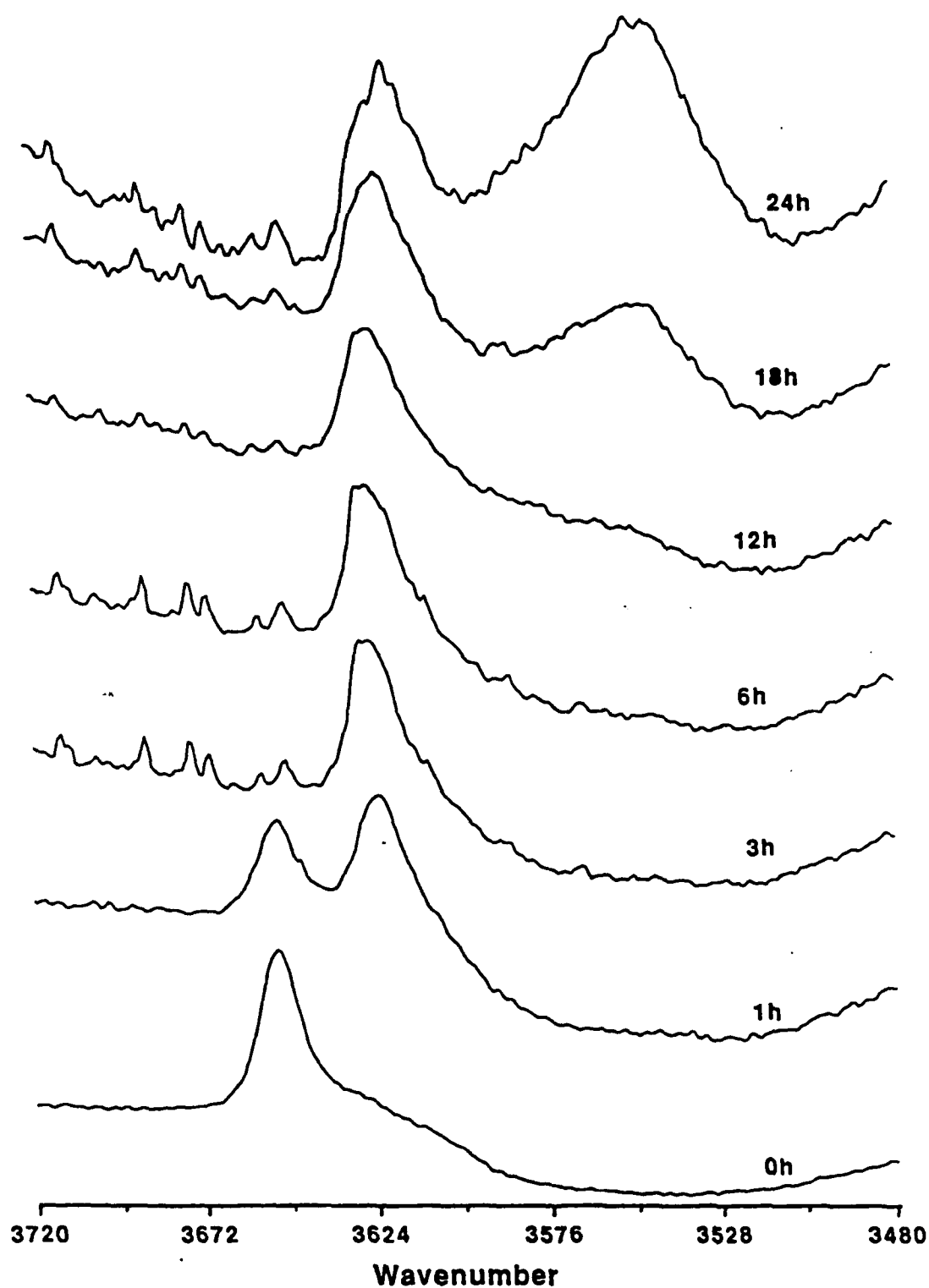


Figure 92. FTIR absorbance spectra of the liquid products obtained from reactions of Jet A-1 + 0.3% A. O. at 425°C for 0-24 h in air.

Jet A-1 + 0.3% A.O. under 100psi nitrogen at 425°C

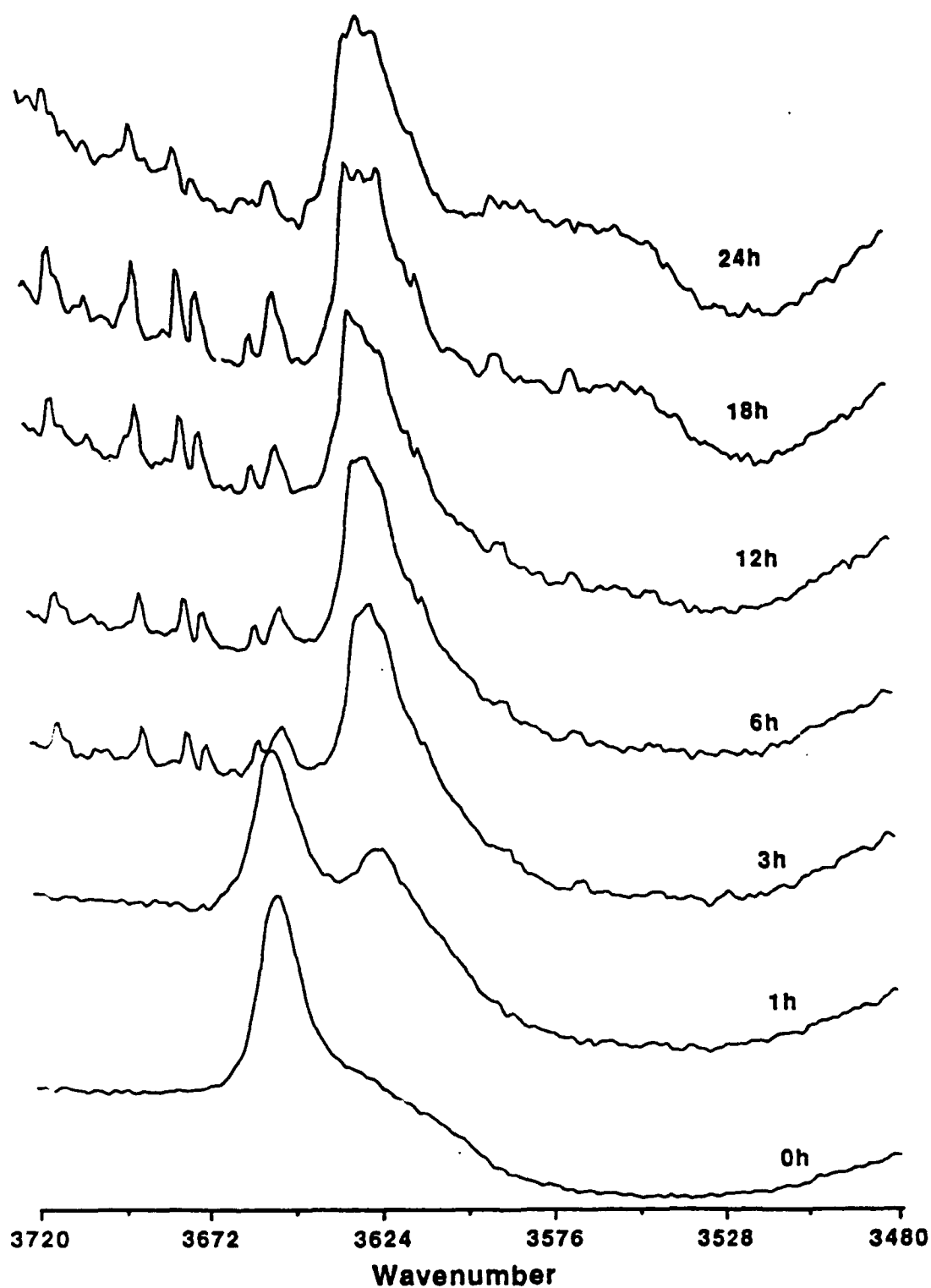


Figure 91. FTIR absorbance spectra of the liquid products obtained from reactions of Jet A-1 + 0.3% A. O. at 425°C for 0-24 h in nitrogen.

Jet A-1 + 0.3% A.O. under 100psi air at 425°C

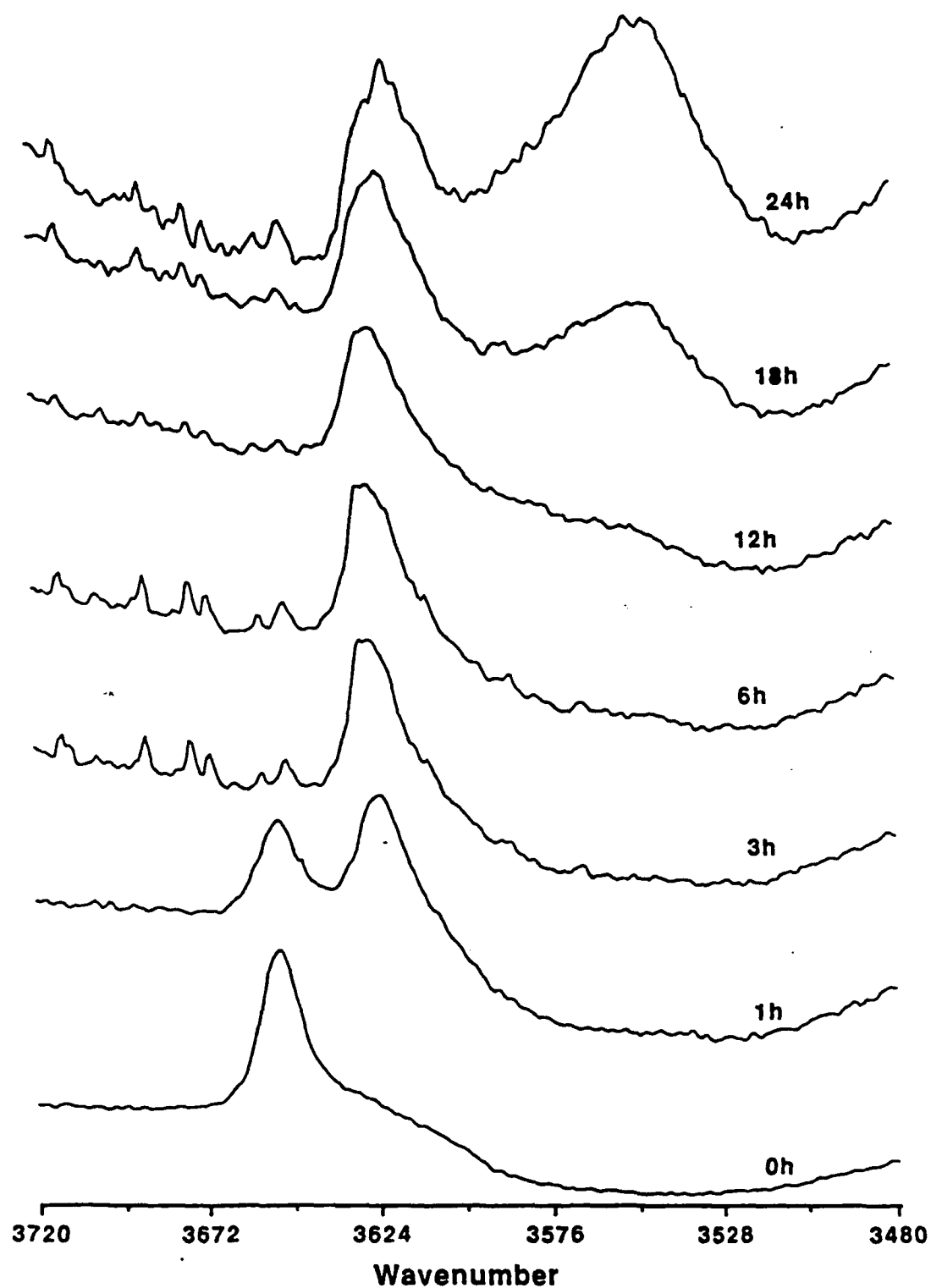


Figure 92. FTIR absorbance spectra of the liquid products obtained from reactions of Jet A-1 + 0.3% A. O. at 425°C for 0-24 h in air.

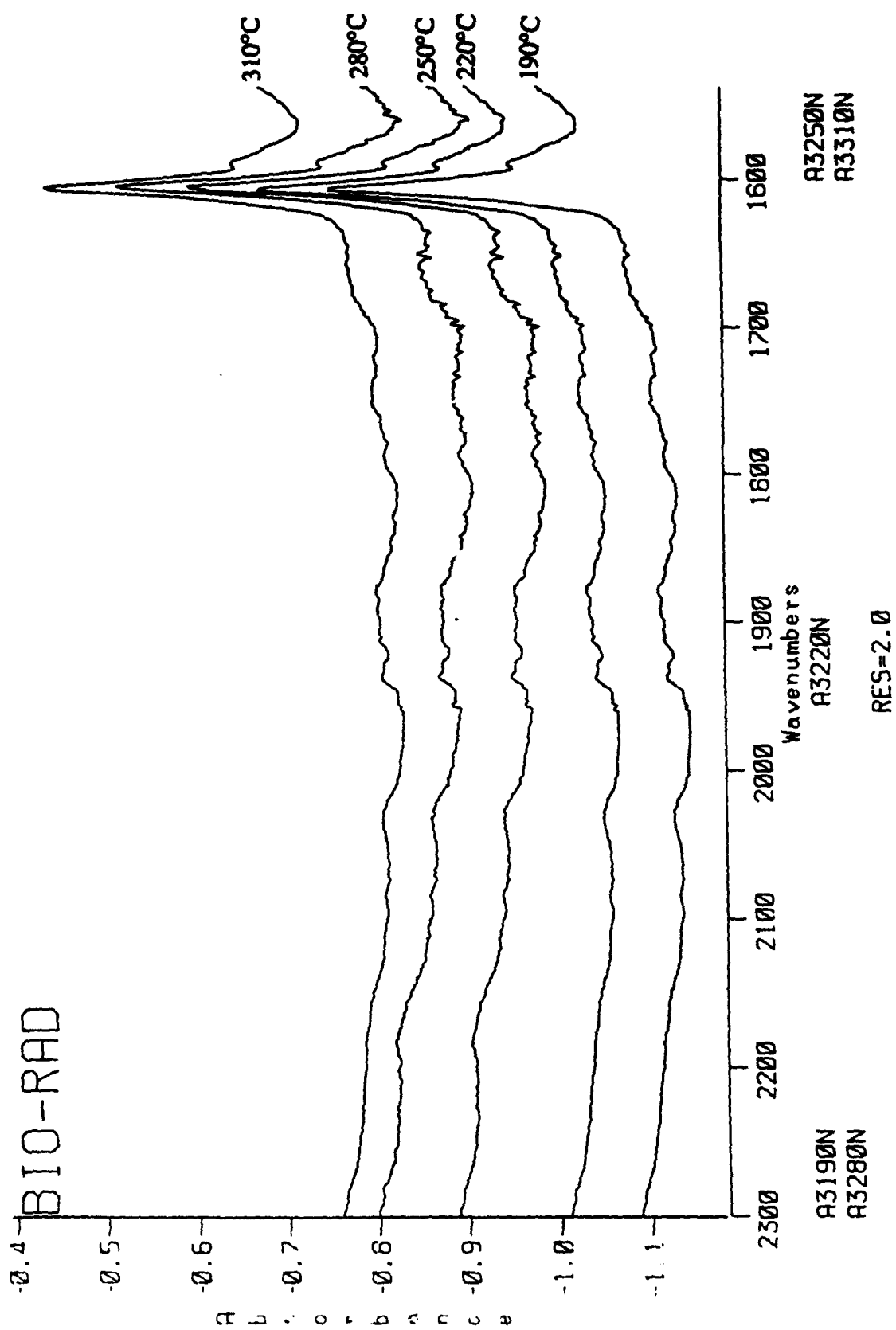


Figure 93. FTIR absorbance spectra of the liquid products obtained from reaction Jet A-1 + 0.3% A. O. at temperatures 190°C-310°C for 4 h in nitrogen.

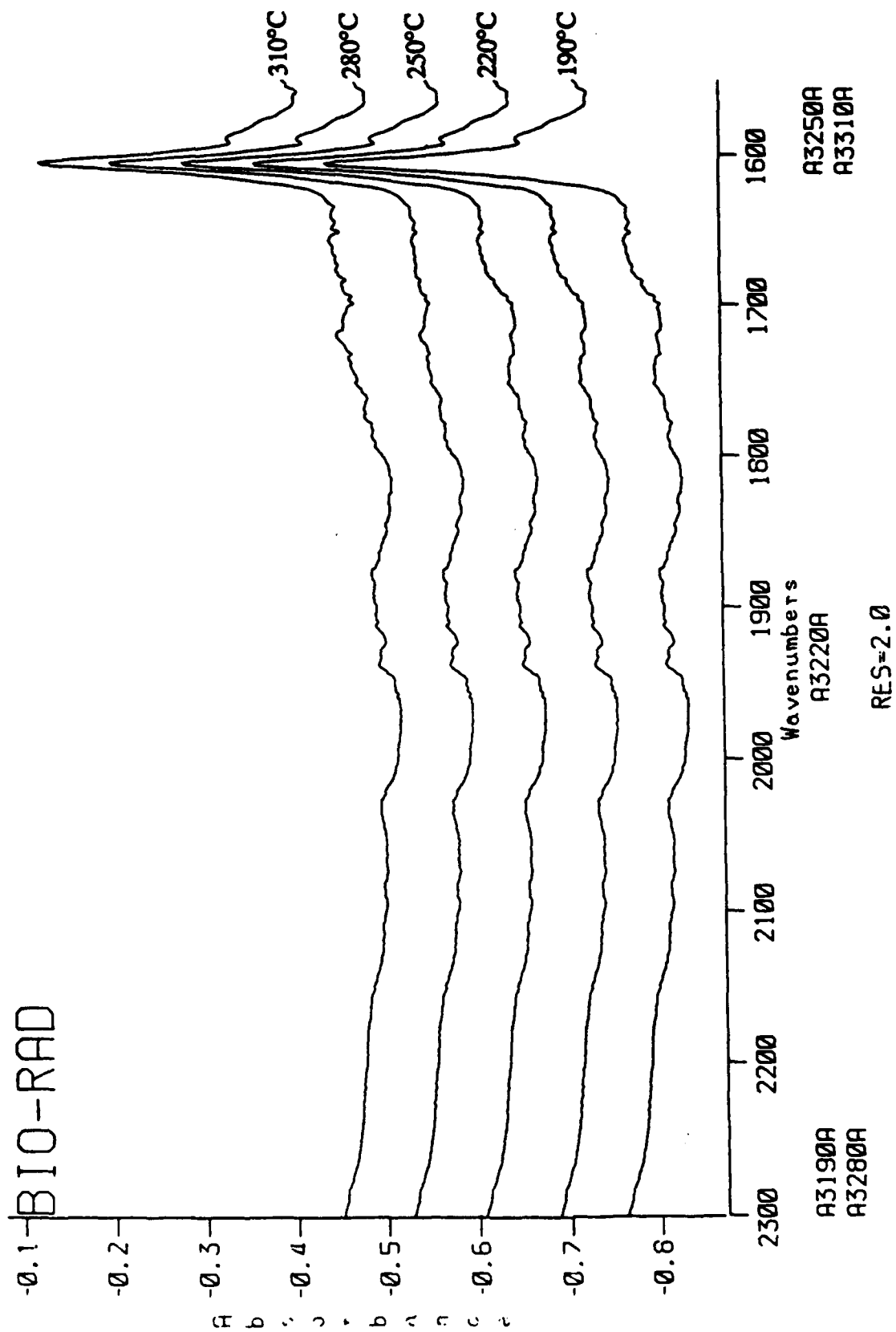


Figure 94. FTIR absorbance spectra of the liquid products obtained from reactions of Jet A-1 + 0.3% A. O. at temperatures 190°C-310°C for 4 h in air.

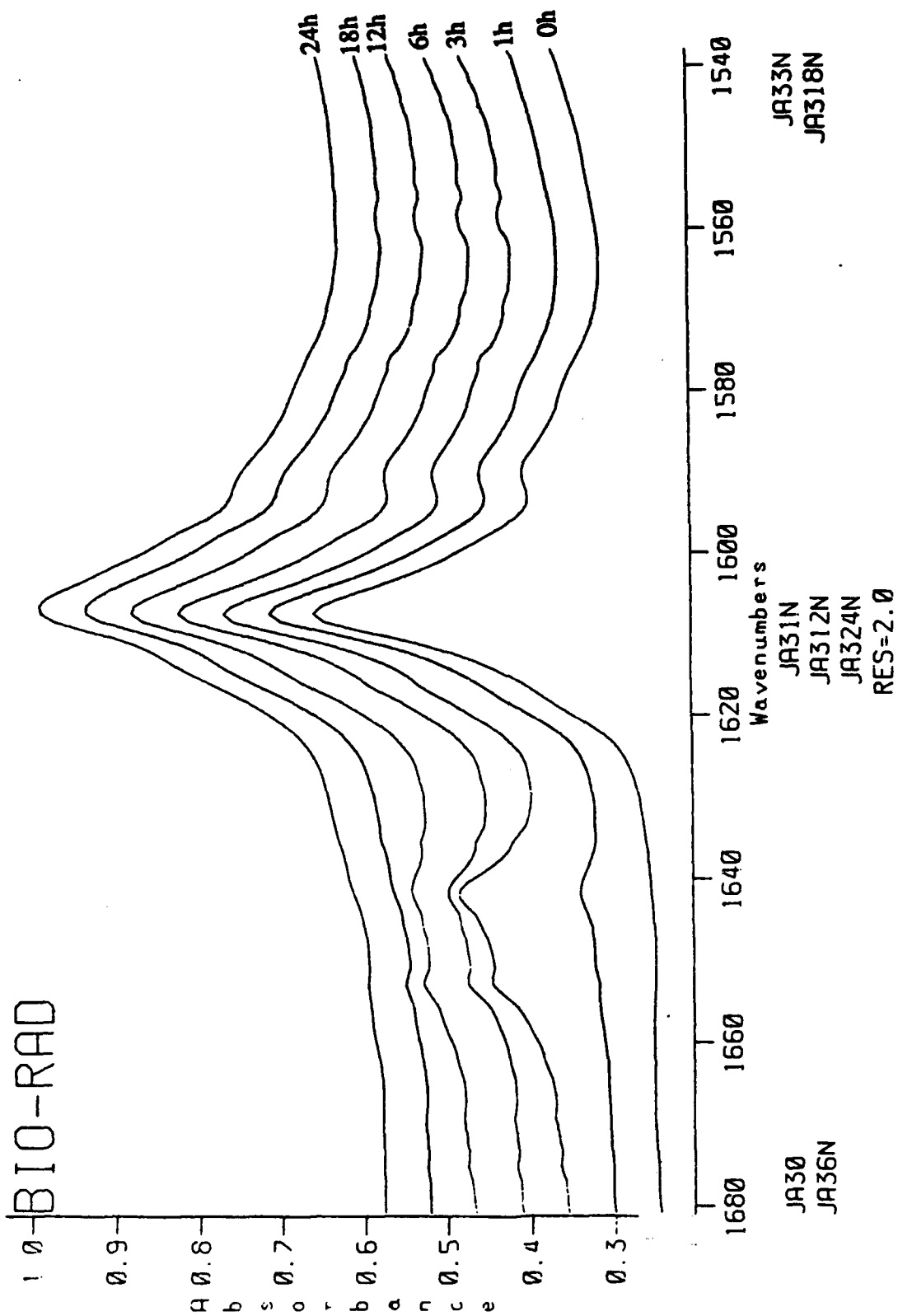


Figure 95. FTIR absorbance spectra of the liquid products obtained from reactions of Jet A-1 + 0.3% A. O. at 425°C for 0-24 h in nitrogen.

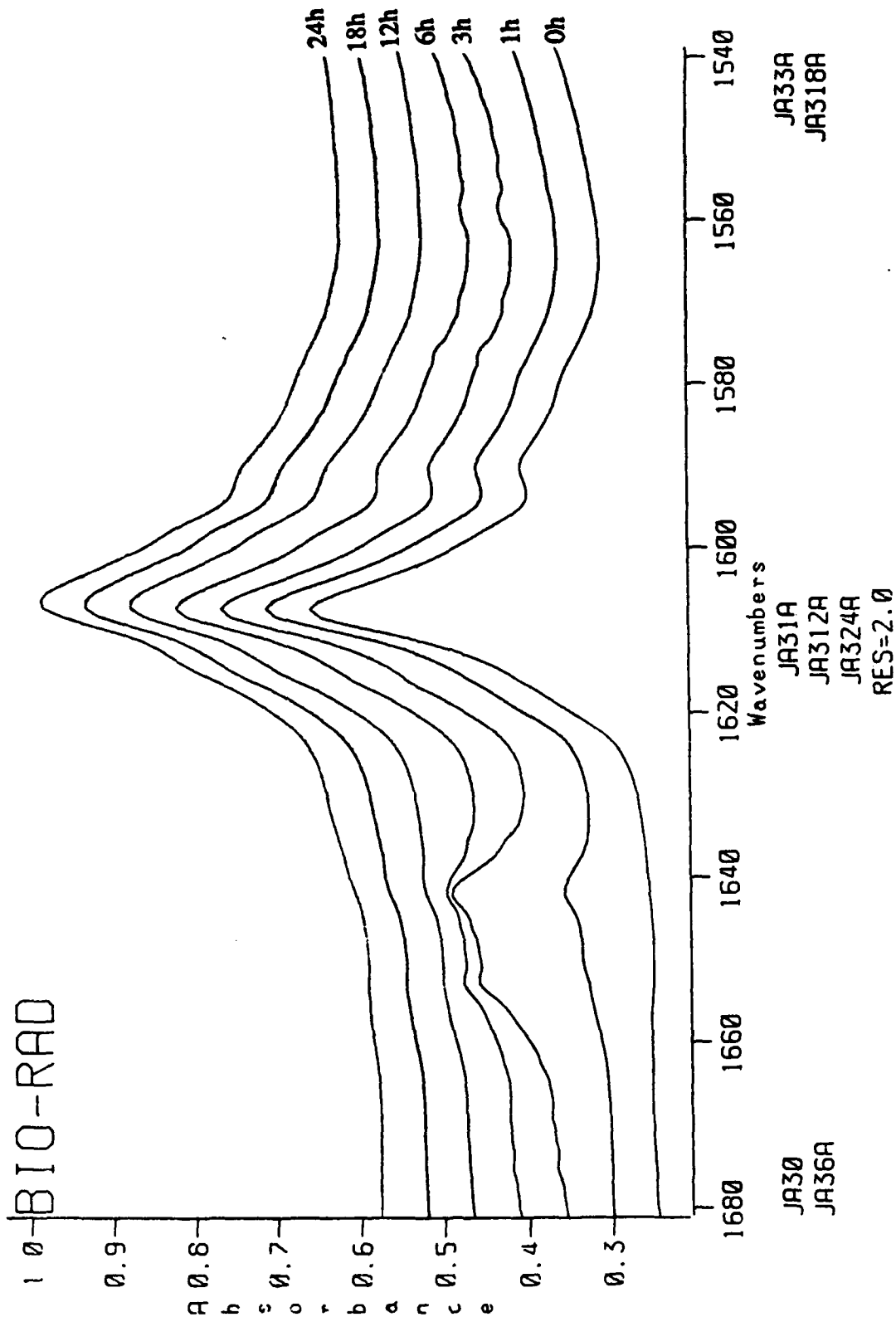


Figure 96. FTIR absorbance spectra of the liquid products obtained from reactions of Jet A-1 + 0.3% A. O. at 425°C for 0-24 h in air.

Figures 97 and 98 show the infrared spectra in the region of $1320\text{--}1080\text{ cm}^{-1}$ of the Jet A-1 fuel stressed for 4 h at temperatures between 190 and 310°C under an overpressure of nitrogen and air, respectively. Once again no change is detected in this region as compared to the infrared spectra of the unstressed Jet A-1 fuel with A.O. Figures 99 and 100 show the infrared spectra in the same region for Jet A-1 fuel stressed at 425°C for various time duration under nitrogen and air overpressure respectively. We notice the development of the peaks at 1265 , 1208 , 1125 , and 1093 cm^{-1} , and these bands are more clearly seen on stressing the fuel under an overpressure of air as compared to that in nitrogen. Although the changes in this region of the spectrum may be significant we will not dwell upon them now as the final region between 660 and 860 cm^{-1} is much easier to interpret.

Figures 101 and 102 show the infrared spectra in the region of $860\text{--}660\text{ cm}^{-1}$ of the Jet A-1 fuel stressed for 4 h at various temperatures under both nitrogen and air. Once again in this region we do not detect any change the infrared spectra on comparing the stressed and unstressed fuels. Figures 103 and 104 show the infrared spectra in the same region for the fuel stressed at 425°C for various time duration under nitrogen and air. There are a number changes in this region of the spectra as a function of time, but we will emphasize only on those which we believe are most important to our studies. The major infrared band in this region of the spectrum of the unstressed fuel can be assigned to vibrational bending modes attributed to aliphatic groups (e.g., the rocking modes of methylene sequences). Thus the band at $\sim 1724\text{ cm}^{-1}$ may be classically assigned to the rocking mode of CH_2 group in sequence of greater than or equal to four. We notice that the intensity of this band decreases with time and appears to have been eliminated after 6 h which suggests that we are observing the degradation of methylene sequences. Concurrently, the bands at 729 and 675 cm^{-1} which are not present in the unstressed fuel increase with time. These bands are tentatively assigned to aromatic species. Thus we appear to have an excellent method of determining the transformation of the aliphatic to aromatic species.

Addition of 2,4,6-tri-tert-butylphenol and 2,4,6-trimethylphenol to JP 8 Neat Fuel

Our previous study on the thermal behavior of alkylated phenols has indicated that the 2,4,6-trimethylphenol is the most stable and the 2,4,6-tri-*t*-butylphenol is the most reactive compound among the phenols studied. In general, the methylphenols have been found to have a higher thermal stability in both inert and oxidizing atmospheres than the *t*-butylphenols [1]. For a preliminary examination of the effect of alkylated phenol addition on the thermal stability of a jet fuel, both 2,4,6-tri-*t*-butylphenol and 2,4,6-trimethylphenol were added at different concentrations to a jet fuel sample (JP8 Neat) prior to thermal treatment in a nitrogen atmosphere. The concentrations of the alkylated phenols additives varied in the range from 10 mg to 500 mg per 10

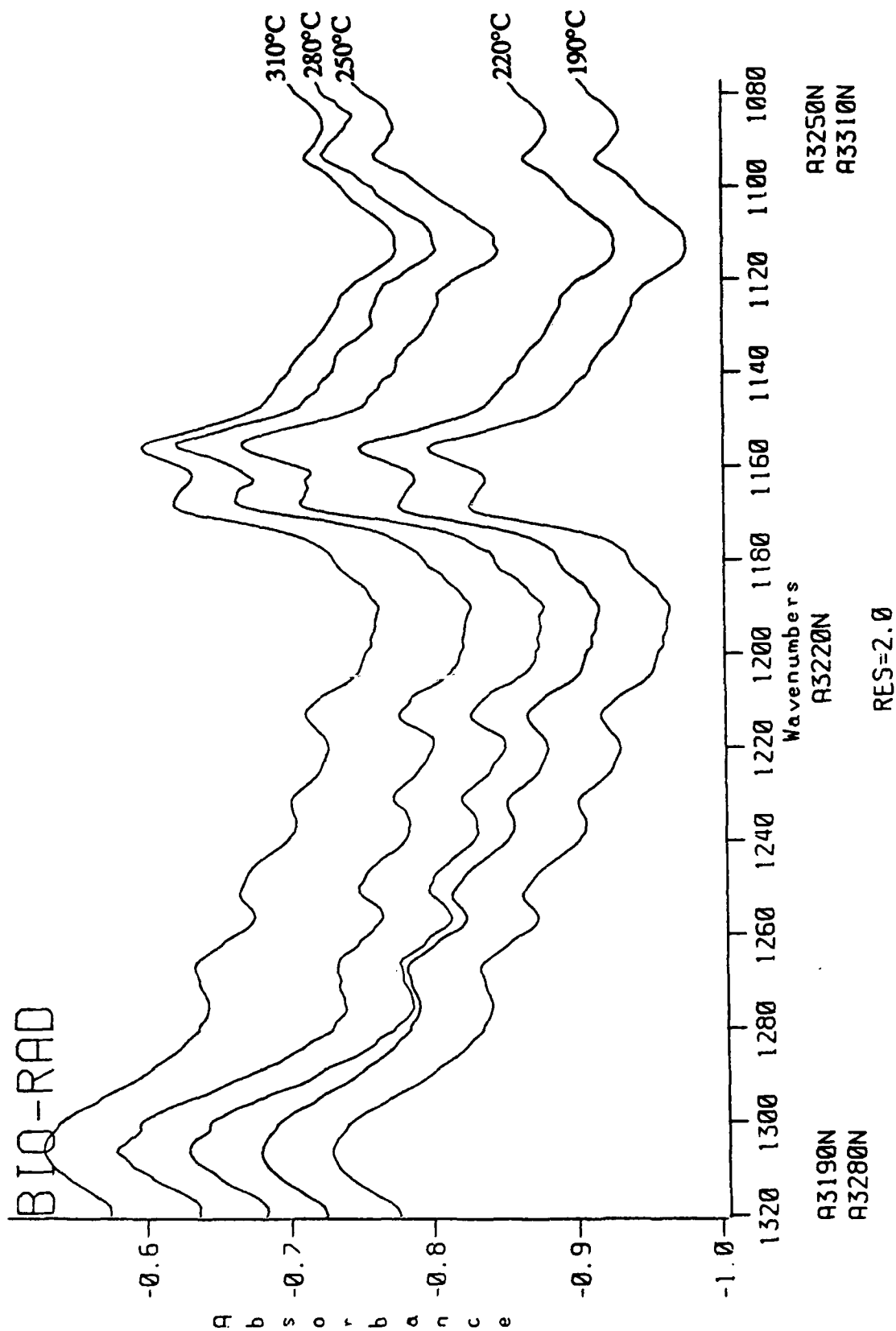


Figure 97. FTIR absorbance spectra of the liquid products obtained from reactions of Jet A-1 + 0.3% A. O. at temperatures 190°C-310°C for 4 h in nitrogen.

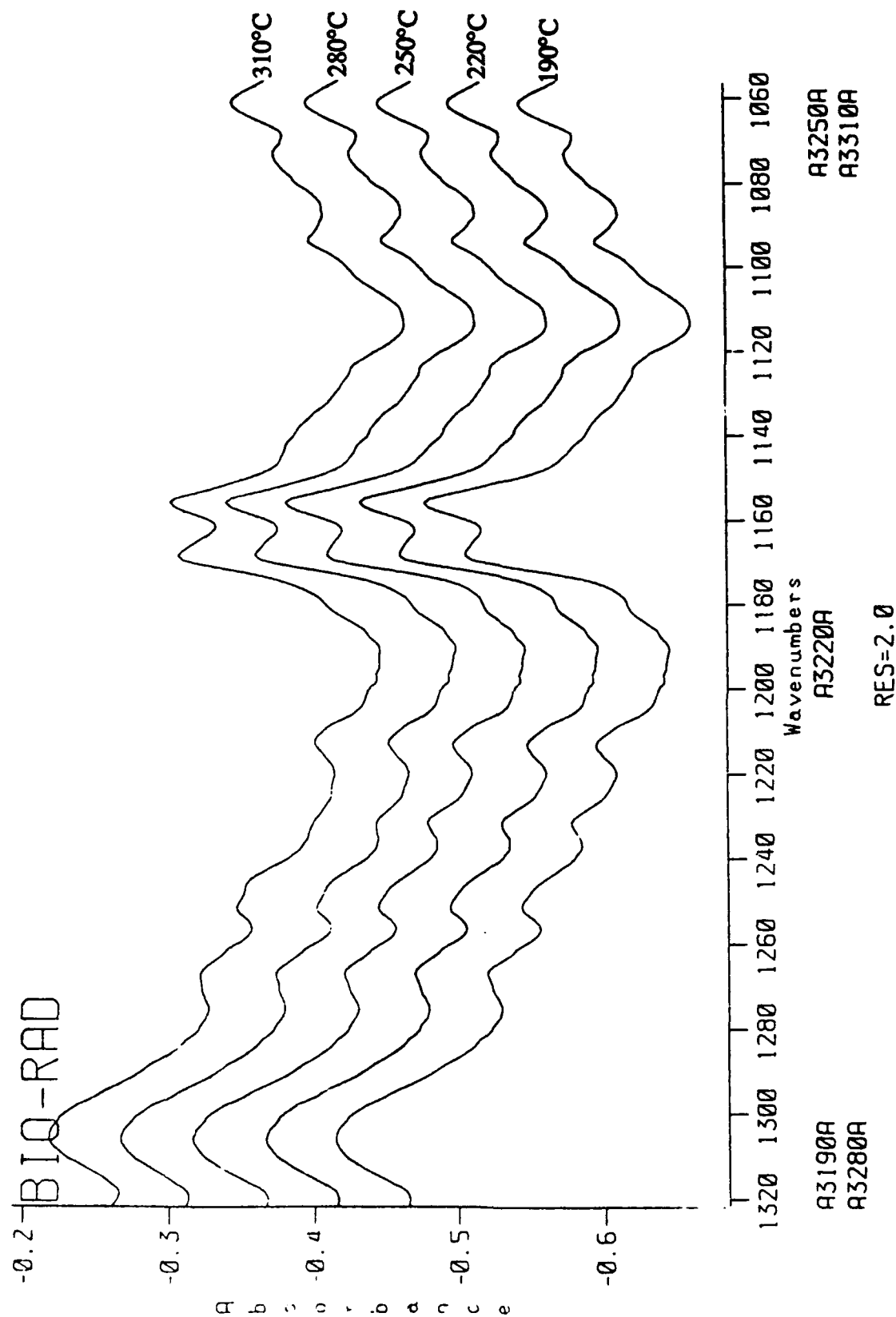


Figure 98. FTIR absorbance spectra of the liquid products obtained from reactions of Jet A-1 + 0.3% A. O. at temperatures 190°C-310°C for 4 h in air.

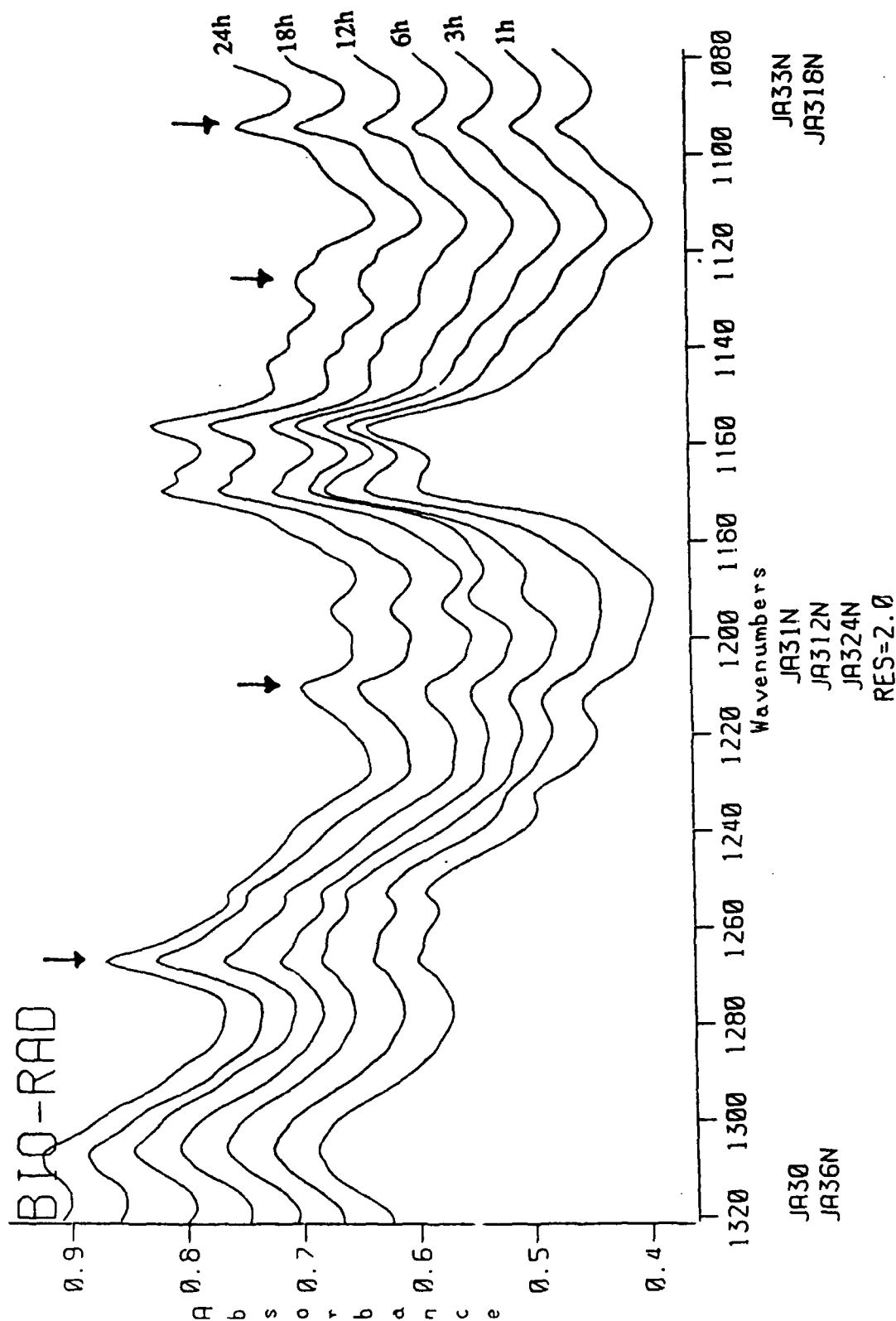


Figure 99. FTIR absorbance spectra of the liquid products obtained from reactions of Jet A-1 + 0.3% A. O. at 425°C for 0-24 h in nitrogen.

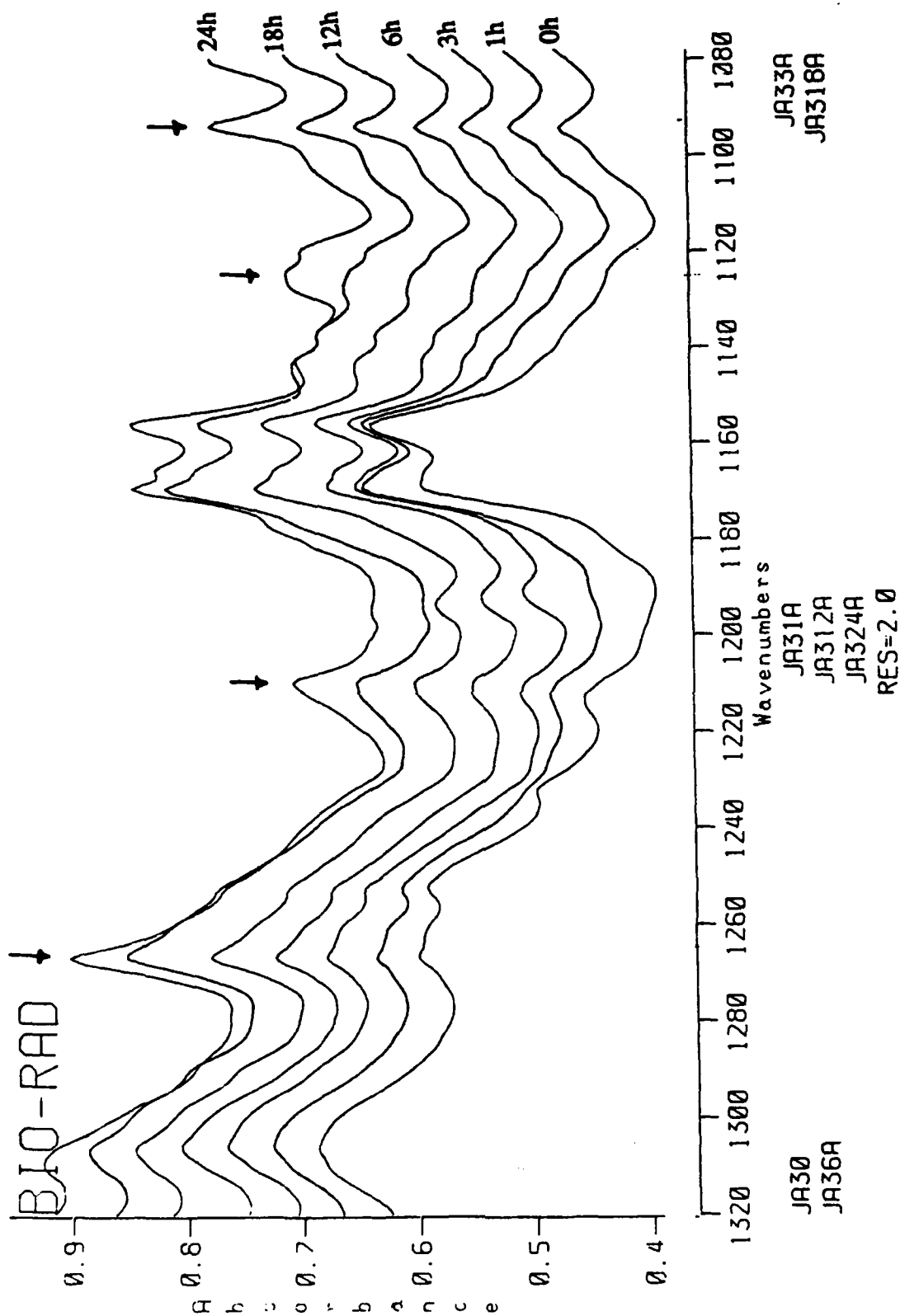


Figure 100. FTIR absorbance spectra of the liquid products obtained from reactions of Jet A-1 + 0.3% A. O. at 425°C for 0-24 h in air.

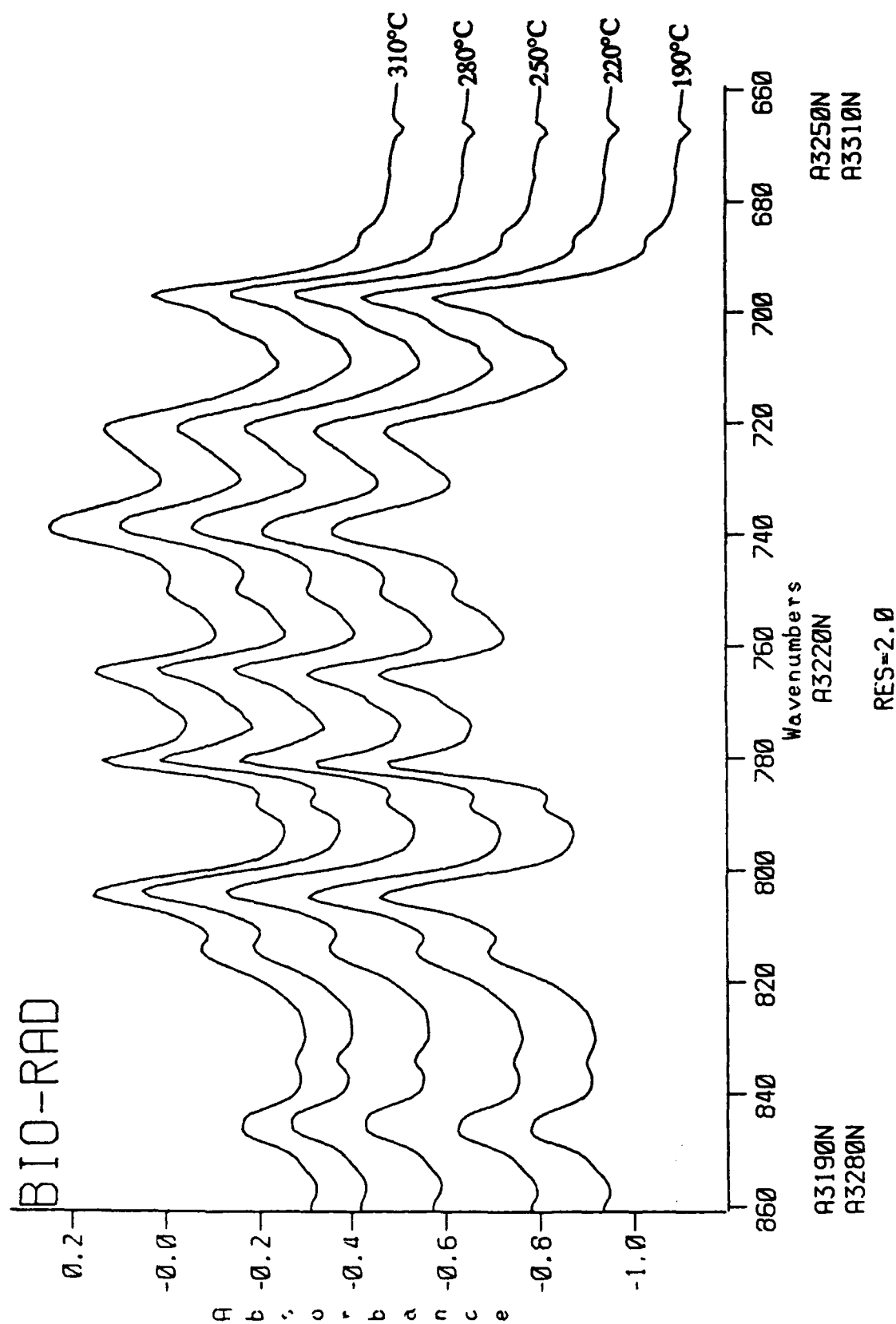


Figure 101. FTIR absorbance spectra of the liquid products obtained from reactions of Jet A-1 + 0.3% A. O. at temperatures 190°C-310°C for 4 h in nitrogen.

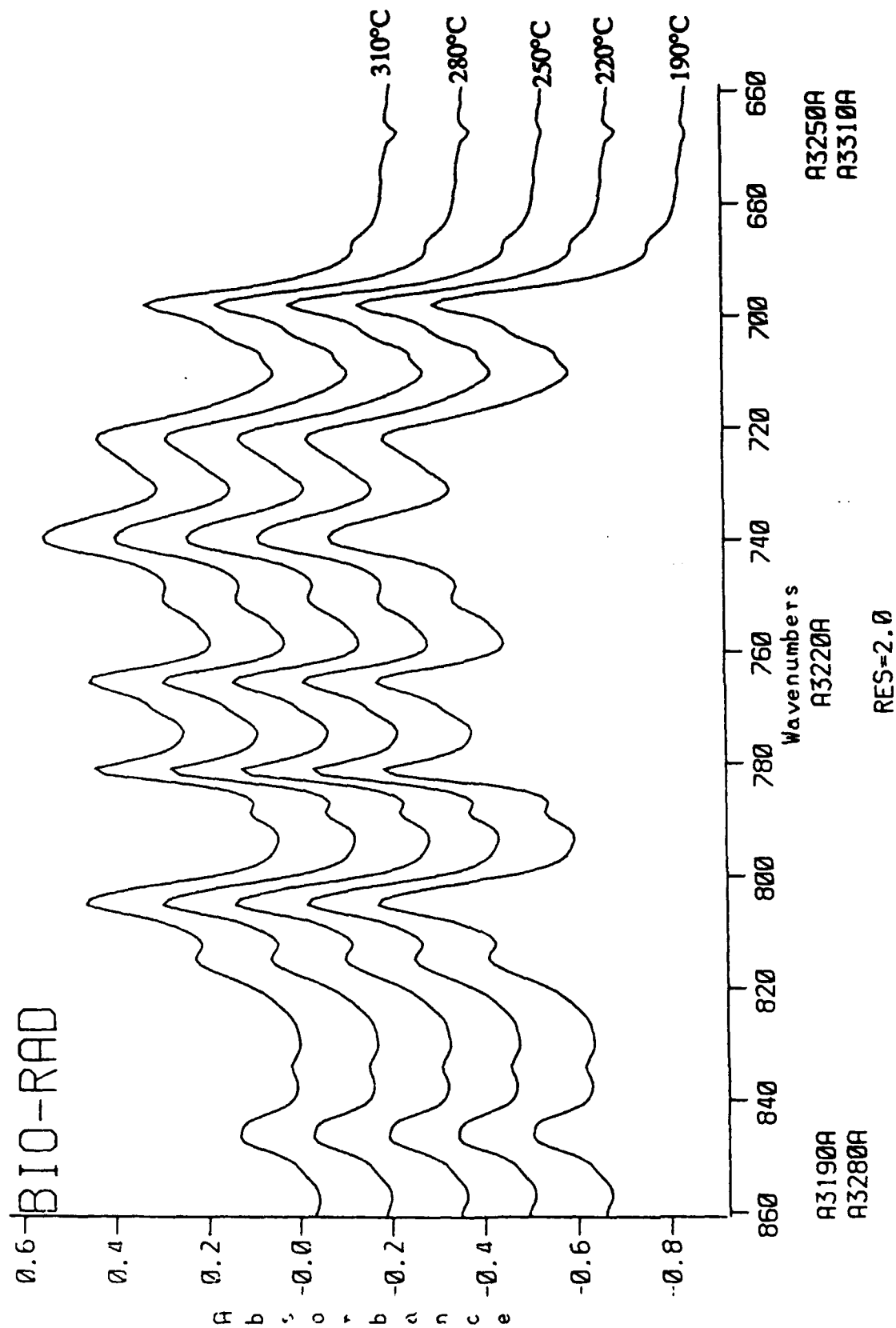


Figure 102. FTIR absorbance spectra of the liquid products obtained from reactions Jet A-1 + 0.3% A. O. at temperatures 190°C-310°C for 4 h in air.

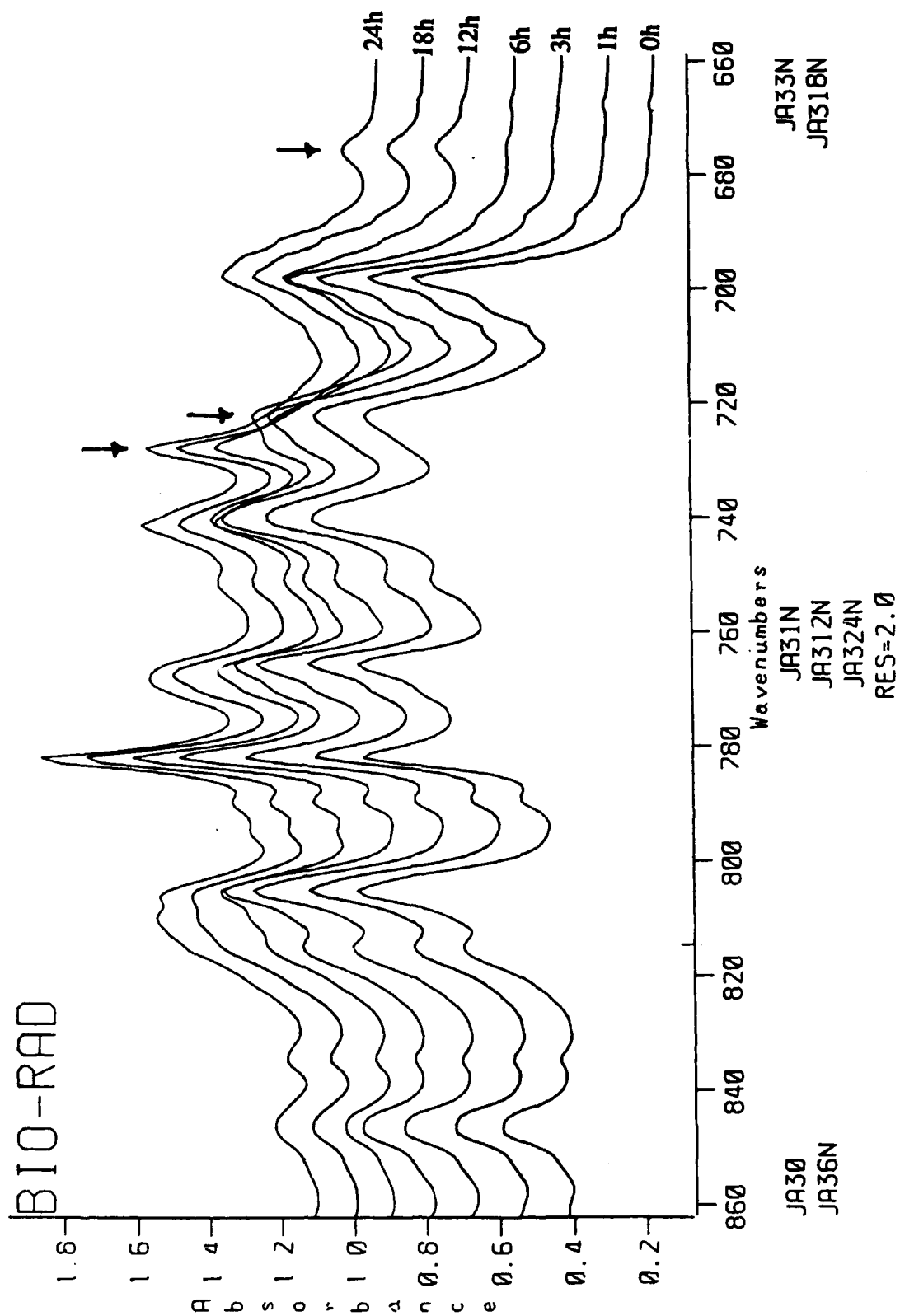


Figure 103. FTIR absorbance spectra of the liquid products obtained from reactions of Jet A-1 + 0.3% A.O. at 425°C for 0-24 h in nitrogen.

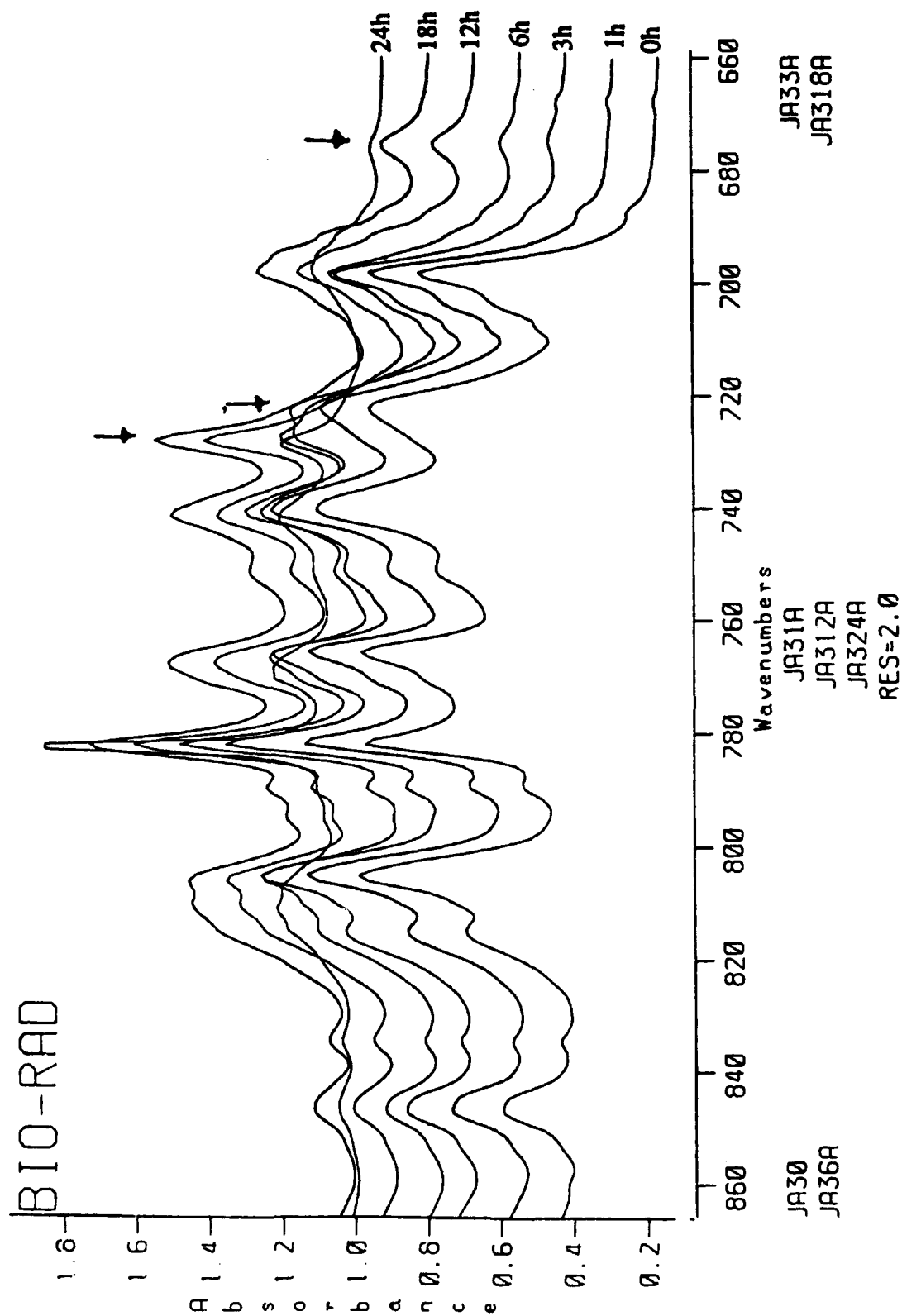


Figure 104. FTIR absorbance spectra of the liquid products obtained from reactions of Jet A-1 + 0.3% A. O. at 425°C for 0-24 h in air.

ml of JP-8 Neat. Both pure JP-8 Neat and the mixtures of JP-8 neat and the additives were heat treated at 400°C for 2 h under 100 psig (cold) nitrogen pressure. The treatment products showed different extents of discoloration and in some cases significant amounts of solids were formed as a result of the thermal treatment. The differences in discoloration of the degradation products were quantified on a comparative scale by measuring the percent transmittance of 520 nm wavelength light through the product samples. Transmittance measurements were based on 100% transmittance through distilled water [1]. The results of the transmittance measurements are shown in Figure 105 where percent transmission of the products is plotted versus the mass of the additives. The transmittance values shown in Figure 105 are the mean values calculated from the transmittance measurements on the products obtained from duplicate treatment experiments.

When JP8 neat was treated alone, there was a slight discoloration in the product indicated by 94% transmittance on the plot in Figure 105 without the formation of any solids. The addition of 2,4,6-tri-*t*-butylphenol produced an increasing extent of thermal degradation of the mixture with the increasing additive concentration, where the product obtained in the presence of 500 mg became almost opaque, accompanied also by the formation of solids (approximately 10 mg) as marked by the letter S in Figure 105. In a distinct contrast, the addition of 2,4,6-trimethylphenol did not produce any change in the thermal stability of the mixtures with the increasing concentration of the additive up to 500 mg per 10 ml.

GC and GC/MS analyses of the treated mixtures indicated that TMP survived the thermal treatment without any degradation, while TTBP was almost completely converted into other products including *tert*-butylphenol and di-*tert*-butylphenol. Figures 106 and 107 show the GC traces of the mixtures of JP8 neat with TMP and TTBP treated at 400°C for 2 h. The peak marked as P in Figure 106 is the TMP peak. One can see that the relatively mild treatment did not cause any discernible change in the chemical constitution of JP-8 neat or the mixtures of JP-8 neat with TMP. In contrast, Figure 107 shows that TTBP was completely converted into other products including *tert*-butylphenol (marked as 1P) and di-*tert*-butylphenol (2P). It is interesting to note that there is no change in the composition of JP-8 neat even in the presence of 500 mg of TTBP. Considering that both mixtures (with 100 and 500 mg TTBP) produced solids, it can be concluded that all the solids produced resulted from the self condensation reactions of TTBP without causing any visible degradation of JP 8 neat. It should, however, be expected that, at higher temperatures, there would be cross reactions between the free radicals formed by degradation of TTBP and the reactive components of jet fuel. Even at a low concentration of TTBP addition, there may be a destabilizing effect of TTBP at high temperatures, as it can become a free radical initiator rather than a free radical scavenger.

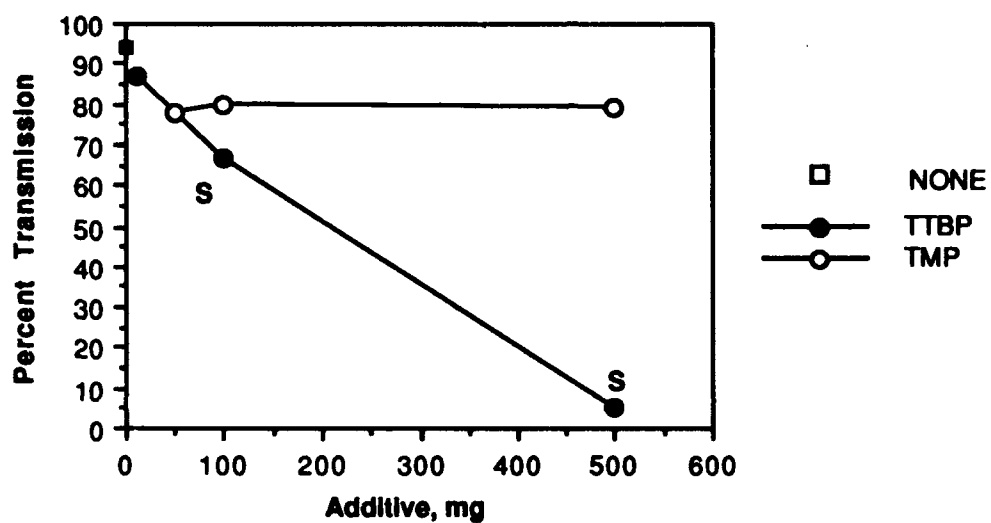


Figure 105. Percent transmittance of the products obtained from thermal treatment of 10 ml JP 8 Neat alone and in the presence of 2,4,6-tri-*t*-butylphenol (TTBP) and 2,4,6-trimethylphenol (TMP).

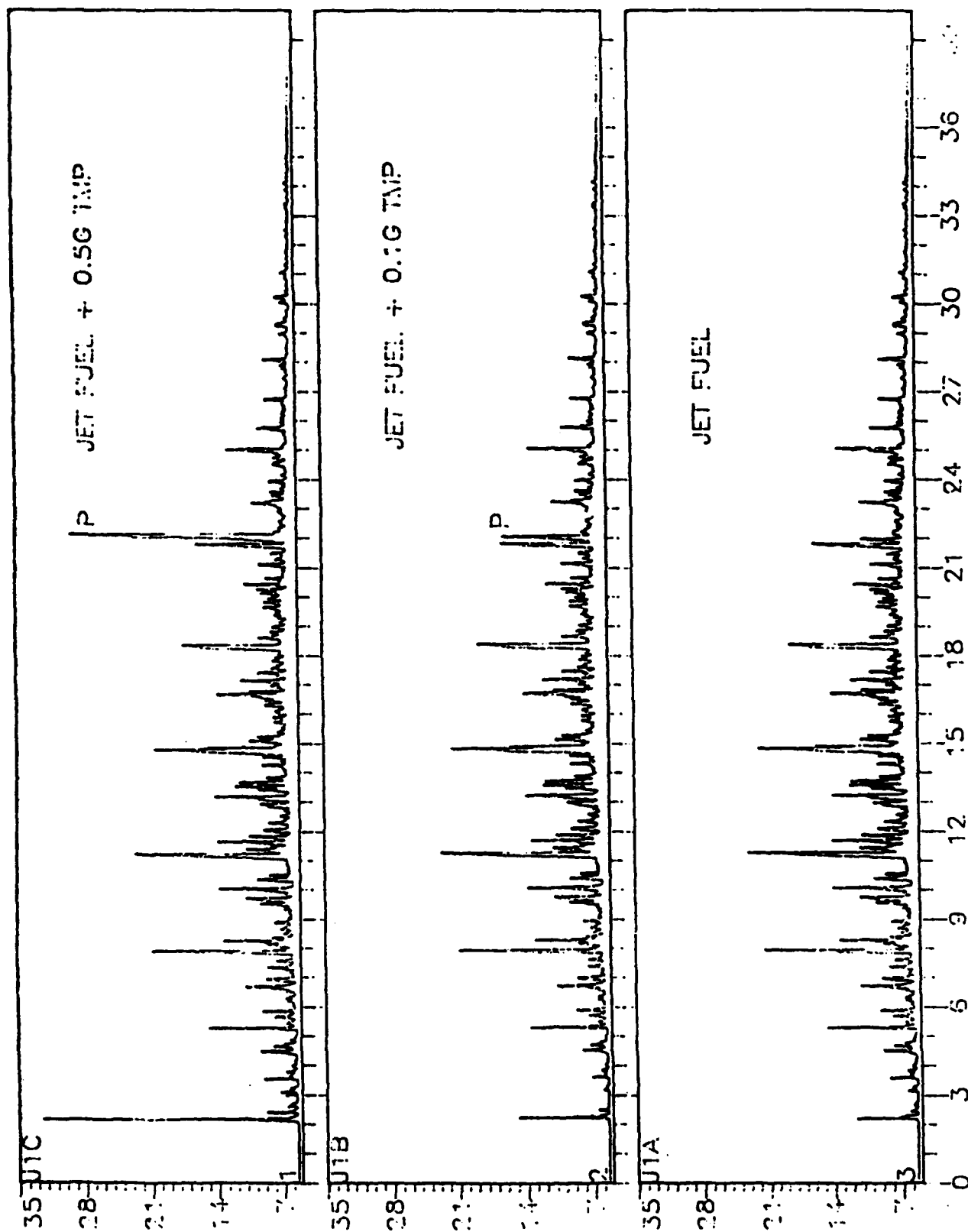


Figure 106. GC trace of JP-8 neat and mixtures of JP-8 neat with 2,4,6-trimethylphenol treated at 400°C for 2 h in 100 psi N₂.

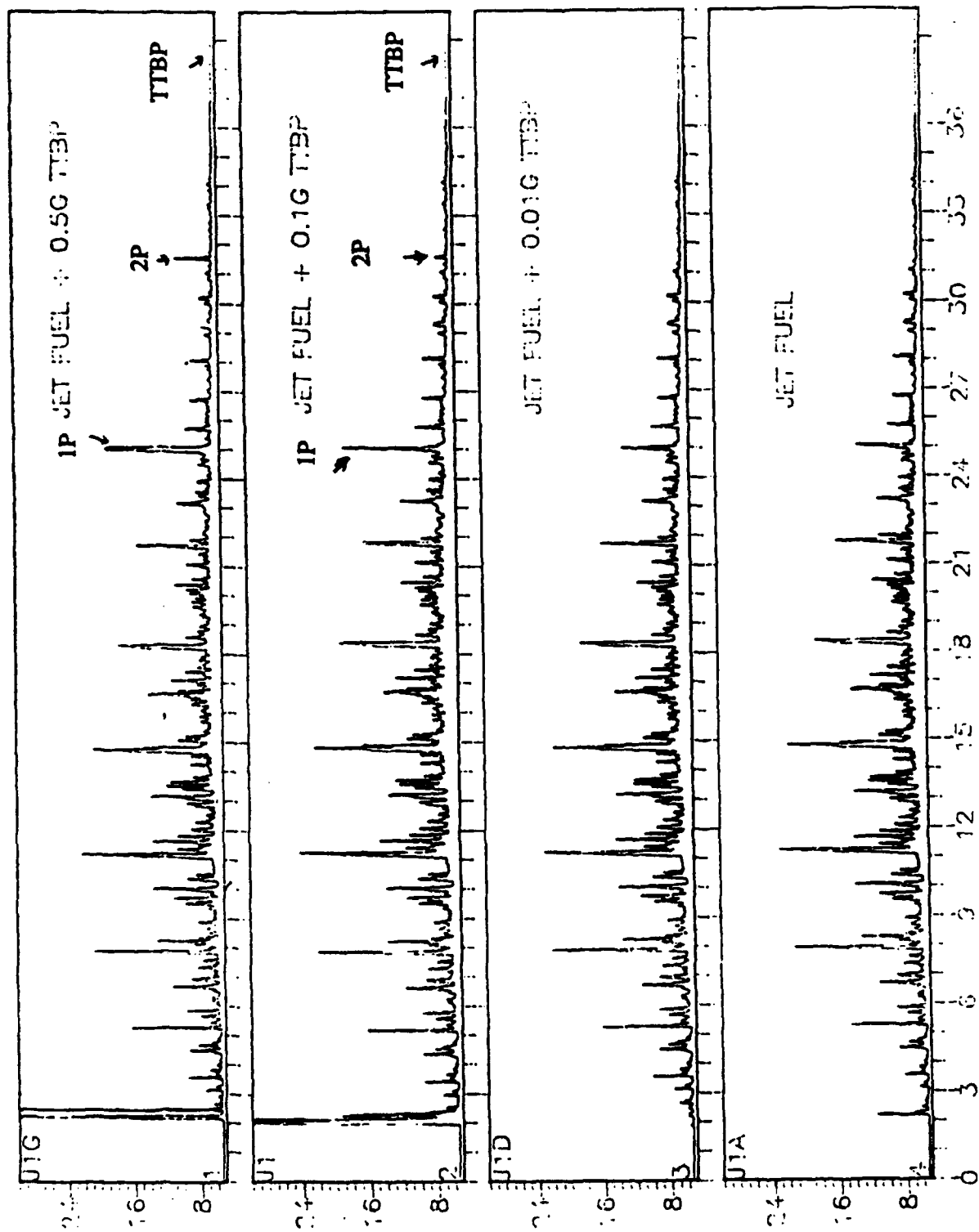


Figure 107. GC trace of JP-8 neat and mixtures of JP-8 neat with 2,4,6-tri-t-butylphenol treated at 400°C for 2 h in 100 psi N₂.

References

1. S. Eser, C. Song, H. H. Schobert, P. G. Hatcher, R. Copenhaver, H. Jiang, R. Li, M. Parzynski, and Y. Peng, Advanced Thermally Stable Jet Fuels Development Program Annual Report, Volume II "Compositional Factors Affecting Thermal Stability of Jet Fuels," Interim Report for period July 1989 to June 1990, DOE/Sandia National Laboratory, June 1990, WRDC-TR-90-2079, Vol. II, Sep. 1990.
2. S. V. Gollakota, O. L. Davies, P. Viamalchand, J. M. Lee, and C. E. Cantrell, "Recent Progress in the Direct Liquefaction of Two Low-Ash Powder River Basin Coals and a Deep Cleaned Pittsburgh Seam Coal," Proceedings of Direct Liquefaction Contractors' Review Meeting, Sept. 24-26, 1990, pp. 129-158.
3. M. Furlong, J. Fox, and J. Masin, "Production of Jet Fuels from Coal-Derived Liquids. Vol. IX - Results of Bench-Scale and Pilot Plant Testing," Interim Report for period February 1988 to March 1989, AFWAL-TR-87-2042, Vol. IX, June 1989.
4. F. W. McLafferty, "Interpretation of Mass Spectra," University Science Books, Mill Valley, California, 1980, Chapter 9.
5. C. Song, K. Hanaoka and M. Nomura, Energy & Fuels 2, 639, 1988.
6. D. J. Cookson and B. E. Smith, Fuel, 68, 776, 1989
7. The Aldrich Library of NMR Spectra, 2nd Ed., Vol.1, 1983.
8. C. R. Martel, "Military Jet Fuels 1944-1987," Summary Report for period Oct. 85 - Oct. 87, AFWAL-TR-87-2062, November 1987.
9. S. Eser, C. Song, H. H. Schobert, Y. Peng, M. Parzynski, L. Selvaraj, R. C. Copenhaver, and P. G. Hatcher, "Compositional Factors Affecting Thermal Degradation of Jet Fuels," Technical Progress Report for the Period July 1990 - September 1990, DOE/Sandia National Laboratory, October 1990.
10. C. Song, S. Eser, H. H. Schobert, P. G. Hatcher, M. M. Coleman, R. M. Copenhaver, Y. Peng, L. Selvaraj, and M. Parzynski, "Compositional Factors Affecting Thermal Degradation of Jet Fuels," Technical Progress Report for the Period October 1990 - January 1991, DOE/Sandia National Laboratory, February 1991.
11. C. Song, S. Eser, H. H. Schobert, P. G. Hatcher, M. M. Coleman, Y. Peng, L. Selvaraj, M. Parzynski, J. Bortiatynski, Y. Liu, R. M. Copenhaver, R. Arumugam, "Compositional Factors Affecting Thermal Degradation of Jet Fuels," Technical Progress Report for the Period February 1991- April 1991, DOE/Sandia National Laboratory, May 1991.
12. J. C. Bokros, in "Chemistry and Physics of Carbon," (Ed. P. L. Walker, Jr.), Dekker, NY, Vol. 5, 1, 1969.
13. J. Smith and H. Marsh, in "Analytical Methods for Coal and Coal Products," (Ed. C. Carr, Jr.), Academic Press, NY, Vol. 2, 371, 1978.
14. H. B. Palmer and C. F. Cullis, in "Chemistry and Physics of Carbon," (Ed. P. L. Walker, Jr.), Dekker, NY, Vol. 1, 265, 1965.
15. J. D. Brooks and G. H. Taylor, in "Chemistry and Physics of Carbon," (Ed. P. L. Walker, Jr.), Dekker, NY, Vol. 4, 243, 1968.